NASA-CR-182214

P-276

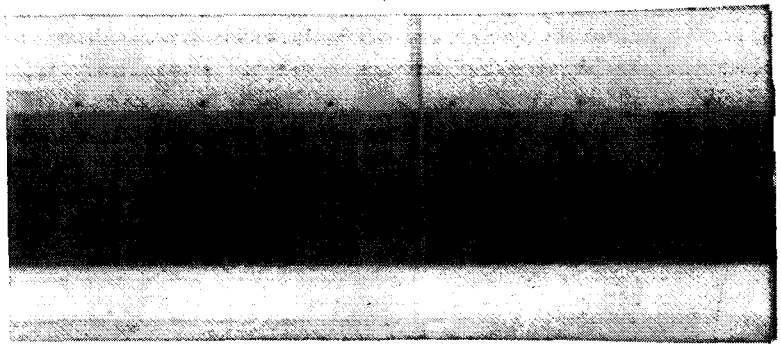

NASA-CR-182214

NAG3-501

Technological Institute

NORTHWESTERN UNIVERSITY

EVANSTON, ILLINOIS

To my dearest

Father - Mr. P. T. Lei

and

Mother - Mrs. C. F. Chen Lei

NORTHWESTERN UNIVERSITY

ELECTRICAL PROPERTIES OF MATERIALS FOR ELEVATED TEMPERATURE RESISTANCE STRAIN GAGE APPLICATION

A DISSERTATION

SUBMITTED TO THE GRADUATE SCHOOL

IN PARTIAL FULFILLMENT OF THE REQUIREMENTS

for the degree

DOCTOR OF PHILOSOPHY

Field of Materials Science and Engineering

By

JIH-FEN LEI

Evanston, Illinois

June 1987

ABSTRACT

ELECTRICAL PROPERTIES OF MATERIALS FOR ELEVATED TEMPERATURE RESISTANCE STRAIN GAGE APPLICATION

By

Jih-Fen Lei

The objective of this research is to study the electrical resistances of materials that are potentially useful as resistance strain gages at 1000°C.

A set of criteria were set and used in selection of strain gage candidate materials that are electrical stable and reproducible at all temperatures up to the operating temperature (1000°C) and have small temperature coefficient of resistance (TCR). Transition metal carbides and nitrides, boron carbide and silicon carbide were selected for the experimental phase of this research. The electrical resistance of these materials was studied in the temperature range of 23-1000°C under vacuum via dc or automatic ac four probes methods. The electrical resistance of boron carbide in an oxidizing environment was also measured.

The resistivities of the transition metal compounds increased and their TCRs and electrical stabilities decreased with an increase in the vacancy concentrations. The resistivity saturated at about 1000 microohm-cm, for resistivities larger than 1000 microohm-cm, negative TCR

were observed.

The TCR of stoichiometric transition metal nitrides decreased monotonically in going from compounds of metal of group VI to those of group V then to those of group IV of the period table. Also the TCR of transition metal nitrides and carbides with transition metals in the same column of the period table decreased as quantum number of the transition metal increased. Carbides had lower TCR than the corresponding nitrides.

The change in resistance of B_4C with temperature followed a form of $R=ATexp(E_A/kT)$, with activation energy E_A of about 0.14 ± 0.005 eV. The change in its strain sensitivity with temperature were also tested.

The decrease in resistance with increase in temperature was faster in α-SiC than in β-SiC. Nitrogen doping effect was studied in the case of β-SiC, doping resulted in a decrease in TCR and electrical stability.

Due to their low TCR and good stability, TiC, ZrC, B_4C and β-SiC are suggested to be good candidate for high temperature resistance strain gage application.

Approved

Professor J. O. Brittain
Thesis Advisor
Department of Materials Science
and Engineer
Northwestern University

ACKNOWLEDGEMENTS

The author would like to express the most sincere gratitude and deepest appreciation to her advisor Prof. J. O. Brittain, without whom this work would not be possible, his scientific guidance, continual encouragement, inspiration and understanding have been invaluable in its completion. She also thanks Prof. C. R. Kannewurf, Prof. B. W. Wessels, and Prof. D. H. Whitmore for many enlightening comments and suggestion provided prior to and while serving on the author's committee.

The helpful discussions and warm friendships of many colleagues will not be forgotten. In particular, Mr. D. Geslin, C. Haney, E. Yoshitake, and Dr. J. Zelimir, M. Shaarbaf, S. C. Chen, C. F. Yang, and C. S. Hwang are appreciated for their help, advice and general interest.

The personnel of the Materials Science Machine Shop, SEM facility, X-ray facility and Metallograph Lab at Northwestern University are thanked for their help and cheery hellos over the years.

The financial support for this work provided

through a grant from the NASA is acknowledged. Dr. H. Okimura of Tokyo Institute of Technology in Japan, Mr. C. Haney of Dow Chemical Co. are thanked for providing specimens for this study. Dr. S. Schwartz and M. Shaarbaf are appreciated for proof reading of the manuscript and Mr. E. Yoshitake for the technical drawings in this dissertation.

Finally, the author would like to thank her parents- Mr. and Mrs. Lei, foster parents- Mr. and Mrs. Schwartz, parents in law to be- Mr. and Mrs. Mao and Jun Mao for their love, understanding, and moral support.

TABLE OF CONTENTS

TABLE OF CONTENTS - Continued

TABLE OF CONTENTS - Continued

TABLE OF CONTENTS - Continued

LIST OF TABLES

LIST OF FIGURES

LIST OF FIGURES - continued

LIST OF FIGURES - continued

LIST OF FIGURES - continued

LIST OF FIGURES- continued

LIST OF FIGURES- continued

LIST OF fIGURES - continued

CHAPTER 1

INTRODUCTION

Historically, the development of strain gages has followed many different paths, and gages have been developed based on electrical, mechanical, optical, acoustical, and pneumatic principles. During the past 40 years electrical strain gages have become so widely accepted that they now dominate the entire strain gage field except for a few special applications. This is because they very closely meet the requirements of the optimum gage, arising from their simplicity, high sensitivity, reliability and low costs. The most important electrical strain gage is the resistance type. Two less commonly employed electrical strain gages are the capacitance type and the inductance type, which have lower sensitivities compared to that of the resistance type.

The discovery of the principle upon which the electrical resistance strain gage is based was made in 1865 by Lord Kelvin, who loaded copper and iron wires in tension and noted that their resistance increased with the strain applied to the wires (piezoresistance effect)

[1]. Much work has been carried out on electrical resistance strain gages since then in an attempt to evolve a generally applicable gage for the measurement of strains at increasingly higher temperatures.

In recent years, the rapid progress in aerospace and nuclear fields, in which extremely high operating temperatures are prevalent, not only resulted in a search for new, heat-resisting materials but also in need for high-temperature resistance strain gages. Since existing high temperature resistance static strain gages are not reliable for use above 600^{o}C, there is an urgent need to find new sensor materials which can be used at higher temperatures.

As the operating temperature level increases, the problems associated with the use of strain gages also increase. The main difficulty with static strain measurements is that the strain gages will not retain (or vary predictably within acceptable limits) their characteristics over a long period of time at elevated temperatures. Therefore, the basic requirement for a strain gage material is to be electrical stable and reproducible over the entire range of the operating

temperatures.

While the specific goal of this work is the development of resistance strain gages for applications at about 1000°C, the objective of this research is not to build a gage itself but to study the electrical resistances of materials that are potentially useful as resistance strain gages at 1000°C [2]. The results of this investigation should lead to an improvement in the material selection process for elevated temperature resistance strain gages application.

This dissertation is divided into eight chapters. In chapter two we review the development of different resistance strain gages and analyze the properties of an ideal resistance strain gage. From these requirements, a set of simple and rough selection criteria were derived and several candidate materials were chosen in the chapter three. Chapter four describes the experimental procedures and techniques adopted for the electrical resistance measurements. In chapter five and six results of the electrical resistance measurements for several conducting and semiconducting materials are discussed respectively. Chapter seven is concerned with the strain

sensitivity measurements for one of the best candidate materials. Based on the work in preceding chapters, the selection criteria for high temperature resistance strain gage materials were modified and are discussed in the final chapter.

CHAPTER 2

RESISTANCE STRAIN GAGE

2.1 Definition of A Resistance Strain Gage

An electrical resistance strain gage is a strain-sensing element which changes its electrical resistance with an applied strain. The strain sensitivity (also called "Gage Factor" G) of a gage is defined as [3]:

$$G = dR/(R\,d\varepsilon) \tag{2-1}$$

where R is the electric resistance of the gage material, ε is the applied strain ($d\varepsilon=dL/L$, L is the length of the gage). Therefore, by detecting the change in resistance and knowing the gage factor, one can measure the applied strain.

For a material with length L, cross-section A, and resistivity ρ, its electrical resistance R becomes

$$R = \frac{\rho L}{A} \tag{2-2}$$

If an uniform stress σ is applied in longitudinal direction to it, the variation in R is then

$$\frac{dR}{d\sigma} = \frac{d(\rho L/A)}{d\sigma} = \frac{\rho}{A}\frac{\partial L}{\partial \sigma} - \frac{\rho L}{A^2}\frac{\partial A}{\partial \sigma} + \frac{L}{A}\frac{\partial \rho}{\partial \sigma} \qquad (2\text{-}3)$$

or, if referred to the initial resistance R,

$$\frac{1}{R}\frac{dR}{d\sigma} = \frac{1}{L}\frac{\partial L}{\partial \sigma} - \frac{1}{A}\frac{\partial A}{\partial \sigma} + \frac{1}{\rho}\frac{\partial \rho}{\partial \sigma} \qquad (2\text{-}4)$$

Eqs. (2-3) and (2-4) show that for a finite stress variation the total resistance change is due to

(1)change in length: dL/L

(2)change in cross-section A, or diameter D:

$$-\frac{dA}{A} \approx -2\frac{dD}{D}$$

(3)change in specific resistivity ρ: $d\rho/\rho$.

With Poisson's ratio η, the lateral contraction is

$$\frac{dD}{d} = -\eta\frac{dL}{L}$$

then Eq. (2-4) becomes

$$\frac{dR}{R} = \frac{dL}{L}(1 + 2\eta) + \frac{d\rho}{\rho} \qquad (2\text{-}5)$$

this yields the gage factor G :

$$G = \frac{dR/R}{d\varepsilon} = 1 + 2\eta + \frac{d\rho/\rho}{d\varepsilon} \qquad (2\text{-}6)$$

with $d\varepsilon = dL/L$.

Experimental results show that G varies from about 1 to 6 for metallic materials at room temperature and about ±100 to ±200 for semiconductors [4]. Since $0<\eta<1/2$ for all materials, equation (2-6) indicates that the change in specific resistivity with strain can be quite large for certain alloys and especially for semiconductors. The change in resistivity with strain (piezoresistive effect) can be further analyzed as follows.

When the stress σ applied on a sample with a resistivity ρ is along the same direction as electric field E, and current density i, the simple relation between these factors is [4]:

$$\frac{E}{\rho} = i\,(1 + \pi_1\sigma) \qquad (2\text{-}7)$$

where ρ is the resistivity of sample under no stress, π_1 is a longitudinal piezoresistive coefficient which depends on the crystallographic direction in a crystalline materials.

The ratio E/i describes the quantity, i.e., the longitudinal resistivity of the sample that is changing

under the stress σ and can be denoted by :

$$\frac{E}{i} = \rho + d\rho \qquad (2\text{-}8)$$

then, from equations (2-7) and (2-8), the fractional change of ρ due to a stress σ is

$$\frac{d\rho}{\rho} = \pi_l \sigma \qquad (2\text{-}9)$$

By using Young's modulus $Y = \sigma/\varepsilon$, where ε is the longitudinal strain resulting in from the tensile stress σ, Eq. (2-9) can be rewritten

$$\frac{d\rho}{\rho} = \pi_l Y\varepsilon = m_l \varepsilon \qquad (2\text{-}10)$$

where

$$m_l = Y\pi_l$$

then the gage factor G in Eq. (2-6) becomes

$$G = \frac{dR}{Rd\varepsilon} = 1 + 2\eta + \frac{d\rho}{\rho d\varepsilon} = 1 + 2\eta + m_l \qquad (2\text{-}11)$$

One of the most important qualities of a strain gage is that its gage factor should be stable; it should not vary with either temperature or time. Ideally, any change in resistance should only be due to the change in strain. However, in general, the change in the resistance of a gage is not only a function of strain (ε), but also

a function of temperature (T) and time (t), i.e., R = f(ε, T, t). To a first approximation, the relative change in resistance of a gage is [5]:

$$\frac{\Delta R}{R} = \frac{1}{R}\frac{\partial R}{\partial \varepsilon}\bigg|_{T_o, t_o} \Delta\varepsilon + \frac{1}{R}\frac{\partial R}{\partial T}\bigg|_{\varepsilon_o, t_o} \Delta T + \frac{1}{R}\frac{\partial R}{\partial t}\bigg|_{\varepsilon_o, T_o} \Delta t \qquad (2\text{-}12)$$

The first term $(\partial R/(R\,\partial \varepsilon))_{T_o,\ t_o}$ is the gage factor G of the gage material at temperature T_o, and time t_o. The second and third terms in Eq. (2-12) combine effects which produce a temperature- and time- induced resistance change. To have the resistance change due to the strain alone, one would have to avoid or eliminate those effects which cause the resistance to change with either temperature or time.

In the next section, we will review the development of high temperature resistance strain gages, and see why the existing gages fail to work at higher temperatures. Then we will define the purpose of this work.

2.2 Historical Development Review

2.2.1 Conventional Resistance Strain Gage

The search for suitable alloys for high-temperature

strain gages has been under way since the introduction of the wire resistance strain gages some fifty years ago. In 1968, Bertodo [6] after examining over 500 individual alloy systems, announced that the existing gages at that time could only measure the static strains up to 300°C. The properties of the alloys he used for evaluation included:

(1) a high degree of metallurgical stability and oxidation resistance;

(2) a relatively constant temperature coefficient of resistance over the temperature range of interest coupled with a resistivity of at least 40 μΩ-cm;

(3) a moderate change in strain sensitivity with temperature;

(4) adequate mechanical strength.

He claimed that the main source of instability at temperatures above 300°C was associated with oxidation and that the desirability of low drift rates restricted the choice of gage materials to certain precious metal alloys; of these an alloy of tungsten and platinum appeared to have been the most acceptable at that time.

In 1970, Drennen et al. [7] conducted an extensive literature survey and compiled and evaluated information

on potential alloys. They consulted more than 700 articles obtained from the Western world and as well as some from Slavic sources covering the period of 1957 to 1970. They defined the properties that an ideal material should have for strain gage application as follows:

(1) good oxidation resistance at the temperature at which it would be used.

(2) metallurgical and structural stability at service temperatures.

(3) good fabricability to wire or foil.

(4) adequate mechanical strength.

(5) high electrical resistivity.

(6) the same or nearly the same coefficient of thermal expansion as the material to which it is applied.

(7) little variation in gage factor with temperature and strain.

(8) a minimum amount of apparent strain with temperature.

(9) a constant or linear temperature coefficient of resistance.

They concluded that no alloy was known at that time which would retain all of the above properties at temperature up to 600^{o}F (315^{o}C). However, they identified

two groups of materials as promising candidates: the platinum-tungsten system and the iron-chromium-aluminum system. Later Lemcoe [8] concluded that Fe-Cr-Al alloys were better than Pt-W alloys for static strain measurements up to 593°C, because Fe-Cr-Al alloys had a lower resistance drift than platinum alloys.

In the early 1980's Pratt and Whitney made another study to select strain gage materials which could be used at temperature up to 600K (327°C) and 900K (627°C). Their guidelines for selecting such candidate materials were as follows [9]:

(1) The first atomic species in the alloy to be a monomorphic FCC transition metal with:
    (a) a melting temperature about twice the service temperature, and
    (b) high oxidation resistance (at least when in solution with second element discussed below).

(2) The second atomic species in the alloy should be from a different column of the period table with:
    (a) large difference in atomic radius
    (b) large difference in valence
    (c) a range of solid solution (no ordering or

formation of phases or compounds with first species) at all temperatures up to service temperature, and

(d) high oxidation resistance when in solution with the first element.

The contradiction between requirements (a) and (c) for the second species is noted. According to Hume-Rothery rule, the difference between the atomic sizes of the component elements forming an alloy should be smaller than 15%, otherwise solid solubility would become restricted [10].

By using the guidelines mentioned above, Pratt and Whitney selected 41 alloys and then investigated. They classified Pt-W and Pd-Mo in the "should be tried" group, and Ag-Pd, Al-Fe, Pt-Ru and Pt-Cr in the "could be tried" group. The last four systems were placed in this group because of their relatively high temperature coefficient of resistance (>200 ppm/^{o}C). Also, Cu-Ni and Ni-Cr were found suitable for use at 327^{o}C, but were eliminated for use at 627^{o}C because Cu-Ni was too sensitive to oxidation and Ni-Cr underwent an order-disorder transformation.

Recently (March 1985), Hulse et al. [11] ran a

survey concurrently with us to identify new candidate alloy systems for electrical strain gage application at temperature up to 1000°C. The materials were tested for the repeatability of resistivity, the thermal coefficient of resistivity over the temperature range of 23°C to 1000°C, and the drift in resistance during 3 hours soak at 1000°C. Six systems were selected after a literature survey on 140 articles: Pt-Pd-Mo, Pd-Ag-Mo, Pt-W, Ni-Si-Cr, Pd-Cr, and Fe-Cr-Al. Later the Pd-Ag-Mo system was eliminated as a candidate when problems of liquid immiscibility were encountered during alloying. The Ni-Si-Cr system (Nicrosil) was also dropped because its resistance did not vary linearly with temperature and it had a relatively high thermal coefficient of resistivity. After further experimental testings, Pt-W and Pt-Pd-Mo were also dropped from the list of candidate alloys because of problem of internal oxidation. From the remaining two systems, Pd-Cr was regarded as the best candidate, Fe-Cr-Al as a system with possibility.

Very recently, Wu et al. [12] developed a high-temperature resistance strain gage which was fabricated from specially developed Fe-Cr-Al-V-Ti-Y alloy. He claimed that this gage with a specified room temperature

gage factor of 2.62 could be used up to 700°C, and this has been evaluated to be the state of the art [13].

2.2.2 Semiconductor Strain Gages

The semiconductor resistance strain gages have been in commercial production since 1960's. Some of their advantages over metallic strain gages are [14] : high sensitivity (up to two orders of magnitude higher than conventional metallic gages), good mechanical stability at room and elevated temperature (thereby minimizing creep and hysteresis), and ease of gage installation. However, there are some disadvantages, which include relatively large temperature coefficient of resistance (induced large apparent strain), large change in gage factor with temperature, and the problem of brittleness.

The unusually large strain sensitivity (piezoresistive effect) in semiconductors was first noted by Smith [15]. A complex theory which concerns intervalley carrier scattering was analyzed and presented by Mason and Thurston [16], who derived detailed equations to explain this effect in terms of change in properties of the semiconducting materials.

It has been known that for lightly doped semiconducting materials, the gage factor varies inversely with the absolute temperature and that the initial resistance varies considerably, Mason et al. [17] found that these undesirable features could be eliminated to a large extent by using heavily doped materials (e.g., 10^{20} boron atoms per cubic centimeter of silicon). Their experimental results are shown in Figs. 2-1 and 2-2. The gage factor at room temperature for the heavily doped sample is approximately 1/3 that of a lightly doped one. However, it remains more than 30 times as sensitive as a metallic resistance strain gage, and its gage factor and resistivity are almost independent of temperature. This heavily doped material consequently is the most practical gage when the temperature can not be precisely controlled.

Rapid progress has been made in the development of semiconductor strain gages over last 25 years, and as a consequence gages made from n- and p-type silicon and germanium are commercially available with gage factors of $\pm$130, which is about 65 times larger than the conventional metallic gages. However, they can only be used at temperature up to 250^{o}C. At higher temperatures,

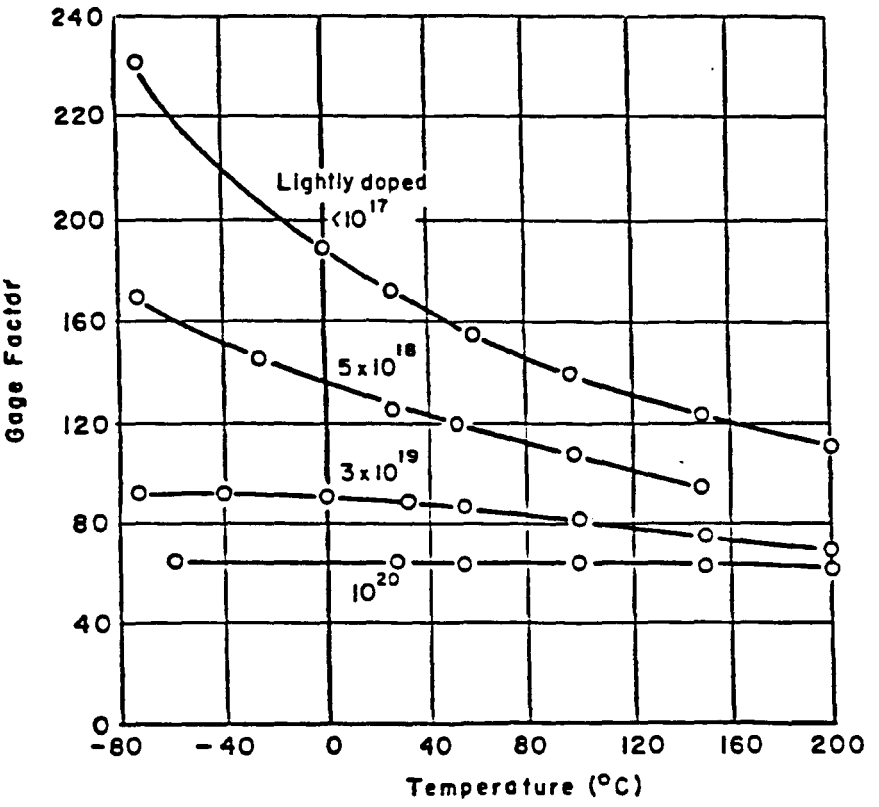

Fig. 2-1. Variation of gage factor with temperature and impurity level for p-type silicon doped with boron (after Mason et al. [17]).

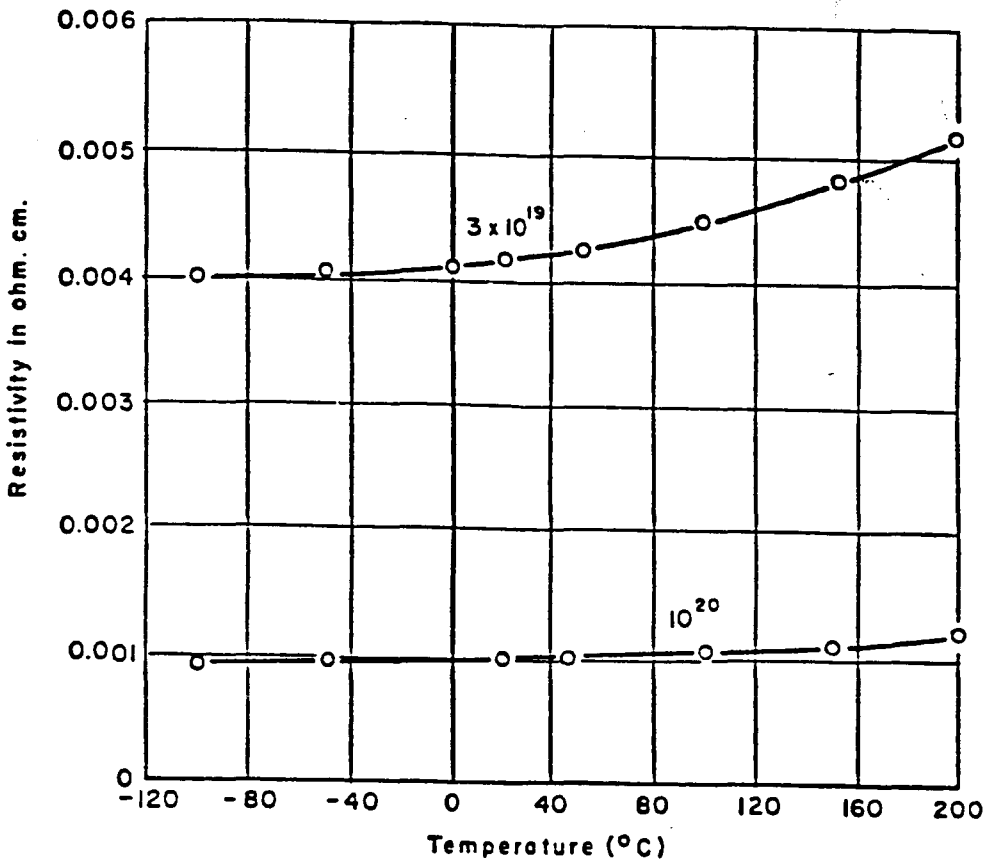

Fig. 2-2. Variation of unstrained resistances with temperature and impurity level for p-type silicon doped with boron (after Mason et al. [17]).

when they reach the intrinsic conduction regions, the temperature effects is too large for compensation.

Recently, a group of scientists in the USSR have been attempting to find a new semiconductor material as a substitute for silicon and germanium for higher temperature usage. They have found that silicon carbide is a promising material for high temperature resistance strain gage application [18-20].

2.2.3 Thin Film Strain Gages

Traditional strain gage technology uses "bonded" strain gages. They are foil gages glued onto the surface of the strainable membrane. The use of glue can, in some instance, limit both the degree of strain transmission from membrane to gage and the temperature at which the device may be used. The use of thin film technology, i.e., vacuum-deposited thin film formed directly on the surface of a strainable member, is seen as a way of obviating the limitations on both temperature and strain.

A number of companies have been involved in research and development in this area since 1970, and it

is clear that thin films will play a leading role in the future transducer technology [21].

2.3 Purpose of this Research

This research is part of a larger investigation conducted by NASA, which is dedicated to the development of a strain gages which can measure the strain up to 2000 micro-strain at a temperature of about 1000^{o}C or above with a total error of no more than $\pm$10% over 50 hours [2].

After reviewing the work in this subjects as cited in the last section, we know that for a resistance strain gage material, the two basic properties are that its electrical resistance should be stable and reproducible at all temperature up to the working temperature and its resistance change must be due to the applied strain. Since a material will be electrically stable only if it is structurally stable, a gage material should therefore not show any structural change with time or temperature up to the operating temperature. To have the resistance change mainly from the applied strain, one would have to avoid or eliminate those effects which causing the

resistance to change with either temperature or time. A gage materials should therefor have (1) the same thermal coefficient of linear expansion as the substrate on which the gage is mounted, (2) a small temperature coefficient of resistance, and (3) good resistance to oxidation, recrystallization or creep.

It is the purpose of this research to study the electrical resistances of the materials which are potentially useful as high temperature resistance strain gages and to develop a set of simple criteria for selections of strain gage materials. We should note here that in this research, we have only studied the intrinsic properties of the gage material itself. We will not consider the problems created when a strain gage is placed on the material to be tested (e.g., the difference in thermal coefficient of linear expansion causing the bonding defects).

In the next chapter, we will discuss the individual requirements which are placed on an ideal strain gage, in order to establish our criteria for selection of high temperature resistance strain gage materials.

CHAPTER 3

DERIVATION OF THE SELECTION CRITERIA

3.1 Introduction

As discussed in the last chapter, we already know that the two basic qualities that an ideal resistance strain gage material should have are :

(1) its resistance change should merely be due to the strain alone, i.e., it should have small temperature coefficient of resistance and good resistance to oxidation.

(2) it should have a stable and reproducible resistance at all temperatures up to the operating temperature. Those phenomena which affect the structural stability and therefore the resistance that should be avoided include: phase transformation, magnetic transition, order-disorder transition, short-range ordering, clustering, plastic deformation, creep or recrystallization.

In the following sections, we will look into these phenomena individually and try to ascertain the intrinsic properties a material should have in order to satisfy

these requirements.

3.2 Small Temperature Coefficient of Resistance (TCR)

Although temperature compensation circuits are often used with strain gages, the compensation problem for a large TCR will be formidable [9]. In addition, for acceptable performance in regions of steep temperature gradients and uncertainty in absolute temperature, which is often the case, the TCR must be reasonably low.

There is no proven basis which exists for the accurate prediction of the electrical properties, particularly, TCR of materials at high temperatures. In fact, the electrical resistance of solids varies from material to material more than any other easily measured property.

3.2.1 Conductors

A treatment of the TCR of metals and alloys requires a detailed consideration of the scattering mechanisms. In a perfect lattice, the charge carriers experience no scattering and the resistivity of the

lattice is therefore zero. Any disturbance of the perfect periodicity of the lattice (e.g., introduction of phonon, impurity, dislocation, etc.) will act as scattering centers and produce resistivity. The electrical resistivity of a nonmagnetic metallic material can in general be separated into two components (Matthiessen's rule), the temperature dependent ideal resistivity ρ_T which results principally from the electron-phonon interaction and the temperature independent residual resistivity ρ_o which is caused by the electron-defects interaction [22]:

$$\rho(T) = \rho_o + \rho_T. \qquad (3-1)$$

The general form of the temperature dependent part of resistivity ρ_T is given by the Bloch-Gruneisen equation:

$$\rho_T = \frac{C}{M\theta_D} \left(\frac{T}{\theta_D}\right)^5 \int_0^{\theta_D/T} \frac{x^5 dx}{(e^x-1)(1-e^{-x})} \qquad (3-2)$$

where C is a constant, M is the atomic mass and θ_D is the Debye characteristic temperature.

For temperatures higher than the Debye characteristic temperature (which is usually above room temperature), the standard integral reduces to an

expression proportional to $(\theta_D/T)^4$, and the Bloch-Gruneisen equation can be approximated by

$$\rho_T = \left(\frac{C}{M\theta_D^2}\right) T, \qquad T > \theta_D \qquad (3\text{-}3)$$

At lower temperatures, the standard integral has a constant value of 124.4, thus ρ_T is proportional to T^5 at low temperatures.

However, Eq. (3-3) is not strictly obeyed for many metallic materials and the departures from a linear temperature dependence of the resistivity are particularly significant for transition metal systems. For example, for transition metals of groups IV and VI, the resistivity usually increases with temperature faster than the linear relation; while for transition metals of group III and V, the resistivity increases with temperature more slowly than a linear relation [23].

According to Mott and Jones [24] and Ziman [25] the Debye temperature of a metal should decrease with increasing temperature as the result of lattice thermal expansion, that is

$$\frac{1}{\theta_D^2} = \frac{1}{\theta_o^2}\,(1+6\beta\gamma T) \qquad (3-4)$$

where θ_o is the Debye temperature at T = O K, β is the linear coefficient of thermal expansion, and γ is the Grüneisen constant. This gives a reasonable explanation of the resistivity deviations from linear temperature dependence for noble metal systems only, but not for most transition metals. In particular, for those transition metals with negative deviation from the linear temperature dependence, one must look for other mechanisms.

A second mechanism to account for the resistivity deviation from a linear temperature dependence in transition metals was also suggested by Mott and Jones [24]. According to their theory, the resistivity is thought to be determined mainly by the scattering processes in which the conduction electrons under the influence of lattice vibrations make transitions to the unoccupied d states. The probability of such process is proportional to the density of states $N_d(E_F)$ and its derivative with respect to the electron energy dE in the d band at the Fermi level E_F. Therefore, taking into account the Debye temperature effect as given by Eq. (3-

4) the ideal resistivity can be written as:

$$\rho_T = (C/M\theta_o^2)\ T\ (1+6\beta\gamma T)\ (1+AT^2), \qquad T>\theta_D \qquad (3\text{-}5)$$

where

$$A = \frac{-1}{6}\ (\pi k)^2\ [3\ (\frac{1}{N_d}\frac{dN_d}{dE})^2 - \frac{1}{N_d}\ \frac{d^2N_d}{dE^2}\ ]_{E_f} \qquad (3\text{-}6)$$

For transition metals with Fermi energies E_F near a maximum position of the density of states curve $N_d(E_F)$, the first term in Eq. (3-6) is small compared to the second term, and A is positive. Then based upon Eq. (3-5) one expects a positive deviation from the linear temperature dependence. On the other hand, for transition metals with Fermi energy near a minimum of the density of states curve, the first term in Eq. (3-6) dominates and A is negative, therefore the resistivity versus temperature curve is expected to deviate negatively from linearity [26]. Materials with a negative deviation in resistivity will have a TCR that decreases with temperature and a low TCR at high temperature.

Aisaka and Shimizu [27] have demonstrated that this simple model agrees well with experimental results for most pure transition metals. In their calculations they made use of $N_d(E_F)$ determined in the rigid-band model

from the low-temperature specific-heat data. Chiu [26] had also applied this model to alloy systems and suggested that this model describes the observed behavior reasonably well for temperature higher than the Debye temperature. However he suggested that the density of states of alloys to be employed in Eq. (3-6) should be calculated via a coherent-potential approximation (CPA) rather than a rigid-band model.

Recently, much work has been devoted to the study of alloys with TCRs much lower than what would be expected from Matthiessen's rule and to the explanation of the existence of zero and negative value of TCR in alloys. These effects are not observed in the pure metals or dilute alloys but only when the alloys are rather concentrated. In strain gage applications, such materials are chosen because the effect of strain cannot be masked by that of temperature. Mooij [28] established a correlation between TCR and the magnitude of the resistivity ρ: if one excludes data on alloys where TCR may be affected by magnetic or structural transition, one concludes that no negative TCR is observed for materials with resistivities below 100 microohm-cm while hardly any positive TCR is found for material with resistivities

above 150 microohm-cm. This TCR-ρ correlation is shown in Fig. 3-1. It is seen that TCR pass through zero at ρ of

(1) Nearly all alloys with a low TCR contain at least one transition element.

(2) No alloy was found with a low TCR at room temperature when the alloy contains only elements from the same column of the periodic table.

(3) Nearly all systems that show a low TCR are disordered.

He then suggested that the occurrence of a low TCR in a concentrated disordered alloy containing a transition metal plus at least one atomic species from a column of the periodic table other than that occupied by the transition metal seems to be the rule rather than an exception.

The high scatter in these materials which results in high resistivity and low TCR value of these materials is usually caused by a high degree of disorder. The origin of the disorder can be the random distribution of the solute elements over the lattice sites or the structural disorder of an amorphous solid. In alloys containing transition metals, the scatter is also

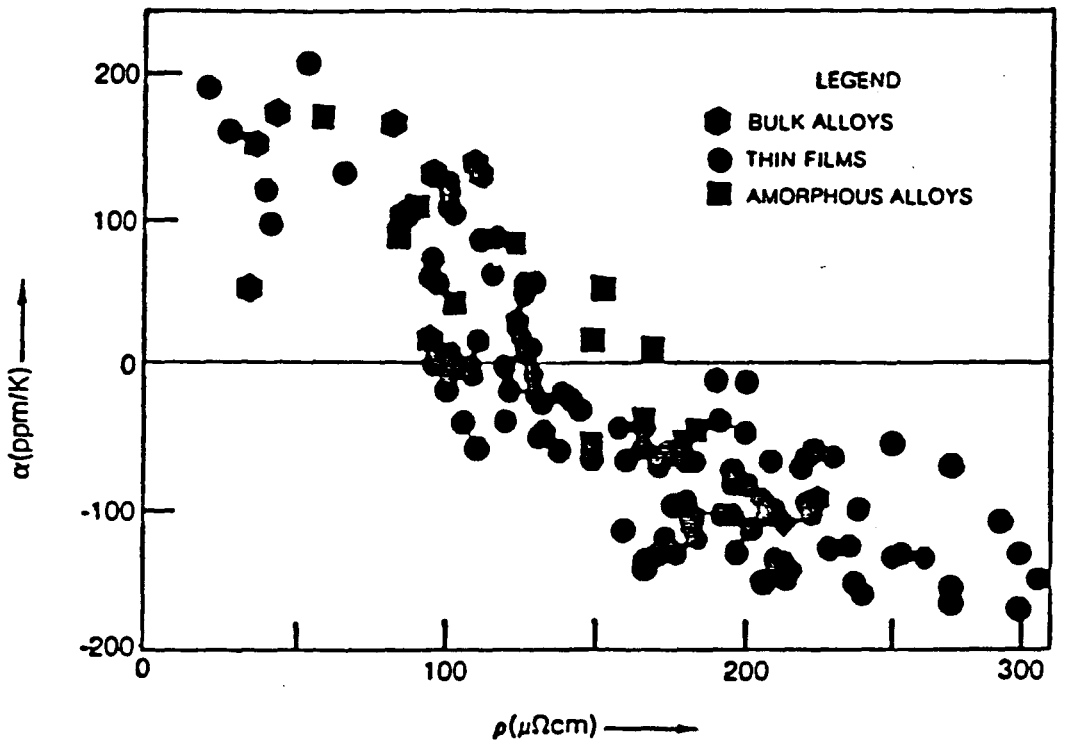

Fig. 3-1. The temperature coefficient of resistance versus resistivity for bulk alloys, thin film and amorphous alloys (after Mooij [28]).

increased by the possibility of s → d electron scattering.

The behavior of electrical conduction in the alloys with a low TCR can be understood to a great extent if it is assumed that in these alloys a lower limit is reached in the electron mean free path, such a limit must exist, as the mean free path cannot be smaller than the interatomic distance [29]. If this limit is reached a further decrease of the mean free path due to phonon scattering is impossible and a low TCR results.

A further consequence of these ideas is that in the absence of phonons, if the mean free path is already short due to the presence of spin fluctuations or of the atomic disorder produced by alloying or the presence of defects, then the magnitude of the temperature dependent (phonon) contribution to the resistivity will be decreased thus resulting in a negative TCR [30]. This phenomenon has been observed for different classes of materials independent of detail of their atomic structures or the electron configurations, for instance in amorphous metals and concentrated crystalline alloys. There is a general tendency for these materials with high

electrical resistivity to have a TCR that decreases linearly with increasing resistivity within a finite fluctuation range (Mooij's rule) [28]. To explain the negative values of TCR, Mooij suggested that in these materials there can be thermally activated releasing sites where electrons are liberated at high temperatures [28].

Recent attempts to explain the negative TCR were based on Ziman's theory [31], coherent potential approximation (CPA) [32,33], and force correlation function method [34]. The basic mechanism for negative TCR has been explained by Richter and Schiller [35] as the mixing of a strong static (electron-disorder) scattering and a dynamic (electron-phonon) scattering, which is described by the CPA model in a simple and straightforward way. For alloys with small "chemical disorder", the electrical resistivity increases nearly linearly with temperature, as the "chemical disorder" becomes larger the slope of the resistivity versus temperature curve decreases. For strong chemical disorder negative temperature coefficients arise.

To further investigate the TCR of alloys of

transition metals, where the disorder effects are mainly due to the d electrons and where the s electrons are the most important current carriers, it is necessary to use a two s-d hybridized band model (BV model) [36] in which transport properties are determined at T=O K. Brauwers and Brouers [37] generalized the work of BV in the case of T>O K by considering that only d electron, which are more localized, interact with phonons. They showed that in concentrated transition metal alloys, the TCR can be negative when the Fermi level lies near a d peak in the alloy density of states. The sign of the TCR results from the competition between two effects: the decreasing of the purely residual resistivity when the Fermi level moves with the temperature and the increasing of the resistivity supposing the Fermi level fixed at its T=O K value.

In summary, it is still too early a stage in the development of an alloy theory to give a quantitative descriptions of the transport properties of concentrated systems. Since the easier and more basic electronic quantity, the static alloy density of state, is just beginning to be understood. At present, there exists, as mentioned in the preceding pages only qualitative or

model description of the transport properties on such alloys. However, these models gave us some guidelines for selecting materials with small TCR. First, from Matthiessen's rule, it is known that alloys generally have lower TCR than single elements. In this research, we only concentrated our efforts on binary alloy systems, excluding alloys with more than two elements because of the complexity of the problem. Second, from Mott and Jones theory, it is known that materials with low density of state at the Fermi energy level may have a low TCR at high temperatures. Third, from Mooij's rule, it is suggested that disordered alloys of transition metals with other elements from the different column of the periodic table will have low TCR. Therefore, disordered binary systems of transition metals were chosen for further studied in order to test the validity of these models.

3.2.2. Semiconductors

The electrical resistivity of a semiconductor is the sum of the resistivities contributed by electron and by hole. The resistivity produced by the two dominant mechanisms, phonon scattering and ionized impurity

scattering, can be expressed as [38]

$$\rho = \frac{1}{en}\left(\frac{1}{\mu_L}+\frac{1}{\mu_I}\right)_n + \frac{1}{ep}\left(\frac{1}{\mu_L}+\frac{1}{\mu_I}\right)_p \qquad (3\text{-}7)$$

where:

n and p are the concentration of electron and hole, respectively,

μ_L is the mobility of carriers for phonon scattering and is usually proportional to $T^{-\eta}$ with $3/2<\eta<5/2$, and

μ_I is the mobility of carriers for ionized impurity scattering and is proportional to $T^{3/2}$.

The processes of electrical conduction for semiconductors can be divided into three sections, depending on the dominate mechanism. At sufficiently low temperatures (extrinsic region), ionized impurity scattering is predominant, and the charge carriers are excited from the impurity levels. The decrease of resistivity with temperature is dependent on the ionization energy (E_i) of the impurity, that is, $\rho \propto \exp(E_i/2kT)$.

In many instances, the charge carriers from all the available impurity levels are excited at room temperature

because the ionization energy of the impurity is much smaller than the band gap. If the number of impurities greatly exceeds the number of intrinsic carriers, the number of carriers will hardly vary at all with the temperature, and the variation of resistivity will be due only to the variation of mobility, and it increases with increasing temperature like that of a metal. This is the saturated extrinsic region [39], and is the working region applicable for resistance strain gages.

As temperature higher enough for electrons to be excited across the forbidden energy gap, intrinsic region begins and the lattice scattering becomes predominant. In this region the concentration of electron n excited from the valence band to the conduction band is equal to the concentration of holes p formed in the valence band, and [38]

$$n = p = 2\left(\frac{2\pi kT}{h^2}\right)^{3/2} (m_n\, m_p)^{3/4} \exp\left(\frac{-E_g}{2kT}\right), \qquad (3\text{-}8)$$

where m_n and m_p are the effective mass of electron and hole, respectively. E_g is the energy gap, k the Boltzman constant and h the Planck's constant.

From Eqs. (3-7) and (3-8), the resistivity is

therefore, approximately proportional to $\exp(E_g/2kT)$ and again decreases with increasing temperatures as in the extrinsic region, but the resistivity decreases at a faster rate with temperature in the intrinsic region because $E_g >> E_i$. For resistance strain gage application, one should avoid the occurrence of this region by choosing materials with larger band gaps so that the temperature of the intrinsic conduction is higher than the resistance strain gage working temperature.

In summary, from the discussion above, it is known that in order to attain small TCR, one should work in the saturated extrinsic region of a semiconductor. This region can be extended to very high temperatures by heavily doping a semiconductor which has large band gap [40].

3.3 Resistance to Oxidation, Creep and Recrystallization

3.3.1 Oxidation

Oxidation results in a reduction of the conducting cross sectional area of the sample which in turn results in changing the resistance of the sample. Nevertheless,

some oxides are stable kinetically, in the sense that they adhere to the material surface and form a tight protective adherent layers. Actually, it is not easy to predict these reactions, since they also depend on the environment. One rule suggests that the alloy should contain at least one species which is resistant to oxidation [7]. It has also been suggested that even noble metals should use a protective coating in order to improve their oxidation resistance [41].

3.3.2 Creep and Recrystallization

The creep effect of a material becomes more prominent at temperature greater than half its melting temperature. Also the recrystallization temperature of most materials are about half the melting temperature [42]. To avoid the occurrence of creep or recrystallization, one should choose materials with melting temperatures higher than twice the operating temperature, i.e., 2000^{o}C for this research. However, the practical strain that these materials will be subjected to are rather small ($\approx$ 2000 microstrain), and these effects may not be important.

3.4 Structure Stability

3.4.1 Phase Transformation and Magnetic Transition

Phase transformation causes lattice periodicity and structural change, thereby perturbating the resistance of a material (see Fig. 3-2, for example). This effect can be considered as being a main cause of electrical resistance irregularities for alloys [22]. The candidate materials should therefore be chosen after consideration of their phase diagrams and by selecting the compositions for which phase transformations do not occur in the range of working temperatures.

Fig. 3-3 shows the resistivity versus temperature for three ferromagnets. One can see that the resistivity decreases more rapidly below the Curie point. This decrease in resistivity is due to the freezing out of the exchange scattering of the electrons from the magnetic moments [43]. This transition frequently occurs in alloys of iron, cobalt, nickel etc., and can be avoided also by checking the existing phase diagrams and selecting a material without magnetic transition.

3.4.2 Order-Disorder Transition and Clustering

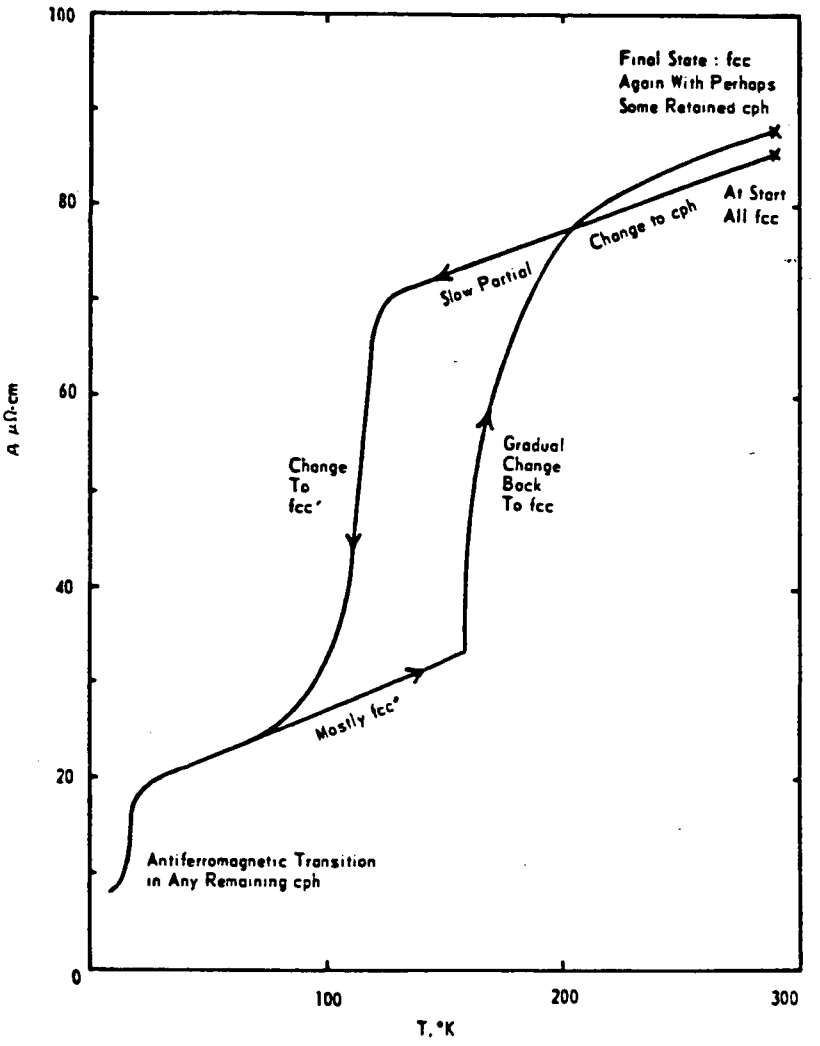

Fig. 3-2. Illustration of the way in which the resistivity of Ce is complicated by phase transformations (after Meaden [50]).

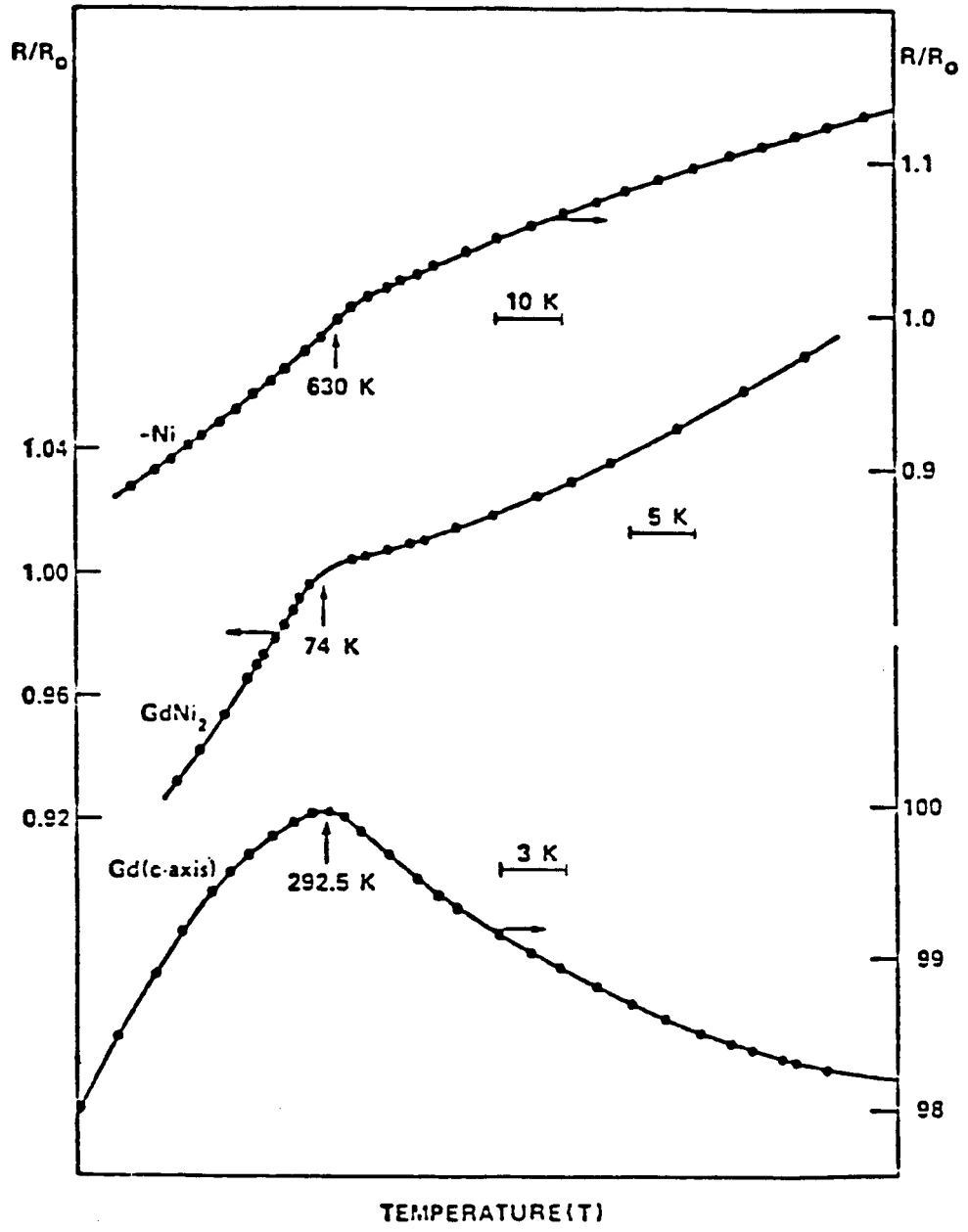

Fig. 3-3. Resistivity change with temperature for three ferromagnets in which magnetic transition occurred. The resistivity is normalized to its value at the Curie point (indicated by the arrow) (after White and Geballe [43]).

Order - disorder transition is a temperature and time dependent reaction. Its major effects on resistivity arise from the influence of the effective number of carriers associated with a splitting of the Brillouin zone during ordering and the presence of Anti-Phase-Boundary scattering mechanism [44]. The effect of order-disorder transition on electrical resistivity of $AuCu_3$, where the resistivity increases abruptly during the order-disorder transition, as shown in Fig. 3-4, is a classical example.

Clustering is another temperature and time dependent reaction. The relation between electrical resistance to clustering has been found to be fairly complex and not yet been completely understood [45]. To have stable and reproducible resistance with temperature and time, one should therefore avoid choosing materials with order-disorder transition or clustering.

From the thermodynamics point of view, these transformations do not occur in ideal solid solutions [46]. The ideal solutions can be characterized by null enthalpy of mixing, or by activity coefficients equal to

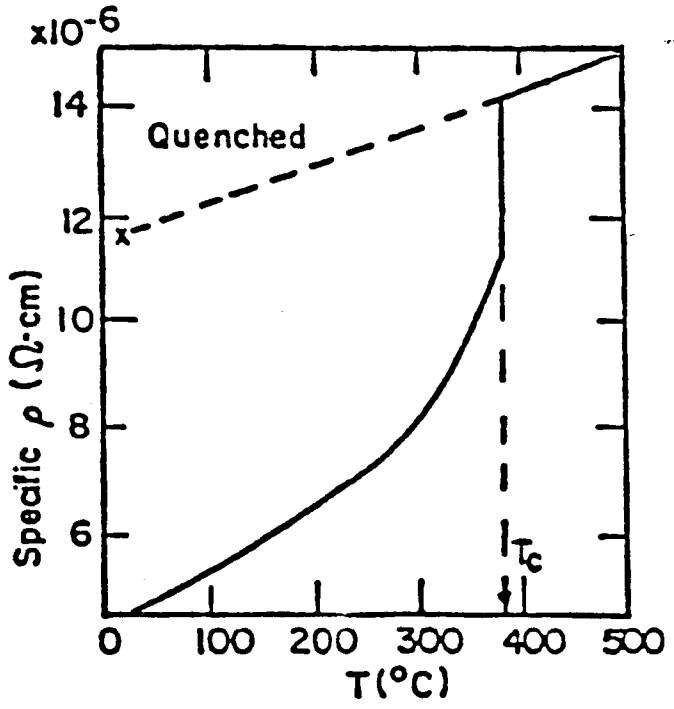

Fig. 3-4. Illustration of the way in which the resistivity of AuCu is affected by order-disorder transition. The resistivity increases abruptly at the transition temperature T_c (after Schroder [22]).

one for both elements [47]. Systems with a negative enthalpy of mixing ($\Delta H_{mix}<0$) may have a tendency to order at low temperature, and systems with a positive enthalpy critical temperature of order-disorder transition is proportional to the enthalpy of mixing and increases with increasing ΔH_{mix}, in many systems the ordered phases are stable up to the melting point without the order-disorder transition [48]. The ultimate selection procedure here is to select either ideal solutions with $\Delta H_{mix}=0$, or intermediate phases with larger negative enthalpy of mixing ($\Delta H_{mix}<<0$).

The structure of intermediate phases is determined by three main factors: relative atomic size, valency and electronegativity. Materials composed of two elements having a large difference in their relative atomic size, valency and electronegativity, will have large negative ΔH_{mix} and a higher order-disorder transition temperature. Interstitial compounds with large difference in atomic size between the components usually have large enthalpy of mixing and therefore have been chosen for further study.

3.4.3 Plastical Deformation

Deformation of materials not only changes the microstructure, but also produces dislocations, vacancies, interstitials etc.. The relative resistivity produced by the defect scatterings with the concentration of defects less than 10%, is [49]

$$\rho = \frac{mN_c\sigma_d v}{Ne^2} \qquad (3\text{-}9)$$

where σ_d is the scattering cross section, v the velocity of electron ($=l_f/\tau_c$, where $l_f=1/N_c\sigma_d$ is the mean free path, and τ_c the relaxation time), N_c the defects concentration and N the concentration of lattice sites.

The relative resistivity (about 1.5×10^{-21} microohm-cm per vacancy, or interstitial, and $(2\text{-}20)\times10^{-13}$ microohm-cm per dislocation line) [50] is negligible in the temperature range of interest unless the material is heavily strained (large plastic deformation). In this case scattering by dislocations ($N_d>10^9$ cm^{-2}) becomes significant [51]. One can avoid plastic deformation by choosing materials with large elastic strain regions. (i.e., σ_e/Y > the maximum strain to be measured, where σ_e is the elastic limit and Y the Young's modulus). Materials then will remain in the elastic domain during

operation and an increase in dislocation density will not occur.

3.5 Selection Criteria and Material Selection

In summary, the selection criteria for materials which are potentially useful as resistance strain gage at 1000°C are materials that have:

(1) Small TCR
   -this screened the potential materials to binary transition metal systems, and heavily doped semiconductors with large band gap.

(2) Good oxidation resistances.

(3) Melting temperature > 2000°C
   -to avoid the occurrence of creep or recrystallization.

(4) No phase transformation or magnetic transition in the temperature range of 0°C - 1000°C.

(5) No order-disorder transition or clustering over the entire temperature range.
   - this requirement screened the candidate materials to either ideal solutions or interstitial compounds.

(6) σ_e/Y larger than the maximum strain to be measured (2000 ppm).

Combining these selection criteria, one will therefore search for candidate materials from the group of (1)ideal solutions, (2) transition metal interstitial compounds, and (3) semiconductors with large band gap.

An extensive survey of the literatures was made taking into consideration the melting temperature, phase diagram, mechanical strength, electrical and chemical stability. Transition metal carbides and nitrides were selected from the group of transition metal interstitial compounds, (the transition metals from which these compounds form come from groups IV, V, and VI of the periodic table) silicon carbide and boron carbide were chosen from the group of semiconductors. The phase diagrams of these materials are shown in Appendix A, and their relative properties (e.g., melting temperature, crystal structure etc.) are listed in the Appendix B. Candidate materials chosen from ideal solution are being studied by another member of our group [52].

CHAPTER 4

EXPERIMENTAL TECHNIQUES FOR RESISTANCE MEASUREMENTS

4.1 Material Preparation

The specimens of transition metal compounds were prepared as thin films by several different evaporation or sputtering techniques including Activated Reactive Evaporation (ARE), Hollow Cathode Discharge (HCD), Chemical Vapor Deposition (CVD) and Radio Frequency Sputtering (RFS) method. These samples were provided through the courtesy of Dr. H. Okimura from Tokyo Institute of Technology and Dr. Y. Onuma of Shinshu University in Japan.

NASA, the sponsor of this work, provided some β-SiC thin films prepared by Chemical Vapor Deposition (CVD) on the silicon substrates. Some β-SiC films prepared by Electron Beam gun Evaporation (EBE) on the alumina Al_2O_3 substrates were also supplied by Dr. Okimura. All these films were cut into about 15mm long by 1.5mm wide samples via a diamond blade.

Thin films of β-SiC on Si substrates were specially treated. Since the resistance of Si substrate was about the same order of magnitude as that of SiC thin film at high temperature, Si substrate had to be removed from β-SiC film. This was done by immersing the cut samples in warm HF-50% HCl etchant solution, this resulted in the removal of the SiC from Si substrate. The 16 micrometer thick SiC films were then attached to Al_2O_3 substrates by using AREMCO high temperature ceramic adhesive (Aremco products, Inc.). The adhesive had to be cured at 370°C prior to the electrical resistance measurements.

Boron carbide and α-silicon carbide bulk samples prepared by hot pressing were supplied by Dow Chemical Co., these samples were then cut into 15x1.5x1 mm specimens via a diamond cut-off wheel.

Specimens for electrical resistance measurements were appropriately chemically cleaned to remove any debris and contaminations. These samples were then sealed in quartz tubes under vacuum and were subsequently annealed for several hours at temperature above 1000°C followed by furnace cooling to room temperature. Table 4-1 lists the preparation methods for all the specimens

studied in this thesis.

4.2 Electrical Resistance Measurements Apparatus

The electrical resistance measurements were conducted inside a Lindberg electric resistance split-type furnace under vacuum. The furnace had a 3-inch bore and 30-inch heating length, which was more than adequate to insure uniform temperature over the entire length of the test section of the specimen. Up to three specimens were placed in a one head opened quartz tube in the furnace. The end of this quartz tube was connected to a stainless steel vacuum cap. The junction between cap and quartz tube was initially sealed simply with a rubber O-ring around the cylindrical quartz tube. Leaks were detected due to the irregularity of the diameter of the tube. This leak problem was solved by acquiring an O-ring sealed hemispheric junction between the quartz tube and the vacuum system, illustrated in Fig. 4-1. In this way, a vacuum better than 2×10^{-5} Torr was usually obtained even at $1050^{\circ}C$. After each experimentation, the quartz tube was cleaned with 5% hydrofluoric acid solution, rinsed with distilled water and then with methanol prior to being dried.

Table 4-1

Preparation Methods for Candidate Materials*

Specimen	Preparation Method	Remarks
TiN-1	HCD, Hollow Cathode Discharge	
-2	CVD, Chemical Vapor Deposition	
ZrN-1		P_{N2}=114 ppm-torr
-2	RFS, Radio Frequency Sputtering	=108 ppm-torr
-3		=96 ppm-torr
-4		=990 ppm-torr
TaN-1		P_{N2}=330 ppm-torr
-2	Magnetron RFS,	=375 ppm-torr
-3		=600 ppm-torr
CrN	HCD	
TiC-1	ARE, Activated Reactive Evaporation	
-2	CVD,	
ZrC	ARE	
B_4C	Hot Pressed	Bulk
β-SiC-1	EBE, Electron Beam Evaporation	
-2	CVD,	with N_2 dopant
α-SiC	Hot Pressed	Bulk

* all the specimens are prepared as thin films on the Al_2O_3 substrates except for B_4C, α-SiC and CVD prepared β-SiC on Si substrate.

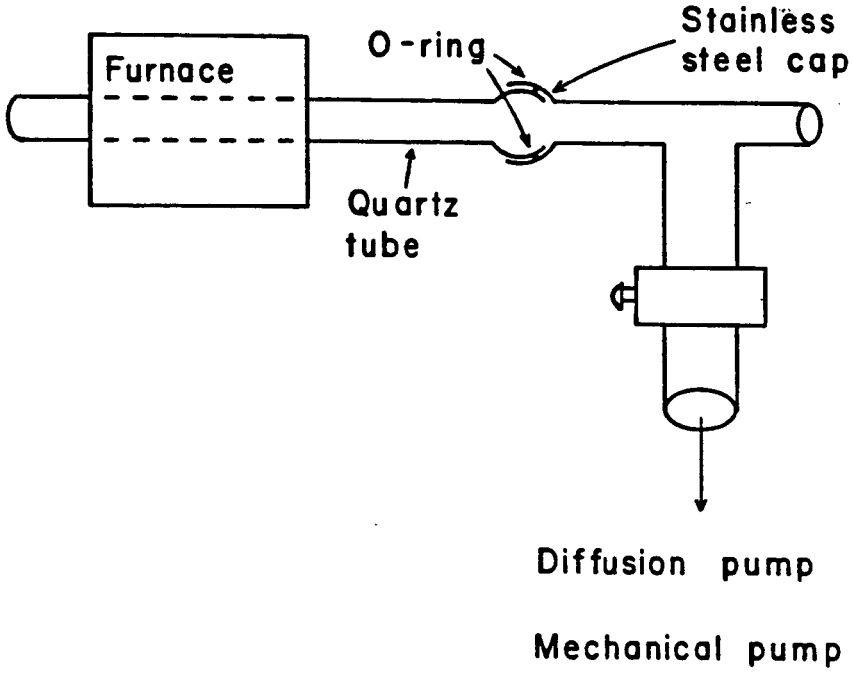

Fig. 4-1. Schematic diagram of the hemispheric junction between quartz tube and vacuum system.

The vacuum cap at the end of the quartz tube was connected to a diffusion pump (made by Consolidered Vacuum Corporation) which in turn was connected to a mechanical vacuum pump. A copper disc was fitted to the front of the vacuum system by means of an O-ring seal. Three grommet vacuum seals were mounted around this disc. Thermocouples and lead wires were introduced into the vacuum system by passing through feed-thru connectors which were mounted on top of the grommet vacuum seals. This construction is illustrated in Fig. 4-2. All leads wires and thermocouples were shielded by insulated woven wire casings or two hole ceramic tubes.

The temperature of the furnace was programmed and controlled by means of a system comprised of a DATA-TRAK temperature programmer, THERMAC temperature controller together with a LABAC power source of the same brand (Research Incorporated). Two platinum/platinum- 13% rhodium thermocouples located on both ends of the specimens were used to monitor the sample temperatures and detect the temperature gradient. Temperatures were determined with a digital nanovoltmeter (Keithley 180), with an Omega reference junction temperature compensator. It was found that by using one of the inner thermocouples

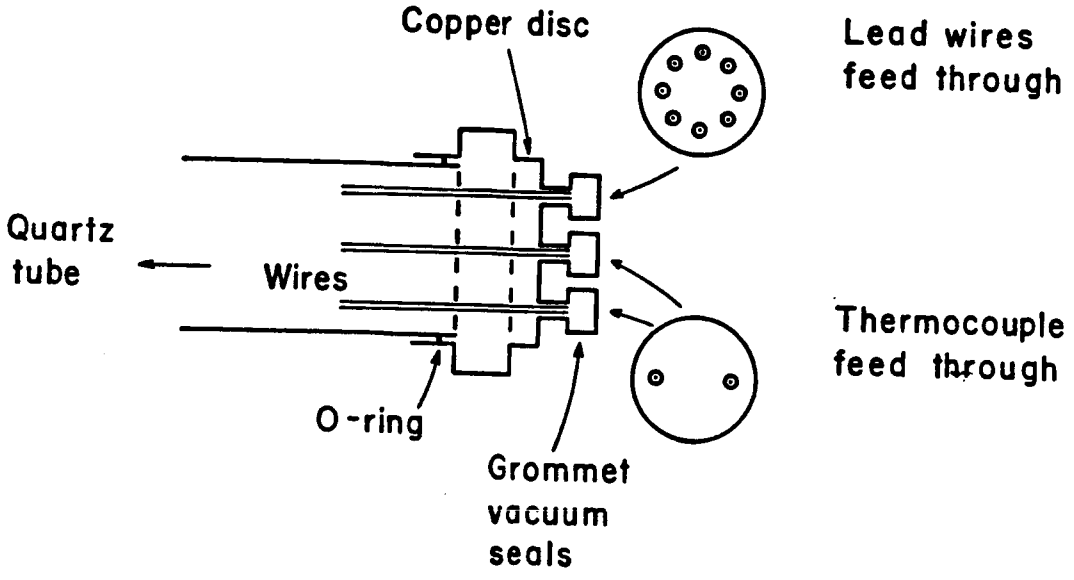

Fig. 4-2. Schematic diagram of the arrangement for introducing lead wires into the vacuum system then to the furnace.

as a temperature sensor for the temperature controller, better temperature control and stability were obtained. The temperature gradient was found to vary by 1-10^{o}C along the length of the specimen holder with a temperature variation over the length of the specimen of 1-2^{o}C at the elevated temperature.

The resistances of samples were measured by the four probes method. This method was chosen because of the small resistances of some of the specimens. It was important to exclude the resistances of lead wires especially if they were of the same order of magnitude as the specimens. Conducting lead wires were taped to the specimen by using pressure contacts. Pressure contacts were chosen because of the difficulty of spot welding lead wires on some of the specimens without breaking them due to thermal shock. In addition, carbide materials will not accept soldered or spot-welded junctions. Another advantage of pressure contact was the possibility to remove the samples after experimentation without breaking them or inducing contamination.

Pressure contacts require some means of holding all four wires to the specimen at identical and constant

pressure. Fig. 4-3 illustrates the ceramic specimen holders designed for resistance measurements. These holders were machined from Aremcolox 502-1100 high temperature machinable ceramics sold by Aremco products, Inc.. This material has a very low coefficient of thermal expansion (1.5 ppm/^{o}F). Grooves were machined into the lower part of the ceramic plates to fix the position of the lead wires used as current and voltage probes. Two holes were drilled at both ends of the upper ceramic holder for placing the thermocouples. After machined, the ceramic specimen holders were fired at 1100^{o}C prior to being used. Samples were positioned on top of the lead wires and between the two ceramic plates which were joined together by ceramic screws to form the pressure contact.

Platinum wires were first chosen to use as lead wires because of the inertness of this noble metal. However, it was found that platinum reacts with some of the specimens, so it was replaced by tungsten.

4.2.1 DC method

At the first stage of the resistance measurement,

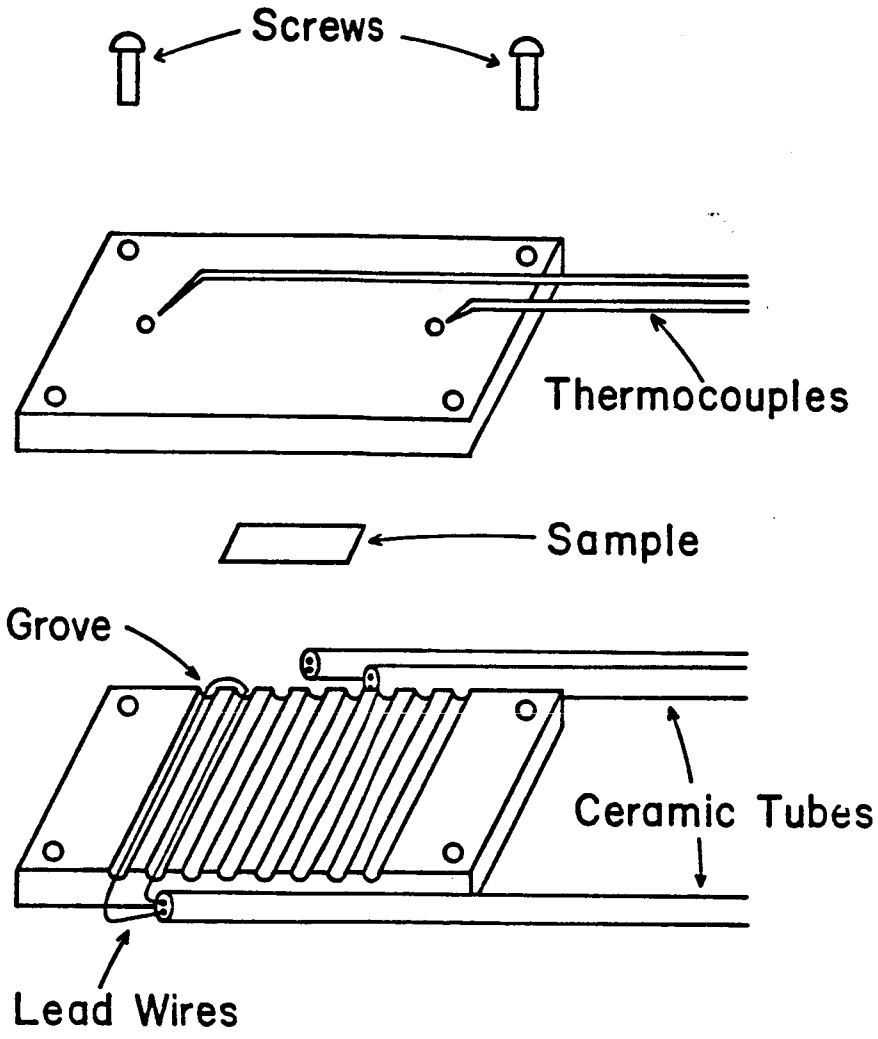

Fig. 4-3. Schematic diagram of the ceramic specimen holder.

the electrical current which applied to the sample were supplied by a constant dc current source (Keithley 227, in the range of $\pm 10^{-5}$ to ± 1 Amp). The current was first measured by measuring the corresponding voltage drop across a standard resistor (Leads and Northrup, 1.00002 ohm with 0.005% accuracy). However, a heating effect was observed in the resistor, and the resistor was not reliable after a longer period, a Keithley 160B Ammeter was then applied for measuring the current instead. The polarity of the current was reversed alternately to compensate the thermal electromotive force (EMF) effects.

The resistance of the specimen was measured at every 80°C intervals, from room temperature to 1010°C, after the specimen stage temperature had been stabilized within 1°C. At each temperature, eight values of direct current both forward and reverse were imposed to the samples and the corresponding voltages drop across the specimens were measured with a digital multimeter (Keithley 192). Resistance of the specimen at this temperature was the average of these eight values of the voltage drop dividing by the supplied current. By using this method, it was possible to check the ohmicity of the electrical contacts at all temperatures. The temperature

was the average of four values given by the two thermocouples, obtained immediately before and after the electrical resistance measurements. Usually two cycles of heating and cooling were conducted to check the reproducibility of the electrical resistance.

Initially measurements were conducted on individual specimen; later up to three specimens were held at the same time to improve the reliability, readings on these three specimens were selected by a mechanic rotary selector switch in the circuit. The electrical circuit for DC resistance measurement is illustrated in Fig. 4-4.

The accuracy of electrical resistance measurement depends on the accuracy of the voltmeter and ammeter. The relation between the resistance R, current intensity I and the corresponding voltage drop across the sample V is:

$$R=V/I$$

therefore, $$dR/R = dV/V - dI/I$$

For example, for a 1 ohm resistance measurement, the currents delivered during the measurements is in the range of 100 to 400 mA, and the corresponding voltage

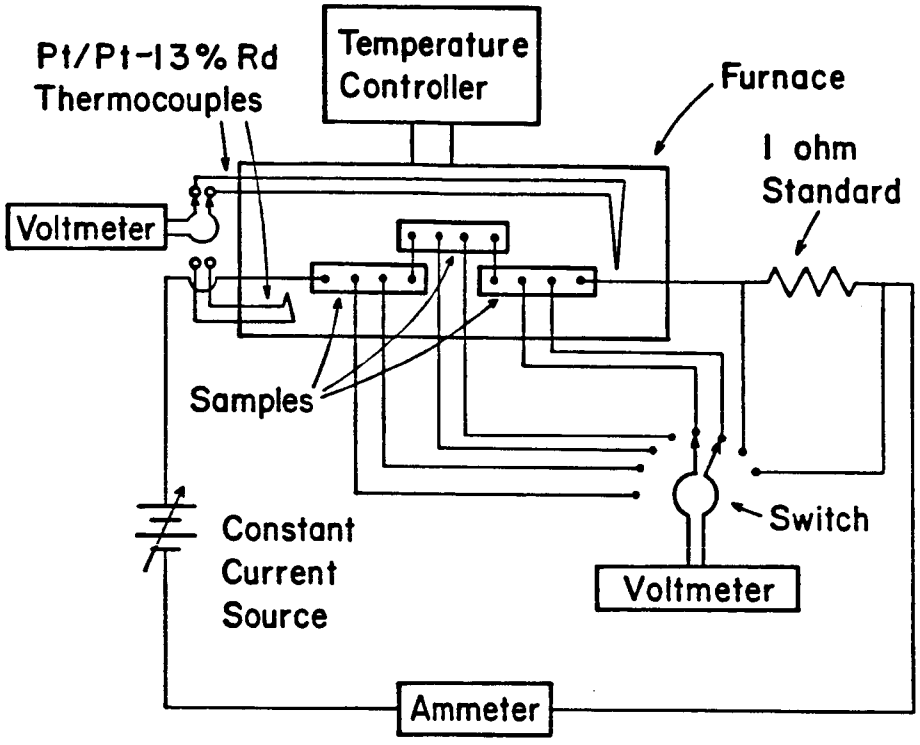

Fig. 4-4. Schematic diagram of the dc circuit for electrical resistance measurements.

measured is varied between 100 mV and 400 mV. The Keithley 160B digit ammeter used for current measurements has an accuracy of 0.2% of reading in this range of currents, and the Keithley 192 digital multimeter used for voltage measurements has an accuracy of 0.004% of reading in this range of voltages. Consequently, the measurement of this 1 ohm resistance had an accuracy of 0.204%. Because of this error no information could be provided concerning the reproducibility of the measurements within 10^{-5}. We assumed that for the very low resistances, which required the use of the least accurate range of the electrical equipments, the measurements could be affected to a large extent by using these Keithley instruments.

4.2.2 AC method

As the research progressed it became evident that improvements would have to be made in the resistance measurements system in order to obtain higher levels of accuracy and stability. This was done by substituting a high precision AC resistance bridge (A∑A model F17A, made by Automatic Systems Lab. limited, England) for the dc current source and digital multimeter, and by using a

high speed scanner (Keithley 705) instead of the mechanical switch box.

The ac bridge had an accuracy of $1x10^{-6}$ of full scale, and a resistance of 1 ohm could thus be measured with 0.0001% accuracy. This accuracy was three orders of magnitude better than that obtained by dc method mentioned above. In addition, by using an AC current, one eliminated the thermal EMF effects along the sample.

A computerized electrical resistance measurements system was constructed in the latter stages of the research for automatically recording the resistances of the specimens between room temperature and 1000°C. The temperature changes of the furnace were programmed to increase or decrease in steps of 80°C, with average heating and cooling rates of 1.85 °C/min and 0.93 °C/min, respectively. Data were taken after the temperature was stabilized.

A standard IBM PC was set up as a system controller and data collector. The computer communicated with the instrumentations by means of an IEEE-488 interface bus. The software (written in Advanced Basic) is attached in

Appendix C. Data read from the instruments were saved on a floppy diskette and were printed on a HP Thinkjet printer. Fig. 4-5 illustrates the electric circuit for this computerized AC resistance measurement.

4.3 Material Characterization

The precise characterization of transition metal compounds is a difficult task. Chemical means of determining the carbon (or nitrogen) to metal ratio are limited by the strong bonding and high melting temperatures of carbides (or nitrides) materials. In addition, the likely major impurities (e.g., oxygen) are most difficult to measure because they are also the constituents of air.

A variety of methods of characterization were used in this work. The structures and lattice parameters of the specimens were determined by X-ray diffraction technique with a Rigaku diffractometer. A correlation of lattice parameters with carbon (or nitrogen) to metal concentration ratio of some transition metal compounds are presented in books by Storms [53] and by Toth [65].

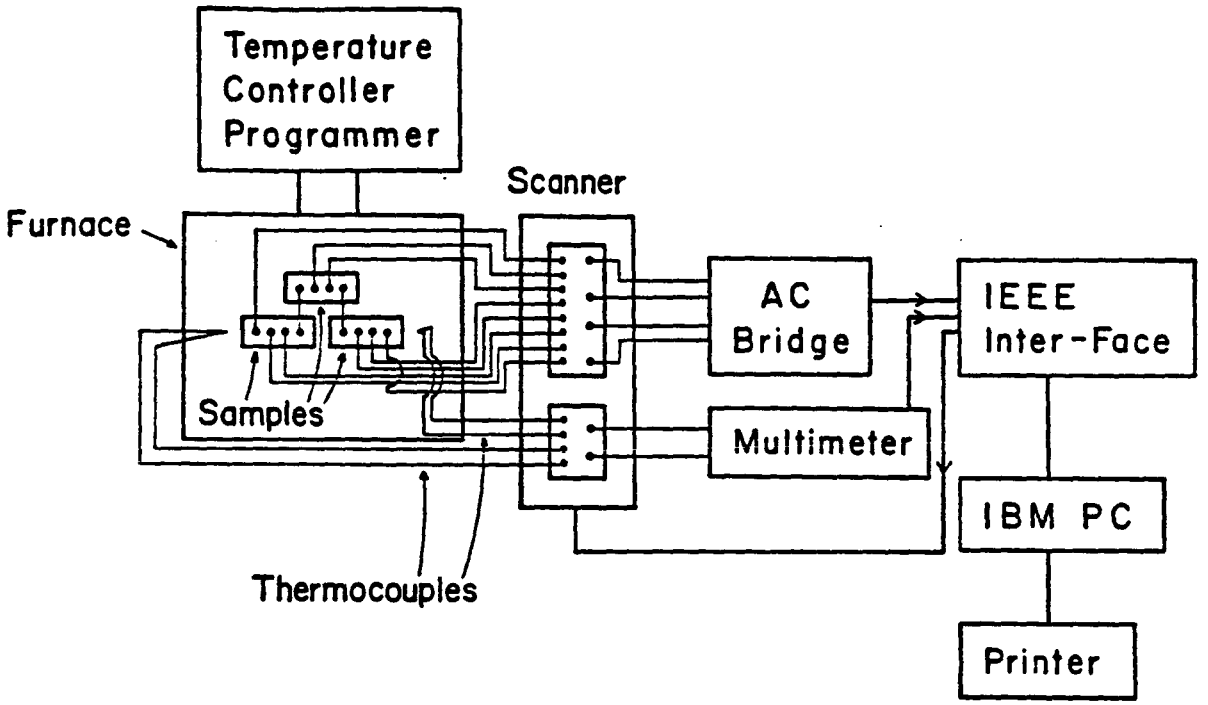

Fig. 4-5. Schematic diagram of the computerized AC circuit for electrical resistance measurements.

Scanning Electron Microscopy (Hatachi) and Auger Electron Spectroscopy (Physical Electronics Co.) were adopted for topology and for determination of the relative amounts of nitrogen or carbon in these compounds. Thickness of some films were determined by Tencor Profilometry.

CHAPTER 5

RESULTS AND DISCUSSION ON THE ELECTRICAL RESISTANCE MEASUREMENTS FOR TRANSITION METAL COMPOUNDS

5.1 Calibration

Before measuring the electrical resistances of the candidate materials, the measurement systems were calibrated. This included the calibrations of the thermocouples and the electrical resistance measurement method.

The platinum/ platinum- 13% rhodium thermocouples were calibrated against four reference temperatures: ice point, boiling point of the distilled water and the melting temperatures of pure aluminum and silver. This consisted of measuring the resistances of two pure aluminum and silver wires as a function of temperature up to their melting temperatures. The melting temperature corresponded to a sudden infinite increase in resistance (when metals melt and the electrical circuit was broken). However, the thermocouples were not in real contact with the pure metals in order to avoid any contaminations, which would result in faulty data. This experiment was

repeated several times, the results are listed below:

Reference Pt.	Expected Temp.	Thermocouple temp. 1	2
ice water	$0^{o}C$	0 ± 0.2	0.4 ± 0.2
boiling water	$100^{o}C$	94 ± 1	96 ± 1
Al melting Pt.	$660^{o}C$	658 ± 2	656 ± 2
Ag melting Pt.	$962^{o}C$	962 ± 3	959 ± 3

The largest inaccuracy in the thermocouples read out was within $6^{o}C$ at $100^{o}C$, this may be due to a possible contact between the thermocouples and the container wall. Since the gradient of temperature in the furnace should be lower than that between boiling water and container wall, it was expected the errors for measurements in the furnace would be lower than those indicated in the table above.

Calibration of the system for electrical resistance measurements was done by measuring the change in resistance with temperature for pure platinum wire and comparing the results with that of Vines [54]. A cycle of heating and cooling between temperatures of $25^{o}C$ and $1000^{o}C$ was performed. Fig. 5-1 illustrates the results of these measurements along with the published results of

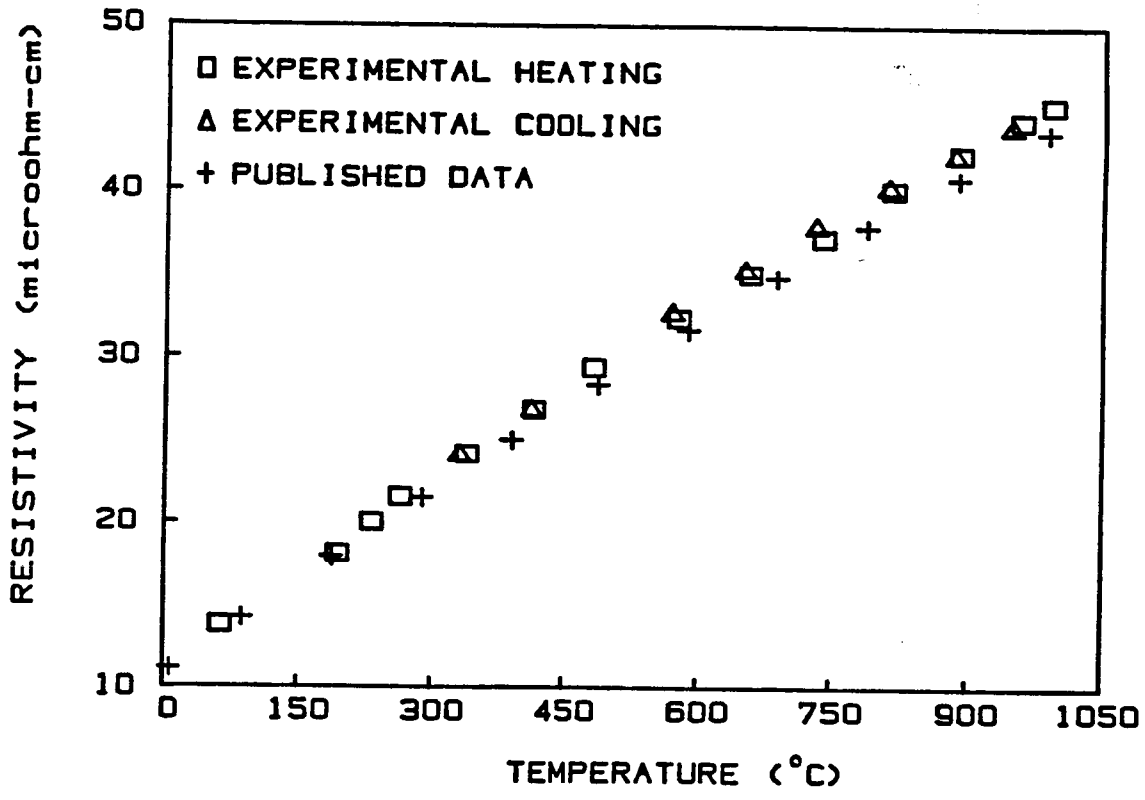

Fig. 5-1. Comparison the results of variation of resistivity with temperature for platinum with the result of Vines [54].

Vines. The resistance of the platinum wire were the same during heating and subsequent cooling which assure the reproducibility of the measurements. The close agreements between the two sets of data indicates the reliable accuracy in the temperature and resistance measurements. An error in the temperature measurements would be detected by a shift of the two curves in the horizontal direction (axis of the temperature).

The accuracy of the resistance measurements was also ascertained by placing a standard resistor of 1 ohm in series with the electrical circuit. The resistance of this standard was determined at the same time with the specimens, values within $2x10^{-3}$ and 10^{-6} were obtained by DC and AC resistance measurement methods, respectively.

5.2 Transition Metal Compounds

5.2.1 Introduction

The refractory carbides and nitrides of the transition metals comprise a class of compounds with many scientifically interesting and useful properties [65] such as :

-high melting temperatures (around 3000°C)

-high electrical conductivity

-great hardness (comparable to diamond)

-wide homogeneity range (e.g., $TiC_{0.5}$ to $TiC_{0.97}$)

-excellent chemical stability

The combination of such properties makes transition metal refractory compounds desirable for many special applications. Perhaps the most important property of this group of materials is their defect structures. Ideal stoichiometry is generally not found in these phases; derivation from stoichiometry are far more common [69]. Most of the transition metal carbides and nitrides have close-packed crystal lattices (NaCl or Hex.), with the carbon or nitrogen atoms in the octahedral sites. If these octahedral sites are not all occupied, the unoccupied sites in the nonstoichiometric compound may be considered as vacancies in the metalloid sublattice [65]. For all rocksalt structured transition metal carbides, non-stoichiometry is due to carbon vacancies only and the metallic sublattice remains completely occupied, as shown by precise density measurements [53]. Some mononitrides such as TiN_x are reported to be nonstoichiometry with x values larger than 1 and these compounds are

characterized as containing metal vacancies [65]. However, this has not been the subject of many studies up to now, and experimental data are still somewhat conflicting.

A wide homogeneity range is characteristic of the cubic transition metal compounds. Titanium carbide, for example, has the NaCl structure from 11 %C to 20 %C by weight. The lower extreme of this range corresponds to a concentration of vacancies in the FCC carbon sublattice of 50 at% and thus has the composition of $TiC_{0.5}$ [67]. The presence of such a large concentration of vacancies would be expected to affect various physical properties. The vacancy concentration is determined by the relative amounts of metal and carbon reacted together to form the compounds.

The transition metals in these compounds are from groups IV (Titanium, Zirconium, Hafnium), V (Vanadium, Niobium, Tantalum), and VI (Chromium, Molybdenum, Tungsten) of the periodic table. However, not all the carbides and nitrides of these elements seemed to be suitable for high temperature resistance strain gage application. Among these materials, nitrides of group VI

were excluded from list of potential compounds because of their chemical instability. These nitrides dissociate rapidly into N_2 and metal at high temperatures. VN, NbN, M_oC and WC were also excluded due to their complex phase diagrams and narrow ranges of homogeneity. However, since we were only able to obtain samples of TiN, ZrN, TaN, CrN, TiC, and ZrC among the remaining possible candidate materials, we only studied the electrical properties on these nitrides and carbides.

The phase diagrams of these transition metal compounds are attached in Appendix A. The relative properties of these materials (e.g., melting temperature, crystal structure, homogeneity range etc.) are listed in Appendix B, and the lattice parameter versus composition curves for some of the materials are attached in Appendix D.

5.2.2 Titanium Nitride

Two titanium nitride thin films were studied, one prepared by hollow cathode discharge (HCD) method and the other by chemical vapor deposition (CVD) method. Both films were deposited on the Al_2O_3 substrates, and had

thicknesses of 2 and 1.2 micrometers, resistivity of 30.5 and 1130 microohm-cm, respectively. Fig. 5-2 presents the results of resistance change with temperature for the specimen prepared by HCD. The electrical resistance of this specimen was measured during two cycles of heating and cooling in the temperature range of 23-1000^{o}C. After heated to 1000^{o}C in the second cycle, the resistance changes during an isothermal sojourn at 1000^{o}C for 8.5 hours were also measured. As can be seen from Fig. 5-2, this titanium nitride film showed metallic conduction; its resistance increased with increasing temperature following a linear regression approximation as:

$$R = 3.55 + (6.65 \times 10^{-4})\ T$$

with a 0.9993 correlation factor. Its temperature coefficient of resistance (TCR) at 1000^{o}C was about 588 ppm/^{o}C, and its resistance drift rate (DR) during 8.5 hours sojourn at 1000^{o}C was about 0.14 %/hrs. Its electrical resistance at any specific temperature was the same during heating and subsequent cooling, i.e., this titanium nitride film had quite good electrical resistance reproducibility.

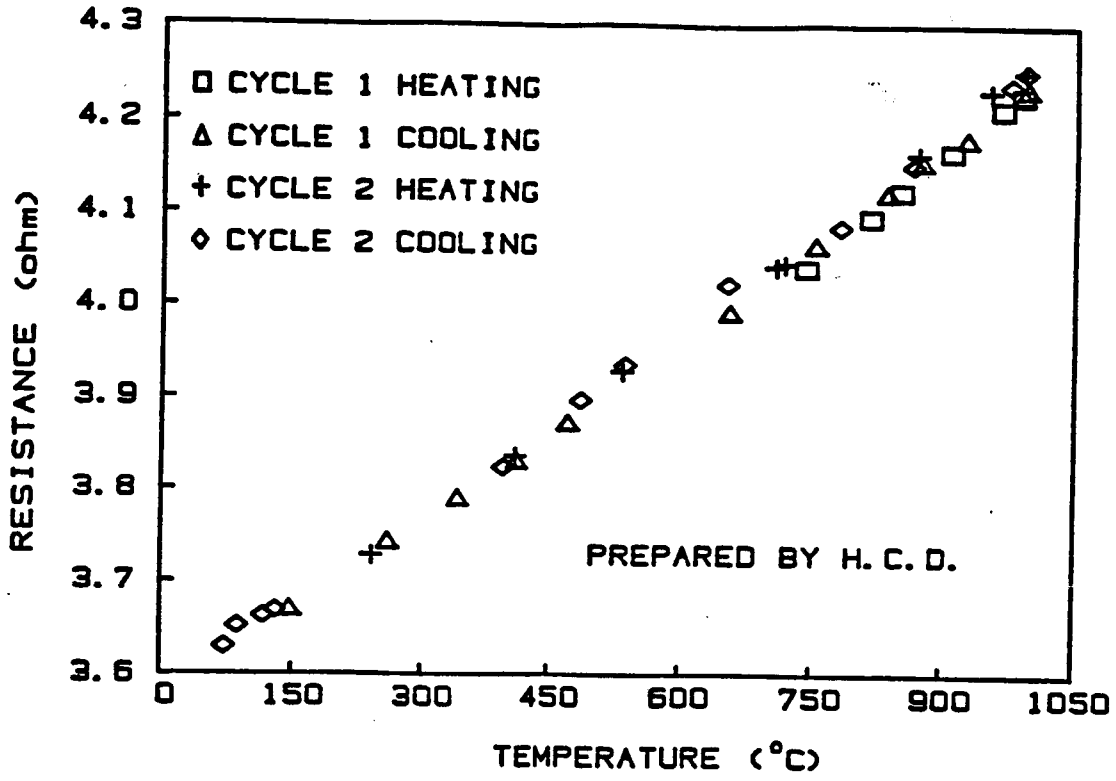

Fig. 5-2. Variation of the resistance with temperature for titanium nitride thin film prepared by hollow cathode deposition.

The TCR of a specimen at temperature T is defined as:

$$TCR = (R-R_o)/R(T-T_o)$$

where R is the resistance of the sample at temperature T, and R_o is the resistance of the sample at a reference temperature T_o. The DR of a specimen at temperature T is defined as:

$$DR = (R-R_o)/R_o(t-t_o)$$

where R_o is the initial resistance of the sample at time t_o and temperature T, and R is the resistance of the sample after drifting for some period of time $(t-t_o)$ at isothermal temperature T.

Fig. 5-3 illustrates the change in resistance with temperature for a titanium nitride thin film prepared by CVD method. This figure shows the resistance of this specimen during three cycles of heating and cooling, and an isothermal sojourn at 1000°C for 9 hours after the second cycle of heating. The average TCR of this sample at 1000°C was about 143 ppm/°C (calculated in the temperature range of 900-1010°C), about one fourth that of the sample prepared by HCD; however, its resistance drift at 1000°C was larger, about 0.22 %/hr., also its resistance reproducibility was not as good as the

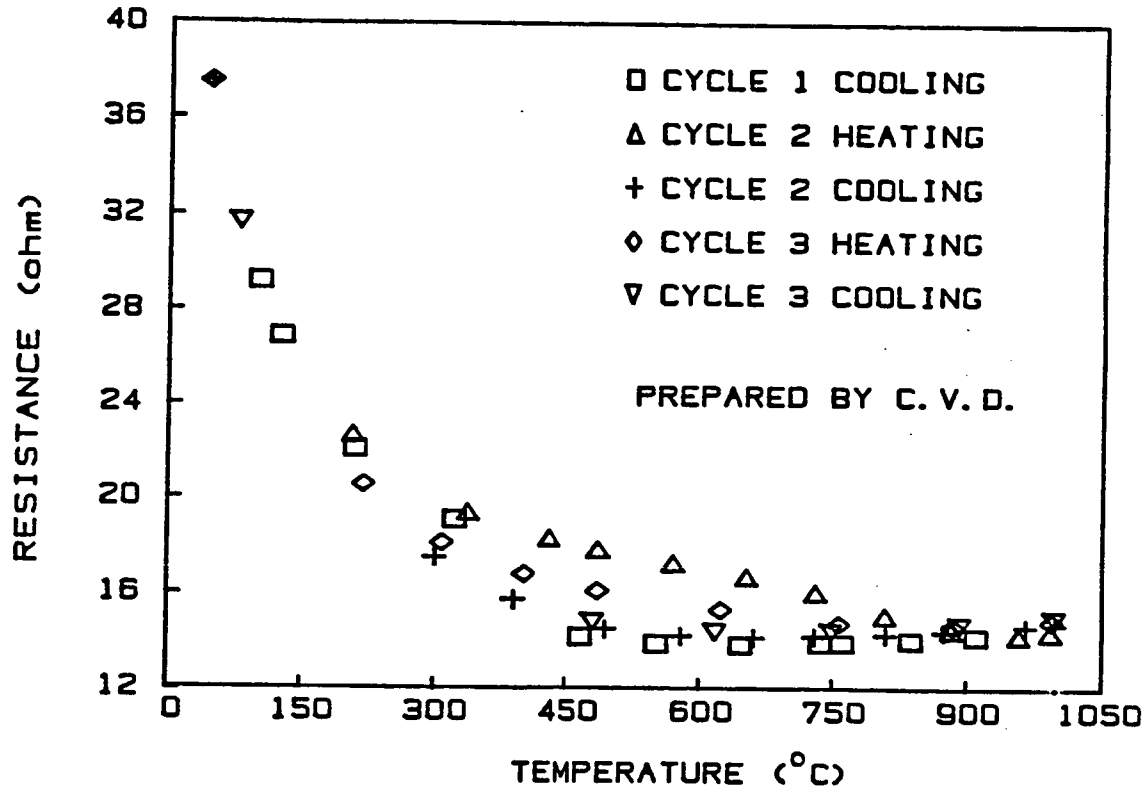

Fig. 5-3. Variation of the resistance with temperature for titanium nitride thin film prepared by chemical vapor deposition.

previous one. Bear in mind, materials with small TCR, small DR and good resistance repeatability are the desired characteristics of materials for resistance strain gages.

A hysteresis was observed for the CVD titanium nitride film in the temperature range of 300-800^{o}C, and this hysteresis decreased with the number of cycles. Fig. 5-4 is the expanded scale of the high temperature region of Fig. 5-3. This figure shows that the resistance first decreased then increased with increasing temperatures. Invariably, the cooling curve exhibits a less abrupt knee than the heating curve. An arrest in the temperature cycling in the hysteresis range for several hours, produced no noticeable resistance change, see table 5-1. In order to investigate the conduction mechanism of this titanium nitride film, a plot of logarithm of resistance versus reciprocal temperature is presented in Fig. 5-5, the slope of this curve changed from positive at low temperature to zero then to negative value at high temperatures. The resistance change of this film did not follow the simple exponential law, however, it followed an empirical expression:

$$R=R_{o} + a\ T + b\ \exp(c/T) \qquad (5-1)$$

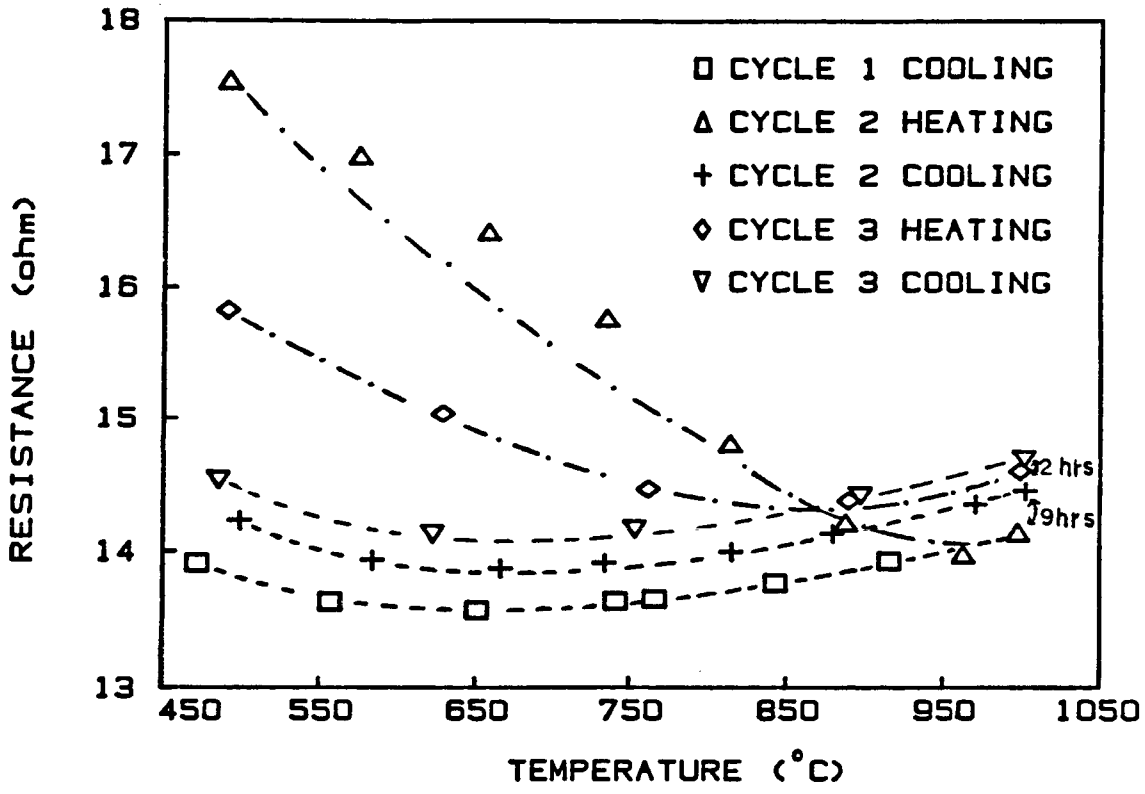

Fig. 5-4. Expansion of the high temperature region of Fig. 5-3.

C-2

Table 5-1

Resistance drift of TiN(CVD) at temperatures in the hysteresis range

Temperature (^{o}C)	Resistance (ohm)	Time (hour)
264	18.178	0
264	18.194	1
265	18.166	2
425	16.532	0
425	16.558	0.28
424	16.596	0.95
424	16.642	1.88
569	15.545	0
567	15.465	0.58
567	15.429	1.1
567	15.336	6.03
568	15.582	22.5

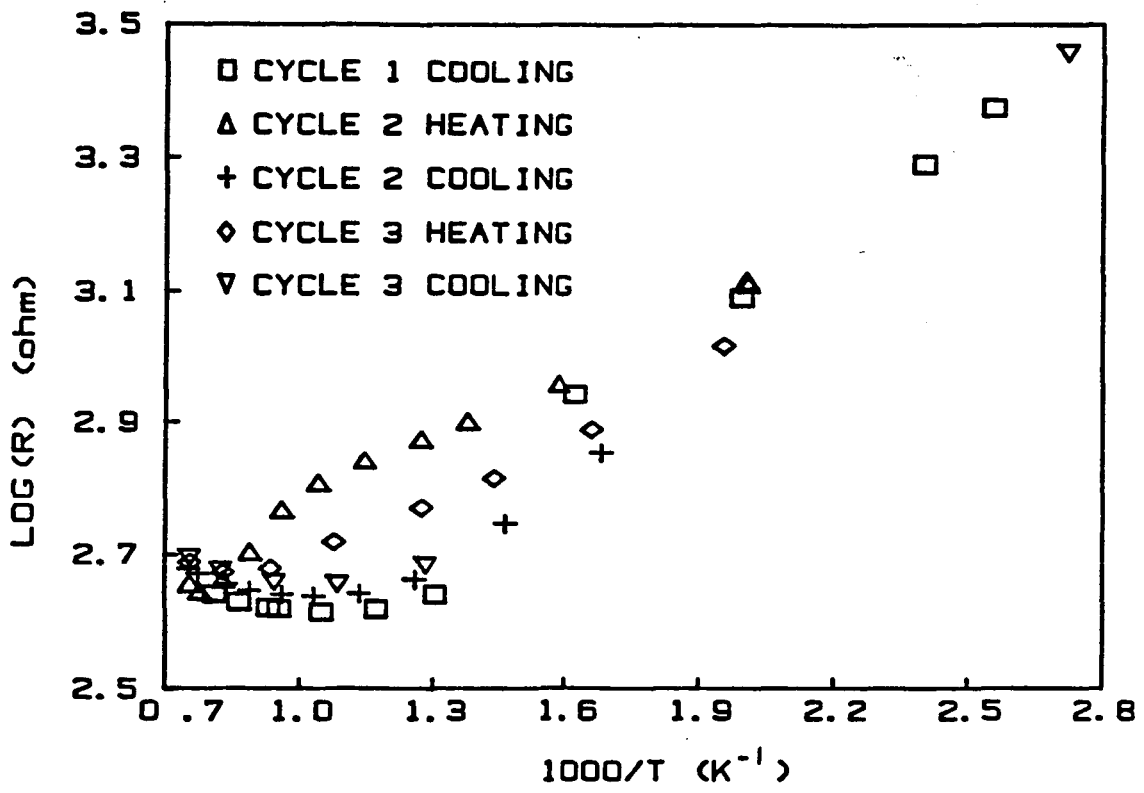

Fig. 5-5. Variation of logarithm of resistance with reciprocal temperature for titanium nitride.

with the fitting parameters R_o, a, b and c equal to -0.13, 0.0064, 4.289 and 708, respectively, i.e., the resistance of this sample depended on temperature based on the following equation:

$$R=-0.13 + 0.0064\ T + 4.289\ \exp(708/T),$$

the consistency between the empirical results and the experimental results for this specimen is shown in Fig. 5-6. A straight line is observed with slope=c=708 K, and intercept=ln(b)=ln(4.289)=1.459. At low temperatures, the third term on the right hand side of Eq. (5-1) was dominate and the resistance decreased with increasing temperature; while at high temperatures, the second term became more important and finally dominate the conduction mechanism, as the resistance of the sample increased with increasing temperature.

The measurements of the change in resistance with temperature of these two specimens were repeated several times, the results were consistent, i.e., the electrical behavior of TiN (HCD) was always metallic while TiN (CVD) was semiconducting. The resistance change with temperature for two other titanium nitrides were also measured; one sample prepared by chemical vapor deposition (CVD) on a glass substrate with a resistivity

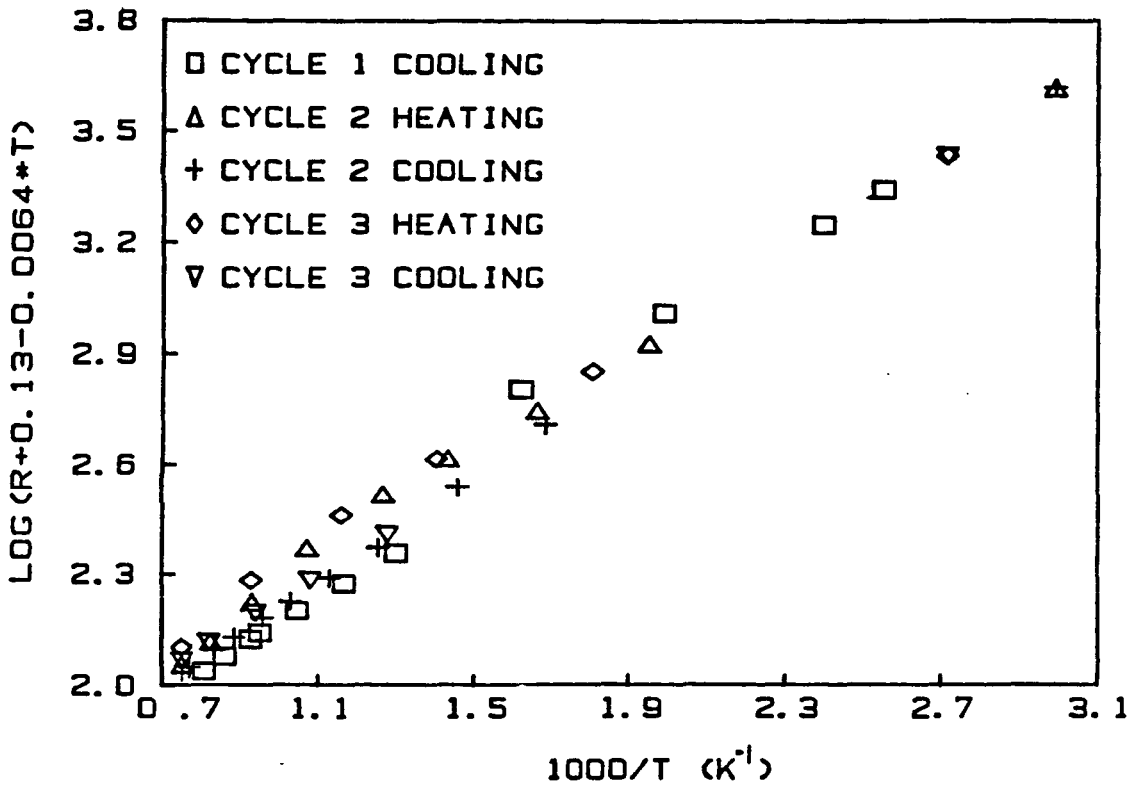

Fig. 5-6. A plot of Log(R+0.13-0.0064T) versus 1/T for titanium nitride. The resistance change with temperature of this sample follows: R=-0.13+0.0064T+4.289exp(708/T).

of about 6290 microohm-cm behaved like a semiconductor, and the other sample prepared by radio frequency sputtering (RFS) on the MgO substrate with 1 micrometer thickness and 129 microohm-cm resistivity, behaved metallic. Therefore, the contradiction of electrical conduction in different titanium nitrides was not coincident. Specimens with small resistivity (<129 microohm-cm) had positive TCRs, while specimens with large resistivity (>1130 microohm-cm) had negative TCRs.

In fact, this phenomenon was not only observed for TiN [56-58], but it has also been observed in the TiC [56,59], ZrC [59], CrN [60,61] and TaN [62] systems. To date there have been no conclusive experiments performed to resolve the conflict between the opposing points of view of classifying these compounds as metallic conductors or semiconductors. There seem to be ample evidence to support both points of view. An unambiguous answer to the question as whether these materials are semiconductor or metallic conductors is still a subject of intense study [61].

In order to explore the reasons which cause the observed behavior, we adopted several techniques to

characterize our two specimens:

(A) X-Ray Diffraction

X-ray diffraction patterns of two titanium nitride specimens with no heat treatment and diffraction patterns of two titanium nitride specimens annealed at 1050°C for 114 hours are illustrated in Figs. 5-7 and 5-8, respectively. These diffraction patterns showed that these specimens all had FCC crystal structures, and the specimen prepared by HCD, with (111) peak predominant, had a lattice parameter of 4.24 Å, corresponding to the composition of TiN; and the other specimen prepared by CVD had (200) peak predominant and a lattice parameter of 4.238 Å, corresponding to the composition of $TiN_{0.9}$ [63]. These patterns also showed the presence of unknown phase in the $TiN_{0.9}$ film with no heat treatment. This phase disappeared during heat treatment. All the rest peaks observed were from the Al_2O_3 substrate.

(B) Auger Electron Spectroscopy

The elemental compositions of these titanium nitride films were analyzed by using Auger electron spectroscopy. The derivative Auger electron spectra of two titanium nitride samples after surface cleaning by

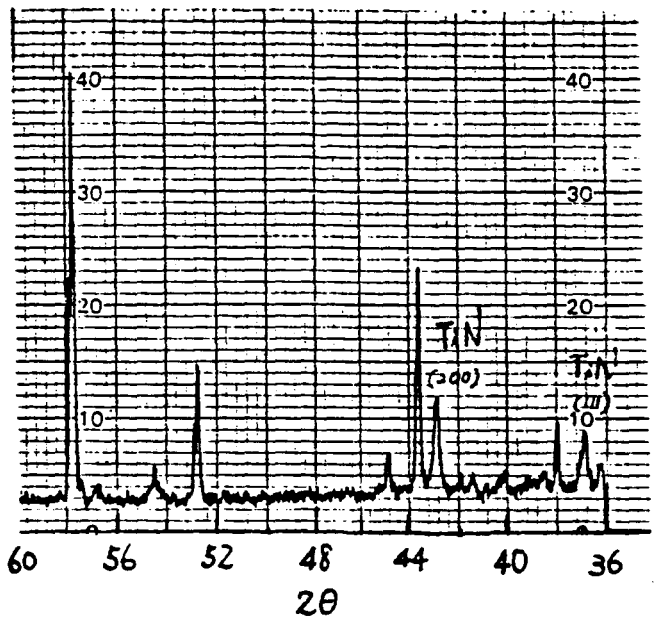

(a)

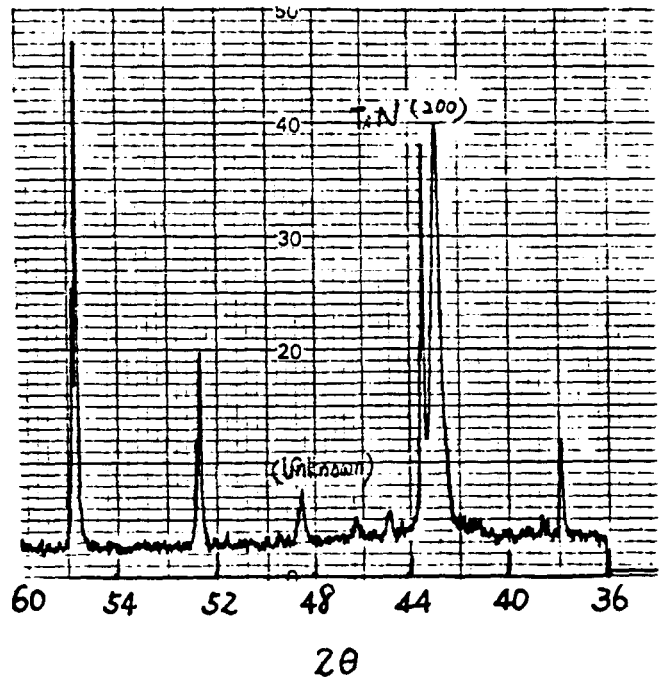

(b)

Fig. 5-7. The X-ray diffraction patterns for TiN (HCD)(a) and TiN (CVD) (b) thin films before the heat treatments.

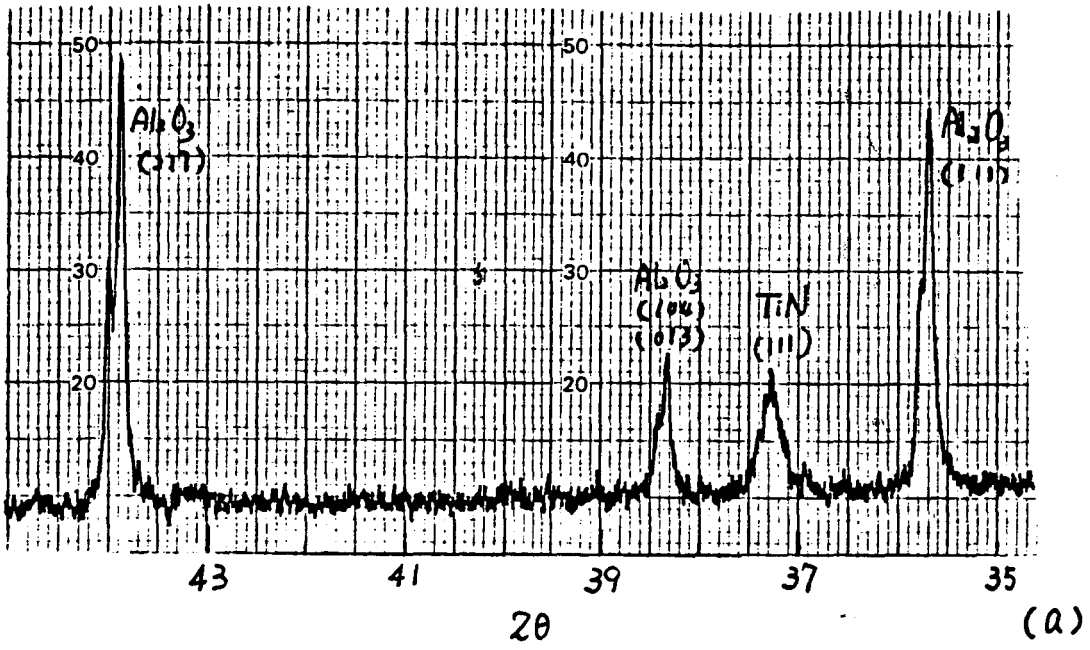

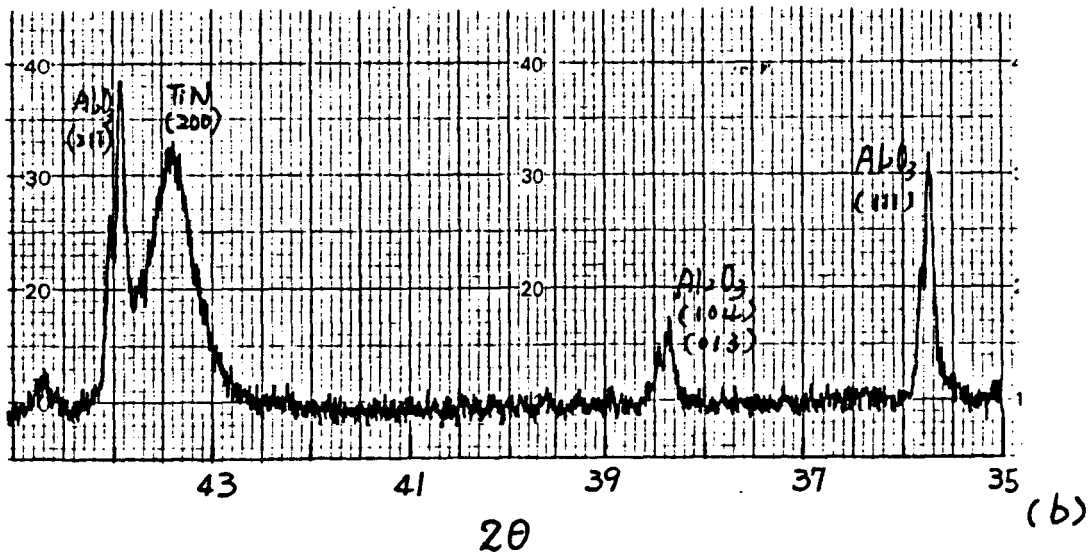

Fig. 5-8. The X-ray diffraction patterns for TiN (HCD) (a) and TiN (CVD) (b) thin films after the heat treatments, 114 hrs. at 1050°C.

means of ion sputtering for 10 minutes are shown in Fig. 5-9. The samples analyzed had not been heat treated. The ratio of the intensities of different chemical compositions to that of Ti are given below:

Specimen	Cl/Ti	Ar/Ti	C/Ti	(Ti+N)/Ti	O/Ti
TiN (HCD)		0.236	0.388	1.988	1.420
TiN (CVD)	0.775	0.176	0.268	1.837	1.521

The major impurity in these TiN films was oxygen. Chlorine signal was rather strong in the CVD film but it was not noticeable in the Auger spectrum for the HCD film. The true atomic composition of these films was difficult to determine by this technique since the strongest $KL_{23}L_{23}$ Auger emission from nitrogen occurs at an energy (378 eV) that completely overlaps the transition from titanium. However, the ratio of the intensity of combined Ti+N peak (378 eV) to that of Ti peak (420 eV) is proportional to the nitrogen concentration [64]. Based on this hypothesis, the sample prepared by HCD appeared to have a higher amount of nitrogen than those prepared by CVD. This is consistent with the results of X-ray diffraction analysis.

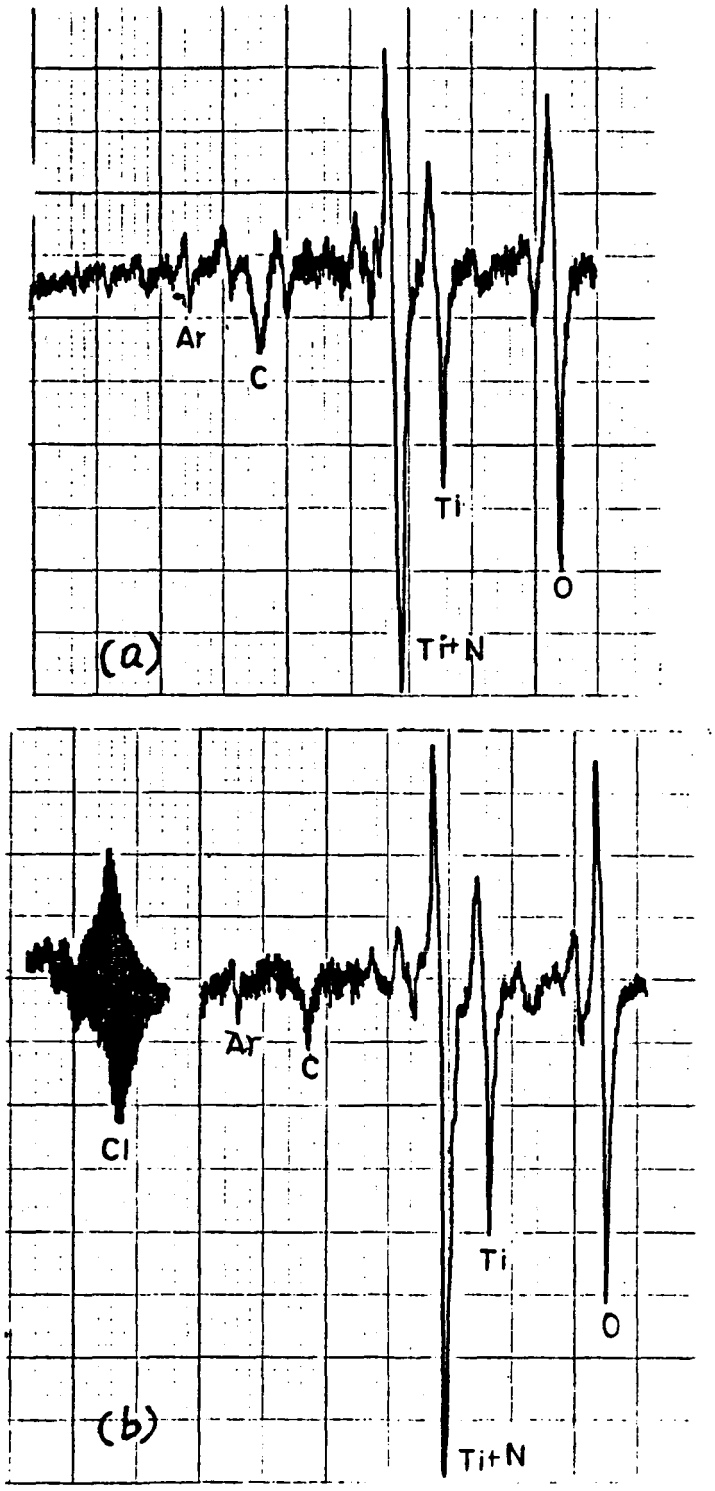

Fig. 5-9. The Auger electron spectra for TiN (HCD) (a) and TiN (CVD) (b).

(C)Scanning Electron Microscopy

Samples for SEM analysis were cleaned by using distilled water : HNO_3 : glacial acetic acid = 1:1:1 etching solution. The scanning electron micrographs of these two specimens before and after the electrical resistance measurements are shown in Fig. 5-10 and 5-11, respectively. The HCD film is more homogeneous, the film prepared by CVD possessed a larger number of voids and a wider range of grain sizes, it also cracked after the electrical resistance measurements. The corresponding EDAX spectra of these two films before the electrical resistance measurements are illustrated in Fig. 5-12. These spectra indicate the presence of some chlorine in the CVD film but not in the HCD film, the chlorine peak again disappeared after heat treatment. Nitrogen could not be detected by this method because of its light atomic weight.

(D)Hall Measurement

Hall measurements were conducted in a 4000 Gauss magnetic field at room temperature. The results of these measurements showed that the specimen prepared by CVD had a Hall mobility of 24.6 $cm^2/v\text{-}sec$ and a charge carrier concentration of 2.08×10^{20} cm^{-3}, and the specimen

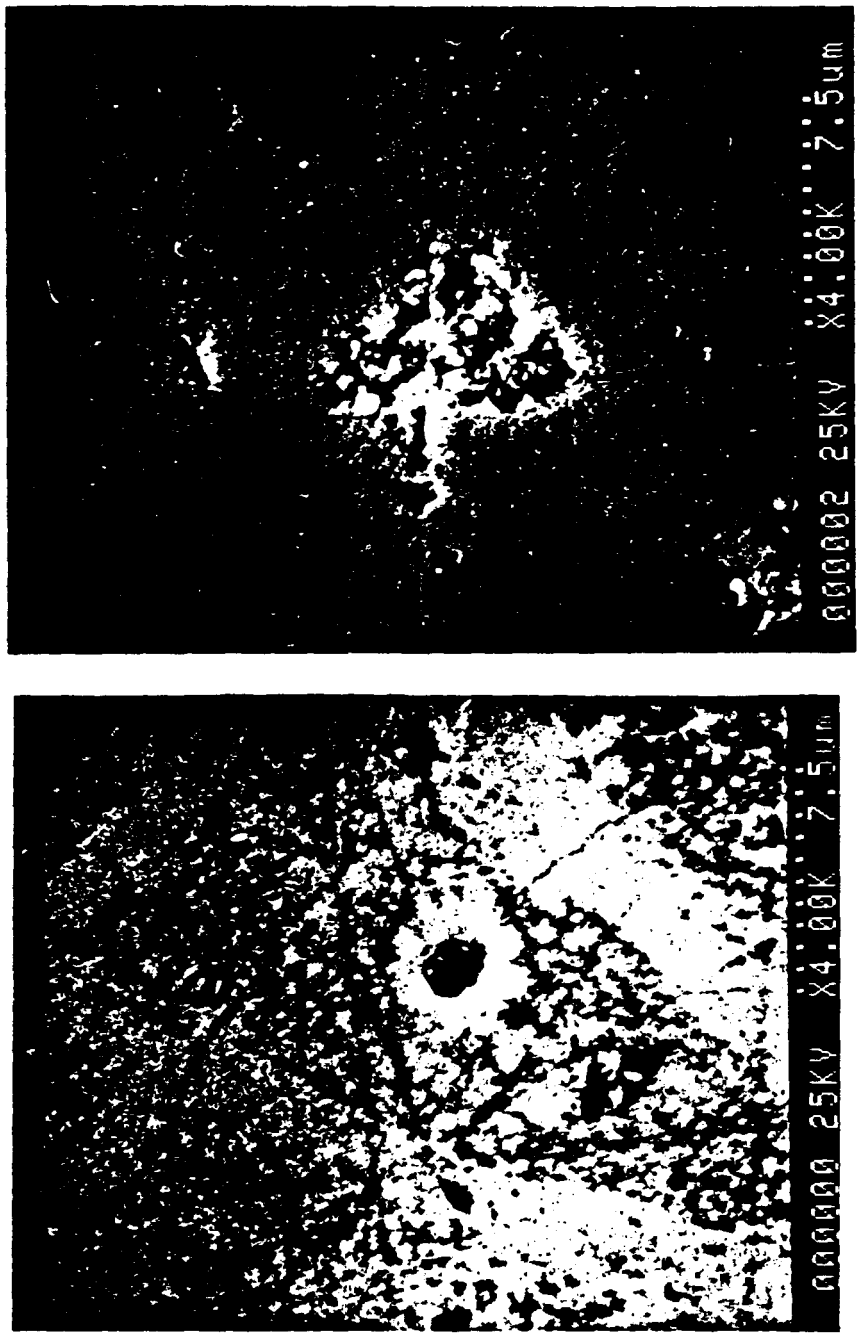

Fig. 5-10. The scanning electron micrographs of TiN (HCD) (a) and TiN (CVD) (b) thin films before the electrical resistance measurements.

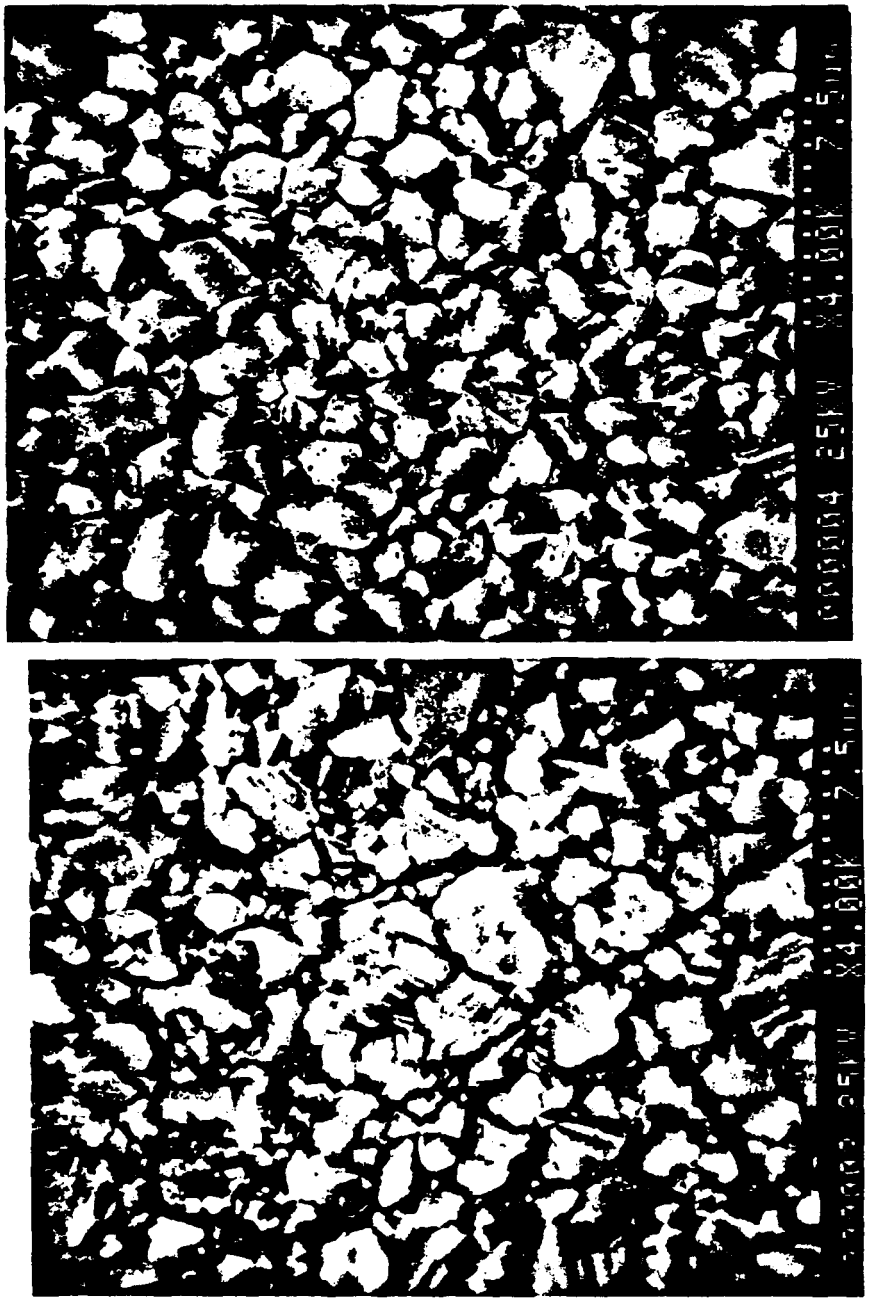

Fig. 5-11. The scanning electron micrographs of TiN (HCD) (a) and TiN (CVD) (b) thin films after the electrical resistance measurements.

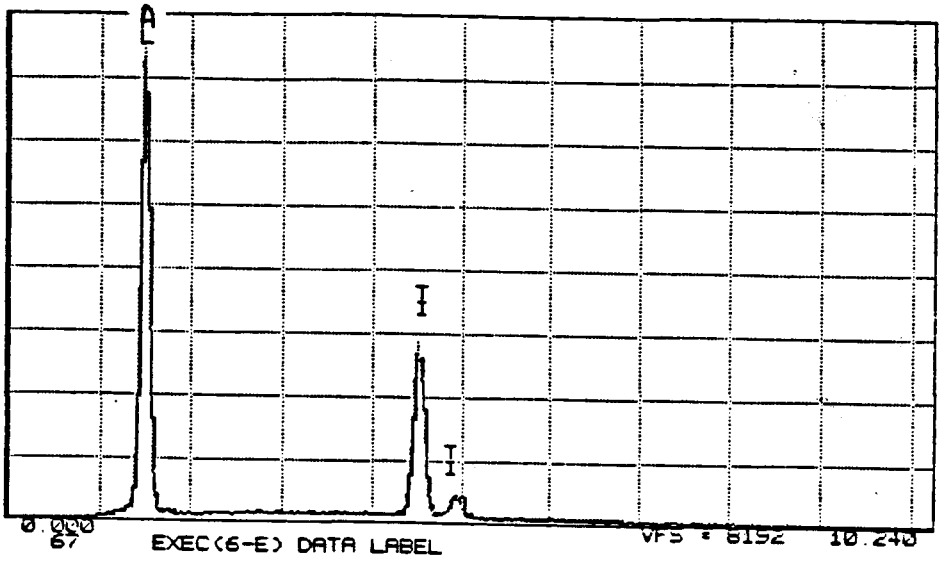

(a)

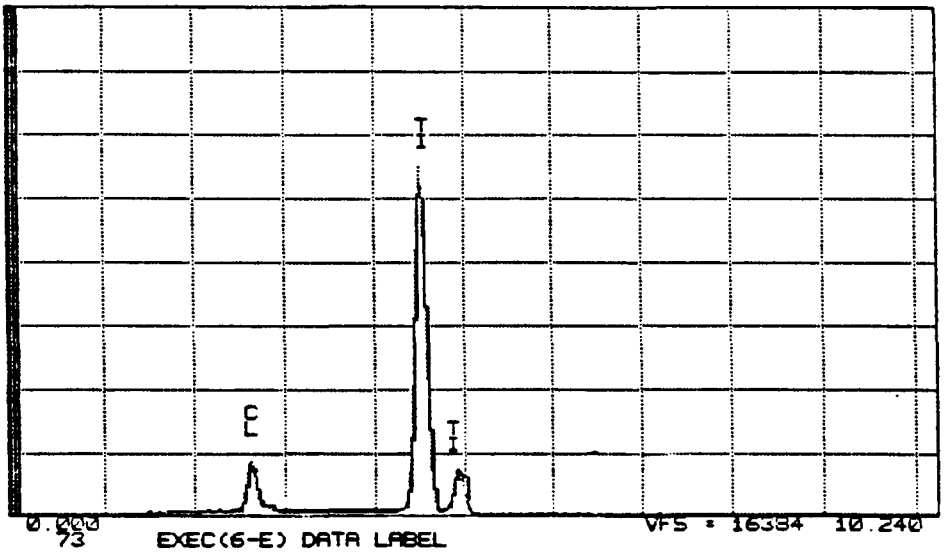

(b)

Fig. 5-12. EDAX spectra of TiN (HCD) (a) ang TiN (CVD) (b) thin films analyzed before the heat treatments. The Al peak observed in TiN (HCD) was from the Al stub.

prepared by HCD had a higher mobility of about 36 cm^2/v-sec, and a larger charge carrier concentration of $1.2x10^{21}$ cm^{-3}.

From all of these analyses the difference between these two films can be summarized as follows:

(1) the concentration of nitrogen was higher in the specimen prepared by HCD than in the specimen prepared by CVD. HCD film corresponded to the composition of TiN and CVD film corresponded to the composition of $TiN_{0.9}$.

(2) TiN (HCD) had higher Hall mobility, larger carrier concentration, and smaller resistivity than $TiN_{0.9}$ (CVD). This suggests that the carrier concentration and Hall mobility of titanium nitrides both increased with increasing nitrogen concentration; and the resistivity of the specimen decreased as nitrogen concentration increased.

(3) Auger spectra and EDAX spectra of the TiN film prepared by CVD showed presence of chlorine in this film and the unknown phases detected by the X-ray diffraction of CVD film may correspond to the existence of a chlorine containing phase, which disappeared upon heating.

It is, therefore, possible to speculate that the

reason for difference in electrical resistances of these two titanium nitride films is either the nonstoichiometry of the film or the presence of Cl. However, the analysis of the heat treated films showed that Cl evaporated during heat treatment, so chlorine would not be the reason for difference in electrical properties of these films and we can therefore conclude that the reason is the defect structure induced by nonstoichiometry. Substoichiometric specimen with a low nitrogen concentration had a larger resistivity and showed semiconducting behavior.

The presence of the structural vacancies would be expected to affect various physical properties of materials. It is obvious that the basis of such behavior is the change in electronic structures due to the presence of vacancies in the crystal lattice. The study of electronic structures of vacancies and perturbations caused by them in the energy spectrum of a crystal is therefore a problem of great interest and importance. This point will be taken up in the final section of this chapter.

5.2.3 Zirconium Nitride

Four zirconium nitride thin films prepared by r.f. sputtering (RFS) in mixed argon and nitrogen reactive gases were studied. The sputtering was performed at a total pressure of 6×10^{-2} torr with different nitrogen partial pressures (P_{N2}). The alumina (Al_2O_3) substrates were maintained at a temperature of 270°C during the sputtering. The relative characteristics of these four specimens are as follows:

Sample	$N_2/Ar+N_2$	P_{N2} (ppm-torr)	Thickness (Å)	Resistivity (microohm-cm)
1	0.19	114	5900	180
2	0.18	108	5750	211
3	0.16	96	5800	255
4	1.65	990	5100	393

The change in resistivity with nitrogen partial pressure and with film thickness are shown in Figs. 5-13 and 5-14, respectively. These figures show that the resistivity of zirconium nitride appears to first decrease and then increase with increasing nitrogen concentration, and the resistivity of the films appears to decrease with an increased in the thickness of the films.

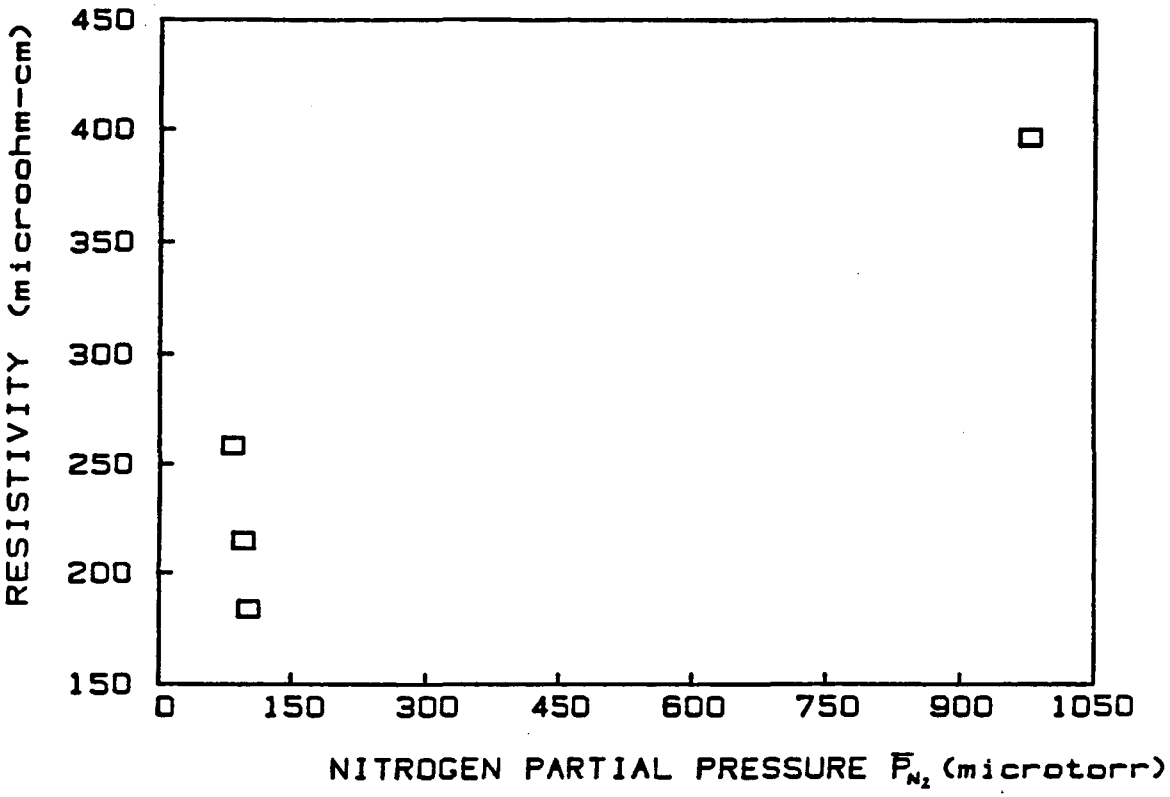

Fig. 5-13. Variation of room temperature resistivity with nitrogen partial pressure for zirconium nitrides thin films.

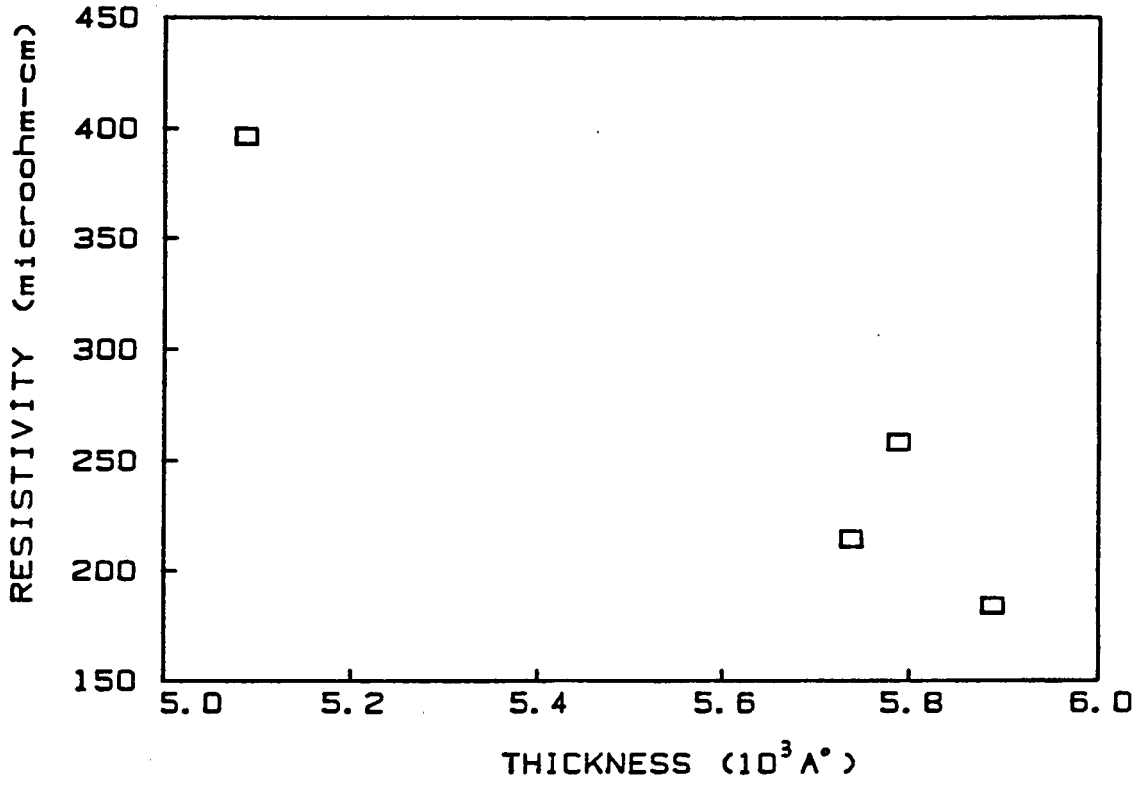

Fig. 5-14. Variation of room temperature resistivity with thickness of the film for zirconium nitrides.

These four zirconium nitride specimens were annealed before electrical resistance measurements. Samples 1 and 2 were annealed at 1007^{o}C for 30 hours, and samples 3 and 4 were annealed at 1050^{o}C for 95 hours. Samples 1 and 2 were tested at one time and 3 and 4 at another time. The change in resistance with temperature and change in resistance during an isothermal sojourn at 1000^{o}C for these samples are illustrated in Figs. 5-15 to 5-18. As seen from these figures, the resistance of these four ZrN films all increased with an increase in temperature. However, their behaviors did not follow a simple linear law, saturation at high temperatures was observed in three of the four films. In order to test whether the theory of Mott and Jones, as presented in the form of Eq. (3-5), could explain this saturation behavior, these resistance data were then plotted as $R(T(1+6\beta\gamma T))^{-1}$ versus T^2. If the data fits Eq. (3-5), one would expect a straight line for all specimens.

Fig. 5-19 shows such a plot for four ZrN samples, data are from the second heating cycle, with the Grüneisen constant γ=1.49, and the thermal linear coefficient of expansion β=7.24x10^{-6} for ZrN [66]. It is seen that the results are indeed linear except at

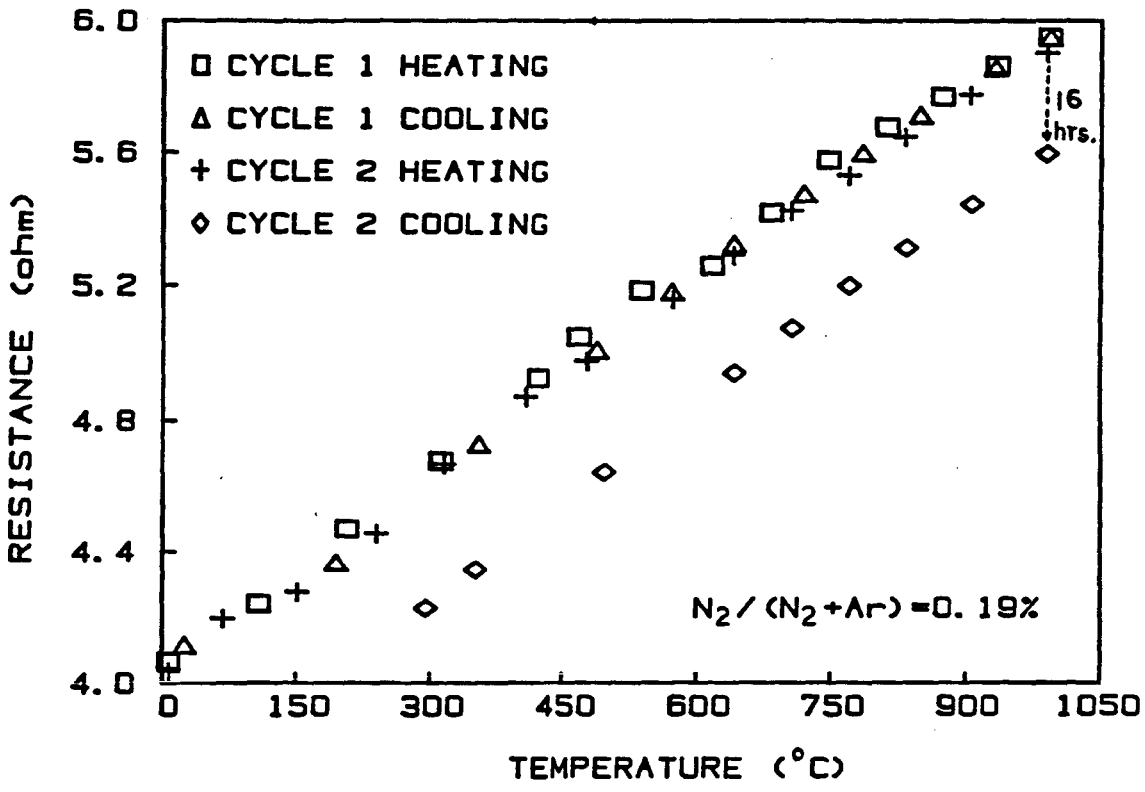

Fig. 5-15. Variation of resistance with temperature for ZrN-1, with P_{N2}=114 ppm-torr during sputtering.

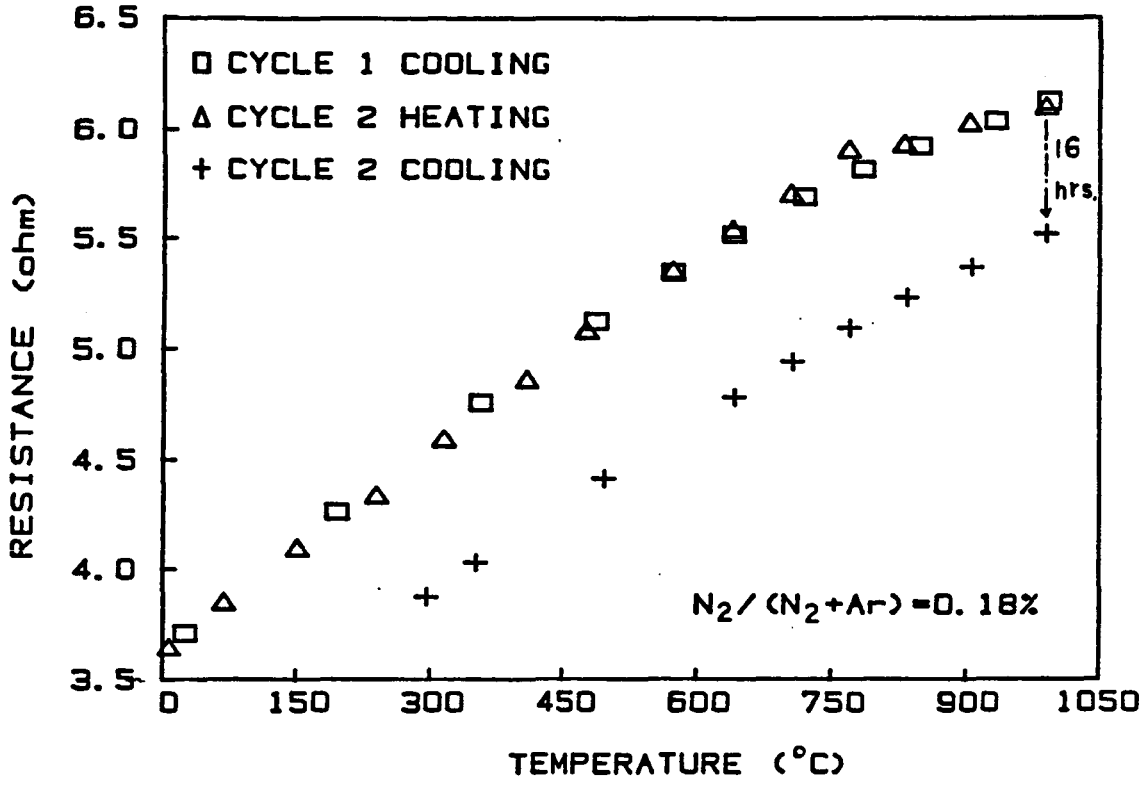

Fig. 5-16. Variation of resistance with temperature for ZrN-2, with P_{N2}=108 ppm-torr during sputtering.

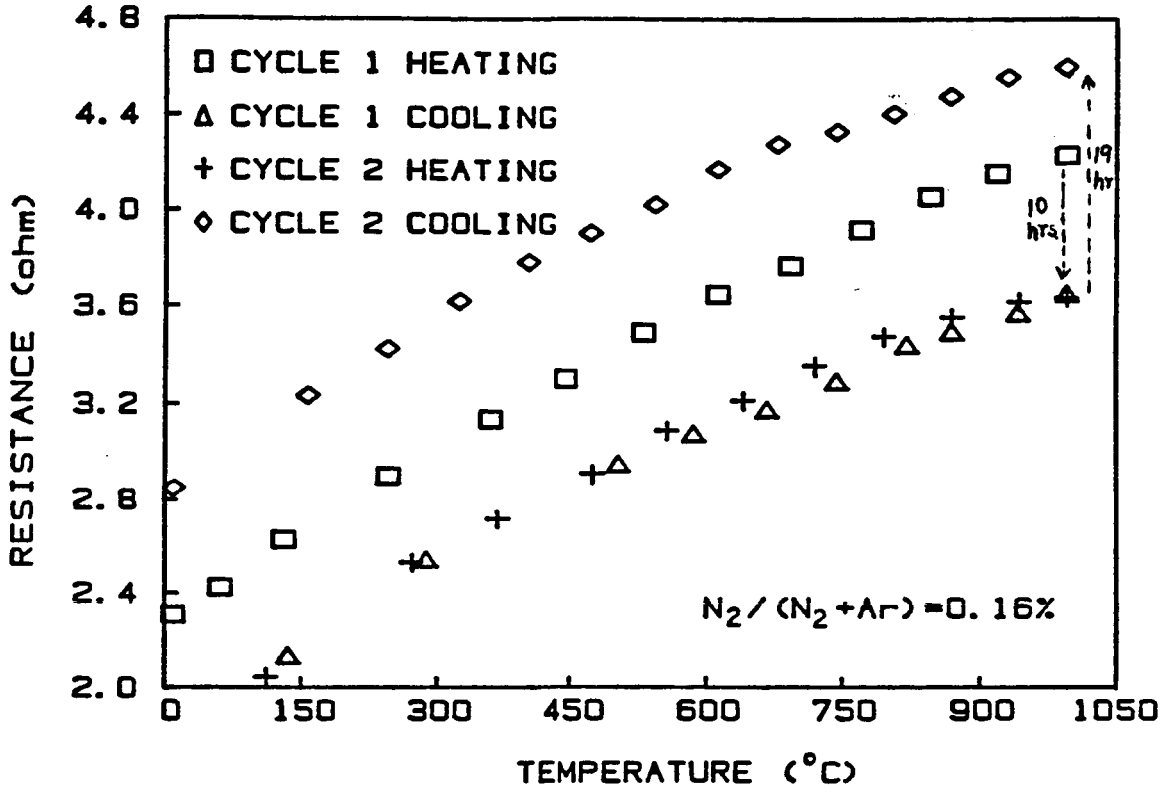

Fig. 5-17. Variation of resistance with temperature for ZrN-3, with P_{N2}=96 ppm-torr during sputtering.

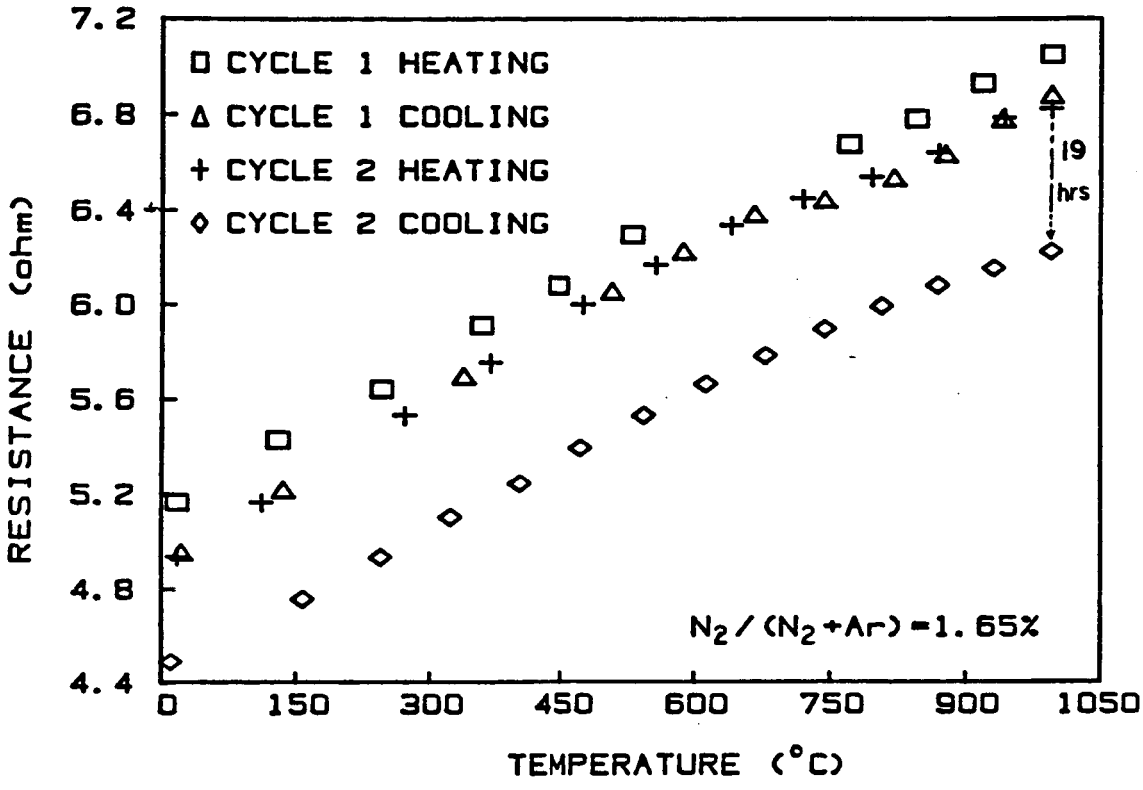

Fig. 5-18. Variation of resistance with temperature for ZrN-4, with P_{N2}=990 ppm-torr during sputtering.

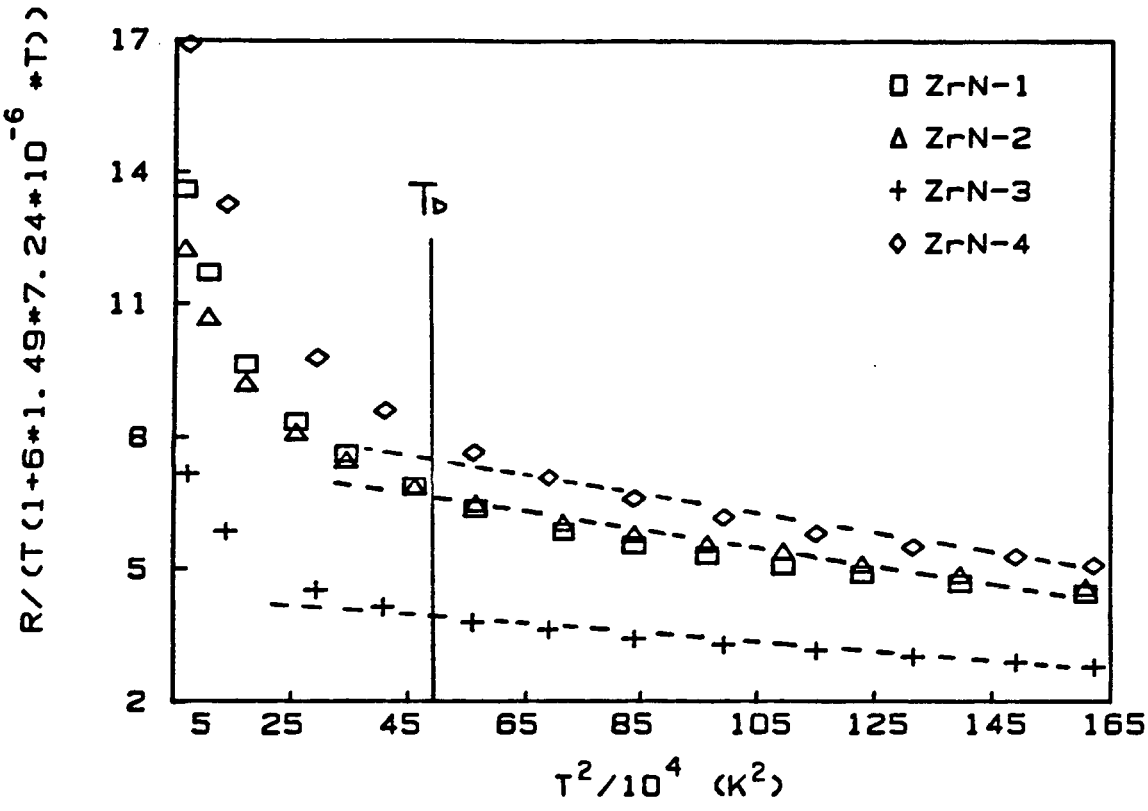

Fig. 5-19. A plot of $R(T(1+6\beta\gamma T)^{-1}$ versus T^2 for four zirconium nitrides.

temperatures below the Debye temperature (T_D=684K) where Eg. (3-5) is no longer valid. Therefore, it is concluded that theory of Mott and Jones is valid for the electrical resistance behavior of ZrN at temperatures higher than the Debye temperature.

The reduced resistance changes with temperature for these four ZrN samples were compared and presented in Fig. 5-20, these data are also from the second heating cycle. It is seen that the relative resistance change from room temperature to 1000°C increased as the nitrogen concentration decreased. However, it was found that the value of TCR at 1000°C, where the resistance saturation was observed, first increased and then decreased with increasing nitrogen concentration. In addition, the resistance drift rates of these four samples all decreased as the number of cycles increased.

The TCR of these specimens at 400°C (below Debye temperature) and 1000°C (above Debye temperature) together with their drift rates at 1000°C were calculated and listed below:

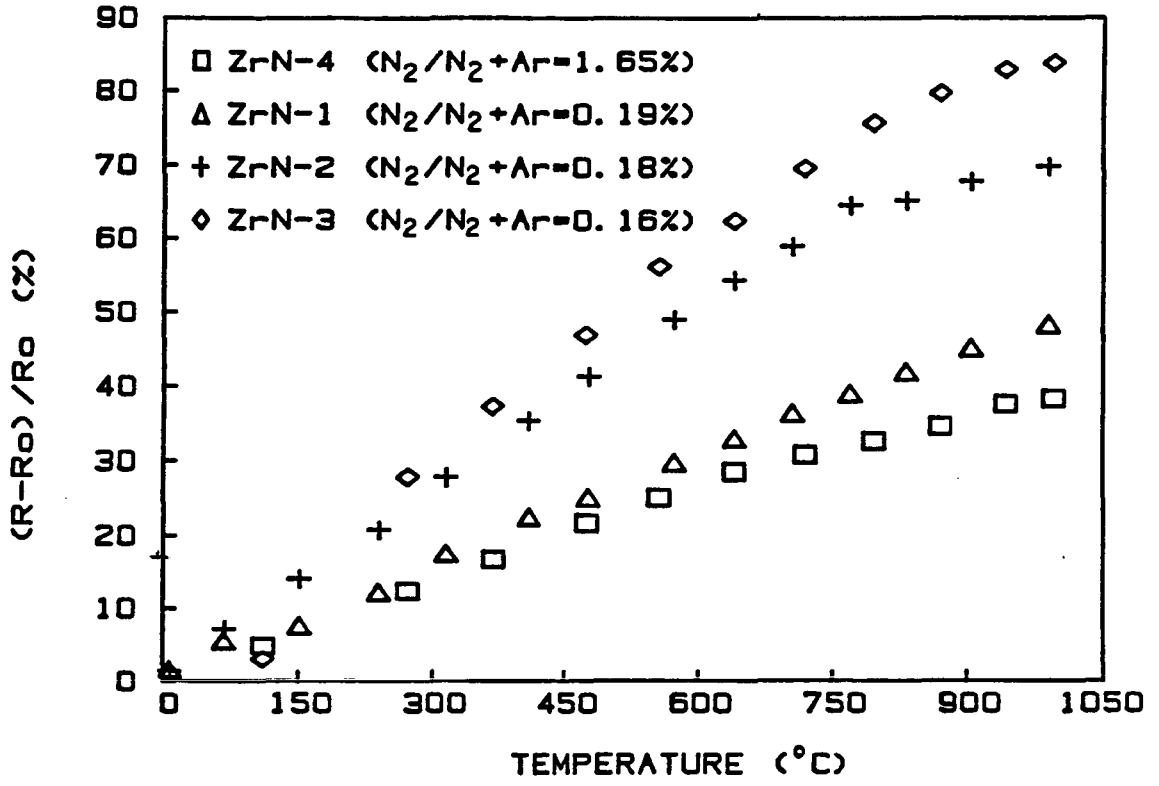

Fig. 5-20. Comparison the change in resistance with temperature for four zirconium nitrides. Resistance is normalized to its value at room temperature.

Specimen	P_{N2} (ppm-torr)	TCR (at 400°C)	TCR (at 1000°C)	DR* (%/hr)
1	114	405	275	-0.26#
2	108	560	228	-0.30#
3	96	574	184	1.60+
4	999	294	212	-0.54+

* data were taken after cycle two heating for a 16 hours(#) or 19 hours(+) sojourn at 1000°C.

The crystal structures of these specimens were studied from their X-ray diffraction patterns. It was found that these four r.f. sputtered zirconium nitride films all had FCC crystal structures. The lattice parameters (LP) and the ratio of the intensity of (111) peak to that of (200) peak of samples, as well as the nitrogen partial pressure (P_{N2}) during sputtering preparation are tabulated as follows:

Sample	P_{N2}(ppm-torr)	LP(Å)	I(111)/I(200)
1	114	4.5785	3/8
2	108	4.5768	1/60
3	96	4.5692	0/42
4	990	4.5717	5/12

Fig. 5-21 illustrates the variation of the lattice

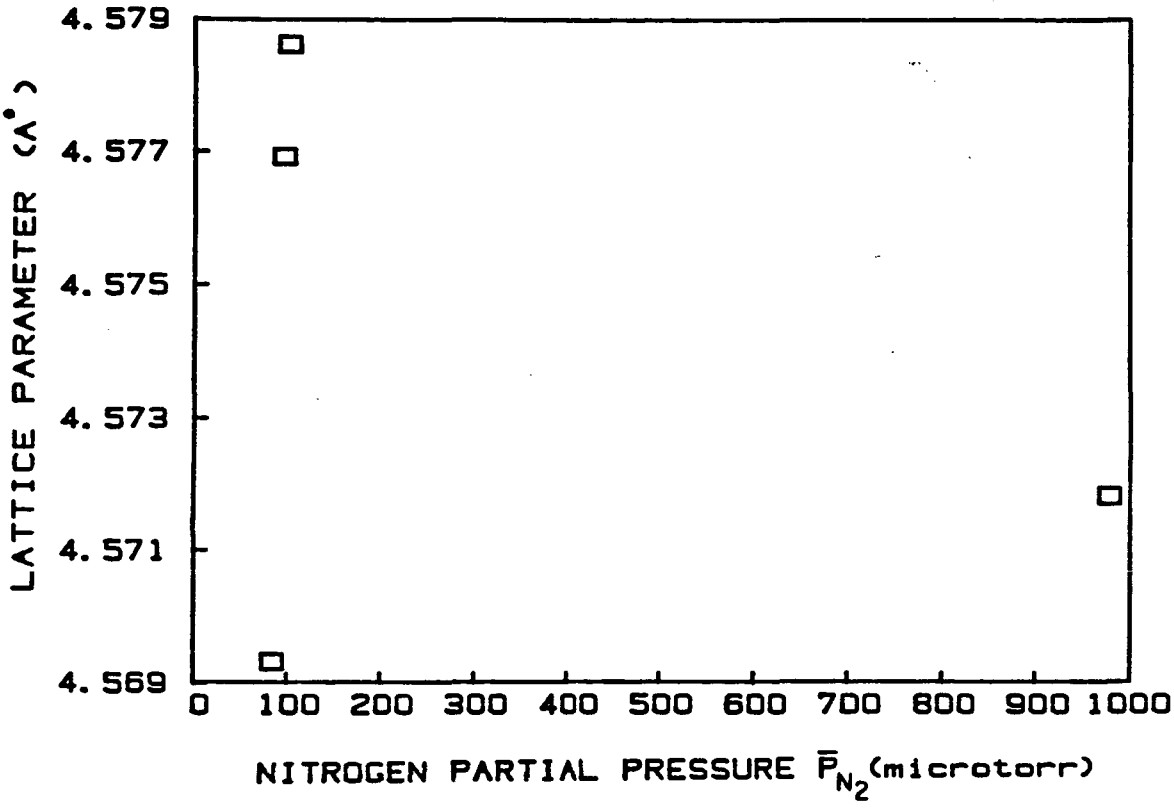

Fig. 5-21. Lattice parameter versus nitrogen partial pressure for ZrN thin films

parameters of these specimens with nitrogen partial pressure. It is seen that the lattice parameters first increased with increasing nitrogen partial pressure up to 114 μtorr. However, at higher nitrogen partial pressures, the lattice parameter decreased with increasing nitrogen partial pressure. Toth [65] and Khaenko [69] found that for transition metal compounds, the lattice parameter is maximum near the stoichiometric composition. The relations between lattice parameter and composition for some of the compounds are shown in the Appendix D. This relati on in ZrN is not well established, however Yajima et al. [70] studied the lattice parameter-composition relation for ZrN_x hyperstoichiometric compound, also shown in the Appendix D, and found that the lattice parameter of ZrN_x (for $x>1$) also had maximum at the stoichiometric composition. Comparing our lattice parameter data with theirs and taking into account the nitrogen partial pressure relation between specimens, sample 1 is expected to have near stoichiometric composition, and samples 4 had hyperstoichiometric composition with $x=1.102$. Sample 2 and 3 are expected to have substoichiometric composition.

The density studies in conjunction with lattice

parameter studies in transition metal compounds have shown that at substoichiometric composition, the nitrogen sublattice is predominantly defective, and at hyperstoichiometric composition, the metal sublattice is defective [65]. Therefore, sample 2 and 3 had more vacant sites on the nitrogen sublattices (V_N) and samples 4 had more vacant sites on the zirconium sublattice (V_{Zr}). The vacant sites on both the nitrogen sublattice and zirconium sublattices are about the same in sample 1.

Therefore, taking into account the composition, resistivity and TCR altogether for four samples, it can be concluded that for zirconium nitrides:

(1) resistivity of the film increased as the concentration of vacancies (both V_N and V_{Zr}) in the film increased. (Fig. 5-13)

(2) resistance saturation at high temperatures was more significant for specimen with higher vacancy concentrations (both V_N and V_{Zr}). The saturation in sample 1 which had near stoichiometric composition was not significant. (Fig. 5-20)

(3) at high temperatures (higher than Debye temperature), TCR of the films decreased as vacancy concentration increased, while at low temperatures TCR

increased with increasing vacancy concentration. (see Fig. 5-20)

(4) the resistance drift rates of these films increased with increasing vacancy concentrations, and decreased with number of thermal cycles.

5.2.4 Tantalum Nitride

Three tantalum nitride thin films prepared by Magnetron r.f. sputtering technique in an argon-nitrogen plasma were analyzed. The total pressure of mixed gases of argon and nitrogen was about 1.5×10^{-3} torr, and the temperature of Al_2O_3 substrate was kept at $250^{o}C$.

The nitrogen partial pressures (P_{N2}), thicknesses and resistivities of the specimens prepared by this technique are as follows:

Sample	$N_2/Ar+N_2$ (%)	thickness (Å)	resistivity (microohm-cm)	P_{N2} (ppm-torr)
1	22	8400	113	330
2	25	12600	103	375
3	40	5300	165	600

Plots of resistivity versus nitrogen partial

pressure and resistivity versus thickness of these specimens are illustrated in Figs. 5-22 and 5-23. It is seen that the resistivity of tantalum nitride first decreased and then increased with increasing P_{N2}, and its resistivity decreased as the thickness of the film increased, as was the case for ZrN.

The resistance versus temperature behaviors of the three specimens for two cycles of heating and cooling, and a sojourn at 1000°C for 11 hours are presented in Figs. 5-24 to 5-26. These specimens all showed metallic behaviors as their resistance increased with increasing temperature. Their average values of TCR and DR at 1000°C are:

Sample	P_{N2}(ppm-torr)	TCR(ppm/°C)	DR(%/hr)
1	330	255	0.53
2	375	301	0.50
3	600	438	-0.16

From these data, it is noted that the TCR of tantalum nitrides decreased with decreasing nitrogen partial pressure, and their DR increased with decreasing nitrogen partial pressure as in the case of TiN and ZrN. It appeared that low TCR and low DR tended to be mutually

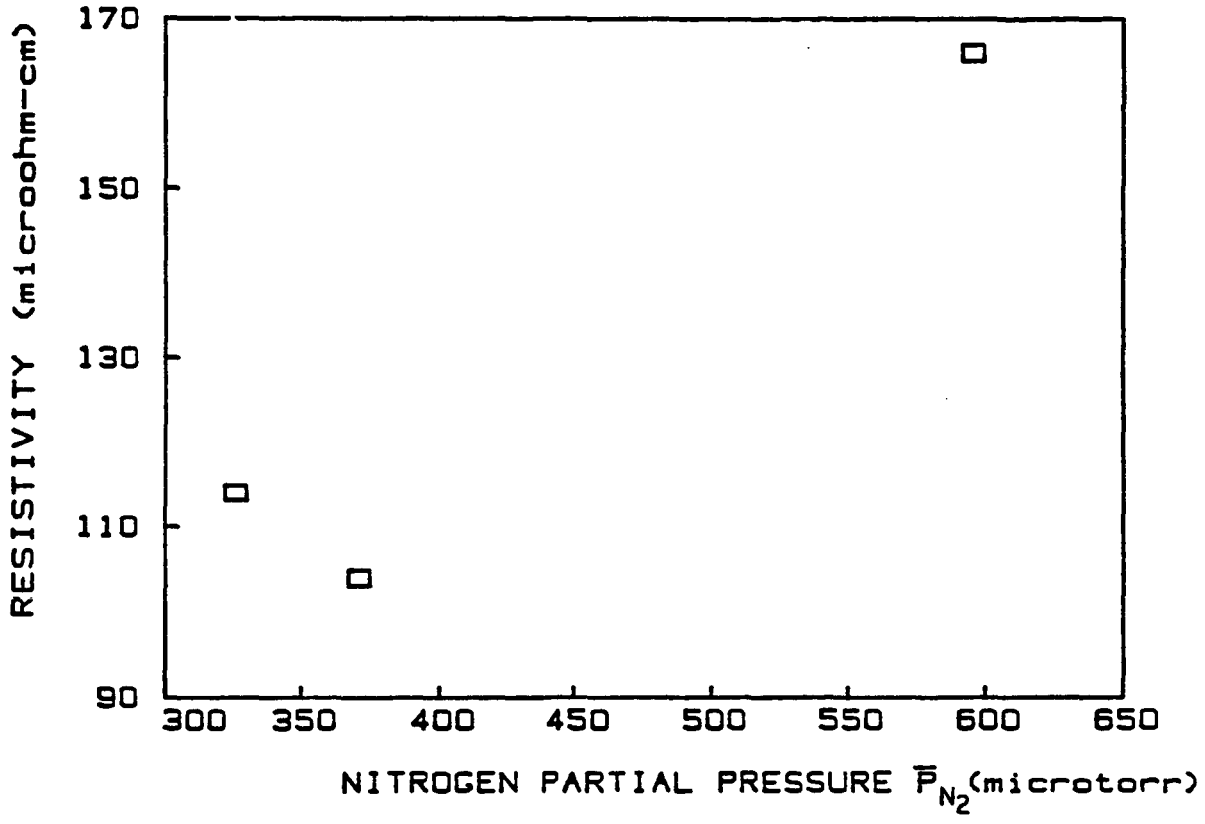

Fig. 5-22. Variation of room temperature resistivity with nitrogen partial pressure for tantalum nitride thin films.

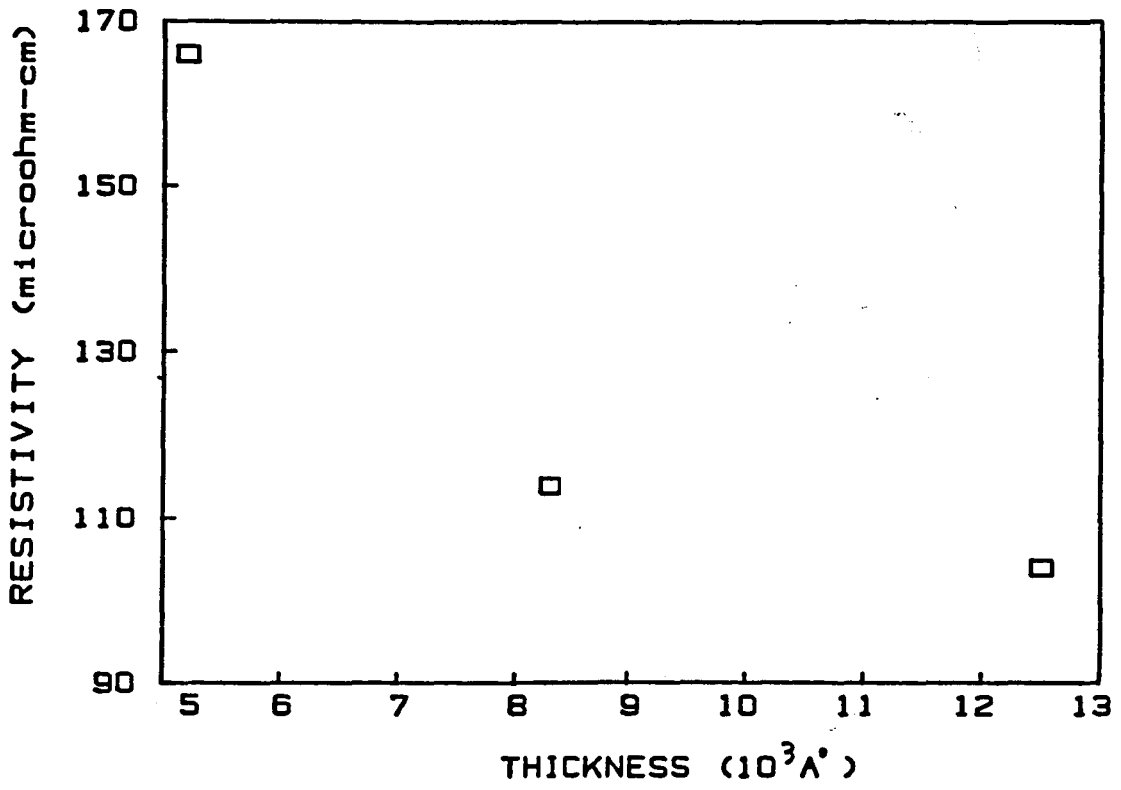

Fig. 5-23. Variation of room temperature resistivity with thickness of the film for tantalum nitrides.

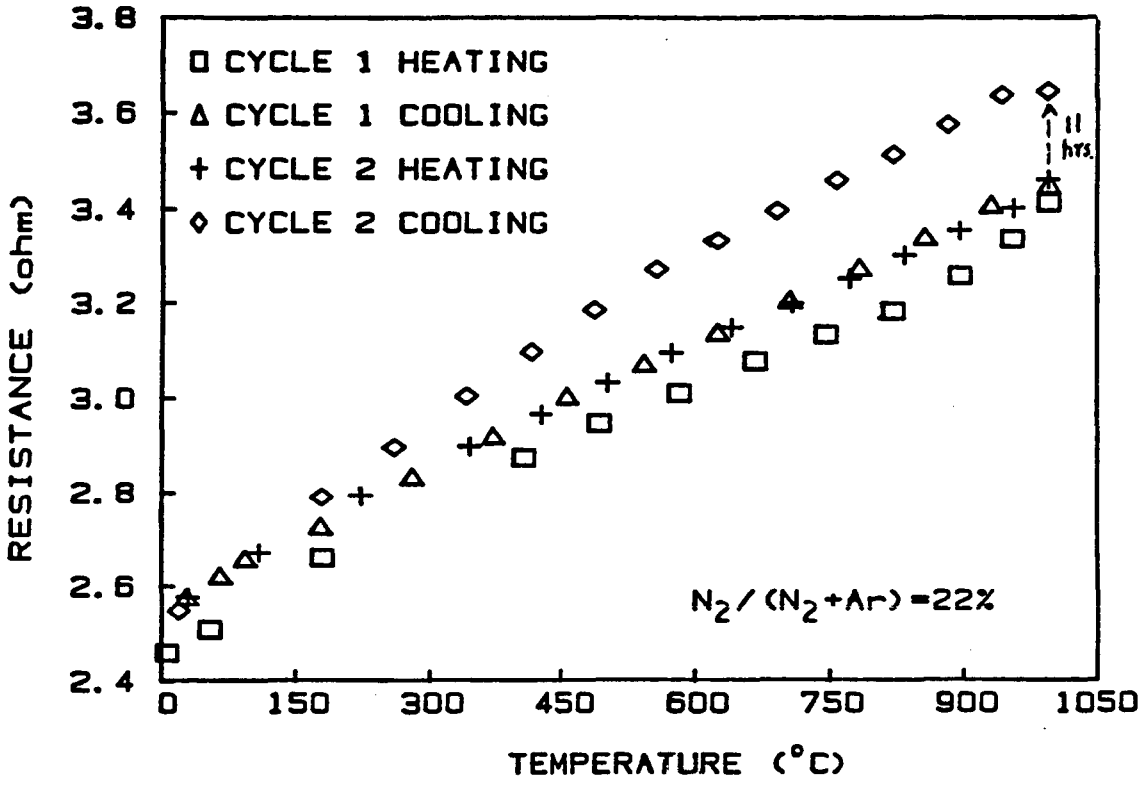

Fig. 5-24. Variation of resistance with temperature for TaN-1, with P_{N2}=330 ppm-torr during sputtering.

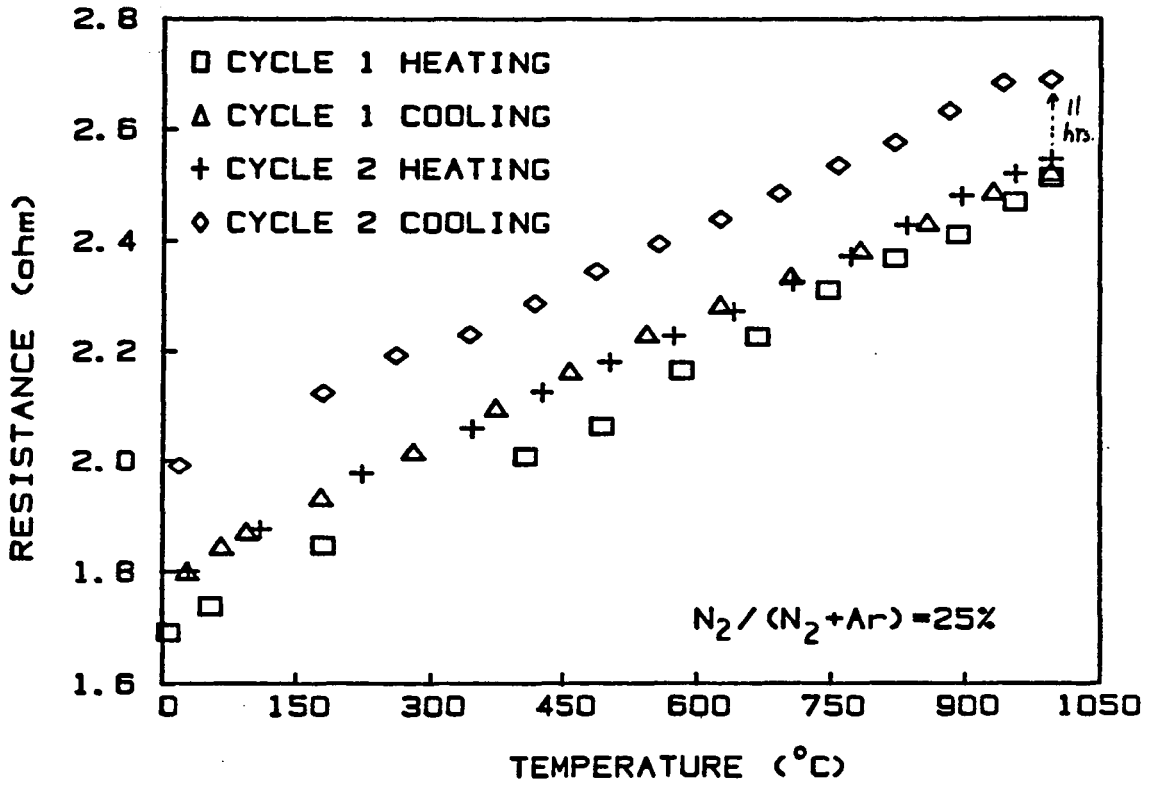

Fig. 5-25. Variation of resistance with temperature for TaN-2, with P_{N2}=375 ppm-torr during sputtering.

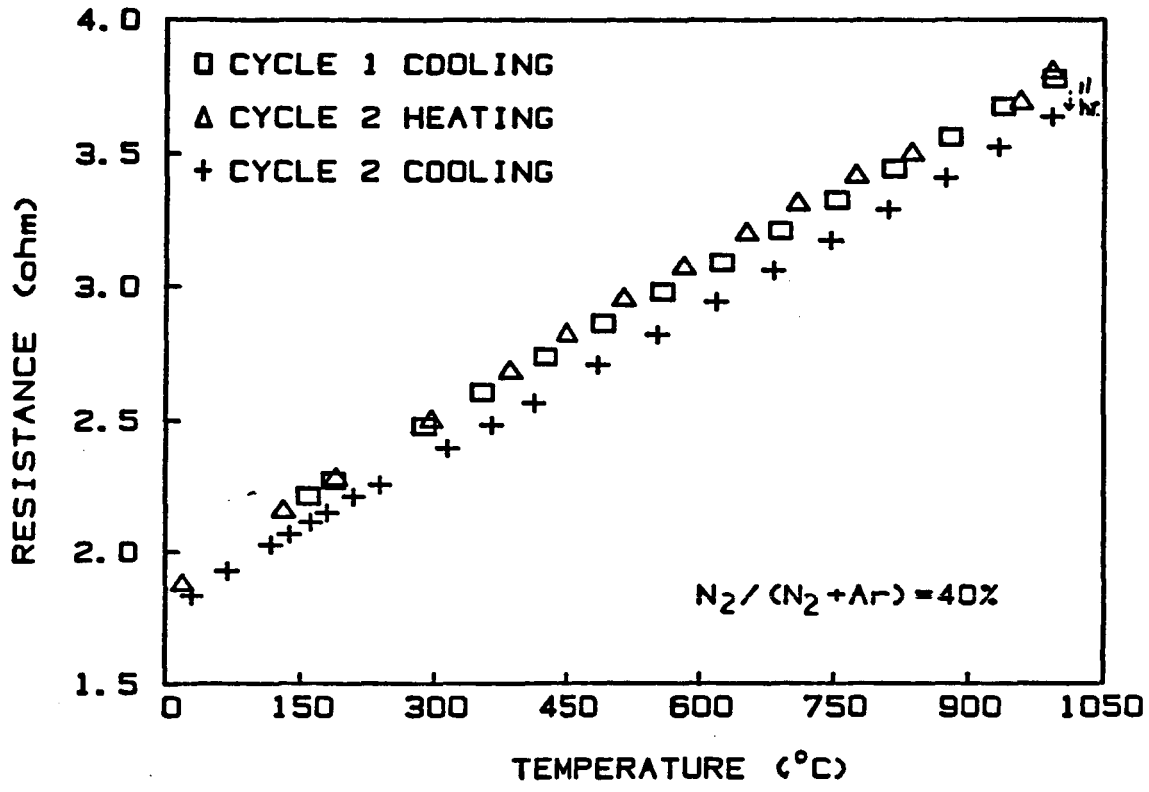

Fig. 5-26. Variation of resistance with temperature for TaN-3, with P_{N2}=600 ppm-torr during sputtering.

exclusive. The reduced resistance change with temperature for these three specimens are compared and illustrate in Fig. 5-27. High temperature resistance saturation which was noticed as in the case of ZrN was not observed for these three TaN film.

The crystal structures of the TaN sputtered films were determined by X-ray diffraction. The diffraction patterns indicated that the structures of the films depended on the nitrogen partial pressure, when P_{N2} was low as in samples 1 and 2, the presence of a mixture of hexagonal ε-TaN together with a small amounts of hexagonal Ta_2N was observed, when nitrogen partial pressure was high, as in sample 3, a mixture of ε-TaN with small amounts of Ta_2N_3 was observed. The lattice parameters of ε-TaN phase in these three films are calculated and listed below:

Specimen	a(Å)	c(Å)	c/a
1	5.2009	2.8662	0.551
2	5.2009	2.8609	0.550
3	5.2097	2.8405	0.545

The chemical compositions of these TaN_x samples were also studied by Auger electron spectroscopy. The

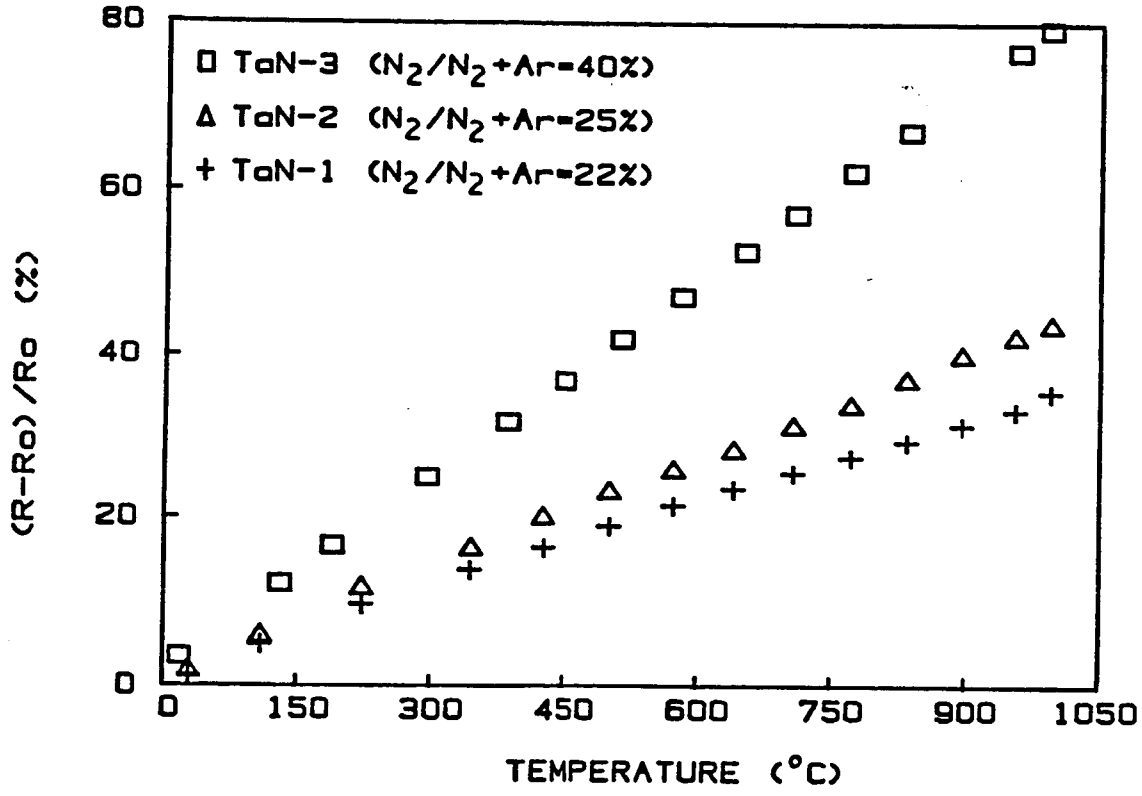

Fig. 5-27. Comparison the change in resistance with temperature for three tantalum nitrides. Resistance is normalized to its value at room temperature.

derivative Auger electron spectra of these TaN_x samples are shown in Fig. 5-28. It was found that the major impurity in these films was oxygen. The ratio of the intensities of nitrogen to that of Ta are as follows:

Specimen	1	2	3
I_{N2}/I_{Ta}	0.460	0.492	0.575

These data suggested that specimen 3 had the highest and specimen 1 had the lowest nitrogen concentration (x).

It is concluded that as the nitrogen concentration (x) in TaNx film increased, the resistivity and DR of the film decreased, while TCR increased (see the second table in this section).

5.2.5 Chromium Nitride

As already mentioned in section 5.2.1, chromium nitride was not in our final list of selected materials due to its dissociation at high temperatures. However, in order to make a systematic analysis of transition metal nitrides, it was included in this research program.

A hollow cathode discharged chromium nitride thin film with a resistivity of 13.8 microohm-cm was studied.

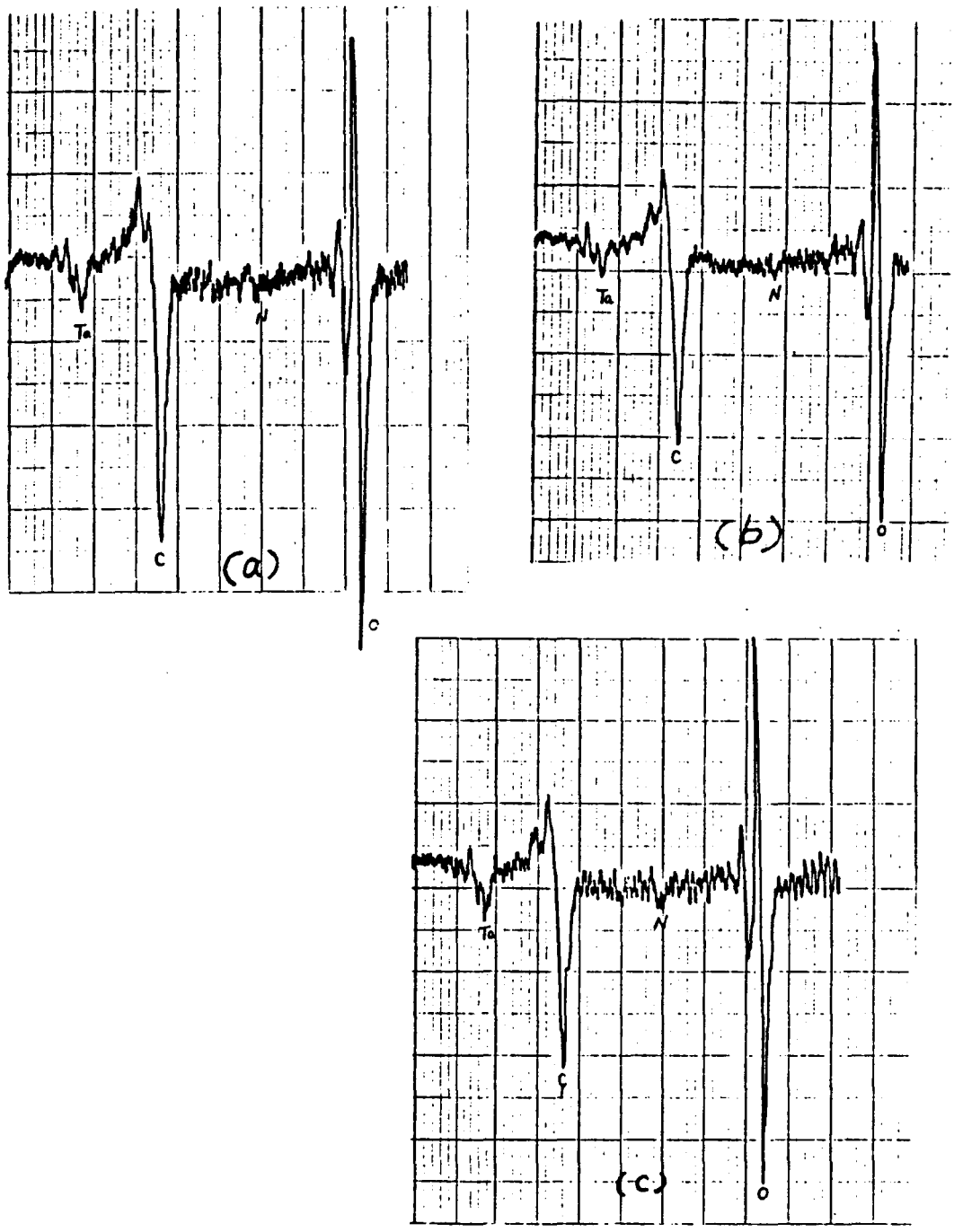

Fig. 5-28. The Auger electron spectra of three TaN_x thin films (a) for TaN-1 (b) for TaN-2 (c) for TaN-3.

Its resistance versus temperature curves for two cycles of heating and cooling are presented in Fig. 5-29. It is seen that the resistance increase had a polynomial instead of linear dependence on temperature. This is due to the dissociation of CrN at high temperatures. Its TCR at 1000^{o}C was about 710 ppm/^{o}C and its DR was 20 %/hr.

5.2.6 Titanium Carbide

Two titanium carbides thin films were studied. One prepared by activated reactive evaporation (ARE) and the other prepared by chemical vapor deposition (CVD). The samples were deposited on the Al_2O_3 substrates to thicknesses of 2.0 and 1.5 micrometers, and had resistivities of 39.4 and 169 microohm-cm, respectively.

Fig. 5-30 presents the resistance versus temperature curves for TiC (ARE) for two cycles of heating and cooling, and Fig. 5-31 presents the results for TiC (CVD). It is seen that the resistance of both samples increased with increasing temperatures with TCR values at 1000^{o}C of 338 and 210 ppm/^{o}C and DR (measured after cycle two heating) of 0.06 and 0.5 %/hr for the ARE and CVD prepared samples, respectively. It was also found

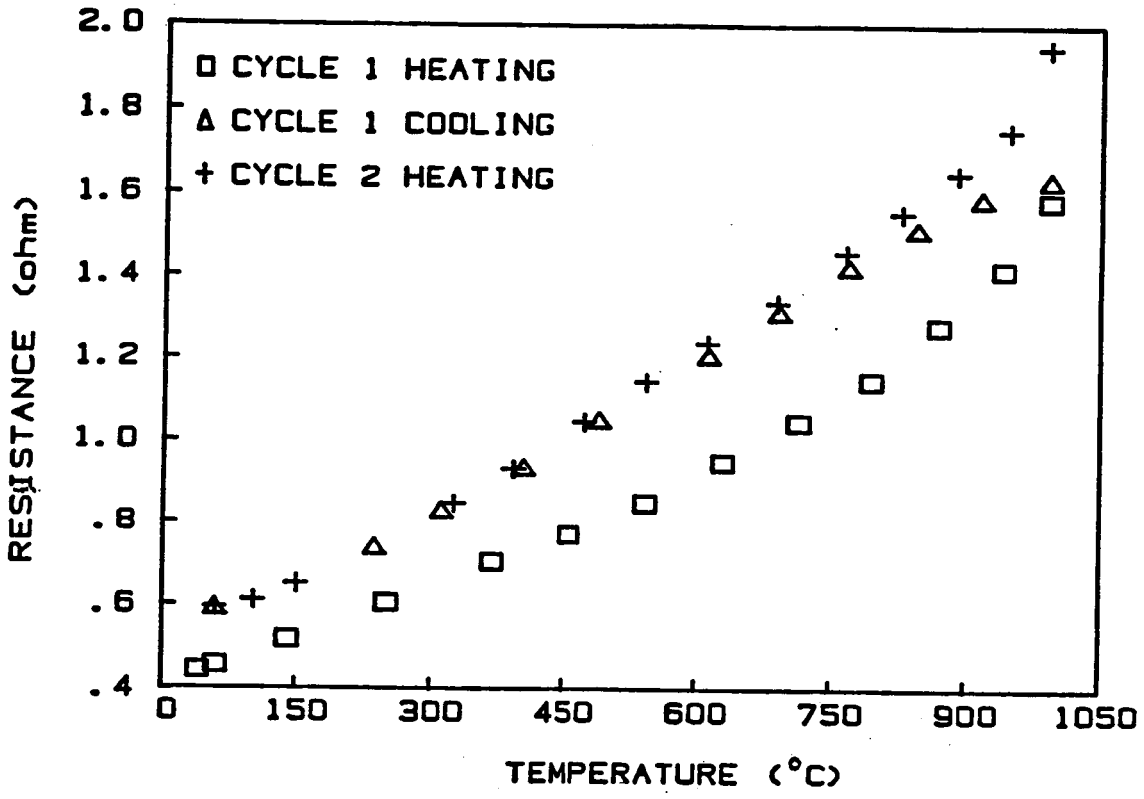

Fig. 5-29. Variation of resistance with temperature for chromium nitride thin film prepared by HCD.

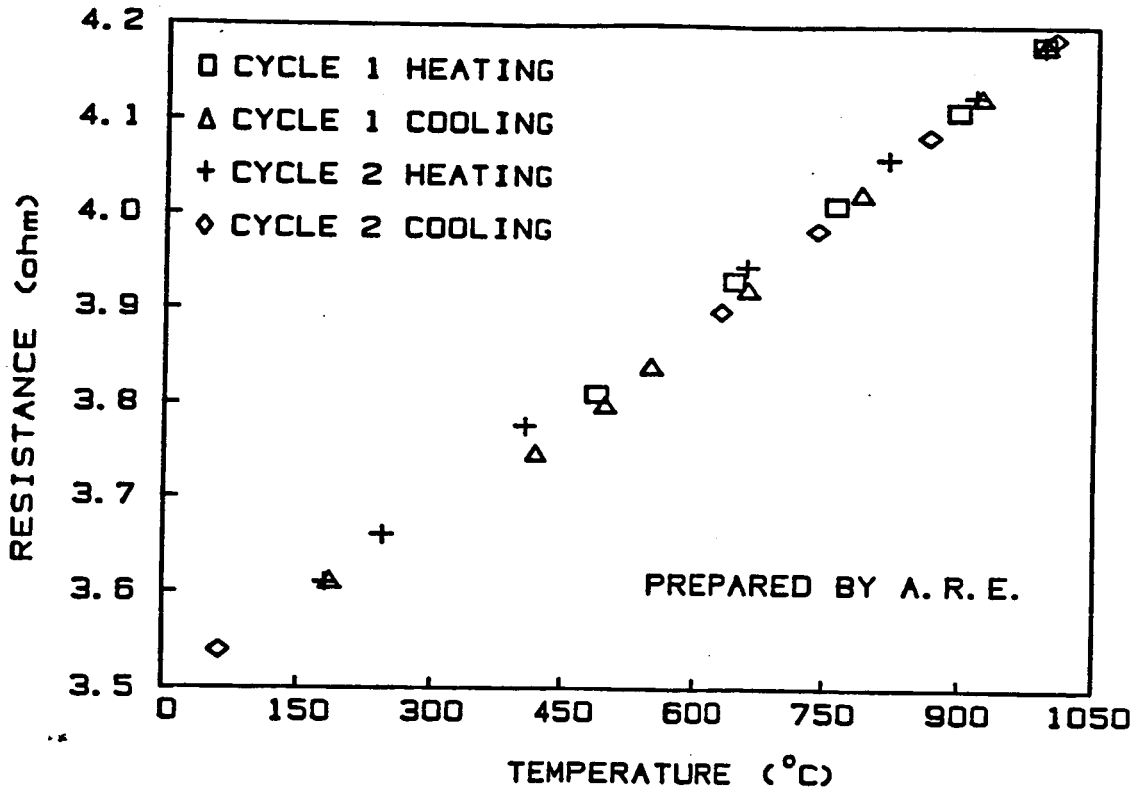

Fig. 5-30. The change in resistance with temperature for titanium carbide thin film prepared by activated reactive evaporation.

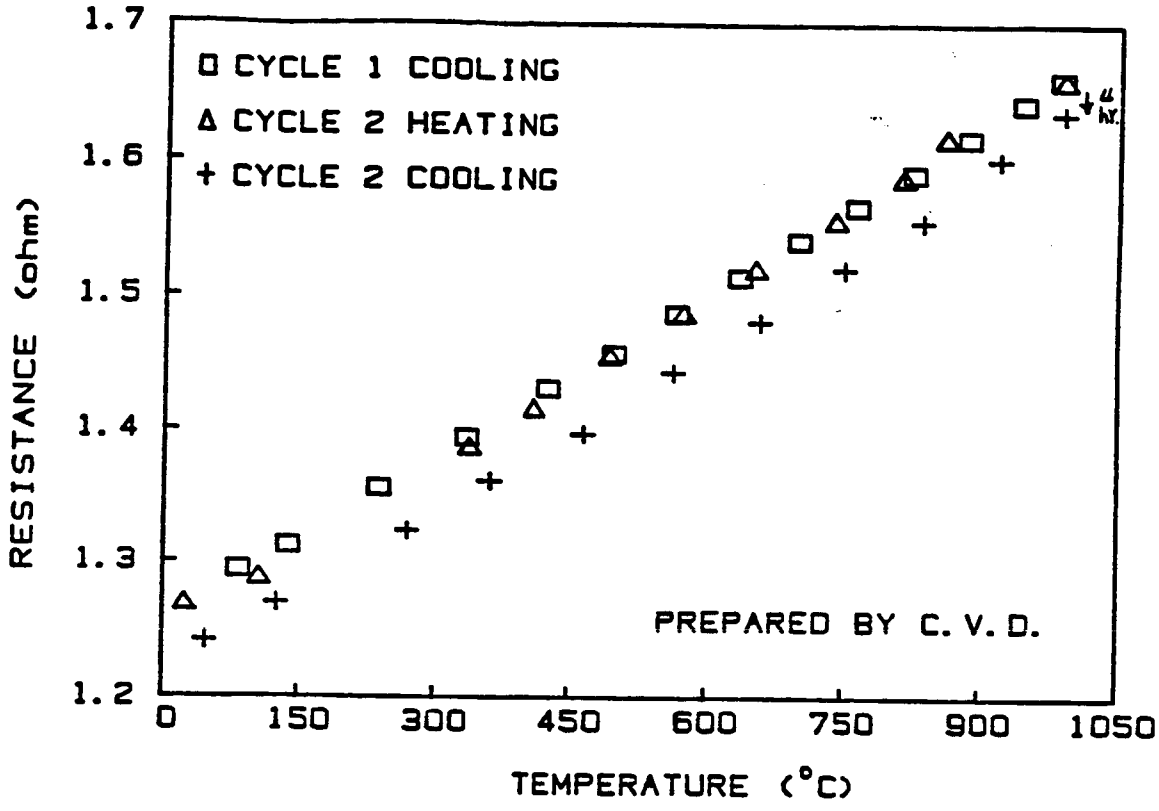

Fig. 5-31. The change in resistance with temperature for titanium carbide thin film prepared by chemical vapor deposition.

that TCR of TiC (ARE) decreased with cycling while that of TiC (CVD) increased with cycling, and as in the case of TiN the specimen prepared by CVD had inferior electrical stability.

The crystal structures of these two specimen were also examined by X-ray diffraction. Both films had FCC structures with lattice parameters of 4.327 Å for TiC (ARE) and 4.331 Å for TiC (CVD). Comparing these values with the relation between lattice parameter and composition data of Stroms [53], shown in Appendix D, it is found that the TiC_x specimen prepared by ARE had higher carbon concentration with x value close to 1, and the sample prepared by CVD had x close to 0.85. The relative properties of these two TiC_x specimens were compared and are listed below:

Specimen	x	resistivity (microohm-cm)	TCR (ppm/°C)	DR (%/hr)
TiC(ARE)	≈ 1	39.4	338	0.06
TiC(CVD)	≈ 0.85	169	210	-0.5

It is therefore concluded that for TiC_x as carbon concentration of the specimen decreased, i.e., as carbon vacancy concentration increased, the resistivities and

the DRs of these specimens increased, while their TCR values decreased. This conclusion is similar to the conclusion made for the nitrides in the previous sections.

Many researchers have investigated the dependence of resistivity upon vacancy concentration on the carbon sites and found that an approximately linear relation exists between them at low vacancy concentrations (<10%). For the particular case of TiC, Williams [68] found that the resistivity of TiC_x varied by 16 microohm-cm per at% vacancies, an order of magnitude larger than the effect found in noble metals. For high vacancy concentrations, resistivity saturates as shown in Fig. 5-32. Data from this work are also shown in this figure (marked as "X"), the resistivities of our two specimens were lower than that of William's samples with same compositions. However the tendency of the resistance change with carbon concentration are the same in two cases.

5.2.7 Zirconium carbide

The zirconium carbide specimen studied was prepared by ARE method. Zirconium was deposited on the Al_2O_3

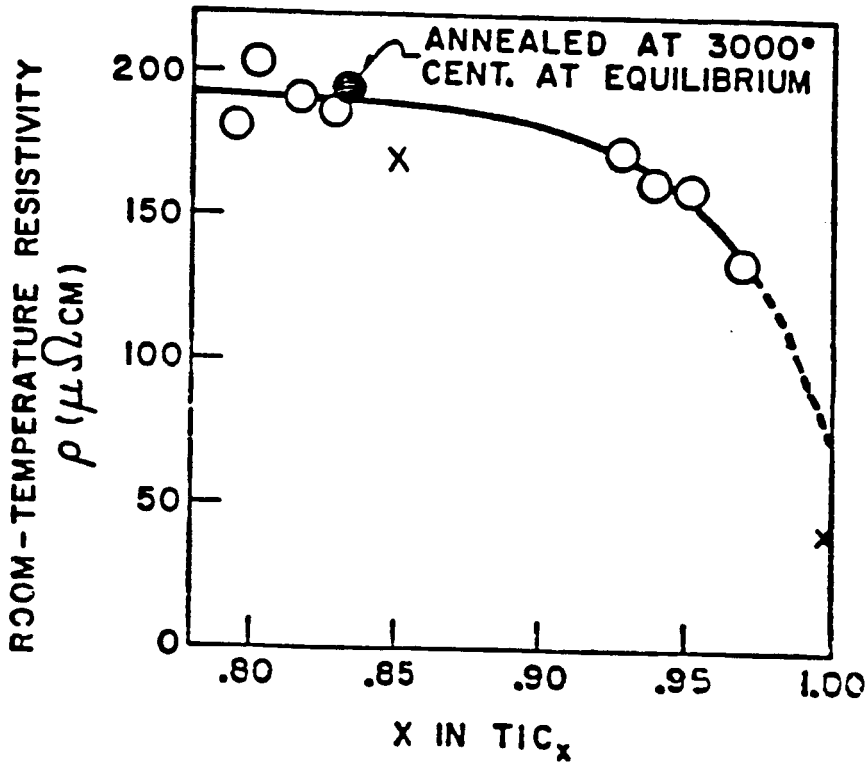

Fig. 5-32. Room temperature resistivities for TiC crystals of various C/Ti ratios. (O, ●) from the results of Williams [68], and (X) from this work.

substrate by electron beam gun in gaseous C_2H_2 at a vapor pressure of $(2-5)x10^{-5}$ torr, with the substrate temperature maintained at 300°C during evaporation. The thickness and resistivity of this film were 2 micrometer and 560 microohm-cm, respectively.

The resistance versus temperature curves for this ZrC sample are presented in Fig. 5-33 for three heating and cooling cycles. Resistance saturation at high temperatures was again noticed as in the case of ZrN. In order to test whether the theory of Mott and Jones also applied to ZrC, a $R(T(1+6\beta\gamma T))^{-1}$ versus T^2 plot was made for ZrC and is shown in Fig. 5-34, taking Gruneisen constant $\gamma = 1.50$, and thermal linear coefficient of expansion $\beta=6.7x10^{-6}$ for ZrC [66]. Again, it was found that the results are indeed linear at temperatures higher than the Debye temperature (744K). Therefore, Mott and Jones theory also described well the observed electrical resistance of zirconium carbide for temperatures higher than the Debye temperature.

The TCR of this sample was about 180 ppm/°C at 1000°C and its DR at 1000°C was about 0.13 %/hr for a 14 hours sojourn after cycle 1 heating and about 0.1 %/hr

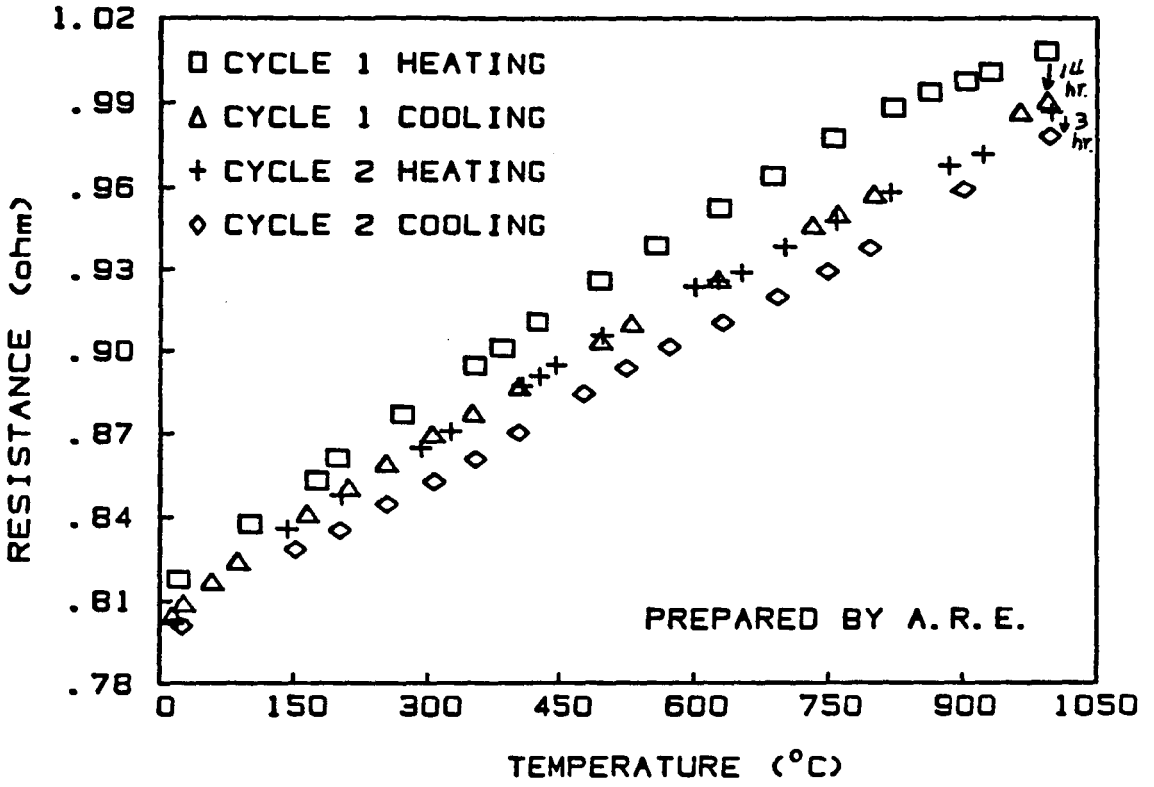

Fig. 5-33. The change in resistance with temperature for zirconium carbide.

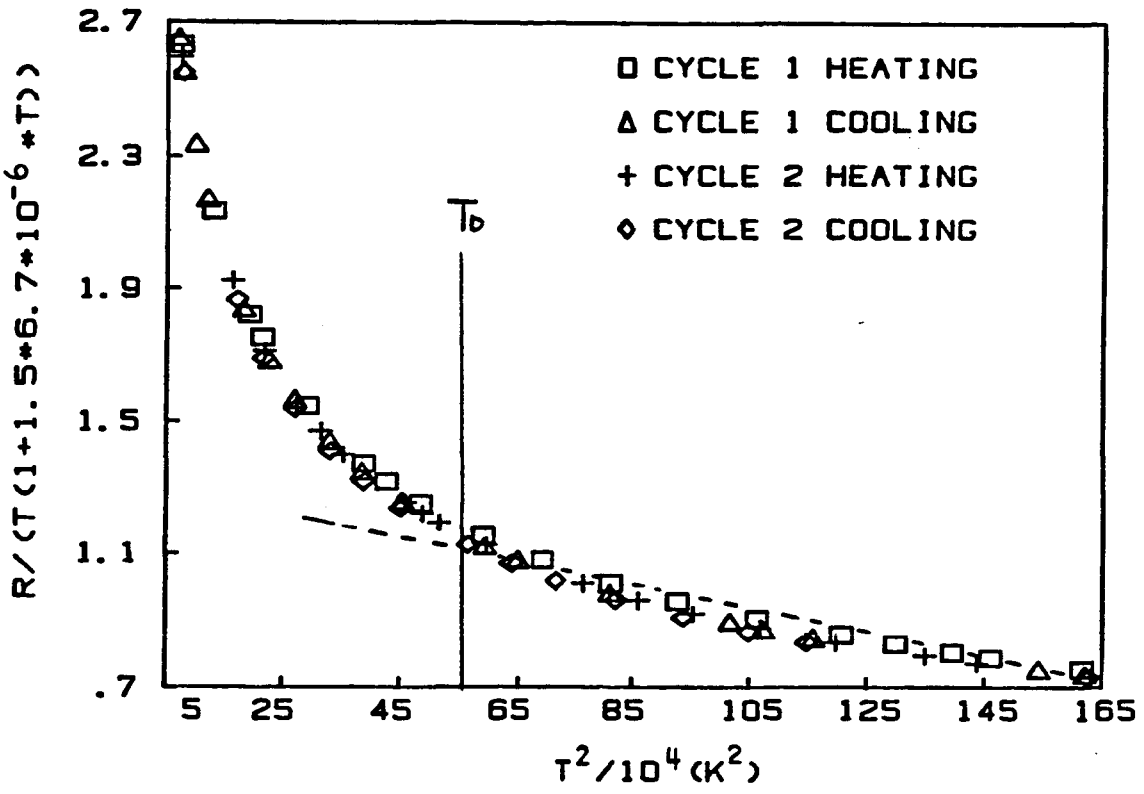

Fig. 5-34. A plot of $R(T(1+6\beta\gamma T)^{-1}$ versus T^2 for ZrC

for 4 hours sojourn after cycle 2 heating. Based on these low values this material was considered to be a good candidate material for high temperature resistance strain gage application.

The crystal structure of this ZrC film was examined by X-ray diffraction. It was found that this ZrC film had FCC structure with lattice parameter of 4.701 Å. Comparing this value with that of Storms [53], shown in the Appendix D, this ZrC_x specimen had a composition either $ZrC_{0.76}$ or $ZrC_{0.9}$.

5.3 Discussion

The experimental results for the transition metal compounds mentioned in the previous section are summarized in Table 5-2. The results suggest the following:

(1) The resistivities (ρ) of these compounds increased with increasing the vacancy concentration (N_v). However, the increase in resistivities with increasing vacancy concentration was much larger in TiN_x than in TiC_x. This result is mainly due to the fact that in TiN_x the concentration of charge carriers (n) decreased as N_v

Table 5-2

Summarized results for transition metal compound MX_x

Specimen	P_N2 (μtorr)	X/M		Resistivity (μohm-cm)	TCR (ppm/°C)	DR (%/hr)
TiN(HCD)		1		30.5	588	0.14
(CVD)		0.9	(V_N)	1130	143	0.22
ZrN-1	114	≈1	(V_N)	180	275	-0.26
-2	108	<1	↓	211	228	-0.36
-3	96	<<1	↓+	255	184	1.6
-4	990	≈1.10	(V_{Zr})	393	212	-0.54
TaN-1	330		↑+	113	255	0.53
-2	375		↑	103	301	0.5
-3	600		(V_N)	165	438	-0.16
CrN				13.8	710	2%
TiC(ARE)		≈1		39.4	338	0.06
(CVD)		0.8	(V_C)	169	210	-0.5
ZrC		0.76 or 0.9	(V_C)	560	180	-0.13

* TCR and DR values are based on the data of 1000°C, and DR were measured after cycle two heating.

increased, while in the case of TiC_x, the concentration of charge carriers increased as N_v increased, and in both compounds, the mobility (μ) decreased with increasing N_v (based upon our Hall measurements results and others [77]). Apparently the vacancy scattering which results in decreasing the mobility offsets sufficiently the increase in charge carriers with increasing carbon-deficient in the case of TiC, since $\rho=1/ne\mu$.

(2) The TCR of these transition metal compounds decreased as the resistivities of the compounds increased. This is illustrated in Fig. 5-35 and this relation between the TCRs and resistivities of specimens is similar to that of Mooij's model [28] for strongly disordered metallic alloys mentioned in chapter 3 (see Fig. 3-1). In the case of these transition metal compounds, high scattering which is caused by the high concentration of vacancies, resulted in high resistivity and low TCR. Extrapolation of the data in Fig. 5-35 suggests that TCR passed through zero at resistivity of about 800-1000 microohm-cm.

(3) The TCR of the stoichiometric carbides were lower than those of their corresponding stoichiometric

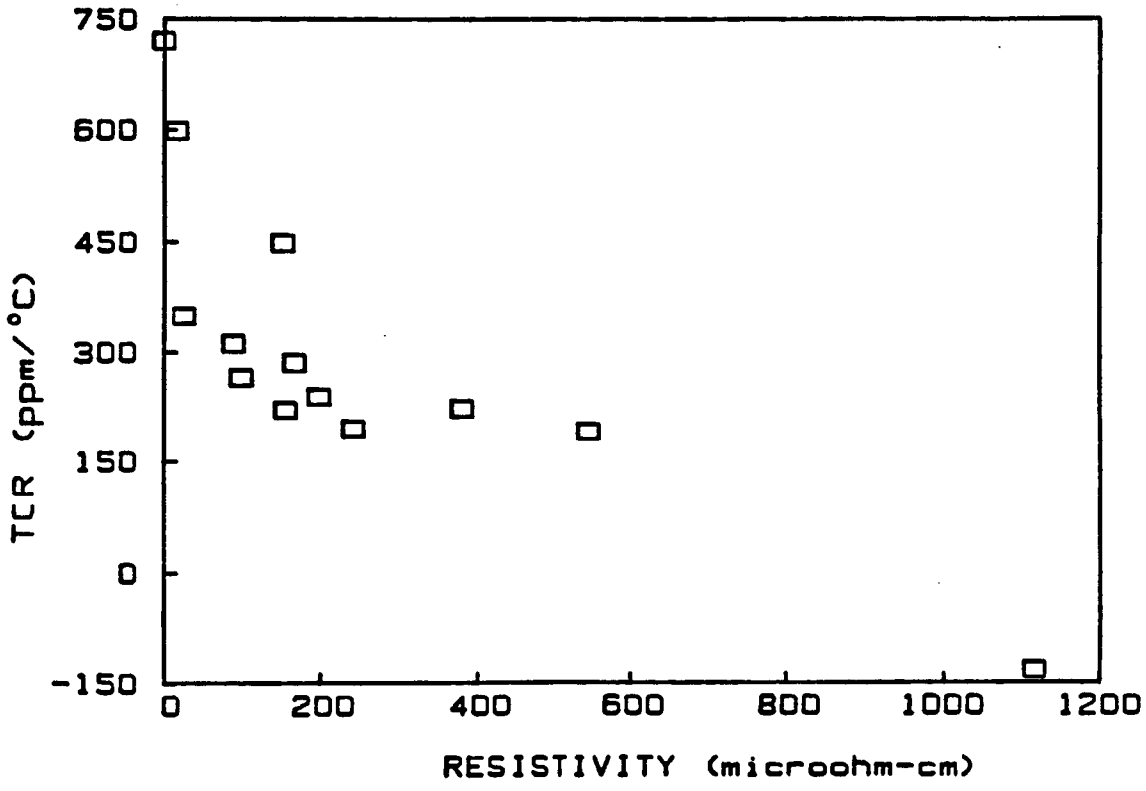

Fig. 5-35. The temperature coefficient of resistance versus room temperature resistivity for transition metal compounds.

nitrides, for examples, TCR of TiC was lower than that of TiN and TCR of ZrC was lower than that of ZrN, as shown in Fig. 5-36. In the figure, TiC (ARE) TiN (HCD) and ZrN-1 all had composition near stoichiometry. Although ZrC was not stoichiometric, it was the only ZrC sample we had, therefore, we used it for comparison. In addition, the TCR of a transition metal nitride (or carbide) at 1000^{o}C decreased with an increase in the vacancy concentration, this may be due to the strong vacancy scattering which compensates phonon scattering.

(4) The TCR of stoichiometric ZrN was lower than that of stoichiometric TaN, which itself was lower than that of stoichiometric TiN which has a TCR value smaller than that of CrN, i.e., $TCR_{ZRN} < TCR_{TaN} < TCR_{TiN} < TCR_{CrN}$, as presented in Fig. 5-37. TCR of ZrC is lower than that of TiC as shown in the Fig. 5-38. These results indicate that the the TCR of transition metal nitrides and carbides with transition metals in the same column of the period table decreased as quantum number of the transition metal increased. Also the TCR of transition metal nitrides decreased monotonically as going from compounds of metal of group VI to those of group V then to those of group IV of the period table.

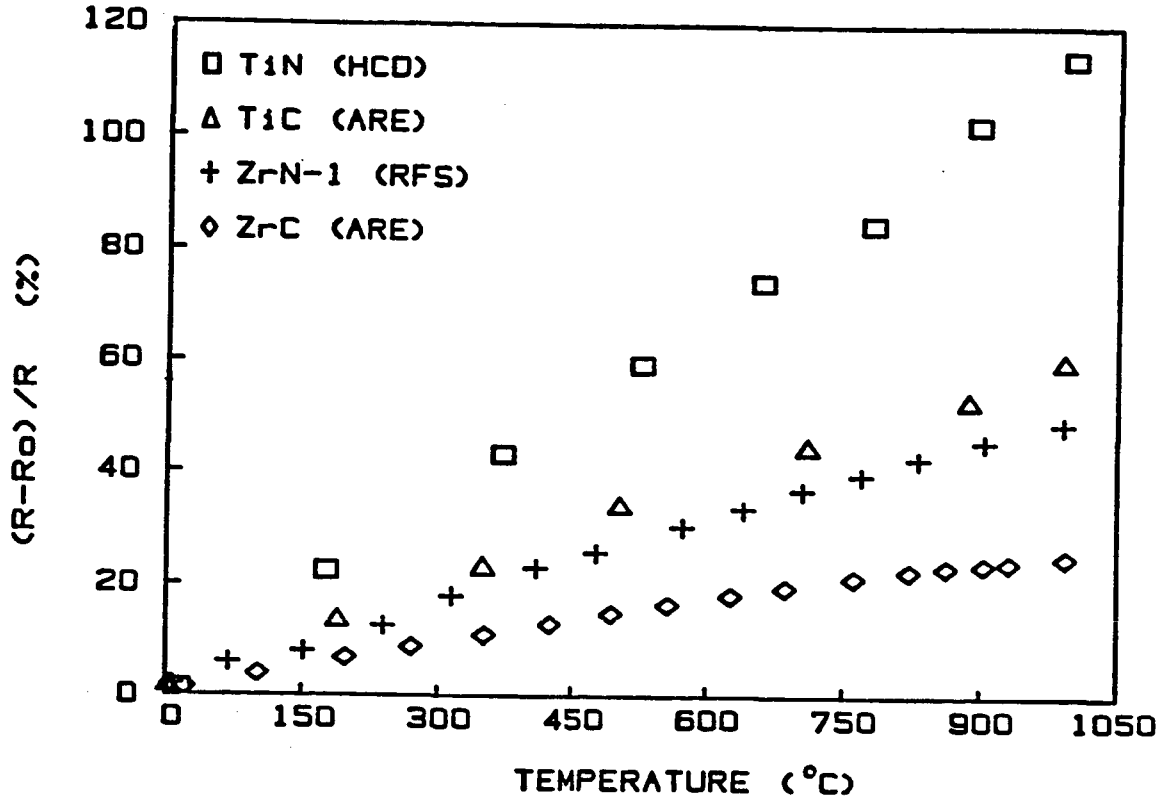

Fig. 5-36. Comparison the resistance change with temperature for TiC and TiN, ZrC and ZrN. Resistance is normalized to its value at room temperature.

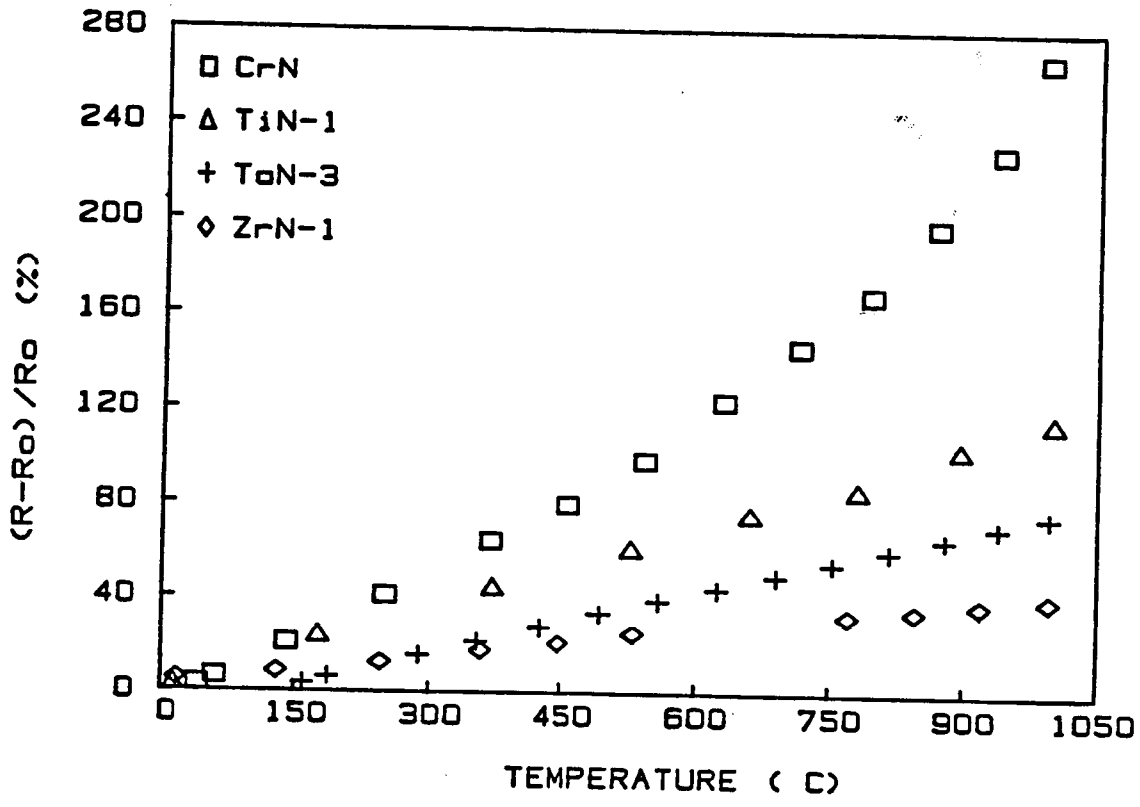

Fig. 5-37. Comparison the change in resistance with temperature for four nitrides. Resistance is normalized to its value at room temperature.

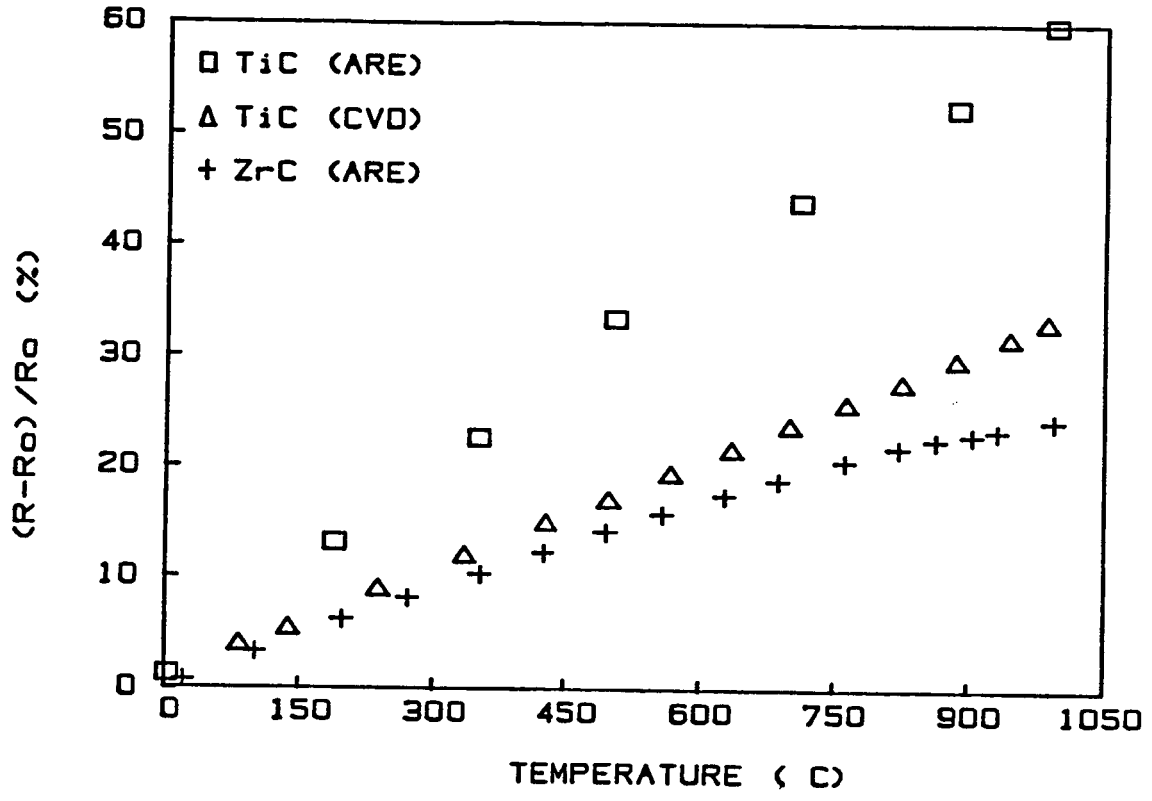

Fig. 5-38. Comparison the change in resistance with temperature for two carbides. Resistance is normalized to its value at room temperature.

(5) High temperature resistance saturations were observed in the ZrC and ZrN systems. These two samples had larger resistivities (in the range of 180 and 560 microohm-cm) that resulted from stronger vacancy scatterings among all of the specimens studied except microohm-cm and resulted in a negative TCR.

(6) The presence of both a small TCR and a small DR value seemed to be mutually exclusive. However, the source of the high temperature resistance drift for the materials investigated was not ascertained. Note that pure platinum also displayed a high temperature resistance drift ($\approx$ 0.2 %/hr).

In order to truly understand the conduction mechanisms of transition metal carbides and nitrides and to make a systematic analysis, we needed more data on some of these materials and therefore it was necessary to adopt the results of other investigators on these group of materials.

As mentioned in the beginning of this chapter, these transition metal nitrides and carbides are of

particular interest, because, on one hand they have high melting temperatures and are ultra hard, properties typical of covalent compounds. On the other hand, they show metallic luster and have high thermal and electrical conductivities. Many of these compounds crystallize in the NaCl structure, typical of ionic crystals. Since some experiments indicate that there is some charge transfer, these compounds actually combine covalent, metallic and ionic binding [55]. Although this has been generally agreed on, there are numerous contradictory theories on the extent or importance of each of these factors in these compounds. In spite of the considerable amount of theoretical work have been carried out, no single theory has been totally successful in explaining their properties. In addition, the question as to whether these materials are metals or semiconductors is unresolved and remains a controversial subject still under study.

Bilz [71] calculated the first band structure for TiC and TiN using a simplified linear combination of the atomic orbitals (LCAO) method. He found that the M-X bonds to be more important than M-M bonds, but, in addition to the covalent aspect, a charge transfer from the metal to nonmetal takes place. A large but opposite

charge transfer was obtained by Costa and Conte [72] and by Samsonov [73], who favored M-M bonding and completely neglected the M-X interaction.

Samsonov and Sinelnikova [74] reviewed previous analyses of the transition metal compounds for the years 1930-1960 and pointed out that the TCR of metal carbides generally decreases as one go from metals in group IV to group V and then to group VI of the periodic system. They compared this with the decrease of the accepter ability of d electron levels of metallic atoms in this series. They asserted that the TCR of silicide is considerably higher than that for the corresponding borides, than carbides, finally nitrides, i.e., $TCR_{MSi2} > TCR_{MB2} > TCR_{MC} > TCR_{MN}$. They related this behavior to the greater ease of detachment of electrons from silicon atoms than from boron atoms, carbon atoms and finally nitrogen atoms, comparing to the difference in their ionization potentials (8.151, 8.298, 11.26, 14.53 eV, respectively). Since his conclusion was based mainly on the M-M interaction, and assumed that the nonmetal atoms donate electrons to the M-M metallic bonds, but totally disregarded the M-X interaction, his model is not accepted today.

Recently, Dunand, Flack and Yvon [76] used high-precision, high-resolution x-ray diffraction measurements to study TiC and TiN refractory compounds. Their analysis showed that ionicity is important, with a charge transfer from the metal to the nonmetal of 2.14e in the carbides and 1.94e in the nitrides. They suggested that the metal-to-metal bonding is similar in TiC and TiN while the metal-to-nometal bonding has greater strength in TiC than in TiN. Maayer and Mackenzie [77] who studied the TiC_x and TiN_x thin films by Hall measurements found that the concentration of electrons increased with decreasing C-content but in the case of the nitride it decreased with decreasing nitrogen content and they concluded that the charge transfer in the TiN occurred from the nitrogen to the titanium atom, while in TiC, the titanium atoms gave up electrons to carbon atoms. Our experimental results of Hall measurements for TiN and TiC supported this argument.

In order to understand the basis of the electrical properties for these materials, a study on the electronic structures of these materials and the changes in electronic structures with the vacancies concentration in these crystal lattices are necessary. Electronic band

structures have been calculated for many stoichiometric transition metal carbides and nitrides. These calculations have been summarized in two review articles by Calais [75] and Neckel [55]. From these reviews the band structures of the transition metal compounds studied in this work are shown in the Figs. 5-39 and 5-40. As a result, which is well confirmed by various experimental measurements, most of the band structure calculations produce a narrow low-lying valence band which is predominantly formed by metalloid 2s states (metalloid 2s band) and is separated by a gap from a set of valence bands resulting from the interaction of metalloid 2p with metal d states. The energetically lower part of these bands corresponding to bonding metalloid-p metal-d interactions (metalloid 2p band) is separated by a deep valley in the density of states (DOS) from the higher part of these bands (metal d bond). This latter part corresponds mainly to the metal-d metal-d bonding, to nonbonding metal d states and also to antibonding metal-d metalloid-p interactions. Therefore, the valence electrons for transition metal compounds can be divided into two groups: (1) electrons essentially localized in Me-X bonds, which play a crucial role in determining lattice properties of the compounds, high melting points,

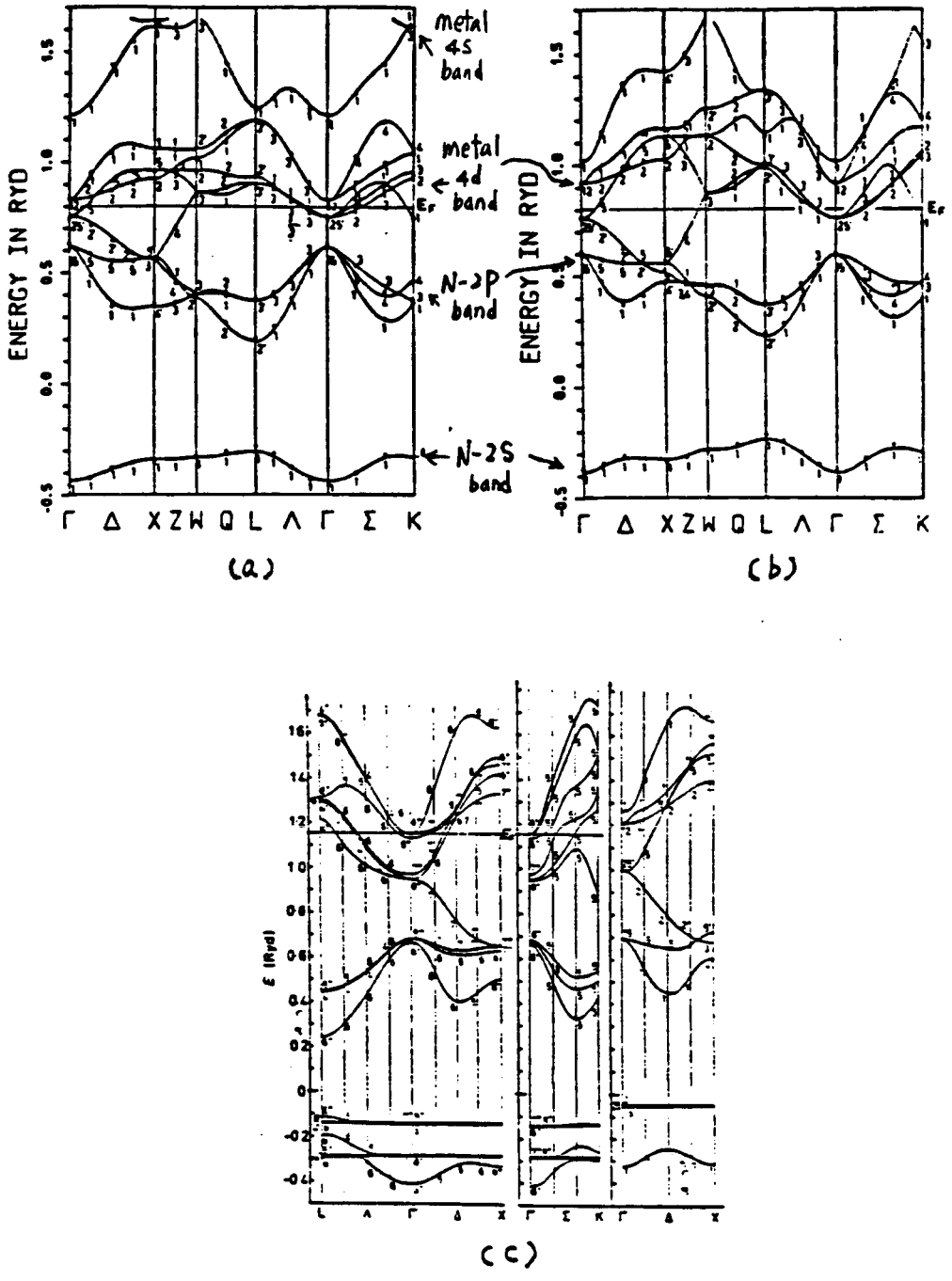

Fig. 5-39. The electronic band structures for TiN (a), ZrN (b) (after Dorrer et al. [117]) and TaN (c) (after Weinberger et al. [112]).

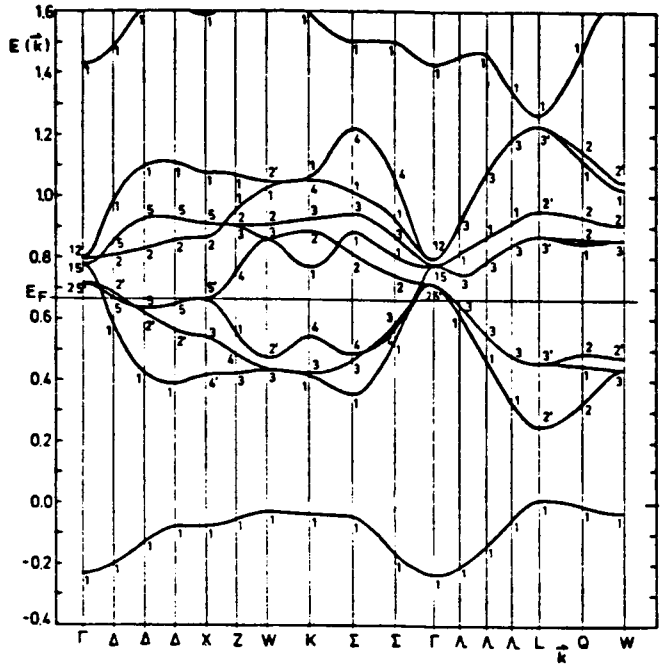

(a)

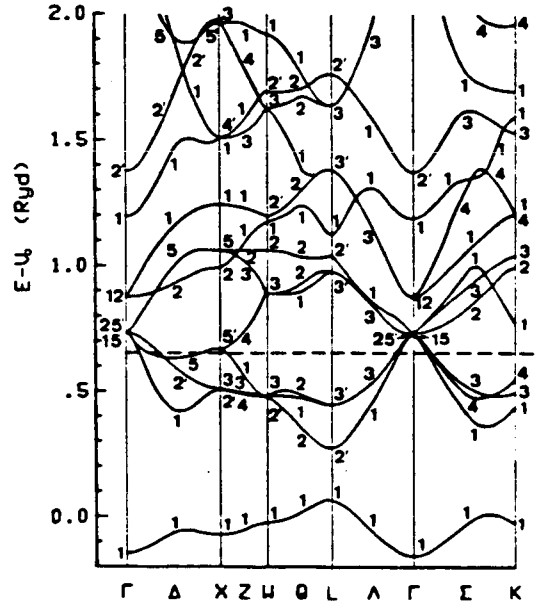

(b)

Fig. 5-40. The electronic band structures for TiC (a) (after Calais [75]) and ZrC (b) (after Schwarz et al. [113]).

hardness etc., (2) electrons in the d-like high-energy states, which are responsible for "electronic" properties [78].

Neshpor and Samsonov [79] studied the electrical properties of molybdenum silicides and quantitatively derived a relation between electronic heat capacity, density of states at the Fermi level $N(E_F)$ and TCR. For a material with a low density of electron states in the conduction band, the scattering probability of the charge carriers is low and therefore carrier mobility is high, which results in low TCR value. Since the determination of $N(E_F)$ is possible with the electronic specific heat constant γ, then we can relate $\gamma \propto N(E_F) \propto$ TCR.

This theory has also been supported by Nemchenko [61] in his study of the nitride interstitial phases. He suggested that the increase in electrical resistivity with the increase in temperature should be greater for conductors with larger $N(E_F)$, which result from a larger heat capacity constant γ. For the nitrides of group IV metals, γ is appreciably higher compared to the carbides of these metals, while in group V this difference virtually disappears, This predicts that nitrides will

have a higher TCR than carbides. This is consistent with the density of states calculations presented in Figs. 5-41 and 5-42. From these figures, it is seen that nitrides of titanium and zirconium, have larger $N(E_F)$ (10.28 and 10 states/Ry unit cell, respectively) than those of their corresponding carbides (3.57 and 3.125 states/Ry unit cell, respectively), while the difference between the $N(E_F)$ of NbN (8,66) and NbC (8.33) is not significant. Therefore, nitrides of Ti and Zr should have greater TCR than their corresponding carbides, while the TCR of NbC and NbN should be about the same. This is confirmed by our experimental results, which indicated that TCR of TiC to be lower than that of TiN, and TCR of ZrC to be lower than that of ZrN (shown in Fig. 5-36). Also noted that the $N(E_F)$ of ZrC (3.125) is smaller than that of TiC (3.57), and $N(E_F)$ of ZrN (10) is smaller than that of TiN (10.28), Fig. 5-41. This is also consist with our experimental results as shown in Fig. 5-37 and 5-38.

All of the existing band structure calculations as well as data on electronic specific heat and magnetic susceptibility in these transition metal stoichiometric compounds have indicated a minimum in the density of states at Fermi level which means minimum TCR for the group IV carbides [80].

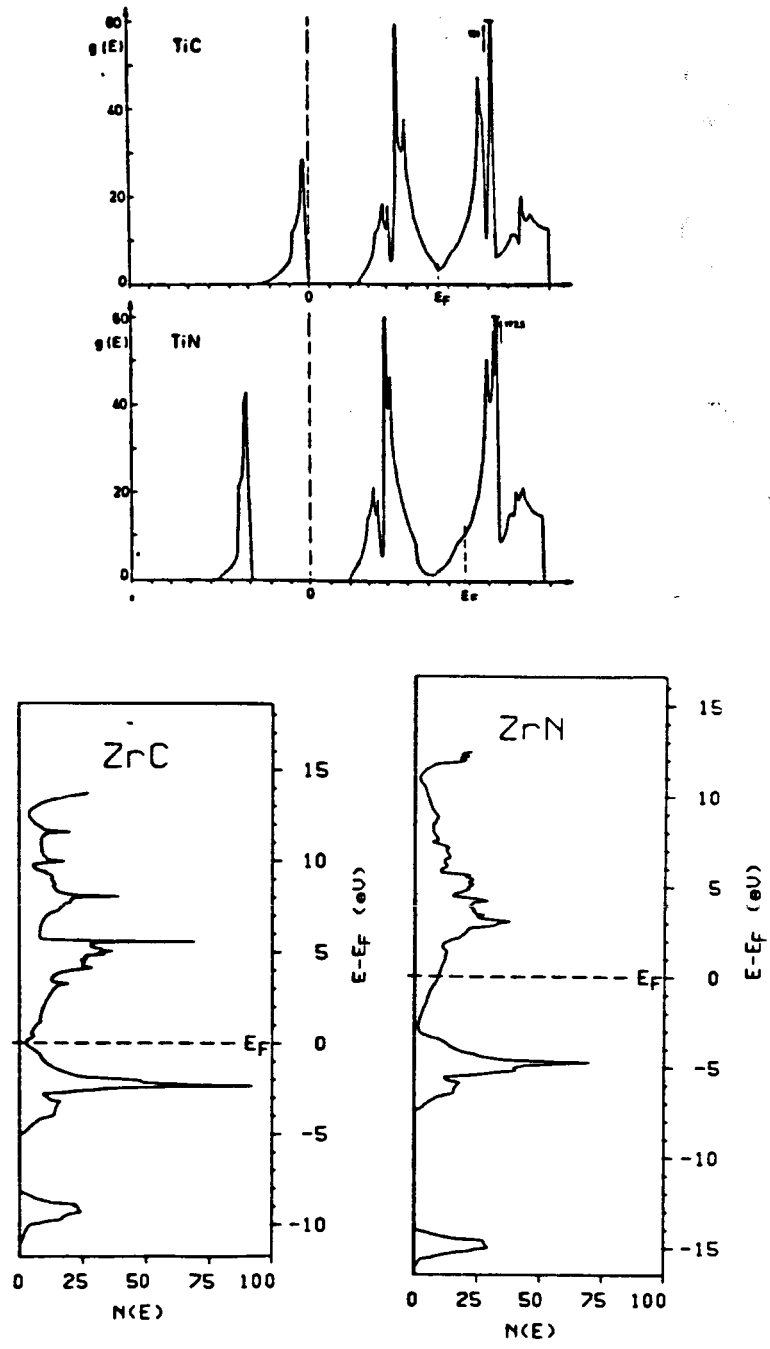

Fig. 5-41. Comparison the density of state at the fermi surface E_F for titanium nitride and carbide (after Calais [75]), zirconium nitride and carbide (after Schwarz [113]).

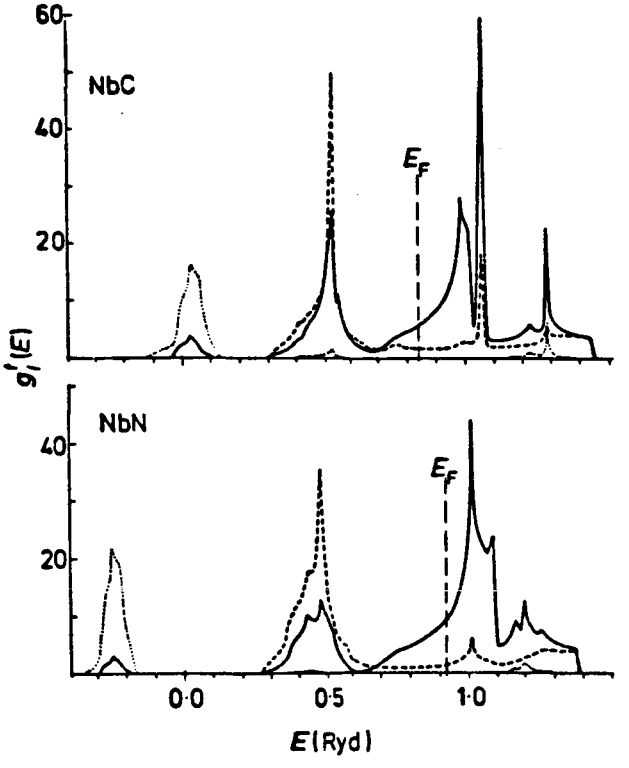

Fig. 5-42. Comparison the density of state at the fermi surface for niobium nitride and carbide (after Schwarz [114]).

In 1980s, results of photoemission spectra of stoichiometric and substoichiometric titanium nitrides [81,82] and niobium carbides [83] showed that a vacancy peak situated in the DOS minimum between metalloid p and metal d band develops with increasing vacancy content in the lattice. Furthermore the Fermi levels of these compounds do not change with increasing vacancy content (see Fig. 5-43). The experimental results of soft X-ray emission spectra [84] and electron energy-loss spectra [85] of substoichiometric titanium carbides and nitrides also suggest the presence of so called "vacancy states" in order to keep the Fermi level fixed when nonmetal atoms are removed from the lattice.

Such a peculiarity of electronic structure enables us to understand the variation of physical-chemical properties of transition metal compound (MX_x). The density of states for some non-stoichiometry transition metal compounds are presented in Figs. 5-44 and 5-45. As can be seen the presence of nonmetal vacancies results in increases in the density of states at the Fermi energy level $N(E_F)$. The consequence is an increase of magnetic susceptibility value X, electronic specific heat γ, and

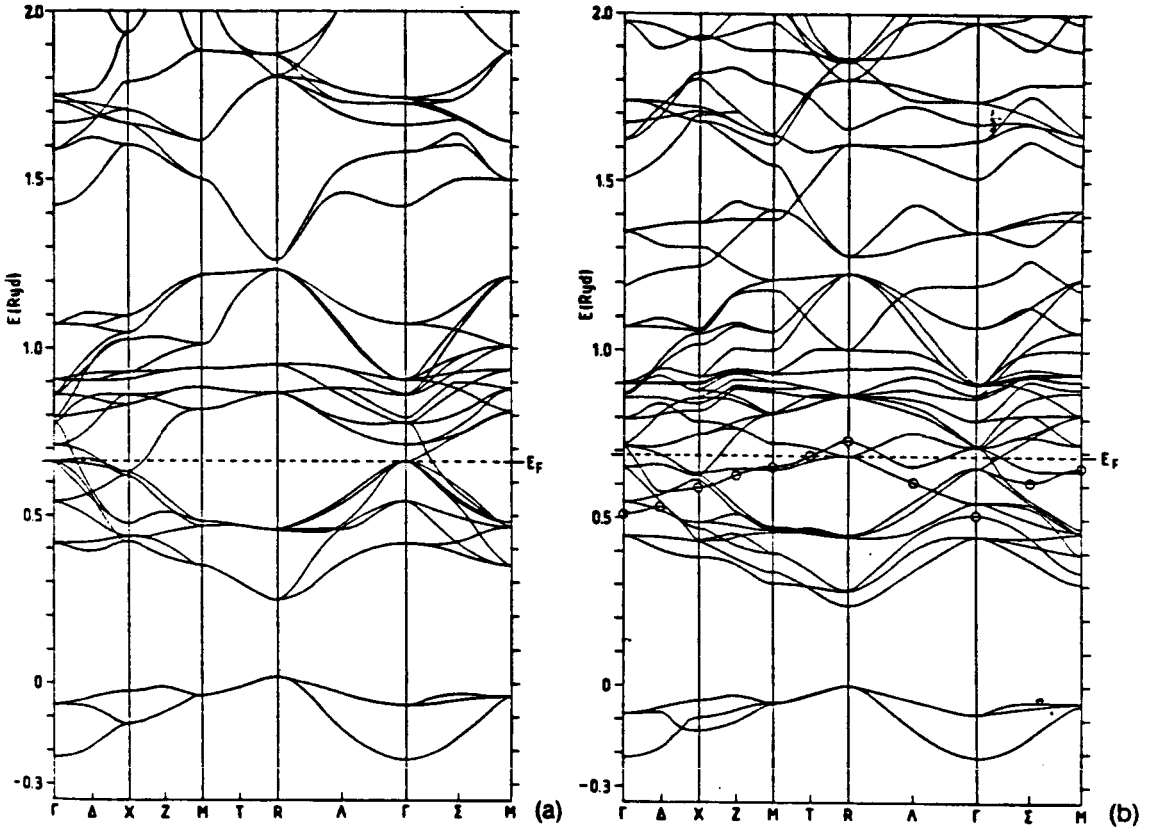

Fig. 5-43. Band structure of TiC (a) and substoichiometric $TiC_{0.75}$ (b) with respect to the constant muffin-tin potential between the spheres. So-called "vacancy states" are encircled in Fig.(b) (after Redinger et al. [115]).

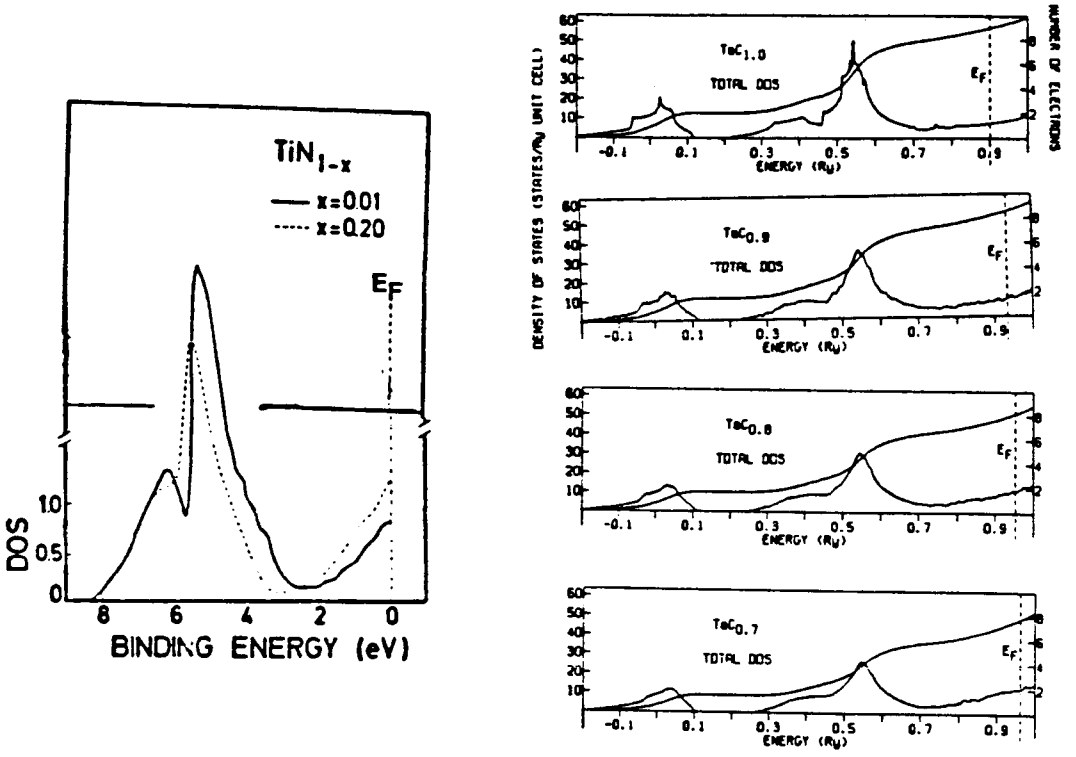

Fig. 5-44. The densities of states for TiN (solid line) and $TiN_{0.8}$ (dashed line) (a) (after Porte et al. [82]) and TaCx (b) (after Klein [116]).

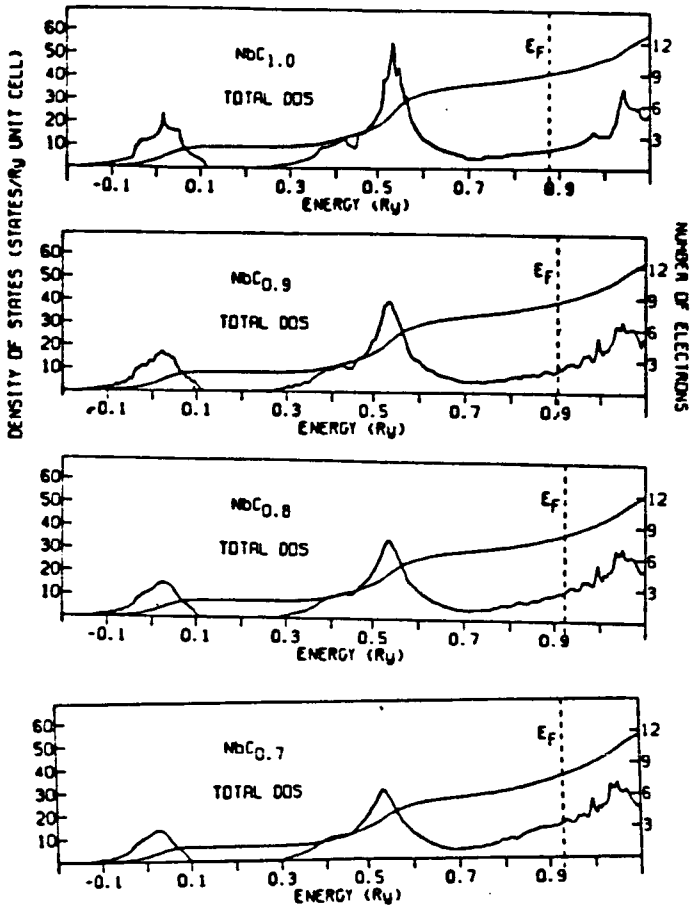

Fig. 5-45. The densities of states for NbCx (after Klein [116]).

TCR. In the present work this behavior was found only in the ZrN system at low temperatures, where its TCR increased as vacancy concentration increased. However, at high temperatures this is not the case for ZrN or other materials. This is because the band structures were calculated for T=0 K and hold only for low temperatures. We infer from the resistivity measurement that the ZrN system had a stronger vacancy scattering than other compounds so the vacancy effect at higher temperatures is more important in this material than in other materials. At high temperatures the resistance thus the TCR of the specimens induced from both temperature and vacancy effects must be considered together.

As has been noted, the dependence of the residual resistivity on defect structure does not follow the simple linear rule for TiN_x. Instead, an exponential behavior was observed [77]. Matthiessen's rule [Eq. (3-1)] is therefore of the form:

$$\rho = \rho_O + \rho_T = a + b\,T + c\,\exp(d\,N_V) \qquad (5\text{-}2)$$

where a, b, c and d are constants, and Nv is the vacancy concentration. For TiC the linearity relation holds [77], and the Matthiessen's rule is written as

$$\rho = \rho_O + \rho_T = a + b\,T + c\,N_V \qquad (5\text{-}3)$$

However, when the vacancy concentration (N_v) is high (Nv > 10%) the simple forms of Matthiessen's rule, which considers the resistivity of defects to be temperature independent, do not hold. Dy and Williams [86] studied the vacancy effects on the electrical properties of NbC system, and Shacklette and Williams [80] studied this effect in VC system, they both claimed that vacancy scattering is important at low temperatures but not at high temperatures. They found that the curve of resistivity versus temperature fitted either of the empirical expression

$$\rho(T) = \rho(\text{ideal}) + c' \exp(d'/T) \qquad (5\text{-}4)$$

or a "parallel resistor" formula

$$1/\rho(T) = 1/\rho(\text{ideal}) + 1/\rho(\text{max}) \qquad (5\text{-}5)$$

where $\rho(\text{ideal}) = \rho_o + b'T$, ρ_o is the residual resistivity, b', c' and d' are fitting parameters, and ρ_{max} is the apparent saturation value of the resistivity at high temperatures. Fisk and Webb [87] have called this effect "saturation" and argue, as does Mooij [28], that this effect is associated with the mean free path decreasing towards a minimum value - the interatomic spacing a.

This saturation effect was also observed in this work for ZrN and ZrC systems. In order to ascertain whether observed data for these systems also satisfied Eq. (5-5), plots of $(R_{max} \times R)/(R_{max}-R)$ versus temperature for ZrN and ZrC were made, taking ρ_{max} as 1000 microohm-cm (from Fig. 5-35). These plots are shown in Figs. 5-46 and 5-47, respectively. Straight lines were expected and are indeed observed. The magnitude of the resistivity saturation value ρ_{max} was larger than that suggested by Mooij [28]. This is due to the smaller mean free path which results from the larger vacancy concentrations in these compounds. The mean free path of the materials is proportional to the reciprocal of defect concentration [49].

When the resistivity of material is larger than the saturation value, one would expect negative TCR as suggested by Mooij [28]. This is observed in the case of $TiN_{0.9}$ in the present work, Fig. 5-3. As discussed in the Section 5.2.1., $TiN_{0.9}$ had resistivity of 1130 microohm-cm, which was larger than 1000 microohm-cm, and its electrical behavior followed Eq. (5-1), which was the same as Eq. (5-4). At low temperature, the exponential term of the Eq. (5-1) dominated and a decrease in

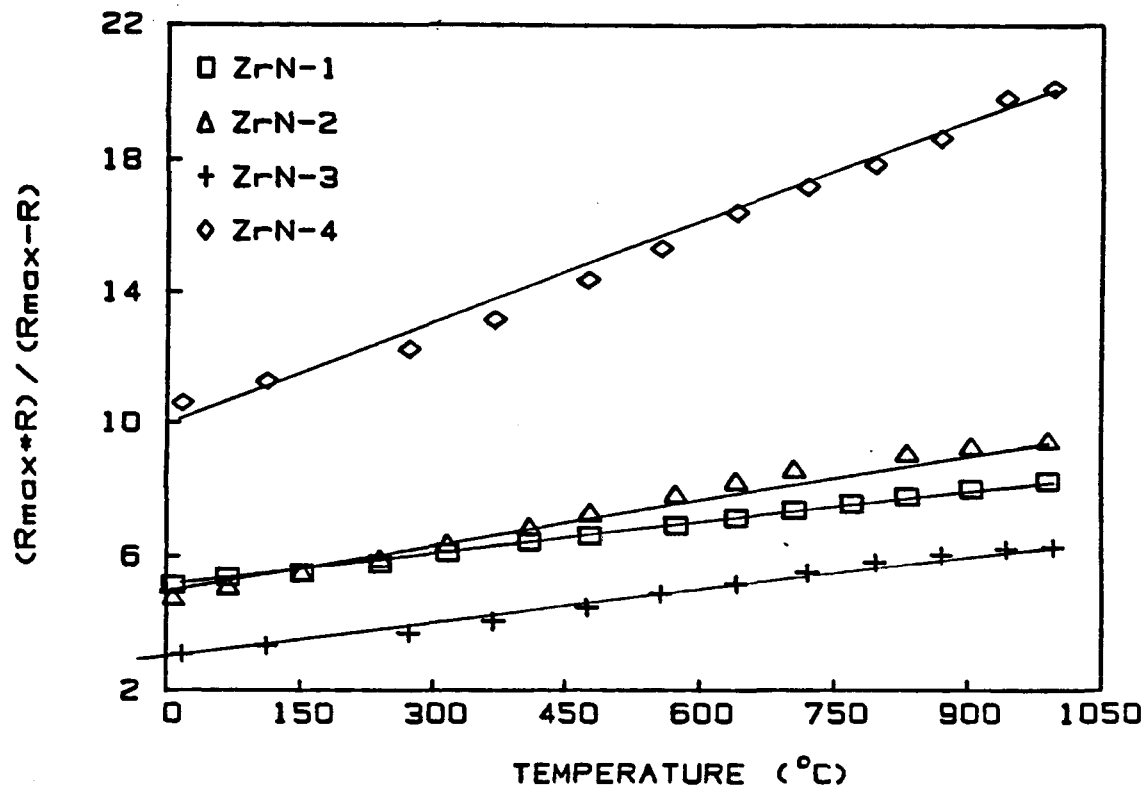

Fig. 5-46. A plot of (Rmax x R)/(Rmax-R) versus T for four zirconium nitrides. Rmax correspondes to ρ_{max}=1000 microohm-cm.

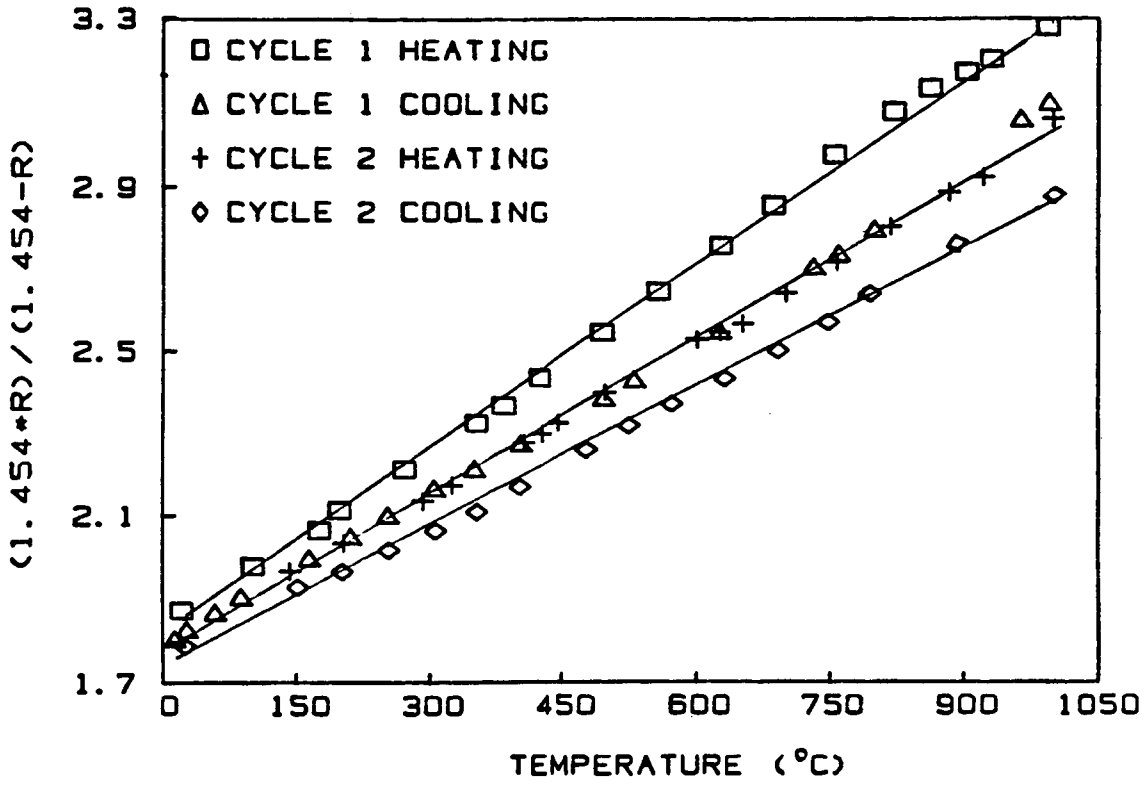

Fig. 5-47. A plot of (1.454xR)/(1.454-R) versus T for zirconium carbide. Rmax=1.454 ohm correspondes to ρ_{max} = 1000 microohm-cm.

resistivity with an increase in temperature was observed. While at higher temperature the second term of the Eq. (5-1) became more important and an increase in resistivity with increasing temperature was observed. Since most of the previous work on transition metal compounds was conducted in the low temperature range, where the resistivity decreased with temperature, the behavior were therefore characterized as semiconducting. However as shown for $TiN_{0.9}$ while the resistivity initially decreased with temperature, it increased at higher temperatures.

Although the order-disorder transition was not observed for materials studied in this work, it does occur in some of the transition metal compounds [118, 119]. The transition temperatures, the range of compositions for ordered phases and some phase diagrams concerning the order-disorder transitions for transition metal compounds are attached in Appendix E. Materials for resistance strain gage application should have compositions with no order-disorder transition in the entire range of the operating temperatures.

5.4 Summary

From this study we conclude that the resistivities of transition metal carbides and nitrides increased and their TCR decreased with increase in vacancy concentration. Resistivity saturated at $\rho_{sat} \approx 1000$ microohm-cm, suggesting the electron mean free path was saturated at its lowest limit- the interatomic spacing. For resistivities larger than 1000 microohm-cm, negative TCR values were observed. Therefore, we suggested that these compounds are metallic in nature, and the semiconducting behavior observed for some specimens are due to the high vacancy concentration in these materials, which results in higher resistivity than the saturation resistivity.

Materials with small electronic specific heat constants had low density of states at the Fermi levels, and therefore had low TCR values. Among the stoichiometric carbides and nitrides, carbides had lower TCR than nitrides, Group IV carbides had the lowest TCR, and TCR of ZrC was smaller than that of TiC.

CHAPTER 6

RESULTS AND DISCUSSION ON THE ELECTRICAL RESISTANCE MEASUREMENTS FOR SEMICONDUCTORS

6.1 Introduction

Traditional semiconductor resistance strain gages are made of silicon or germanium, which have band gaps of 1.11 and 0.67 eV, respectively. In order to extend the working temperature of the strain gages to higher temperatures, semiconducting materials with band gaps larger than 1.11 eV are therefore needed. α-Silicon carbide, β-silicon carbide and boron carbide with band gaps of 2.86, 2.3 and 2.5 eV, respectively, were chosen for this study. Their intrinsic conductions all occur at temperatures above 1000^{o}C.

Boron carbide and silicon carbide have the highest chemical resistances among the refractory carbides. They are not decomposed by mineral acids or mixtures of them, including the mixture of nitric and hydrofloric acids which decomposes almost all the transition metal carbides (except those of chromium). The high chemical resistance of the boron and silicon carbides may be attributed to

the strong covalent bonds between the atoms of carbon and boron or silicon and to the very low concentration of unlocalized electrons. This property makes these compounds suitable for application in the severe environment.

6.2 Boron Carbide

The boron carbides $B_{1-x}C_x$ in the composition range of $0.1 \leq x \leq 0.2$ represent a class of single-phase solids with remarkable mechanical and electronic properties [88]. They are believed to crystallize in a rhombohedral structure $R\bar{3}m$ consisting of a twelve-atom deformed icosahedra shared at the corners of the unit cell and a three-atom chain, containing one or more carbon atoms, along the cell diagonal connecting the icosahedra [89,90] (see Fig. 6-1). The boron carbides are highly stable (melting temperature $\approx 2470^{\circ}C$) and have high electrical conductivities and Seebeck coefficients as well as low thermal conductivities [89]. These features have stimulated considerable interest in these materials for possible applications in efficient high-temperature thermoelectric generators. More generally, these materials have potential applications as very- high -

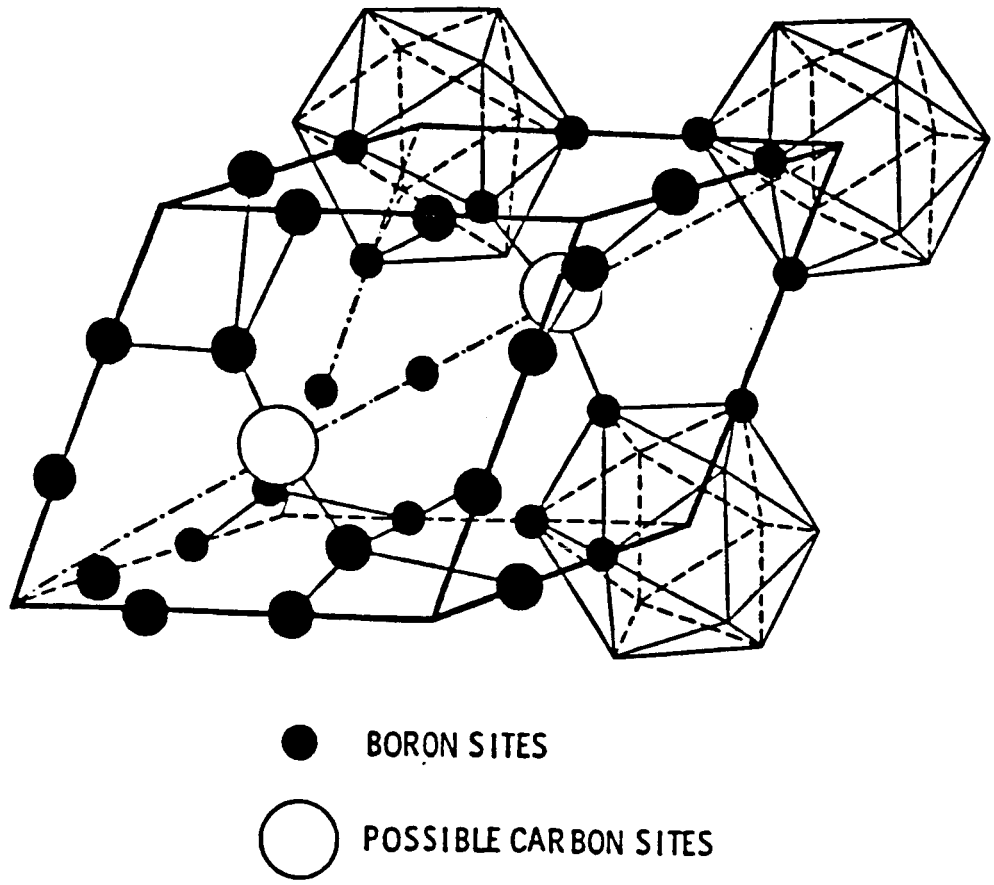

Fig. 6-1. Crystal structure for boron carbide; carbon atoms are distributed among open circles and within icosahedra (after Wood and Emin [89]).

temperature semiconductors.

The change in resistances with temperatures for a hot pressed B_4C was first measured under vacuum during two cycles of heating and cooling. These data are shown in Fig. 6-2, a decrease of the resistance with increasing temperature was observed. Furthermore, the resistance was altered somewhat with thermal cycling, the magnitudes and directions of the changes depended on the temperature and previous history of the sample, this is shown in the Fig. 6-3, which is an expanded scale of the high temperature section of Fig. 6-2. These changes, amounting to at most 4 %, occur on thermal cycling to temperatures in the vicinity of, or above, a knee in resistance curves occurring at about 750^{o}C and above.

A resistance which decreases in an activated manner with temperature can arise from two causes. First, it can, as in conventional high-mobility semiconductor, be ascribed to an increase in the carrier density with temperature. In this situation the resistance (R) decreases with temperature (T) as

$$R = A\exp(Eg/2kT),$$

where A is a constant, Eg is the band gap of the

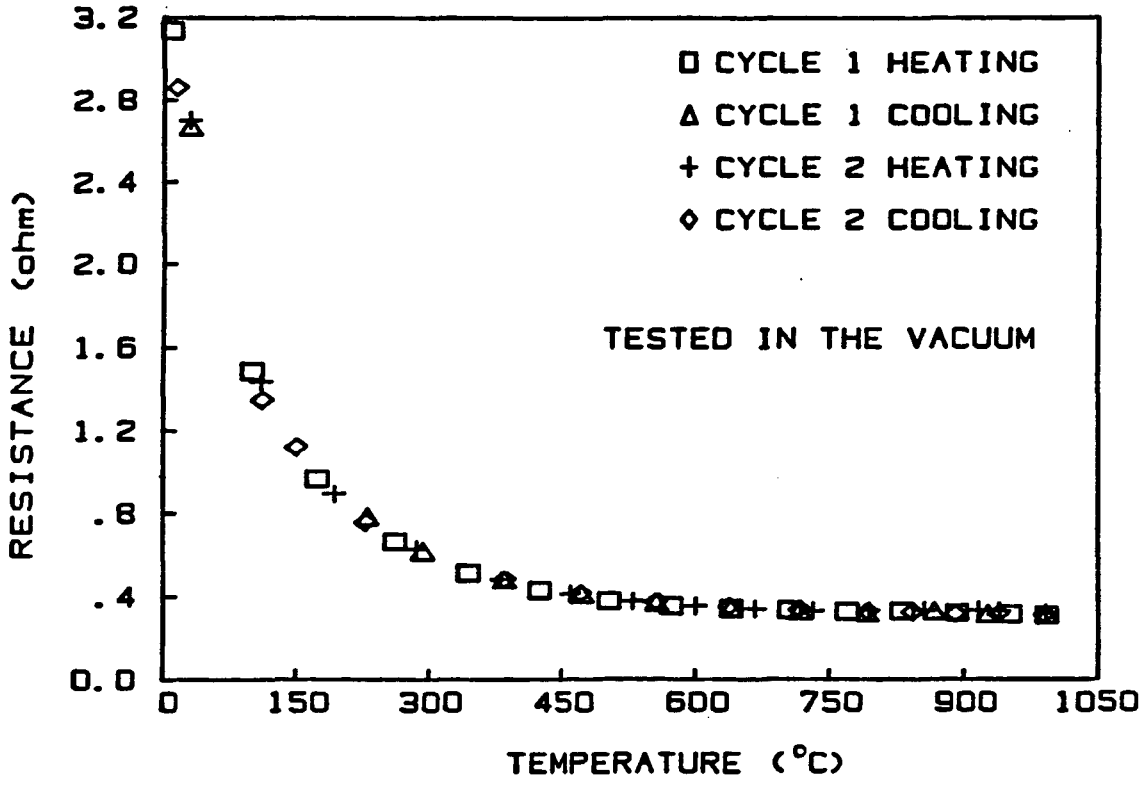

Fig. 6-2. Variation of resistance with temperature for hot pressed boron carbide tested in the vacuum.

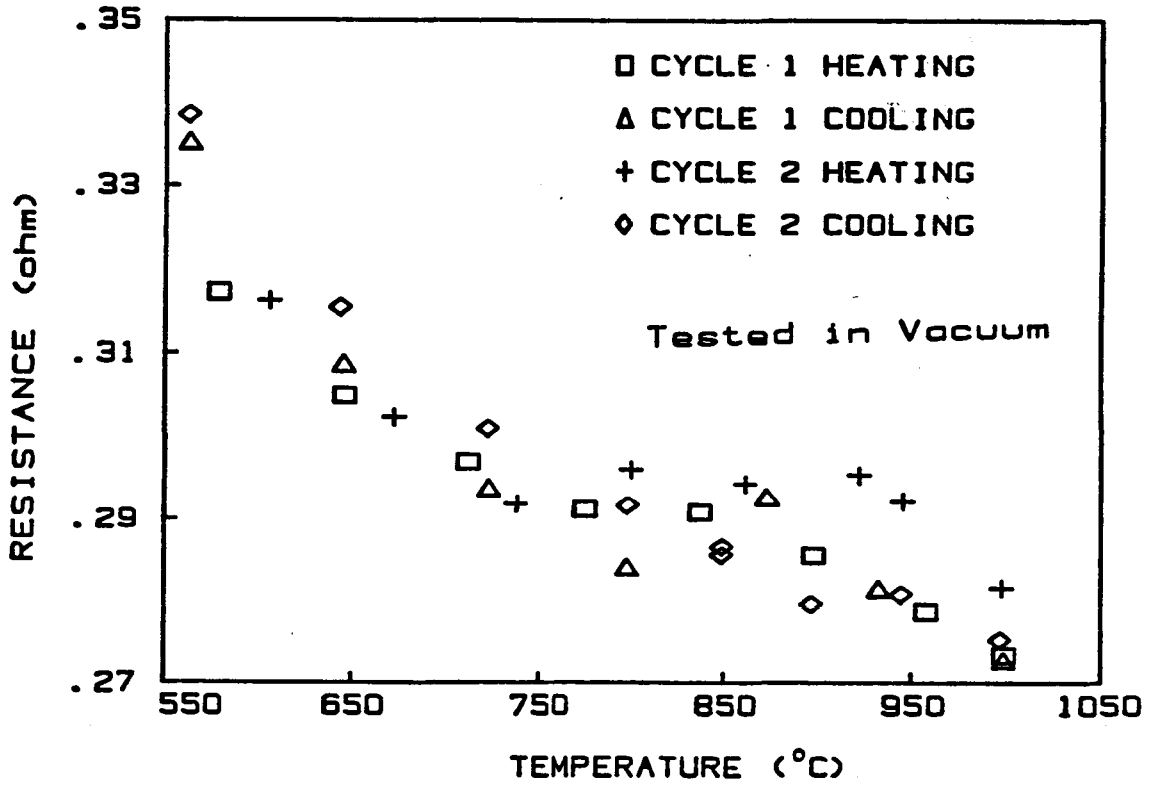

Fig. 6-3. Expansion of the high temperature region of Fig. 6-2 for boron carbide tested in vacuum.

specimen, and k is the Boltzman constant. The second possibility is that electronic transport proceeds via low-mobility hopping of a temperature-independent density of small-polaronic charge carriers. The carrier mobility varies as $T^{-n}\exp(-E_A/kT)$ where E_A is the activation energy for hopping, and n is either 3/2 or unity depending on whether the hopping is nonadiabatic [91] or adiabatic [92]. Thus, the resistance falls with increasing temperature as $R = A\,T^{n}\exp(E_A/kT)$.

In order to understand the electrical conduction mechanism of boron carbide, plots of log(R) and log(R/T) versus reciprocal temperature (1/T) are drawn in Figs. 6-4 and 6-5, respectively. A straight line is found in Fig. 6-5 but not in the Fig. 6-4, therefore, the change in resistance of B_4C with temperature followed a form of

$$R = AT\exp(E_A/kT) \qquad (6\text{-}1)$$

with activation energy E_A of about 0.14 $\pm$ 0.005 eV. The form of this expression is that appropriate to the adiabatic hopping of a constant number of small polarons, the temperature dependence of the resistance is actually the temperature dependence of the mobility.

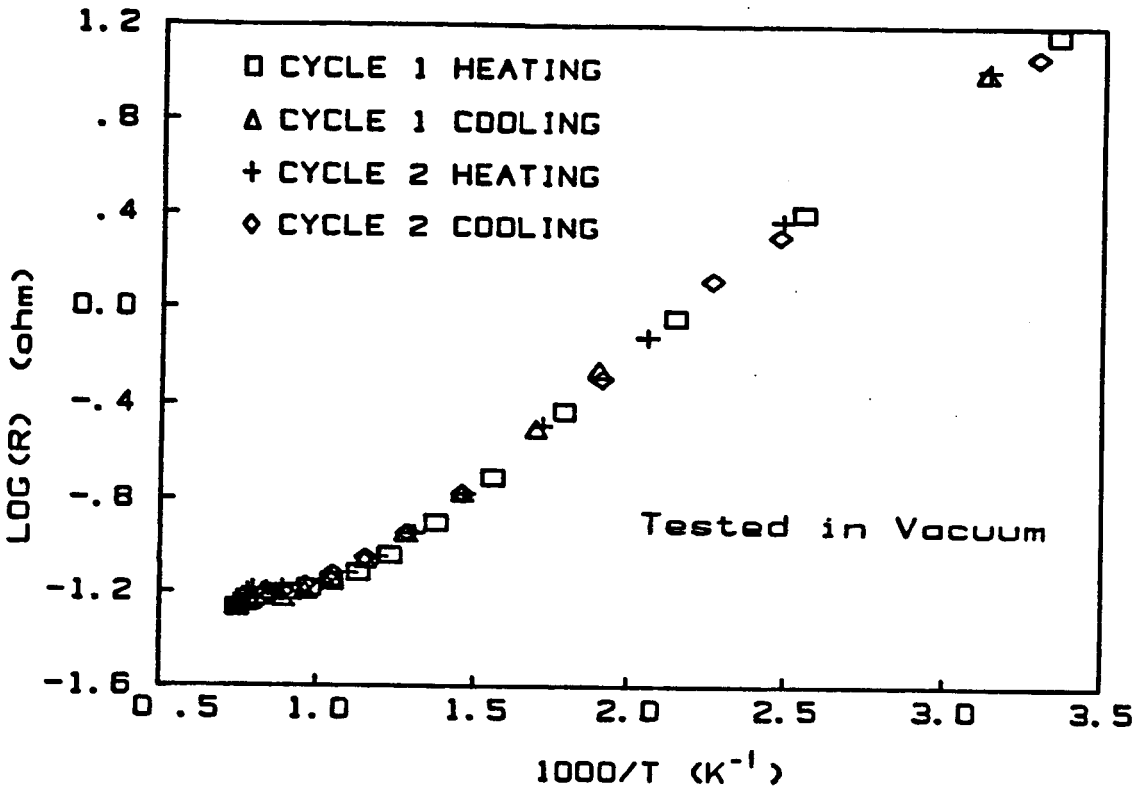

Fig. 6-4. A plot of Log(R) versus 1/T for boron carbide.

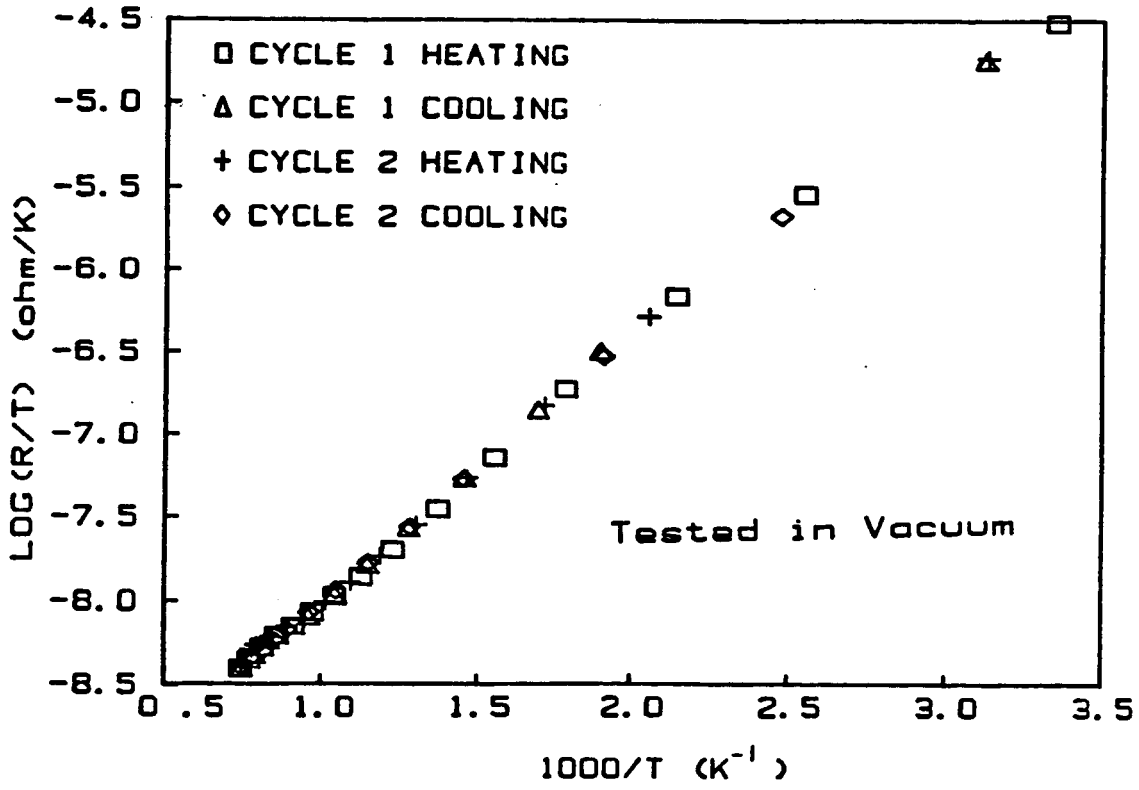

Fig. 6-5. A plot of Log(R/T) versus 1/T for boron carbide.

The elemental composition of this B_4C sample was analyzed by chemical analysis and the results are shown in weight percent as follows:

	B	C	O	N	Fe	Ca
wt %	78	19.6	0.65	0.92	0.053	0.041

This boron carbide $B_{1-x}C_x$ specimen therefore had a composition with x=0.18.

Recently, Wood and Emin [89] studied the high temperature transport properties of boron carbide. Their experimental results on the electrical conduction mechanism were similar to ours with activation energy of 0.16 eV. Their results on the Hall effect and Seebeck-coefficient measurements suggested that the electrical conduction of boron carbide results from the hopping motion of a large ($\approx 10^{21}$ cm^{-3}) temperature-independent density of small-polaron holes. In addition, they studied the relation between carbon concentration and electrical conduction, and they found that an increase in the carbon concentration decreases the magnitude of the preexponential factor of the conductivity. However, the temperature dependence of the conductivity was independent of carbon concentration and the current is carried by small-polaronic carriers whose density falls

with increasing carbon content [89].

It has been almost 50 years since Lev Davidsvich Landau set forth the notion of the small polaron. Nonetheless, it is only in recent years that have seen the rapid accumulation of evidence of small polarons and the development of the theory. A small polaron is a severely localized extra electron or a hole within a potential well that it creates by displacing the atoms that surround it. The polaron is the entire unit made up of the self-trapped carrier and the atomic-displacement pattern. A polaron is called "small" when the spatial extent of the wave function of the excess electron or the hole is less than or comparable to the separation of the atoms or molecules. The charge carrier then moves only in response to appropriate motions of the surrounding atoms.

The properties of small polarons are often opposite those of quasi-free charge carriers. Because of its connection with surrounding atoms, a small polaron has a mobility of less than 1 cm^2/V-sec, which is very much lower than that generally associated with quasifree motion. While the mobility of a quasifree carrier typically falls with increasing temperature, small-

polaron mobility usually increases with temperature. The highest mobility of small-polaronic hopping occurs in the adiabatic region where [93]:

$$\mu = qa^2v/kT \exp(-E_A/kT) \qquad (6\text{-}2)$$

Here q is the carrier's charge, a is the characteristic hopping distance, and v is the vibrational frequency which characterizes the atomic displacements with which the electronic carriers interacts most strongly.

Most recently, Emin [94], who studied the structural and electronic model of the boron carbides, found that the charge carriers in boron carbide are really bipolarons, i.e., with two extra electrons or holes trapped, instead of polarons. Azevedo et al. [95] found that the charge carriers of boron carbide provide neither an ESR signal nor a contribution to the magnetic susceptibility, i.e., they are spinless. With q being the charge of a bipolaron, twice the elemental electronic charge, a being the separation between the centroids of adjacent icosahedral, $\approx$ 5 Å, and the phonon temperature being close to room temperature, Emin calculated the preexponential prefactor of the mobility by using Eq. (6-2) to be about 1 cm^2/V-sec. A low and thermally activated mobility with an activation energy in excess of a typical

phonon energy is the hallmark of small polaron or small bipolaron motion.

Emin's study [94] also suggested that it was the additional localizing forces in the crystal, such as disorder that were effected in fostering self-trapping. The disorder provides a trigger for the collapse of a quasifree carrier into a small polaron. The structures of the boron carbides are inherently disordered, the basic structural picture of the boron carbides is that carbon is distributed substitutionally in some icosahedra and occupies sites within the intericosahedral linkages. For B_4C, the material is viewed as composed of $B_{11}C$ icosahedra with C-B-C intericosahedral chains [94]. The presence of disorder, e.g., carbon inclusions and a high density of twin planes, encourages electronic self-trapping in the boron carbides.

Hot-pressed boron carbide samples have highly disordered structures with the degree of disorder subject to modification by heat treatment. These effects are most pronounced at the knees of the resistance curves. Emin conjectured that temperature cycling to the vicinity of, or above, the knees in the resistance curves produces a

change in the degree of disorder of the boron carbide and in a rearrangement of the distribution of C atoms in energetically favorable hopping sites. Thermal cycling appears to change the distribution of carbon atoms in energetically favorable hopping sites.

In summary, boron carbide is a degenerate semiconductor in which the predominant conduction mechanism is small-bipolaron hopping between carbon atoms at energetically inequivalent sites in highly disordered structures. The activation energy associated with such correlated hopping can be large enough that the small-polaron mobility has a very weakly temperature-dependent value of about 1 cm^2/V-sec [93]. The TCR of our bulk B_4C at 1000°C was rather small, around 200±10 ppm/°C (calculated in the temperature range of 900 to 1010°C), and its average resistance drift rate at 1000°C was about 0.095 %/hr for 17 hours. Based on these low values, boron carbide was considered to be good candidate for high temperature resistance strain gage usage.

The change in resistance of boron carbide with temperature was also conducted in the air with results shown in the Fig. 6-6. Data was collected after two

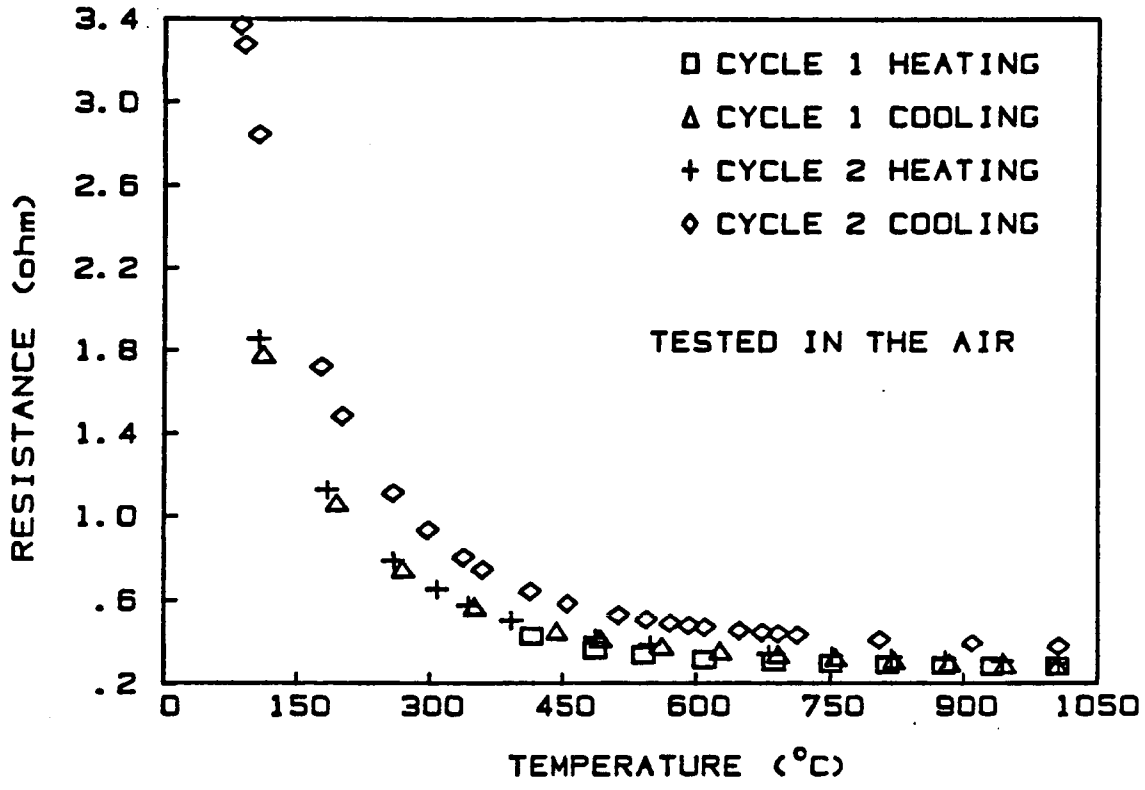

Fig. 6-6. Variation of resistance with temperature for pure boron carbide tested in the air.

C-3

cycles of heating and cooling. The hysteresis effect which was noted for sample without heat treated (shown in Fig. 6-3) was not observed for this sample with heat treatment, (see Fig. 6-7, which is the expanded scale of Fig. 6-6). Therefore, the reproducibility of B_4C could be improved by thermal cycling in air. The conduction mechanism also followed the form of Eg. (6-1), with activation energy of 0.139 eV. This result together with that of the test in the vacuum are compared and illustrated in the Fig. 6-8. The TCR at 1000°C was around 250±10 ppm/°C, and the resistance drift rate was about 0.9 %/hr. for 14 hours. The sample after electrical resistance measurements in air was heavily oxidized and had changed its color from a grey to a dark black.

Nazarchuk and Mekhanoshina [96] who investigated the oxidation of boron carbide powder, had shown that oxidation began at 600°C, and the oxidation rate increased sharply with rise in temperature up to 800 - 1000°C, it then became slower followed by a sharply increasing between 1200 and 1300°C. At all temperatures oxidation proceeded only for a certain period of time, after which it ceased. They suggested it was probably due to the formation on the B_4C particles of a B_2O_3 film

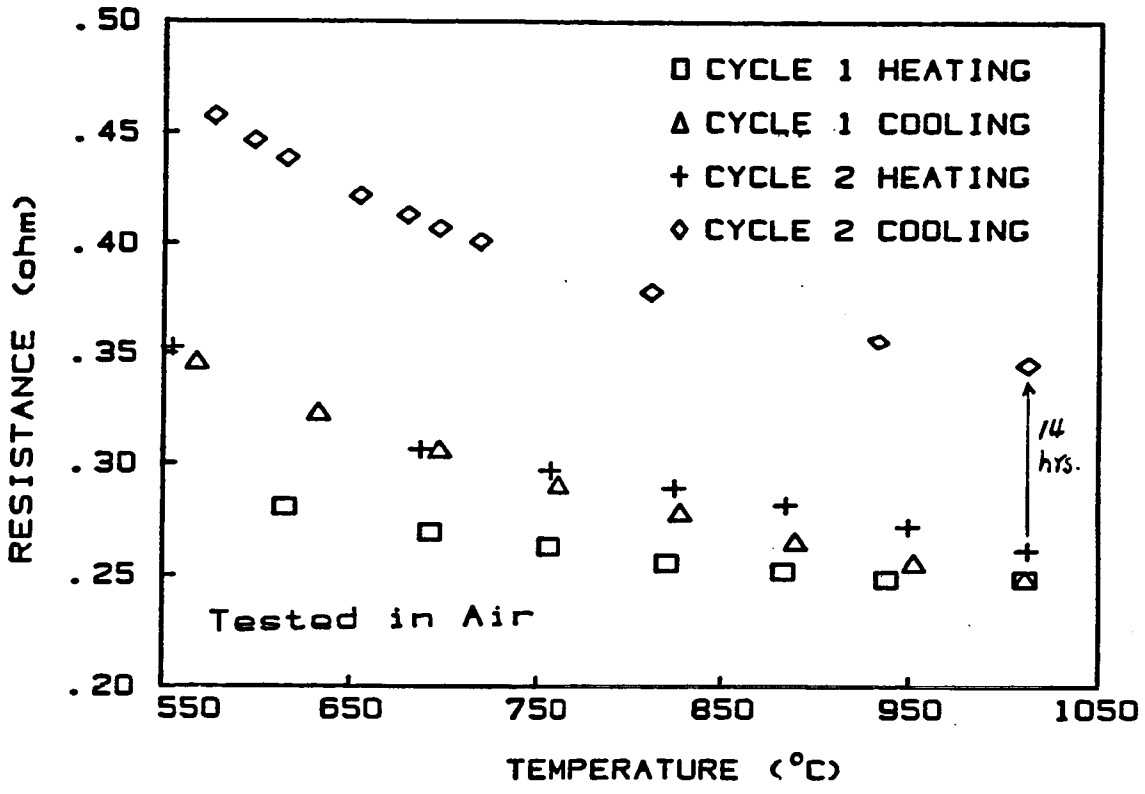

Fig. 6-7. Expansion of the high temperature region of Fig. 6-6 for boron carbide tesed in the air.

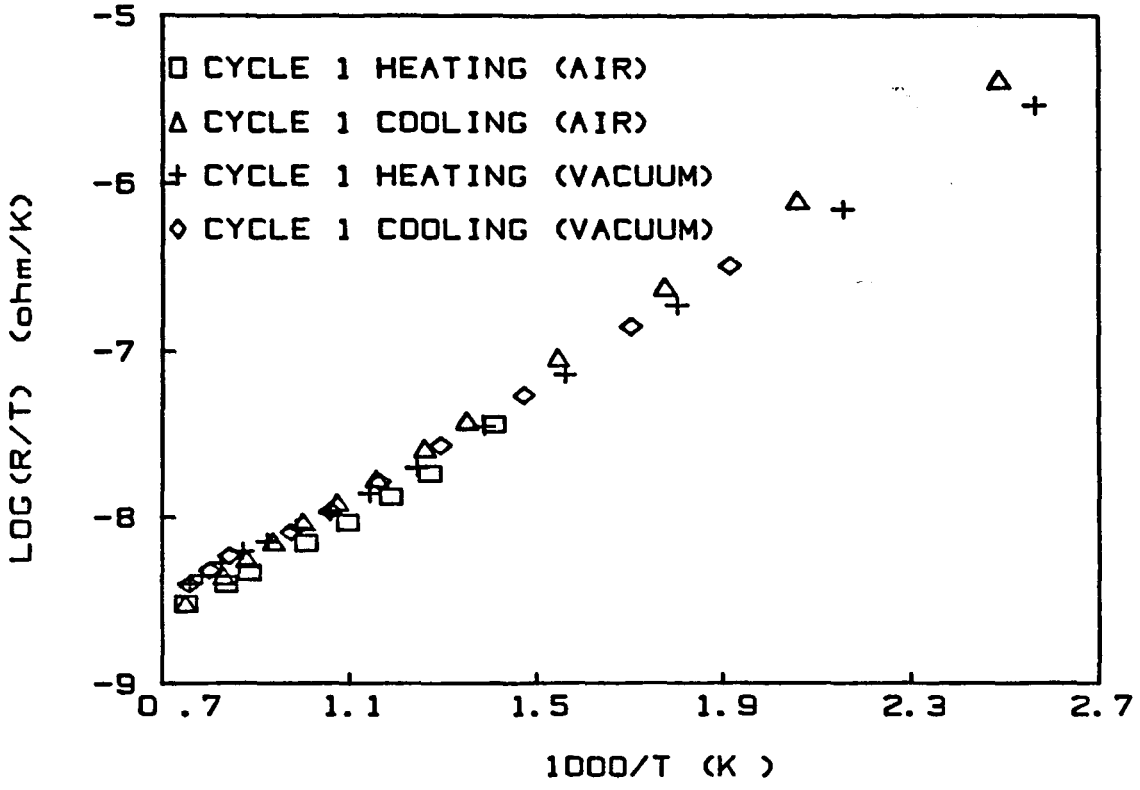

Fig. 6-8. A plot of Log(R/T) versus 1/T for boron carbide tested in air and in vacuum. Data are from the first cycle of heating and cooling.

which prevented further oxidation not only of the carbide but also of the carbon. They also found that the greater the carbon content in the boron carbide, the higher the oxidation rate. A study of the oxidation mechanism and protection method for boron carbide films is suggested for further work.

6.3 Silicon carbide

6.3.1 β-SiC

The physics of silicon carbide and the possibilities of its use in device design have been subjects of considerable interest for the past decade. Its relevant electrical characteristics appear to qualify it as a more promising material than silicon and germanium for electronic device applications at high temperatures. In addition, its strong chemical bonding and physical stability are favorable for the development of devices which must withstand radiation and other severe environments. β-SiC is expected to be an excellent material for electronic devices operated at high temperature because of its wide band gap (2.2 eV) and high electron mobility ($\approx$ 1000 cm^2/V-sec) comparable to

that of silicon.

A β-SiC thin film prepared by electron beam gun evaporation (EBE) on an alumina (Al_2O_3) substrate was tested. The substrate temperature was kept at 875-900°C during the deposition, and the thickness of the film was 0.25 micrometer. The change in the electrical resistance with temperature for this β-SiC film is shown in Fig. 6-9. These data show a decrease in resistance with increasing temperature and a average TCR of 330 ppm/°C at 1000°C. In addition, the change in resistance with temperature occurred at a higher rate in the heating cycle than in the cooling cycle at high temperatures (T>900°C). Resistance drift at 1000°C was measured during three cycles, the drift rates decreased with cycles from 1.16 %/hr for the first cycle to 0.32 %/hr for the third cycle. The electrical resistance stability of this β-SiC film was improved by thermal cycling.

The change in resistance with time at three different temperatures (900°C, 950°C, and 1007°C) are shown in the Fig. 6-10. The drift rates at these three temperatures were about 0.066 %/hr, -0.075 %/hr and -0.36 %/hr, respectively. SiC does not melt congruently,

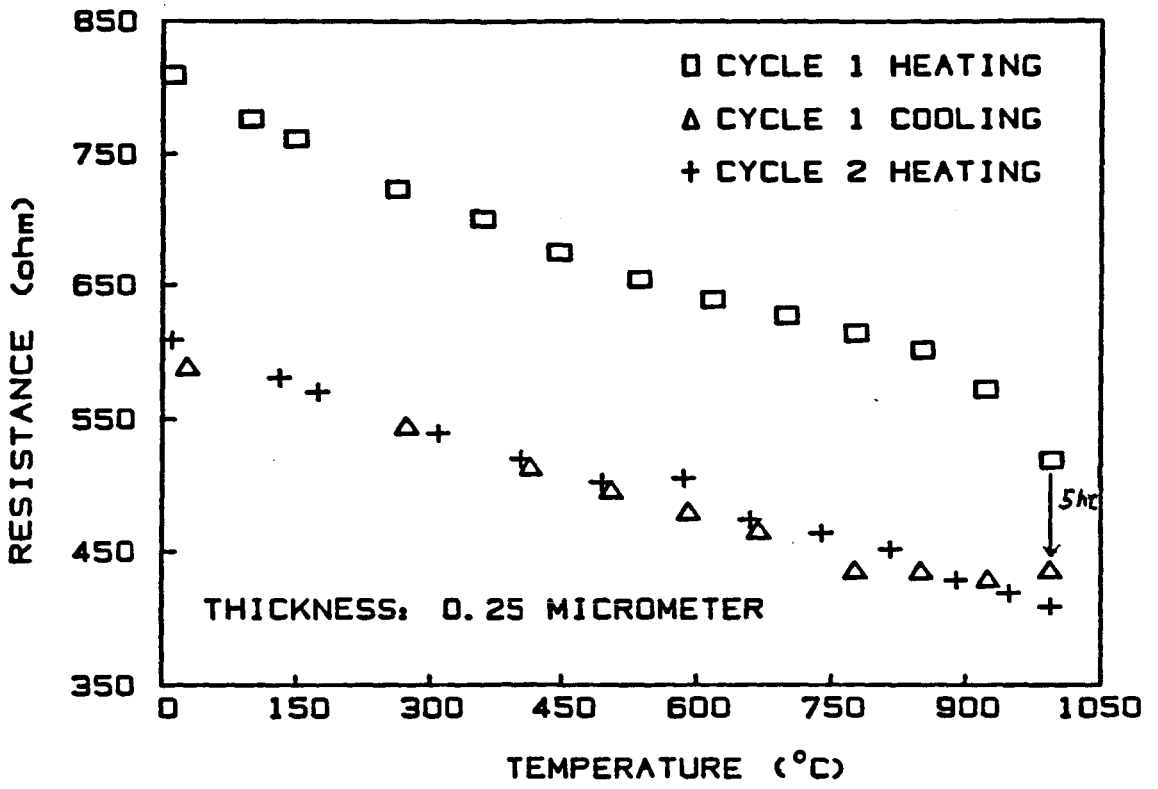

Fig. 6-9. Variation of resistance with temperature for β-silicon carbide thin film prepared by electron beam gun evaporation.

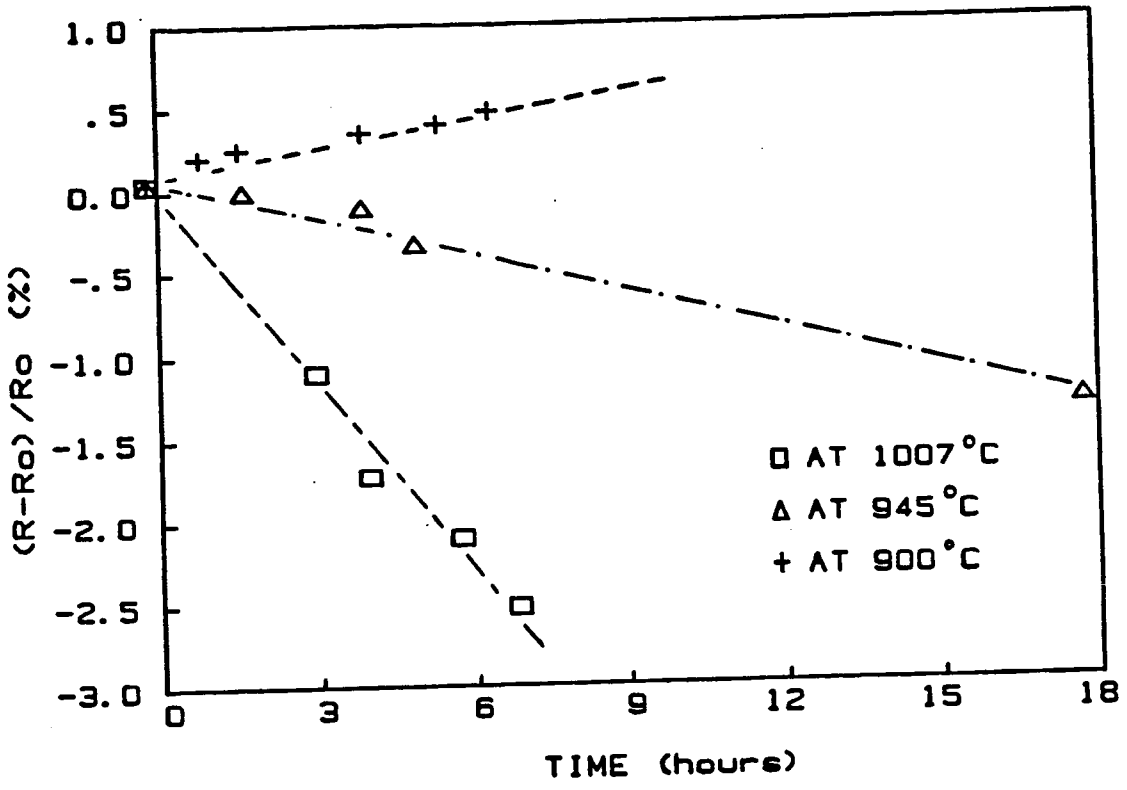

Fig. 6-10. Resistance drift of β-silicon carbide at three different temperatures.

instead it begins to dissociate into graphite and silicon vapor between 900 and 1000°C [97]. Assuming the resistance drift at high temperature was due to the growth of the graphite layers, the growth rates of the graphite layers calculated from the resistance changes were about 1.68 Å /hr at 1007°C and 0.32 Å/hr at 950 °C. For a thicker specimen, this phenomenon would not be significant, therefore, the drift effects would most probably decrease in thicker specimens.

A plot of log(R) versus 1/T for this specimen illustrated in Fig. 6-11 indicated that the slope of this curve increases with increasing temperature and the activation energy calculated from the slope, varied from 0.005 eV at low temperature to 0.074 eV at high temperatures. Nagai et al., (98) who studied the effects of nitrogen on the electrical properties of the sputtered SiC_x films, found that the addition of a small amount of nitrogen gas (<9 %) to the argon sputtering atmosphere markedly affected the properties of the SiC_x films, particularly the electrical properties. The temperature dependence of the resistance was found to be represented by the following empirical equation:

$$R = AT^{-n} \exp(m/T) \qquad (6-3)$$

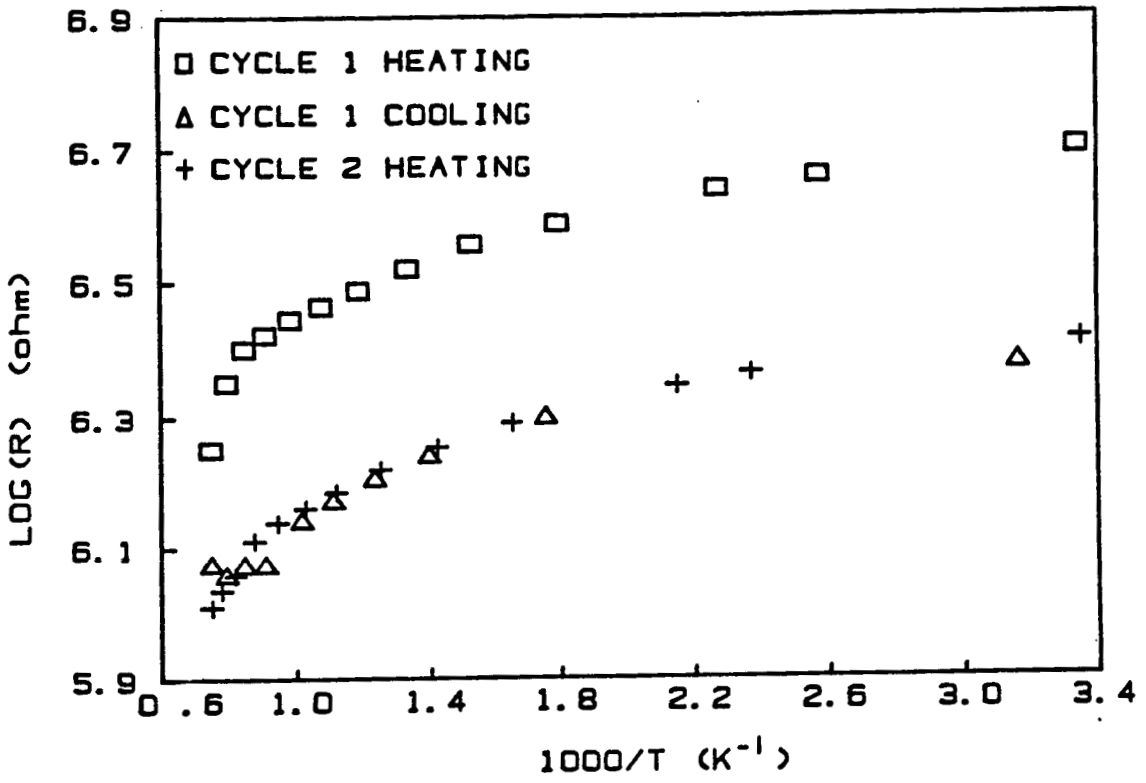

Fig. 6-11. A plot of Log(R) versus 1/T for β-SiC prepared by EBE.

where A, n and m are constants and are determined experimentally and depend on the sputtering condition. A plot of log(RT) vs. 1/T for the β-SiC film used in present work is shown in Fig. 6-12. A straight line was observed in the high temperature region. Therefore, the temperature dependence of the resistance of this β-SiC thin film at temperature higher than 250°C can be described by

$$R = AT^{-1} \exp(429/T)$$

with n=1 and m=429 K.

Another β-SiC film prepared by chemical vapor deposition (CVD) on a silicon substrate was also tested. This specimen had a greater thickness (7 micrometers) than the former one and with some nitrogen dopants ($n=1.1\times10^{17}$ cm^{-3}). The temperature dependence of the resistance for this β-SiC film on Si is illustrated in Fig. 6-13. As can be seen, it has positive TCR at low temperatures and negative TCR at high temperatures, this results from the change in resistance of a 7 micrometer β-SiC (with room temperature resistivity of 0.2 ohm-cm) together with that of a 381 micrometers Si (with a room temperature resistivity of 20 ohm-cm). Since the resistance of the Si substrate was about the same order

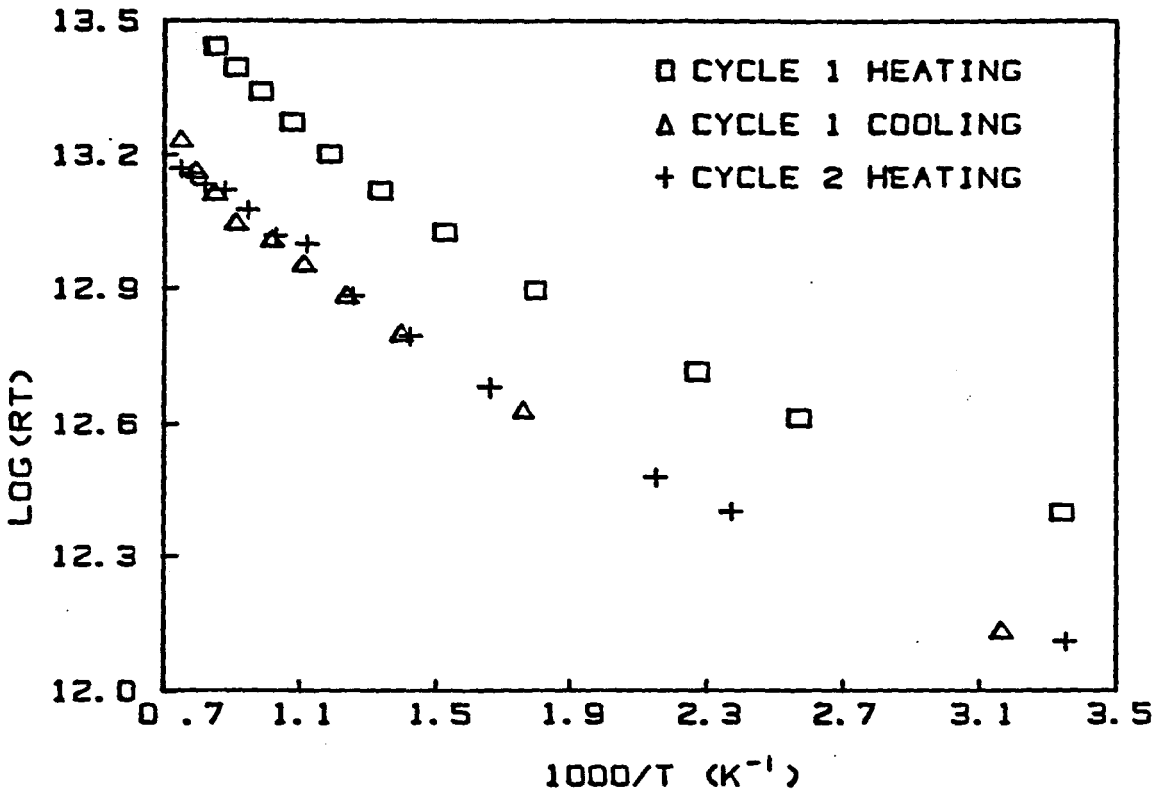

Fig. 6-12. A plot of Log(RT) versus 1/T for β-SiC prepared by EBE.

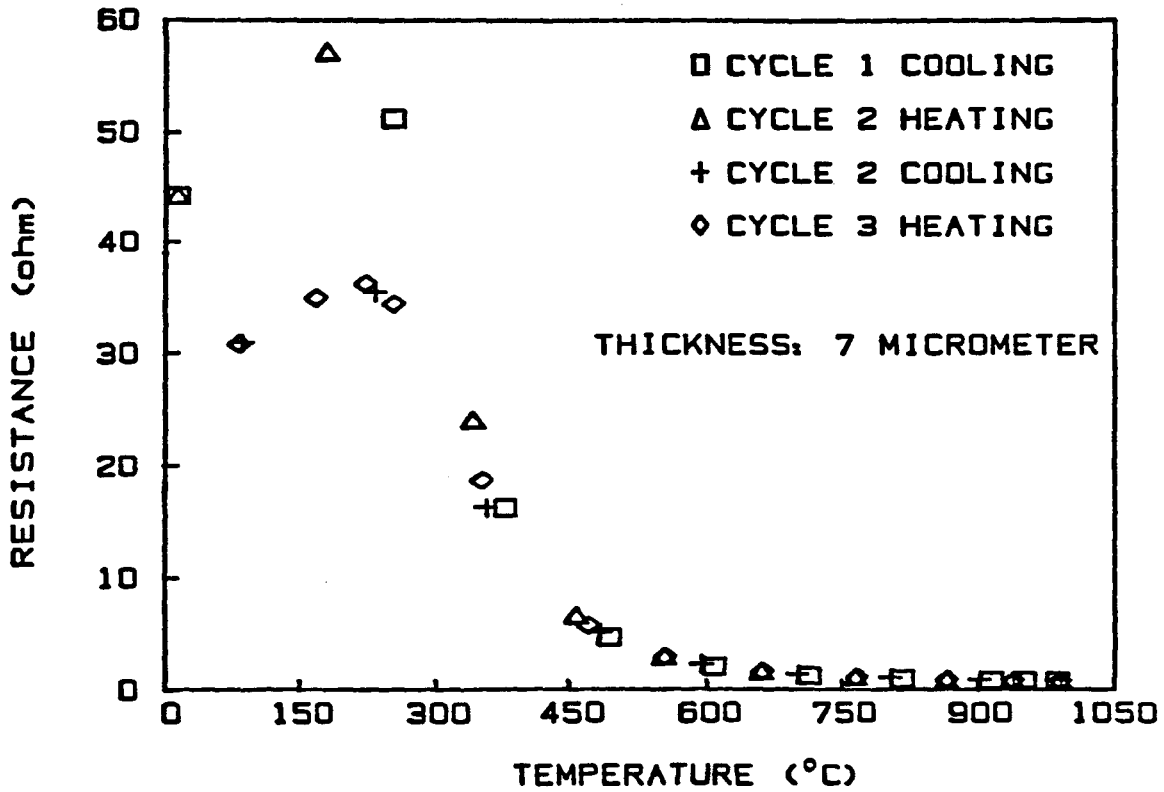

Fig. 6-13. Variation of resistance with temperature for β-SiC thin film on Si substrate. SiC film was prepared by CVD.

of magnitude as that of the SiC film, the temperature dependence of this β-SiC film is difficult to resolve.

A similar β-SiC film was tested again without the Si substrate. After removing the Si substrate, this 7 micrometer film was attached to a alumina substrate by means of a high temperature adhesive. The alumina substrate had very high resistance compared to that of the SiC. The change in resistance with temperature and with reciprocal temperature for this specimen are illustrated in Figs. 6-14 and 6-15, respectively. It can be seen that this sample has a negative TCR at low temperature region and but a positive TCR at high temperature region. The changeover point may be due to the sample going from a region of extrinsic conduction at the lower temperatures to a region of saturated extrinsic conduction in the higher temperature. The plot of log(R) verse 1/T as in Fig. 6-15 shows a linear relation at the temperature between room temperature and 600^{o}C. The TCR of this β-SiC film at 1000^{o}C was about 223 ppm/^{o}C, which was smaller than that of the β-SiC (EBE) film, and its average DR was 0.53 %/hr for four hours, which is larger than that of the β-SiC (EBE) film.

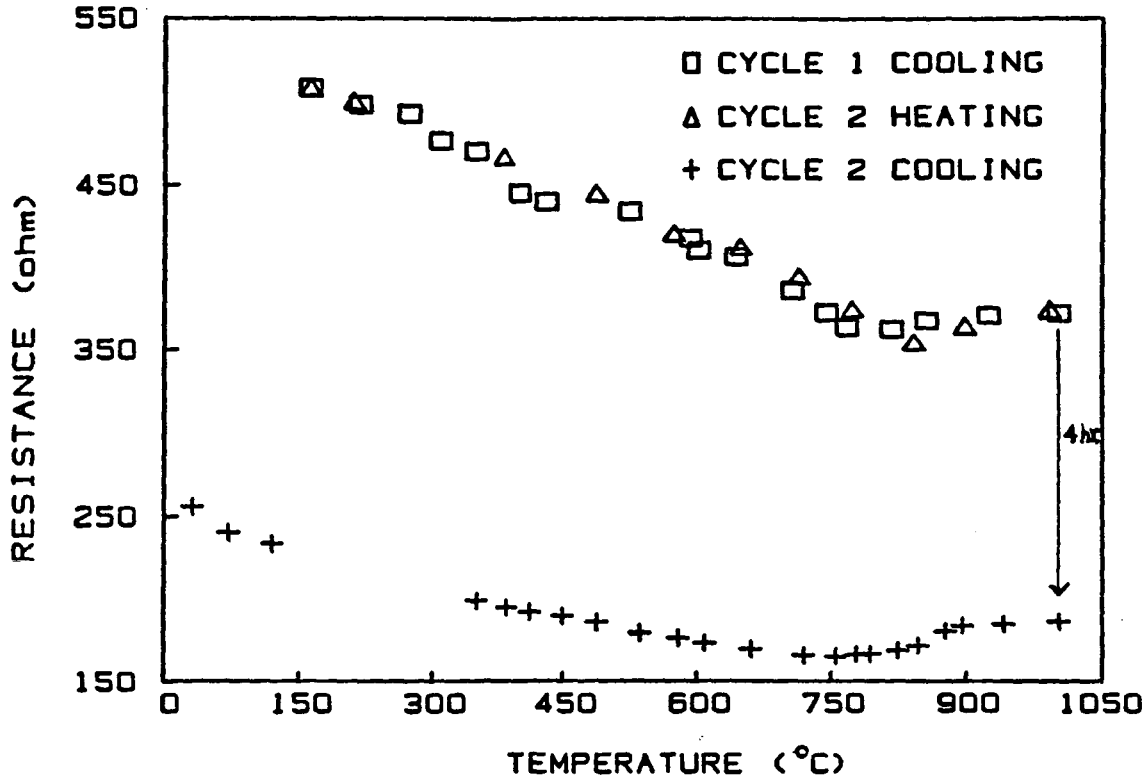

Fig. 6-14. Variation of resistance with temperature for β-SiC thin film prepared by CVD, film was attached to the Al_2O_3 substrate by using adhesive.

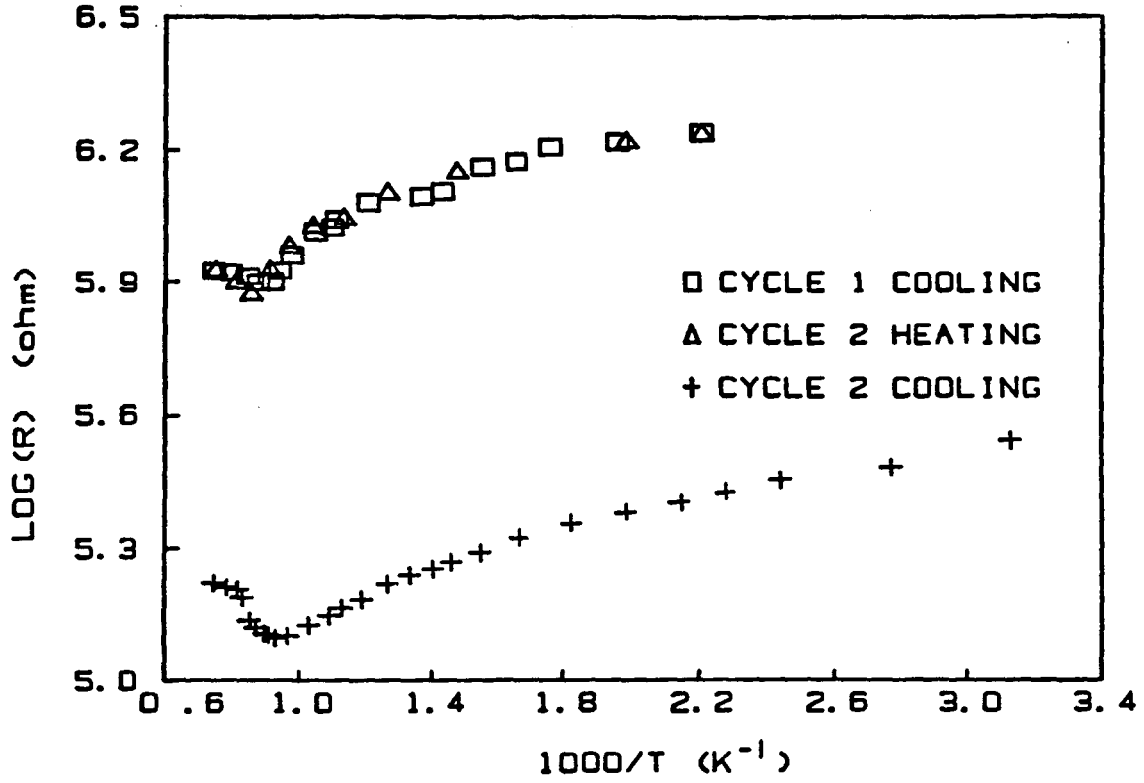

Fig. 6-15. A plot of Log(R) versus 1/T for β-SiC on the Al_2O_3 substrate.

6.3.2. α-SiC

Silicon carbide exists in the form of the cubic β-SiC and the hexagonal α-SiC. β-SiC is unstable above 2000°C, and is converted into α-SiC. The α- β transition at high temperature is accompanied not only by a change in structure and color but also by a strong increase in the resistivity [100]. It has been noted that the mobility of electrons scattered by phonons in α-SiC is much lower than that in β-SiC [101].

The resistance versus temperature and reciprocal temperature curves for a hot pressed α-SiC are presented in Figs. 6-16 and 6-17, respectively. The electrical resistance of the specimen in the temperature range investigated was the same during heating and subsequent cooling, i.e., the results were reproducible. The resistance of the sample decreased with increasing temperature in an activated manner with activation energies of 0.0058 eV at low temperatures and 0.36 eV at high temperatures. The TCR of this bulk α-SiC at 1000°C was 2100 ppm/°C and its DR was about 0.04 %/hr for 9 hours.

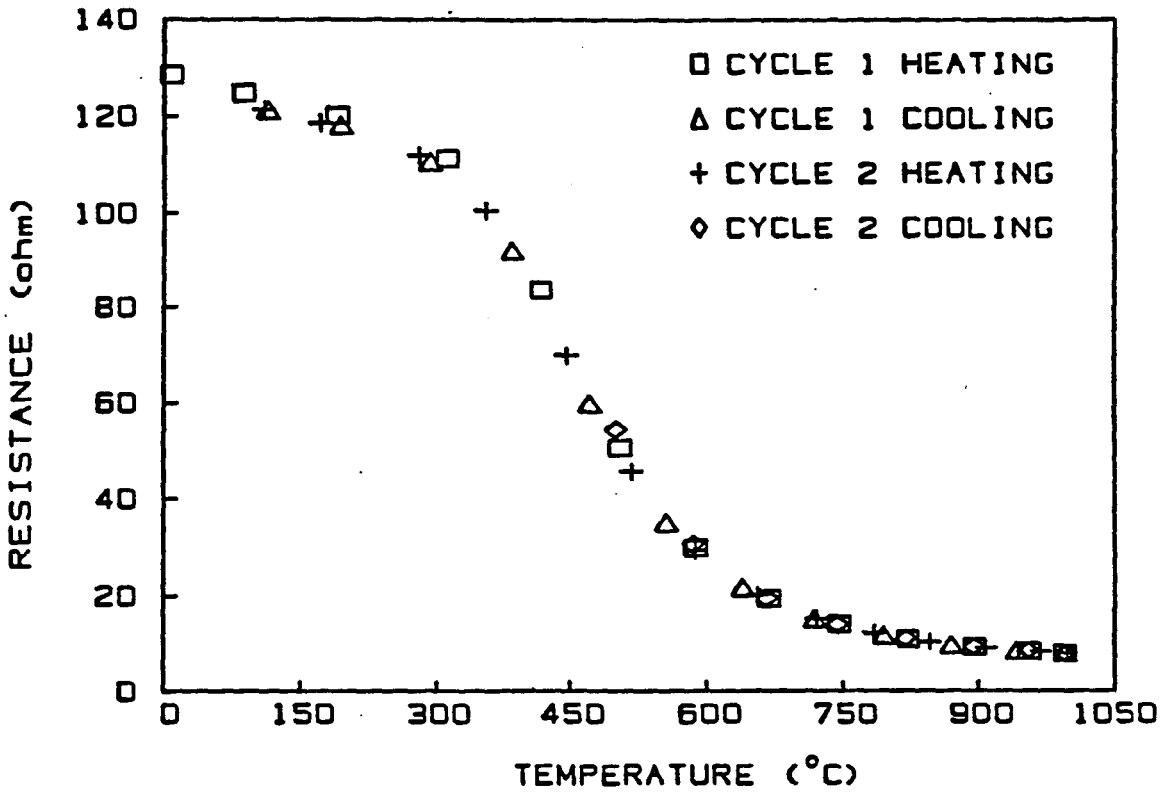

Fig. 6-16. Variation of resistance change with temperature for α-SiC bulk sample prepared by hot pressing.

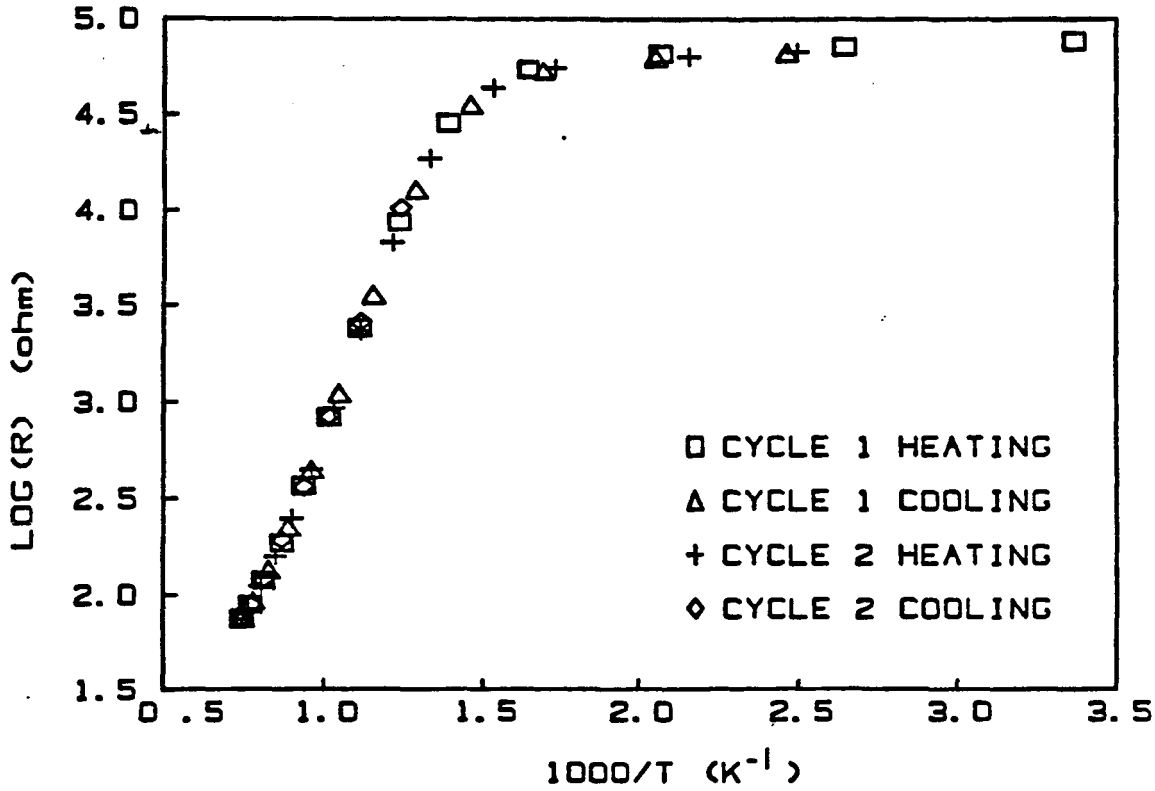

Fig. 6-17. A plot of Log(R) versus 1/T for hot pressed α-SiC.

Comparing the results of β-SiC with those for α-SiC, it was noticed that the decrease of resistance with increasing temperature was faster in α-SiC than in β-SiC. This is because, in the case of α-SiC, the electron mobility at high temperatures is restricted by intervalley scattering as well as acoustic phonon scattering [102,103], which results in the steep decrease of mobility with increasing temperature. On the other hand, in the case of β-SiC, the mobility is little affected by intervalley scattering because of its crystal symmetry. Therefore, it was anticipated that the change in the mobility of β-SiC with temperature would be smaller than those of other polytypes and its mobility would be large even at high temperatures.

Sasaki et al. [101], who studied the high temperature (<850^{o}C) electrical properties of β-SiC epitaxial layers grown by chemical vapor deposition, also found that β-SiC had weaker temperature dependence of mobility and larger mobilities compared with other polytypes of SiC, and they suggested that β-SiC is more promising material for devices that operate at high temperatures.

Analysis of the X-ray diffraction patterns of these SiC specimens indicated that both β-SiC samples had FCC crystal structures, with lattice parameters of 4.2807 Å and 4.3583 Å for the samples prepared by EBE and CVD methods, respectively. α-SiC had a hexagonal crystal structure with a lattice parameter of a=3.0805 Å and c=15.117 Å.

The oxidation of SiC begins at above 1000°C [104]. The principal oxidation product of this compound is SiO_2, whose volume is greater than that of SiC. With time a dense film of SiO_2 forms which is protective and retards further oxidation of SiC film.

6.4 Summary

Table 6-1 summarizes the experimental results for the semiconducting materials mentioned in the preceding sections. Due to its special conducting mechanism, the temperature dependence of resistance in B_4C is actually the temperature dependence of its mobility, and the activation energy was large so that its mobility had a weakly temperature dependent value and resulted in a small TCR value at high temperatures. In addition the

electrical resistance reproducibility of boron carbide was improved by thermal cycling.

β-SiC had weaker temperature dependence of resistance compared with α-SiC, and it is more promising for use at high temperature. The TCR of silicon carbon was decreased by doping effect. However, its resistance stability was slightly diminished. It is also concluded that the resistance stability of thin films depends on their thickness; with better stabilities for thicker films.

Table 6-1

Summarized results for semiconducting candidate materials

Specimen	ρ (Ω-cm)	TCR (ppm/°C)	DR (%/hr)	Remark
B_4C	0.24	-200	0.095	tested in vacuum
		-250	0.9	tested in air
				hot pressed bulk
β-SiC-1	0.01	-330	-0.32	"pure", 0.25 μm thick, prepared by EBE.
-2	0.2	-223	-0.53	with N_2 dopants, 7μm thick, prepared by CVD.
α-SiC	10.1	-2100	0.04	hot pressed bulk

CHAPTER 7

GAGE FACTOR MEASUREMENT

7.1 Introduction

Although the main concern of this work was to study the electrical resistance properties for those materials which were potentially useful for resistance strain gage application, a preliminary study on the piezoresistance effect for one of the best candidate materials, boron carbide, was also undertaken.

In this chapter the experimental apparatus which was adopted for strain measurements and the theory behind it are described and the results of gage factor measurements for boron carbide are discussed and compared with that of Wu's Chinese strain gage [12], which is the present state of the art.

7.2 Experimental Apparatus

In order to determine the gage factor, it is necessary to simultaneously strain the sample and measure

the change of resistance with strain. Strain is most commonly applied to the specimen by means of a direct pull on a tensile specimen, the bending of a beam, or the deflection of a cantilever beam. Due to its simplicity, small size and the fact that it requires virtually no auxiliary equipment, a device which consisted of a cantilever beam designed first by McClintock [105] was adopted and modified to measure the gage factor of the specimens in this work.

The principle of operation of this strain gage calibration device was a constant strain cantilever beam, an element frequently used by civil and aeronautical engineers. The width of a fixed-end cantilever beam of a homogeneous material of constant thickness was varied along its length so that upon loading in the elastic region the stress and consequently the strain was the same everywhere on its upper and lower surfaces [105]. If L is the length of such a homogeneous isotropic beam, t its thickness, P a force applied at its free end, and taking the origin of linear Cartesian coordinates at its fixed end as shown in Fig. 7-1, then in order to achieve a constant stress σ at its surface, the width b must vary linearly along the length of the beam according to [106]:

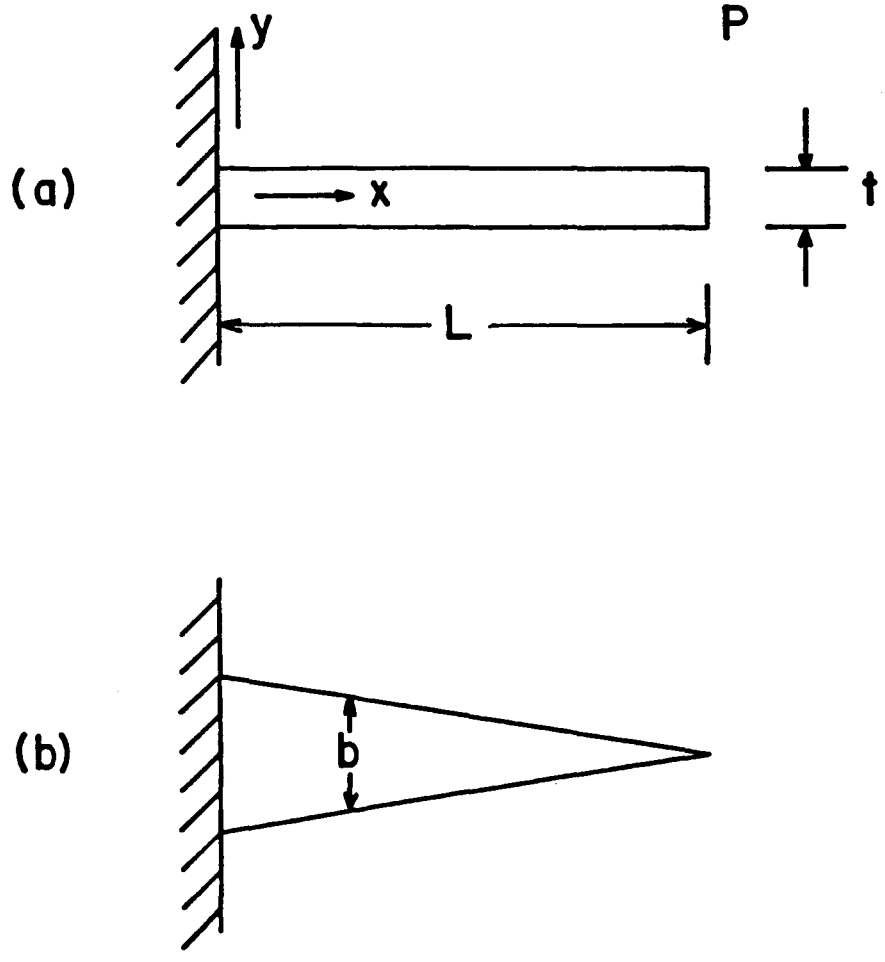

Fig. 7-1. Schematic diagram of cantilever beam (a) side view and (b) top view.

$$b=6P(L-x)/\sigma t^2. \qquad (7-1)$$

The relation between deflection of the free end of the beam and the strain at its surface can be deduced from the condition of equilibrium for an elastic member [106],

$$M=EId^2y/dx^2, \qquad (7-2)$$

where M is the bending moment, I is the moment of inertia of the cross-sectional area about its central axis, and E is the modulus of elasticity. For the free body diagram shown in Fig. 7-1, this moment becomes

$$EId^2y/dx^2 = -P(L-x). \qquad (7-3)$$

For a beam with rectangular cross section $I=bt^3/12$, and for the constant strain beam

$$b=6P(L-x)/\sigma t^2,$$

so

$$d^2y/dx^2 = -2\sigma/Et. \qquad (7-4)$$

Integrating both sides of this equation twice with respect to x and applying the following conditions

(a) $dy/dx = 0$ at $x=o$,

and (b) $y=0$ at $x=0$

yields the following relation:

$$y = -\sigma x^2/Et.$$

Maximum deflection, y^*, occurs at $x=L$ and since $\sigma=E\varepsilon$, where ε represents strain, thus,

$$\varepsilon = -y^{*}t/L^{2} \qquad (7\text{-}5)$$

This shows the strain at the surface of the cantilever beam to be dependent only upon easily measured deflectional and geometric factors.

Fig. 7-2 is a drawing of the apparatus designed on this principle. This includes a cantilever beam with a 5.27 inch length, a 0.13 inch thickness and a 1 inch width at the fixed end. Every 0.1 inch deflection of this cantilever beam at the free end will result in a microstrain of 468 at the surface of the beam. Since strain at the surface is constant over the length of the beam except near the ends, the location of the gauge was not critical. Part number 2 is a stepped, sliding block in contact with a screw which is fixed at the free end of the beam. The block was accurately machined so that the difference in height between any two steps (0.022 in) represents a known deflection of the free end of the beam, and consequently a known strain of 103 microstrain (calculated from Eq. (7-5)) at the beam surface. The frame (part number 3) which fixed the relative position of the cantilever beam and the sliding block by means of screws are heavy enough to minimize the error caused by deflection of the frame. The sliding block, beam, frame,

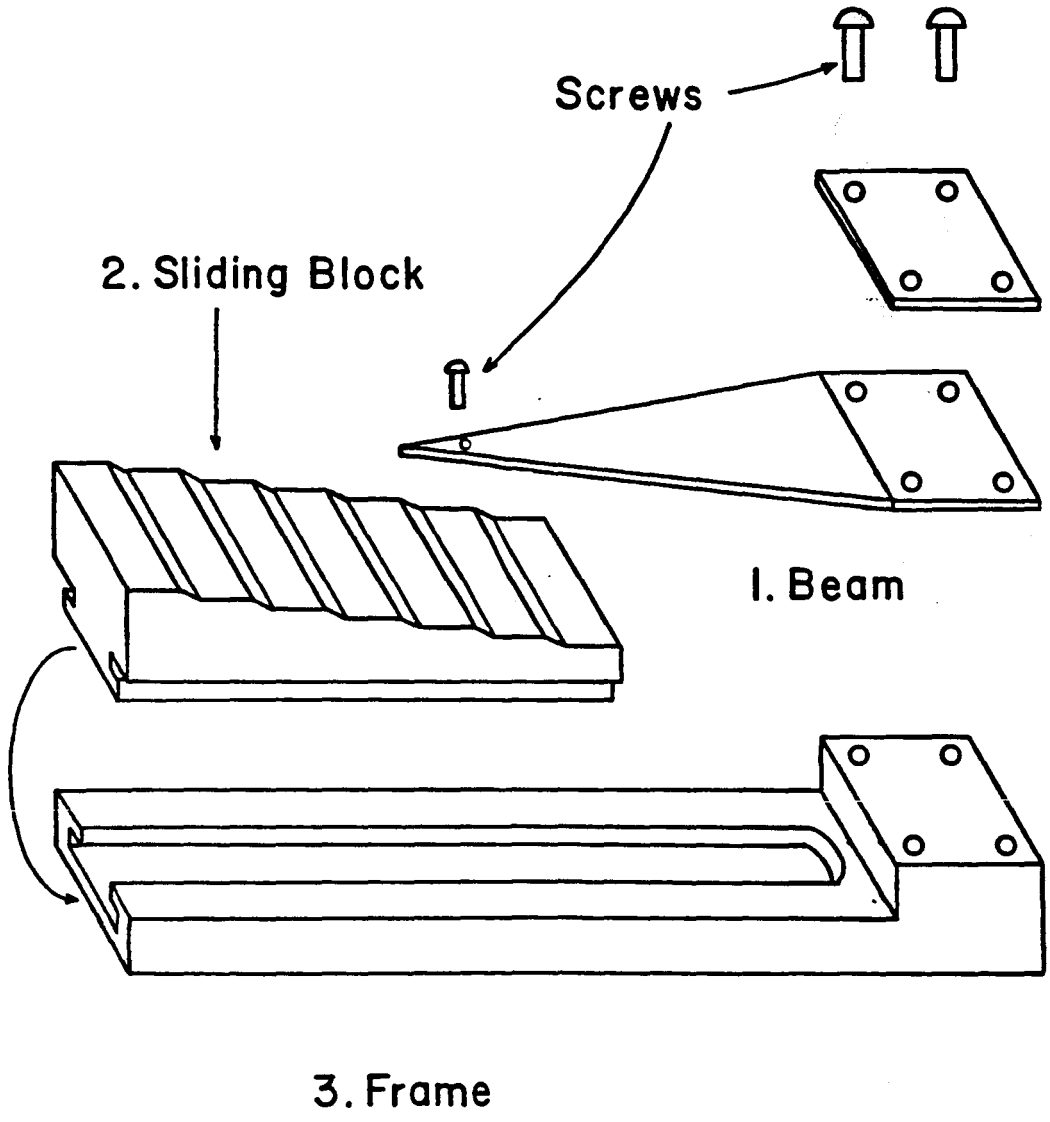

Fig. 7-2. Schematic diagram of the apparatus for gage factor measurements.

and screws were all made of the same material (Aremcolox 502-1100 high temperature low thermal expansion machinable ceramics, AREMCO) to minimize relative dimensional changes of these parts resulting from the thermal expansion.

This whole device was then inserted in a two head opened quartz tube, the quartz tube with one head connected to the vacuum system, and one head to a micrometer was placed in a furnace described in chapter 4. The position of the frame in the furnace was fixed by a rod extending outside the furnace and fixed by means of screws. The sliding block was actuated by a micrometer through another rod extending through the same end of the furnace. This system is illustrated in Fig. 7-3. Two rows of small diameter holes were drilled in the cantilever beam to fix the positions of the led wires used as current and voltage probes by winding the wires through the holes. Samples were placed under the lead wires and attached to the surface of the cantilever beam by means of a high temperature ceramic adhesive (AREMCO products), which was cured at 370^{o}C prior to making measurements. This arrangement is illustrated in Fig. 7-4.

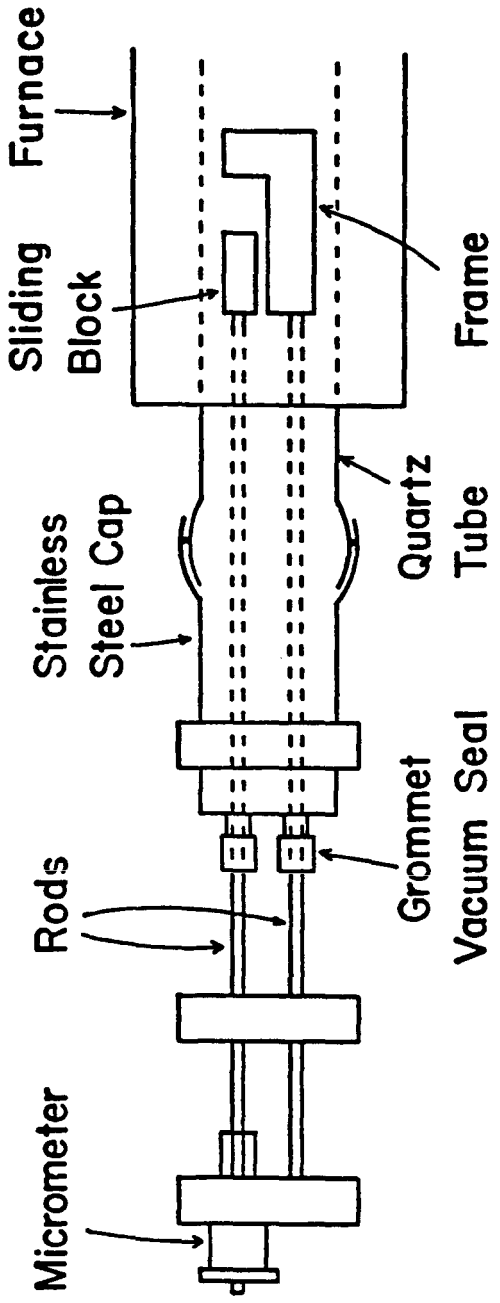

Fig. 7-3. Schematic diagram of the arrangement for actuating the sliding block to apply a strain to the specimen.

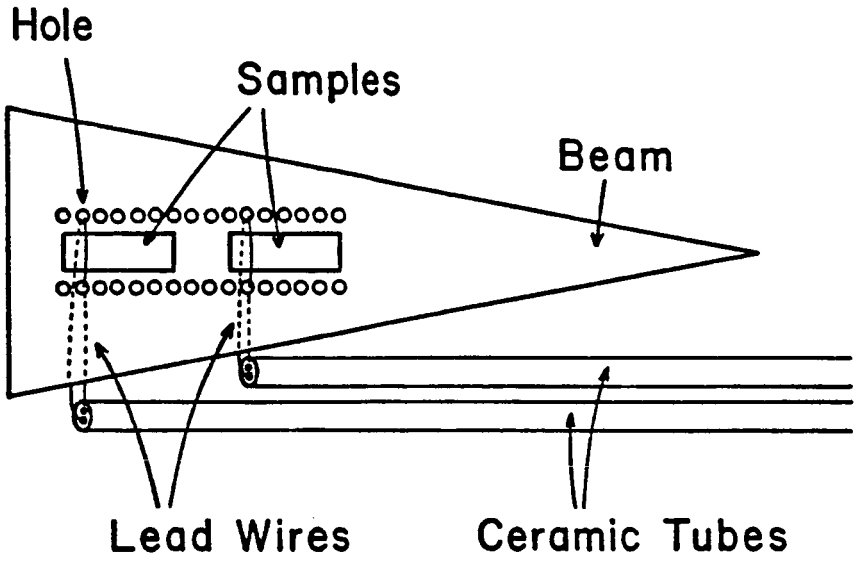

Fig. 7-4. Schematic diagram of the arrangement between specimen, lead wires and cantilever beam.

Platinum wires were first used as lead wires. However it was found that platinum wires reacts with the ceramic adhesive, and they were replaced by tungsten wires. The gage factor of the specimen was measured every 100°C intervals from 1010°C to room temperature after the furnace temperature had been stabilized within 1°C. The procedure for controlling the furnace temperature and for measuring the temperature and resistance of the specimen were the same as those described in chapter 4. At each temperature, 3 levels of strain were applied to the specimen by moving the sliding block forward through three steps, which resulted in strains of up to 306 microstrain in the specimen, and then back to the original position. The gage factor of the specimen at each temperature was the resistance change divided by the original resistance multiplied by applied strain, as defined by Eq. (2-1):

$$G=dR/(R\,d\varepsilon).$$

7.3 Result and Discussion

The gage factor measurement system was first calibrated with commercial resistance strain gages at room temperature. Three EA strain gages (Micro-

measurements Co.) with resistance of 120 ± 0.15 % ohm and gage factors of 2.105 ± 0.5 % at room temperature were attached to the cantilever beam and tested all at the same time. By applying a total 103 microstrain to the specimens, which corresponded to the deflection of the beam by one step height of the sliding block, the three gages showed resistance changes corresponding to 103.7, 103.2, and 103.4 microstrain deformation, respectively. The largest inaccuracy in these strain measurements was about 0.68 %.

The use of a simple cantilever beam can result in a number of possible errors. The most important of these is probably that due to the thickness of the adhesive layer. The strain in the gage differs from the surface strain of the beam by an amount directly proportional to the adhesive thickness. If the adhesive has a thickness δ at the center of the gage, because of the radius of the curvature of the deflected beam, the gage is subjected to a strain greater than that at the beam surface by an amount of $2\delta y^*/L^2$ [105]. For example, with a 0.13 inch thick beam and 0.004 inch thick adhesive, the strain at the gage element is 6 % greater than that at the surface of the beam. Errors arising with the effects of

nonuniform shear stress could be neglected provided L>>D, where L is the length and D the depth of cross section of the cantilever beam. The beam used in this work was suitably designed to satisfy this requirement.

A hot pressed boron carbide (B_4C) with a 0.24 ohm-cm resistivity was then attached to the cantilever beam with the ceramic adhesive and tested in the furnace under vacuum. Resistance of this sample was measured from room temperature to 1000°C. The change in resistance with temperature curve of this sample was compared to that of the resistance data from a sample without applying adhesive (shown in Fig. 6-2). The comparison is shown in Fig. 7-5 where the consistence between two curves indicates the inertness of the adhesive.

Fig. 7-6 illustrates the resistance versus strain characteristics for boron carbide at three different temperatures. A linear change in resistance of the boron carbide with applied strain at strain levels less than 306 microstrain was observed. The gage factor drift at 1000°C was also investigated for B_4C and was found to be about 0.22 %/hr for period of 6 hours.

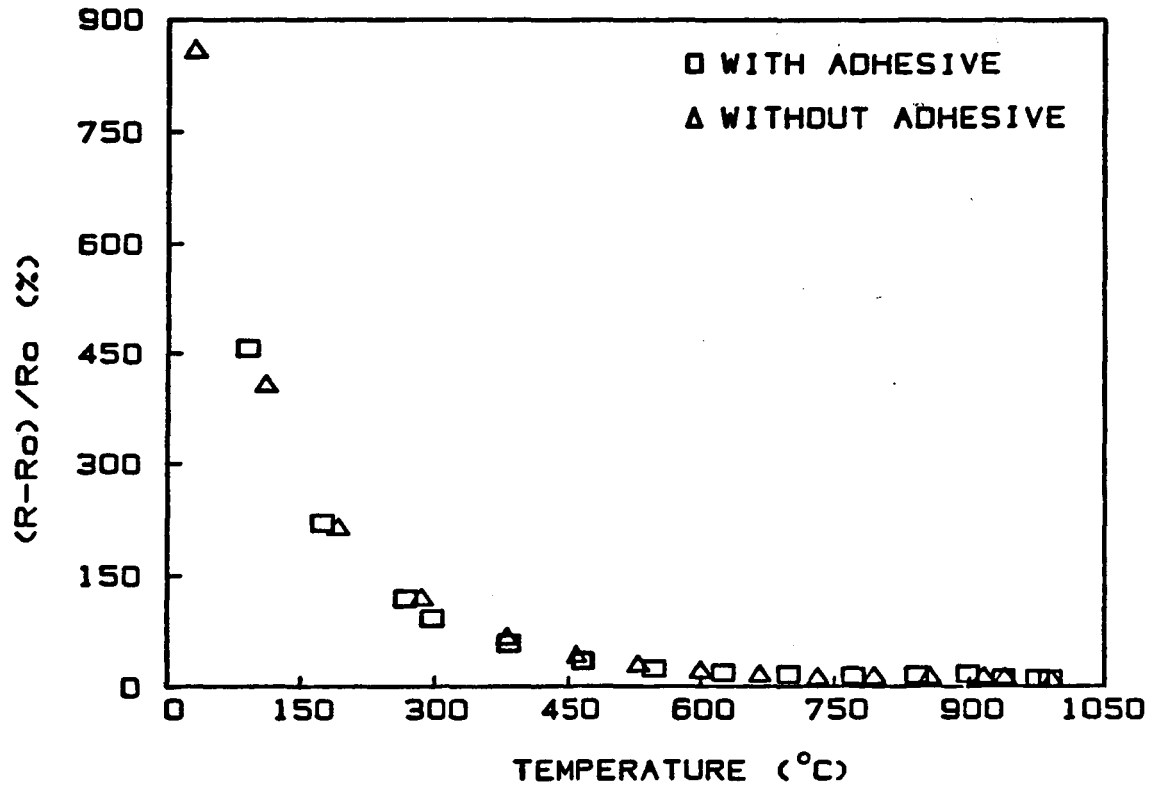

Fig. 7-5 Comparison the change in resistance with temperature of two boron carbides, one with adhesive and one without adhesive.

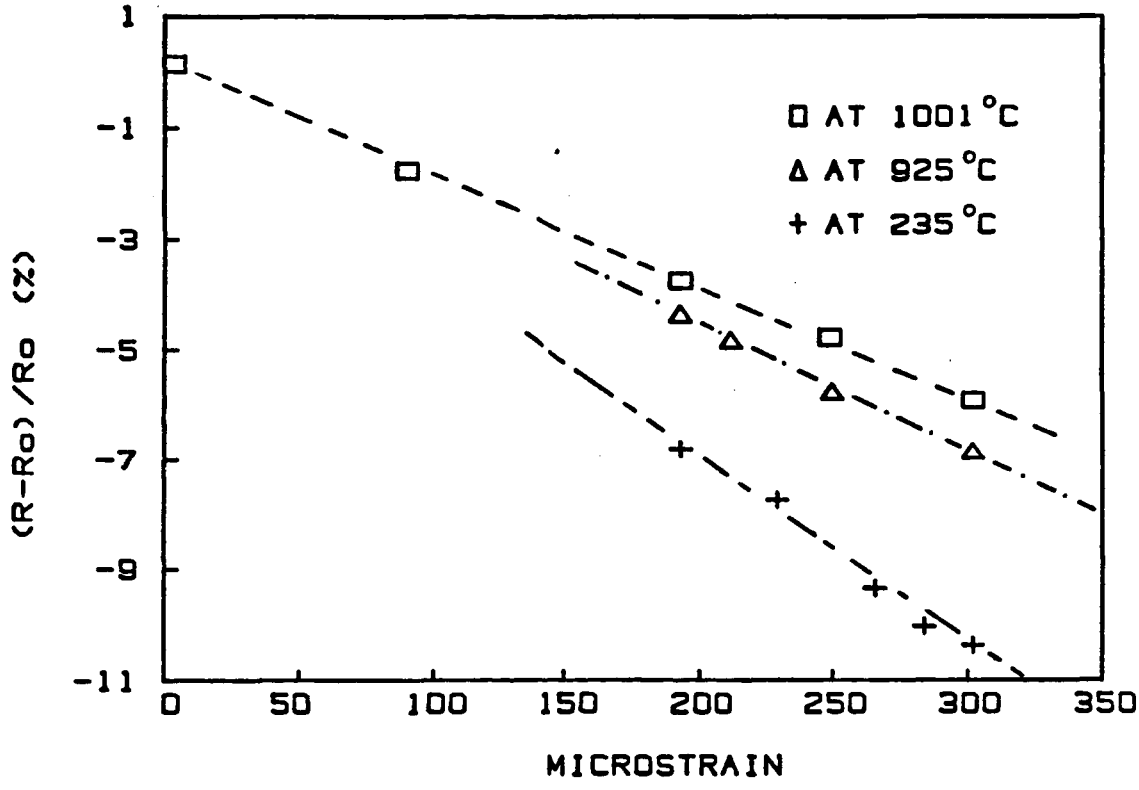

Fig. 7-6. Variation of resistance with strain at three different temperatures for boron carbide. Resistance is normalized to its value under no strain.

Fig. 7-7 is a plot of percentage change in gage factor from its room temperature value versus temperature for the B_4C specimen in the temperature range of 23°C to 1000°C. This figure shows that the gage factor of B_4C decreased with increasing temperature. This gage factor characteristics is similar to that of the comparssion curve for Wu's gage [13], shown in Fig. 7-8. The gage factor of boron carbide was about 196±1 % at 1000°C and 455±2 % at room temperature, respectively. It varied by about 57% from room temperature to 1000°C. The gage factor of Wu's Fe-Cr-Al-V-Ti-Y gage was 2.56 at room temperature and 1.9 at 700°C which varied about 26% in the temperature range from room temperature to 700°C. In the same temperature range the gage factor variation for B_4C was about 32%. Since no effort has been made to optimize the performance of B_4C, the comparison is rather favorable.

The usually large piezoresistive effect in semiconductors was first noted by Smith [15] and explained later by Herring [107], and others [16,108]. The optimum piezoresistive effect depends on physical form, type of material, its resistivity or doping, and crystallographic orientation. P-type silicon with a

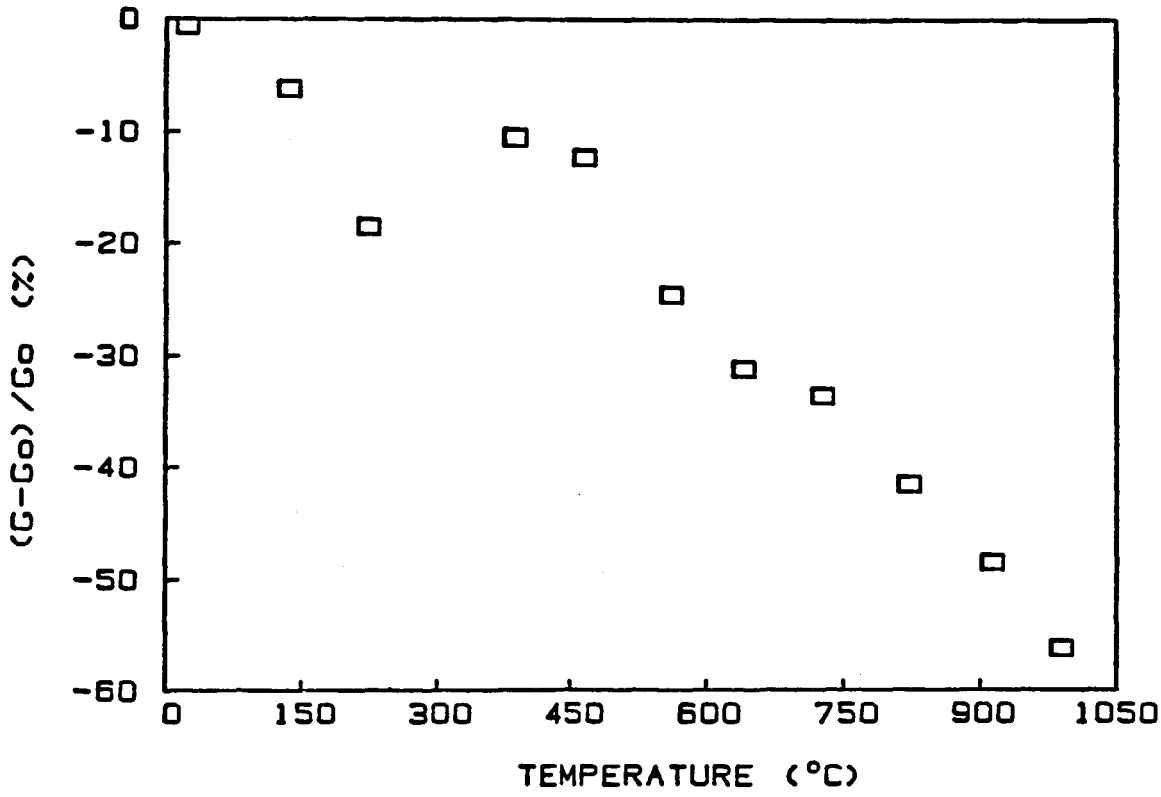

Fig. 7-7. Variation of gage factor with temperature for boron carbide.

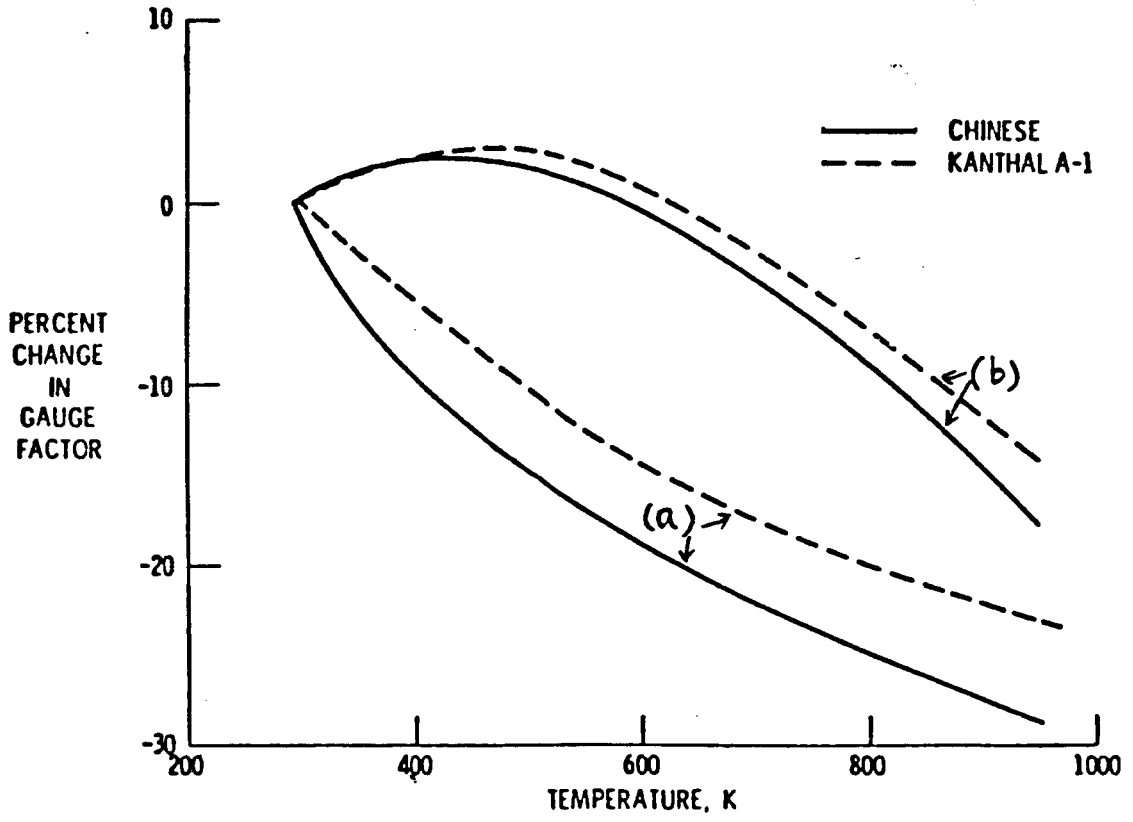

Fig. 7-8. Variation of gage factor with temperature in both tension (a) and compression (b) for Wu's Chinese gage and Kanthal A-1 gage.

resistivity of 0.1 ohm-cm in [012] orientation is the most widely used strain gage material and has a high gage factor of 125, which is 62.5 times larger than those of conventional conductors [4]. This large piezoresistive effect in silicon is attributed to the large values of piezoresistance coefficients that are associated with the symmetrical structure of silicon. The theory is quite complex and concerns intervalley carrier scattering and in some cases, impurity scattering [109]. The theory behind the even larger piezoresistive effect in B_4C is a subject suggested for further study.

The boron carbide studied in this work had Rhombohedral crystal structure with a=5.60 Å and c=12.08 Å, determined by X-ray diffraction pattern. Its elemental composition determined by chemical analysis are as follows:

	B	C	O	N	Fe	Ca
wt %	78	19.6	0.65	0.92	0.053	0.041

This boron carbide $B_{1-x}C_x$ thus had a composition with x=0.18.

CHAPTER 8

CONCLUSION

From the review of the previous works on high temperature resistance strain gages it was realized that the two characteristics of these gages, namely, the stability of their electrical resistance with temperature and time and their low temperature coefficient of resistance (TCR) are the controlling factors in the selection of candidate sensor materials. This induced the need for studying the electrical properties of the materials which are potentially useful for high temperature resistance strain gage applications.

After an intensive literature survey, a group of materials was selected for electrical resistance evaluation based on the criteria defined in chapter 3. These candidate materials included transition metal carbides and nitrides, silicon carbide and boron carbide. All the materials studied in this work showed no phase transformation in the temperature range of 23°C-1000°C and they all had some degree of electrical reproducibility and stability.

The resistivity of the transition metal compounds increased and their TCR values decreased with increasing the vacancy concentrations. The resistivity saturated at about 1000 microohm-cm, suggesting the electron mean free path was saturated at its lowest limit - the interatomic spacing in these compounds. For resistivities larger than 1000 microohm-cm, negative TCR values were observed. This suggested that these transition metal compounds are metallic in nature and the semiconducting behavior observed for some specimens are due to the large vacancy concentration in these materials which results in higher resistivity than the saturation resistivity.

The low values of TCR of these compounds were associated with highly defective lattice structures. However, structures with high concentration of defects were often unstable at high temperatures, this was observed from the resistance drift at 1000^{o}C. Actually, this dilemma between low drift and low TCR has appeared often in the annals of strain gage development of the past 30 years. Therefore, the selection of the composition of these transition metal compounds depends on which one of the two factors is more dominate.

This work on transition metal compounds supported the theory of Neshpor and Samsonov [79], which relates the electronic heat capacity, density of states at the Fermi level, and TCR. The stoichiometric materials with small electronic specific heat constants would have low density of states at the Fermi levels, and therefore have low TCR values. The relation between these three factors can complement the selection criteria of materials with small TCR.

It was also found that the TCR of transition metal nitrides decreased monotonically in going from compounds of metal of group VI to those of group V then to those of group IV of the period table. Also the TCR of transition metal nitrides and carbides with the transition metals in the same column of the period table decreased as quantum number of the transition metal increased. Carbides had lower TCR than the corresponding nitrides.

The study of the electrical resistance of boron carbide brought focused attention on a material in which the electronic transport proceeds via a low-mobility hopping of a temperature independent density of small-polaronic charge carriers. This kind of material has a

small TCR at high temperatures and their electrical stability is generally improved by thermal cycling and perhaps by controlled oxidation.

In the case of silicon carbide, it was found that β-SiC was more suitable than α-SiC for high temperature resistance strain gage applications. It was noted that the decrease in resistance with an increase in temperature was faster in α-SiC than in β-SiC. One of the effect of doping nitrogen in β-SiC was a decrease in TCR values at high temperatures, however, this resulted in an increase in the drift rate. Again, we have to compromise between the two factors: low TCR and low drift. It was also found that the resistance stability of thin film specimens depends on their thickness; the thicker the film, the higher the stability.

For a resistance strain gage to be useful for 2000 micro static strain measurement at 1000^{o}C for 50 hours within 10 % accuracy, (TCR x ΔT)/G of its material must be below 200 ppm, and the DR/G must be less than 4 ppm/hr, calculated from Eq. (2-1), where ΔT is the uncertainty in temperatures, G the gage factor. For alloys, the gage factor (G) is usually close to 2, so the

value of (TCR x ΔT) should not be larger than 400 ppm/^{o}C. For semiconductors, G has large values, usually of the order of 100 to 200. As a result (TCR x ΔT) value should be less than 2000 ppm/^{o}C. For example, for a performance in a region with 2K temperature uncertainty, the TCR of the alloys should be lower than 200 ppm/^{o}C, and TCR for semiconductors should be lower than 1000 ppm/^{o}C. Based upon the data presented in Table 5-2 and 6-1 which summarize the experimental results, we conclude that TiC, ZrC, B_4C, and β-SiC have the potential to be used in production of high temperature resistance strain gages. However, further studies on the optimization of their electrical behaviors and protection of these materials from oxidation at high temperature is necessary before these materials could be utilized in strain gage.

REFERENCES

1. L. Kelvin, "The Electrodynamical Qualities of Metals", Phil. Trans., vol. 146, p. 649-672 (1856).

2. J. O. Brittain, Research Proposal Submitted to NASA, Oct. 26 (1984).

3. G. S. Holister, Experimental Stress Analysis, Cambridge University Press, p. 53-54 (1967).

4. E. D. Padgett and W. V. Wright, "Silicon Piezoresistive Devices" in Semiconductor and Conventional Strain Gages, Ed. by M. Rean, III, Academic press, London, p. 1-19 (1962).

5. W. N. Sharpe, Jr., "Strain Gages for Long Term High Temperature Strain Measurements", Experi. Mech., p. 482-488, Dec., (1975).

6. R. Bertodo, "Precious Metal Alloys for High-Temperature Resistance Strain Gages", Brit. J. Appl., Phys. Ser. 2, vol. 1, p. 1743-1752 (1968).

7. D.C. Drennen, C. M. Jackson, and N. Crites and J. E. Sorenson, " Topical report on LMFBR instrumentation: Strain Gages, Phase V. High Temperature Strain Gage Development Program. Task I. Literature and Field Survey, Contract No. 83-0004, Dept. NITSTID-25816, Nov. 13, (1970).

8. M. M. Lemcoe, "Development of Electrical Resistance Strain Gage System for Use to 2000°F", ISA, vol. 572 p. 1-10 (1975).

9. Pratt and Whitney, "Thin Film Strain Gage Development Program- Strain Gages for Dynamic Measurements", Contract NASA 3-21242, preliminary report (1980).

10. R. W. Cahn and P. H. Haasen, Physical Metallurgy, North-Holland Physics Pub., p. 158-161 (1983).

11. C. O. Hulse, R. S. Bailey and F. D. Lemkey, High Temperature Static Strain Gage Alloy Development Program, NASA report No. CR-174833, March (1985).

12. T. T. Wu, L. C. Ma and L. B. Zhao, "Development of Temperature Compensated Resistance Strain Gages for Use to 700°C", Exp. Mech., vol. 21, no. 3, p. 117-123 (1981).

13. H. F. Hobart, "Evaluation Results of the 700°C Chinese Strain Gages", NASA conference publication 2443, p. 77-84, (1985).

14. J. C. Sanchez and W. V. Wright, "Semiconductor Strain Gages- What Can They Do?", ISA Journal, vol. 9, no. 5, p. 38-40, May (1962).

15. C. S. Smith, "Piezoresistive Effect in Germanium and Silicon", Phys. Rev., vol. 94, p.42-49, (1954).

16. W. P. Mason and R. N. Thurston, "Use of Piezoresistive Materials in the Measurement of Displacement, Force and Torque", Jnl. Acoust. Soc. of Amer., vol. 29, no. 10, p.1096-1101, Oct. (1957).

17. W. P. Mason, J. J. Forst and L. M. Tornillo, "Recent Developments in Semiconductor Strain Transducers", in Semiconductor and Conventional Strain Gages, Academic Press, New York, p. 109-121, (1962).

18. V. Rapatskaya and G. E. Rudashevskii, "Silicon α-Carbide Strain Transducers", Measurements Tech., p.771-772, (1968).

19. G. V. Lomakina, "The Piezoresistance of P-Type 6H SiC", Sov. Phys. Solid. State, vol. 17, no. 9, p.1808-1811, (1976).

20. A. A. Glagovskii, G. N. Guk, V. M. Lyubimskii and M. P. Chertkov, "Temperature Dependence of Piezoresistance Constants of Some Polytypes of n-Type SiC", Sov. Phys. Semicond., vol. 12(1), p. 116-117, (1978).

21. G. R. Witt, " The Electromechanical Properties of Thin Films and the Thin Film's Strain Gage", Thin Solid Films, vol. 22, p. 133-156 (1974).

22. K. Schroder, CRC Handbook of Electrical Resistivities of Binary Metallic Alloys, CRC Rress, p.3-38, 388-390 (1983).

23. S. N. Lvov, P. I. Malko and V. F. Nemchenko, "High-Temperature Resistivity of d-Transition Metals", Phys. Met. Metallogr, vol. 32(3), p. 35-47 (1971).

24. N. F. Mott and H. Jones, The Theory of the Properties of Metals and Alloys, Oxford University Press, p. 268-302 (1936).

25. J. M. Ziman, Electrons and Phonons, Oxford, U. P. London, p. 376-382, (1960).

26. J. C. H. Chiu, "Deviations from Linear Temperature Dependence of the Electrical Resistivity of V-Cr and Ta-W Alloys", Phys. Rev., vol. B13, No. 2, p.1507-1514, (1976).

27. T. Aisaka and M. Shimizu, "Electrical Resistance, Thermal Conductivity and Thermoelectric Power of Transition Metals at High Temperatures", J. Phys, Soc. Jpn., vol. 28, p. 646-654, (1976).

28. J. H. Mooij, "Electrical Conduction in Concentrated Disordered Transition Metal Alloys", Phys. Stat. Sol., vol. (A)17, p. 521-530, (1973).

29. N. F. Mott and E. A. Davies, Electronic Processes in Non-Crystalline Materials, Clorerdon Press, Oxford p. 408-425, (1971).

30. Z. Fisk and G. W. Webb, "Saturation of the High-Temperature Normal-State Electrical Resistivity of Superconductors", Phys. Rev. Lett., vol. 36, no. 18, p. 1084-1086, (1980).

31. L. V. Meisel and P. J. Cote, "Application of the Extended Ziman Theory to Amorphous Nickel-Phosphorus Alloys", Phys. Rev., vol. B15, p.2970-2983 (1977).

32. A. B. Chen, G. Weisz and A. Sher, "Temperature Dependence of the Electron Density of States and dc Electrical Resistivity of Disordered Binary Alloys", Phys. Rev., vol. B5, p. 2897-2924, (1972).

33. K. I. Wysokinski, "Electronic Transport in Disordered Alloys: Effect of Thermal and Off-Diagonal Disorder ", J. Phys., vol. C11, p. 291-302, (1978).

34. V. Christoph, "Temperature Dependence of the Electrical Resistivity of Disorder Metallic Alloys" Phys. Stat. Sol., vol. (b)91, no. 2 , p. 593-603, (1979).

35. J. Richter and W. Schiller, "Temperature Dependence of the Electrical Resistivity of Disordered Alloys", Phys. Stat. Sol., vol. (b)92, p. 511-517 (1979).

36. F. Brouers and A. V. Vedyayev, "Theory of Electrical Conductive in Disordered Binary Alloys. The effect of s-d Hybridization", Phys. Rev., vol. B5, p. 348-360 (1972).

37. M. Brauwers and F. Brouers, "Temperature and Strain Effect on Electrical Resistivity of Transition Metal Alloys: Application to Strain Gages", J. Phys. F: Metal Phys., vol. 6, no. 7, p. 1331-1339, (1976).

38. C. Kittel, Introduction to Solid State Physics, John Willey and Sons, Inc., p. 228-237 (1976).

39. R. A. Smith, Semiconductors, Cambridge University Press, p. 10-23, (1978).

40. R. M. Rose, L. A. Shepard and J. Wulff, The Structure and Properties of Materials, IV. Electronic Properties, MIT Press, p. 149-150, (1975).

41. R. Bertodo, "Platinum Metal Alloys for the Measurement of Strain at High Temperature", Brit. J. of Appl. Phys., Ser. 2, vol. 1, no. 12, p. 1743-1752, Dec., (1968)

42. G. E. Dieter, Mechanical Metallurgy , McGraw-Hill Inc. p. 239-242, 451-453 (1976).

43. R. M. White and T. H. Geballe, Solid State Physics-Long Range Order in Solid, Academic Press, New York, p. 179-181 (1979)

44. J. H. Westbrook, Intermetallic Compounds, John Wiley and Sons, Inc., p. 260-265 (1967).

45. Y. Ochiai and J. O. Brittain, "Anomalous Electrical Resistivity in CoGA Intermetallic Compounds", Phys. Letters, vol. 72A, no. 4, p. 347-349 (1979).

46. O. Kubascheuski and C. D. Alcock, Metallurgical Thermochemistry, 4th ed., p. 15-17 (1967).

47. C. Wagner, Thermodynamics of Alloys, Addison-Wesley Inc., p. 32-40 (1952).

48. D. A Porter, K. E. Easterling, Phase Transformation in Metals and Alloys, Van Nostrand Reinhold Co., p. 35-36, 358-365, (1981).

49. R. J. Elliott, A. F. Gibson, Solid State Physics, Harper and Raw Pub. Inc., p. 299-300 (1974).

50. G. T. Meaden, Electrical Resistance of Metals, Plenum Press, New York, p. 39-41 (1965).

51. ibid 39, p. 261-262.

52. J. O. Brittain, D. Geslin, J. F. Lei, "Elevated Temperature Strain Gages", NASA Conference Publication no. 2444, p. 69-84, (1986).

53. E. K. Storms, The Refractory Carbides, Academic Press, New York and London (1967).

54. R. F. Vines, The Platinum Metals and Their Alloys, International Niclel Co., p. 19-25 (1941).

55. A. Neckel, "Recent Investigations on the Electronic Structure of the Forth and Fifth Group Transition Metal Monocarbides, Mononitrides, and Monoxides", Int. J. Quantum Chem., vol. 23, p. 1317-1353 (1983).

56. A. Munster, K. Sagel and G. Schlanp, "Titanium Nitride and Titanium Carbide as Semiconductores", Nature, vol. 174, no. 4442, p. 1154-1155 (1954).

57. K. Kawabata and T. Muto, "Electrical Properties of Titanium Nitride Thin Films Deposited by Reactive Sputtering", Electrocomponent Science and Technology, vol. 8, p. 249 (1981).

58. W. Posadowski and Lubomila Arol-stepniewska, "Properties of TiNx Films Reactively Sputtered in an Argon-Nitrogen Atmosphere", Thin Solid Films, vol. 62, p. 347-351 (1979).

59. O. A. Golikova, E. O. Dzhafarov, A. I. Avgustinik and G. M. Klimeshin, "Electrical Properties of Carbides of Transition Metal of Group IV in the 20-2000°C Temperature Range", Heat Transfer-Soviet Research, vol. 5, no. 2, p. 11-14 (1973).

60. G. V. Samsonov, S. M. Lvov, and V. P. Nemchenko, "Semiconducting Properties of the Higher Temperature Chromium Nitride", Dopovide Akad. Nauk Ukr. Rsr., no. 7, p. 936-938 (1962).

61. V. F. Nemchenko, "Some Characteristics of the Thermal and Electrical Conductivities of Nitride Interstitial Phase", Poroshkovaya Metallurgiya, vol. 7, no. 223, p. 87-91 (1981).

62. R. Petrovic, T. Nenadovic, N. Kraljevic and T. Dimitrijevic, "Electrical and Structural Properties of Tantalum Nitride Thin Films Deposited by Sputtering", Thin Solid films, vol. 57, p. 333-336 (1979).

63. R. Jenkins, W. F. McClune, et al., Powder Diffraction File, Inorganic Phases , The International Center Press, (1986)

64. P. T. Dawaon and K. K. Tzatzov, "Quantitative Auger Electron Analysis of Titanium Nitrides", Surface Science, vol. 49, p. 105-118 (1985).

65. L. E. Toth, Transition Metal carbides and nitrides, Academic press, London, p. 71-99 (1971).

66. F. I. Ajami and R. K. MacCrone, "Thermal Expansion, Debye Temperature and Gruneisen Constant of Carbides and Nitrides", J. of the Less-Common Metals, vol. 38, p. 101-110 (1974).

67. M. Hansen, Constitution of the Binary Alloys, McGraw-Hill Book Company Inc., New York, 2nd ed., p. 232-233 (1958).

68. W. Williams, "Scattering of Electrons by Vacancies in Nonstoichiometric Crystals of Titanium Carbide", Phys. Rev., vol. 135, p. A505-510 (1964).

69. B. V. Khaenko, "Order in Cubic Carbides and Nitrides of Transition Metal of Group IV and V", Neorg. Mater, vol. 15, no. 15, p. 35-43 (1979).

70. A. Yajima, Y. Segawa, R. Matsuzaki and Y. Saeki, "Reaction Process of Zirconium Tetrachloride with Ammonia in the Vapor Phase and Properties of the Zirconium Nitride Formed", Bull. Chem. Soc. Jpn., vol. 56, p. 2638-2642 (1983).

71. H. Bilz, "Under Elektronenzustande von Harstoffen mit Natriumchloridstruktur", Z. Phys., vol. 153, p. 338-358 (1958).

72. P. Costa and R. R. Conte, Compounds of Interest in Nuclear Reactor Technology, Ed. by J. T. Waber, Institute of Metals Division, Special Report No 13, (1967).

73. G. V. Samsonov, "Continuous-Discrete Character of Variation of the Type of Binding in Refractory Compound of Transition Metals and Principles of Classification of Refractory Compounds", in Refractory Transition Metal Compounds- High Temperature Cermets, Ed. by G. V. Samsonov, p. 1-13, Academic Press Inc., (1962).

74. G. V. Samsonov, V. S. Sinelnikova, "Electrical Resistance of Refractory Compounds at High-Temperatures", in Refractory Transition Metal Compounds - High Temperature Cermets, Academic Press Inc., p. 172-177 (1964).

75. J. L. Calais, "Band Structure of Transition Metal Compounds", Adv. Phys, vol. 26, no. 6, p. 847-885 (1977).

76. A. Dunand, H. D. Flack and K Yvon, "Bonding Study of TiC and TiN. I. High-precision X-ray-diffraction Determination of the Valence-Electron Density Distribution, Debye-Waller Temperature Factors, and Atomic Static Displacements in $TiC_{0.94}$ and $TiN_{0.99}$", Phys Rev., vol. B31, p. 2299-2315 (1985).

77. P. T. P. De Maayer and J. D. Machenzie, "The Electrical Properties of Thin Films of TiNx and TiCx", Z. Naturforsch, vol. 30a, p. 1661-1665 (1975).

78. V. A. Gubanov, A. L. Ivanovaky, G. P. Shveikin and D. E. Ellis, "Vacancies and the Energy Spectrum of Refractory Metal Compounds: TiC and TiO", J. Phys. Chem. Solids, vol. 45, no. 7, p. 719-130, (1984).

79. V. S. Neshpor and G. V. Samsonov, "Electrical Properties of Molybdenum Silicides", in Refractory Transition Metal Compounds-High Temperature Cermets, Academic Press, p. 162-171 (1964).

80. L. W. Shacklette and W. S. Williams, "Influence of Order-Disorder Transformation on the Electrical Resistivity of Vanadium Carbide", Phys. Rev., vol. B7, p. 5041-5053 (1973).

81. H. Hochst, R. D. Bringens, P. Steiner and Th. Wolf, "Photoemission Study of the Electronic Structure of Stoichiometric and Substoichiometric TiN and ZrN", Phys Rev., vol. B25, p. 7183-7191 (1982).

82. L. Porte, L. Roux and J. Hanus, "Vacancy Effects in the X-Ray Photoelectron Spectra of TiNx", Phys. Rev., vol B28, p. 3214-3224 (1983).

83. H. Hochst, P. Steiner, S. Hufner and C. Politis, "The XPS Valence Band Spectra of NbC", Z. Phys, vol. B37, p. 27-31 (1980).

84. V. A. Gubanov, E. Z. Kurmaev and D. E. Ellis, "Valence States of Titanium Atoms in Nonstoichiometric Carbides: X-ray Emission Spectra and Cluster Calculations", J. Phys., vol. C14, p. 5567-5574 (1981).

85. J. Pfluger, J. Flink, G. Grecelius, K. P. Bohnen and H. Winter, "Electronic Structure of Unoccupied States of TiC, TiN and VN by Electron-Energy-Loss-Spectroscopy", Solid St. Commun., vol. 44, p. 489-492, (1982).

86. L. C. Dy and W. S. Williams, "Resistivity, Superconductivity, and Order-Disorder Transformations in Transition Metal Carbides and Hydrogen-Doped Carbides", J. Appl. Phys., vol. 53, no. 12, p. 8915-8927 (1982).

87. Z. Fisk and G. W. Webb, "Saturation of the High-Temperature Normal-State Electrical Resistivity of Superconductors", Phys. Rev. Lett., vol. 36, p. 1084-1086 (1976).

88. D. Emin and C. Wood, in Proceedings of the 18th Intersociety Energy Conversion Conference American Institute of Chemical Engineering, New York, vol. 1, p. 222-226 (1983).

89. C. Wood and D. Emin, "Conduction Mechanism in Boron Carbide", Phys. Rev., vol. B29, no. 8, p. 4582-4597 (1984).

90. D. Emin, G. A. Samara and C. Wood, Prodeedings of the 1984 International Conference on Physics of Semiconductors, Spring, New York, p. 1349-1352, (1985).

91. T. Holstein, "Studies of Polaron Motion Part II. The "Small" Polaron", Ann Phys., New York, vol. 8, p. 343-389 (1959).

92. D. Emin and T. Holstein, "Strdies of Small-Polaron Motion IV. Adiabatic Theory of the Hall Effect", Ann. Phys., New York, vol. 53, p. 439-520 (1969).

93. D. Emin, "Small Polarons", Physics Today, vol. 35(6), p. 34-40 (1982).

94. D. Emin, "Electronic Transport in Boron Carbides" in Boron- Rich Solids, Ed. by D. Emin, T. Aselage, C. L. Beckel, I. A. Hoeard and C. Wood, American Institute of Physics, New York, p. 189-205 (1986).

95. L. J. Azevedo, E. L. Venturine, D. Emin and C. Wood, "Magnetic Susceptibility Study of Boron Carbides", Phys. Rev., vol. B32, p. 7970-7985 (1985).

96. T. N. Nazarchuk and L. N. Mekhanoshina, "The Oxidation of Boron Carbide", Poroshkovaya Met., No.2, p. 46-48 (1964).

97. Jurgen Schlichting, Gerhard Czack and P. Kuhn, Gmelin Handbook of Inorganic Chemistry, 8th Ed., p. 107-109 (1984).

98. Takeshi Nagai, Kazushi Yamamoto and Ikuo Kobayashi, "Effects of Nitrogen on the Electrical Properties of Sputtered SiCx Films", Thin Solid films, vol. 106, p. 303-309 (1983).

99. W. J. Choyke and L patrick, in Silicon Carbide- 1973, Ed. by R. C. Marshall, J. W. Faust and C. E, Ryan, p. 261-265 (1973).

100. S. I. Vlaskina, V. A. Kravets, K. V. Nazarenko, O. T. Sergeev and I. N. Frantsevich (Dopov. Akad. Nauk Ukr. RsR Ser. A Fiz. -Mat. Tekhn. Nauki 1981 No. 3, p. 49-52; C. A. 94, no. 217905 (1981).

101. K. Sasaki, E. Sakuma, S. Misawa, S. Yoshida and S. Gonda, "High Temperature Electrical Properties of 3C-SiC Epitaxial Layers Grown by Chemical Vapor Deposition", Appl. Phys. Lett., vol. 45(1), p. 72-73 (1984).

102. D. L. Barrett and R. B. Campbell, "Electron Mobility Measurements in SiC Polytypes", J. Appl. Phys., vol. 38, p. 53-57 (1967).

103. L. Patrick, "Electron Mobilities in SiC Polytypes", J. Appl. Phys., vol. 38, p. 50-53 (1967).

104. A. Dietzel et al., "Oxidation Mechanism of SiC", Ber. Deut. Keram. Ges., vol. 37, p. 524-525 (1960).

105. R. M. McClintock, "Strain Gage Calibration Device for Extreme Temperature". The Review of Scientific Instruments, vol. 30, no. 8, p. 715-718 (1959).

106. A. P. Poorman, Strength of Materials, McGraw-Hill Book Company Inc., New York. (1945).

107. C. Herring, "Transport Properties of a Many Valley Semiconductor", Bell System Technical Journal 34, p. 237-240, (1955).

108. F. Morin, T. Geballe, C. Herring, "Temperature Dependence of Piezoresistance of High Purity Silicon", Phys. Rev. Jap., vol. 15, p. 525-539 (1957).

109. J. C. Sanchez, "Semiconductor Strain Gages: A State of the Art Summary", Strain Gage Readings, vol. IV, no 4, p. 3-16 (1961).

110. H. J. Goldschmidt, Interstitial Alloys, N. Y. Plenum Press, p. 89, 216 (1967).

111. R. P. Elliott, Constitution of Binary Alloys, 1st Supplement, McGraw-Hill Book Company p. 110-111, 227-228 (1965)

112. P. Weinberger, C. P. Mallett, P. Podloucky and A. Neckel, "The Electronic Structure of HfN, TaN and VN", J. Phys. C: Solid St. Phys., vol. 13, p. 173-187 (1980).

113. K. Schwarz, H. Ripplioger and A. Nechel, "Energy Band Structure and X-Ray Emission Spectra of ZrC and ZrN", Z. Phys. B: Condensed Matter, vol. 48, p. 79-87 (1982).

114. K. Schwarz, "The Electronic Structure of NbC and NbN", J. Phys. C: Solid State Phys., vol. 10, p. 195-207 (1977).

115. J. Redinger, R. Eibler, P. Herzig, A. Neckel, R. Podloucky and E. Wimmer, "Vacancy Induced Changes in the Electronic Structure of Titanium Carbides- 1. Band Structure and Density of State", J. Phys. Chem. Solids, vol. 46, no. 3, p. 383-398 (1985).

116. B. M. Klein, D. A. Papaconstantopoulos and L. L. Boyer, "Linear-Combination-of-Atomic-Orbitals-Coherent-Potential-Approximation Studies of Carbon Vacancies in the Substoichiometric Refractory Monocarbides NbCx, TaCx and HfCx", Phys. Rev. B, vol. 22, no. 4, p. 1946-1966 (1980).

117. M. Dorrer, R. Eibler and A. Neckel, "An Improved LCAO Interpolation Scheme for Energy Band Structures. Application to Four Compounds (ScN, ScP, TiN, ZrN) Crystallizing in the Sodium Chloride Structure", Theoret. Chem. Acta (Berl.) no. 60, p. 313-325 (1981).

118. C. H. de Novion and J. P. Landesman, "Order and Disorder in Transition Metal Carbides and Nitrides: Experimental and Theoretical Aspects", Pure and Appl. Chem., vol. 57, no. 10, p. 1391-1402 (1985).

119. J. Billingham, P. S. Bell and M. H. Lewis, "Vacancy Short-Range Order in Substoichiometric Transition Metal Carbides and Nitrides with the NaCl Structure. I. Electron Diffraction Studies of Short-Range Ordered Compounds", Acta. Cryst. A. 28 p. 602-602 (1972).

APPENDIX A

PHASE DIAGRAMS FOR CANDIDATE MATERIALS

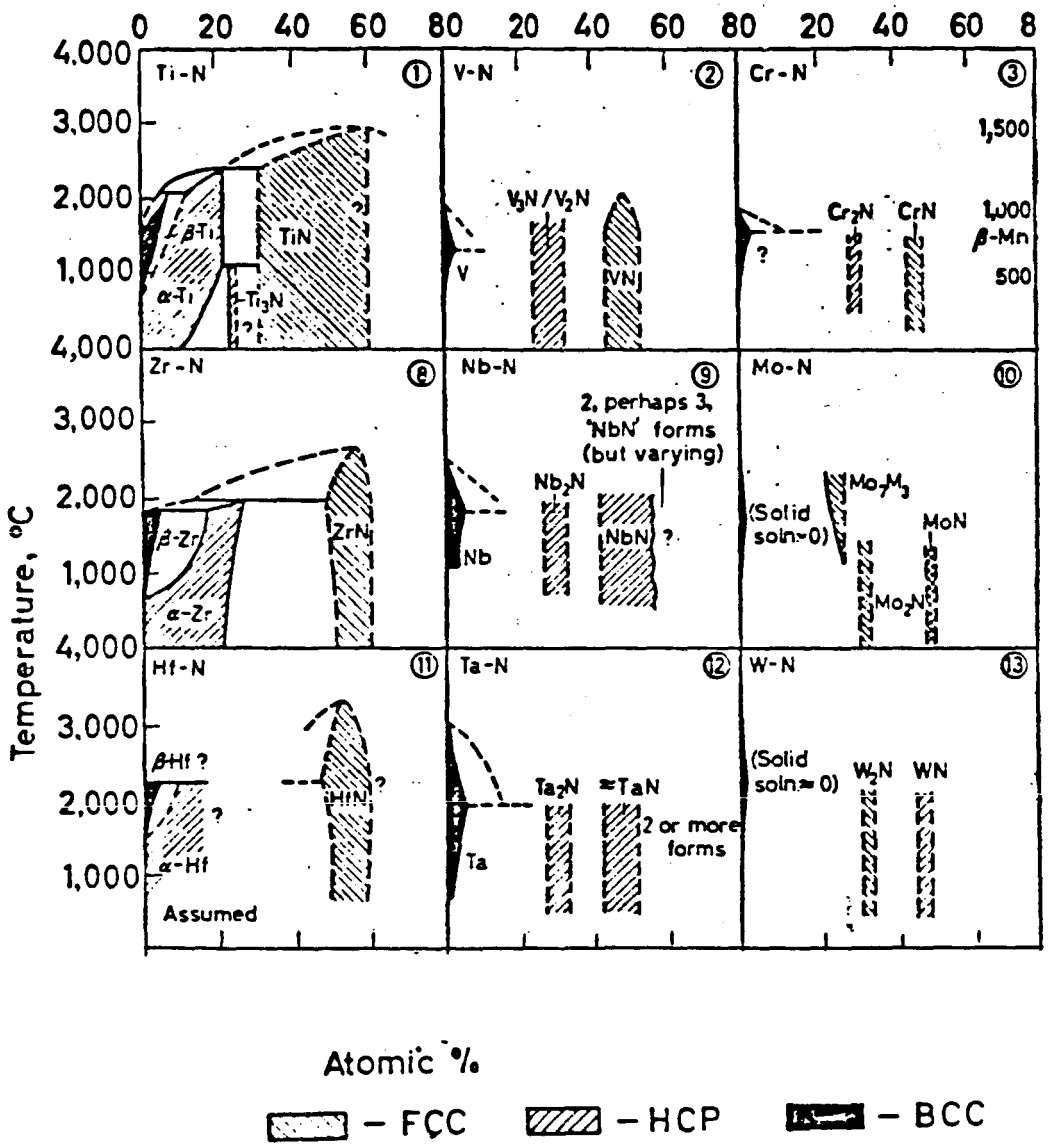

Fig. A-1. Phase diagram of transition metal nitrides (after Goldschmidt [110]).

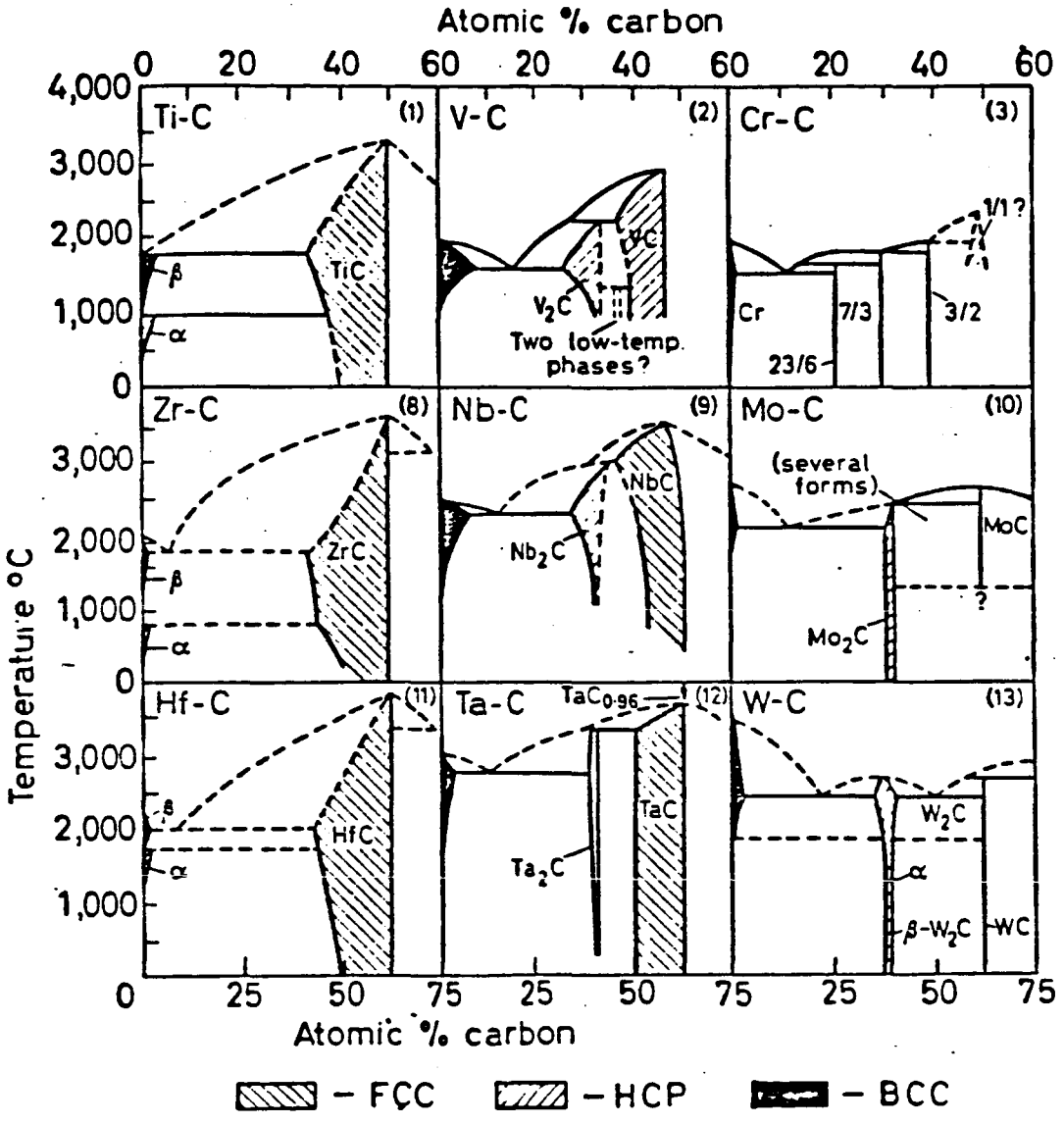

Fig. A-2. Phase diagram of transition metal carbides (after Goldschmidt [110]).

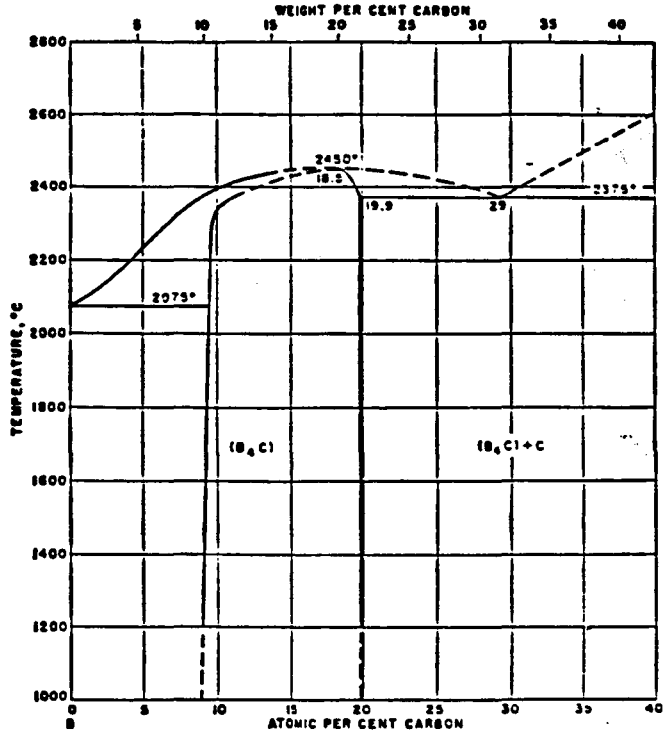

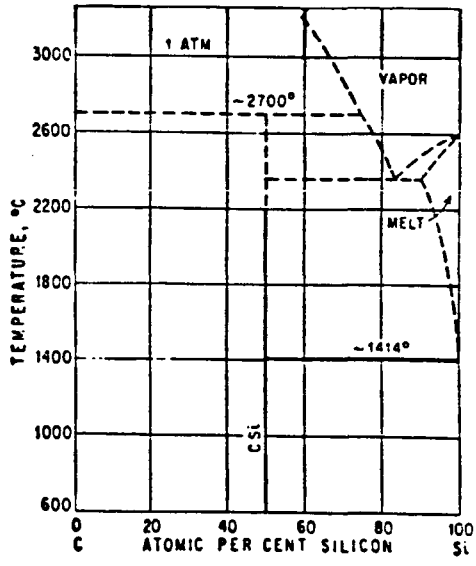

Fig. A-3. Phase diagram of boron carbide (a) and silicon carbide (b). (after Elliott [111]).

APPENDIX B

PROPERTIES OF THE SPECIMENS

Table B-1

Properties of the specimens

Specimen	Homogeneity* range (x)	Structure#	Melting+ temp.°C
TiN_x	0.50-1.15	NaCl	2949
ZrN_x	0.55-1.15	NaCl	2982
TaN_x	0.80-0.90	Hex	3093
CrN_x	0.98-0.99	NaCl	1500
TiC_x	0.50-0.97	NaCl	3067
ZrC_x	0.58-0.97	NaCl	3420
$B_{1-x}C_x$	0.08-0.20	Rhom.	2350
α-SiC		Hex	
β-SiC		FCC	2830

* after Khaenko [69]

after Toth [65] and Samsonov [73]

+ after Toth [65] and Samsonov [73].

APPENDIX C

LISTING OF THE COMPUTER PROGRAM WHICH TAKES DATA FROM THE ELECTRICAL MEASUREMENT INSTRUMENTS AND SAVES THE DATA ON A FLOPPY DISKETTE AND PRINTS OUT ON THE PRINT

```
10 REM*************************************************************************
20 REM*                                                                       *
30 REM*            BASICA PROGRAM TO TAKE DATA AUTOMATICALLY                  *
40 REM*             FROM ELECTRICAL MEASUREMENT INSTRUMENTS                   *
50 REM*                                                                       *
60 REM*                        FILE NAME: INTERFAC                            *
70 REM*                                                                       *
80 REM*************************************************************************
100 DIM TEMP1(200),TEMP2(200),TEMP3(200),TEMP4(200),TEMP(200),RESIST(3,200),NAM$
(5),TIM$(200),DAT$(200),SIGN(3,200)
110 '
120 '
130 '-----------------------------------------------------------------
140 '       default values
150 '-----------------------------------------------------------------
160 '
170 '
190 GRADMAX=5                 'maximum gradient of temperature allowed
200 TEMPMIN=0                 'minimum temperature difference between 2 measuremen
210 TIMMIN=10                 'minimum time difference between 2 measurements
220 DELTATP=40                'minimum temperature change between 2 cycles
225 CYCLNUM=1                 'number of the first cycle
230 UNITEMP$="C": UNIRES$="OHM"
235 TIM$(0)="00:00": DAT$(0)="0-00-1900"      'time for the fictive data "o"
236 I=1                       'number of the first data
250 '
260 '
470 '*****************************************************************
480 '
490  '      BEGINING OF THE PROGRAM
495 '
496 '*****************************************************************
500 GOSUB 3170                'introduction of the information for the table
510 GOSUB 2080                'creation of the table
520 PARAM$="INIT/1/&H310/P/": GOSUB 9600     'initialize IEEE
530 GOSUB 4065                'set-up scanner
540 GOSUB 4165                'set-up multimeter 192 for measuring temperature
545 GOSUB 5400                'set up ac bridge for measuring resistance
550 GOSUB 4250                'read thermocouple voltages
560 GOSUB 5000                'conversion of voltage into temperature
570 TEMP1(I)=TEMP1            'temperature for thermocouple 1
580 TEMP2(I)=TEMP2            '                             2
585  PRINT "TEMPERATURE before: ";TEMP1,TEMP2
590 IF ABS(TEMP1(I)-TEMP2(I))>GRADMAX THEN GOTO 550
600    FOR F=1 TO NSPECI
610      CHANEL$=CHAN$(F)  'channel for specimen F
620  GOSUB 4480         'read resistance of specimen F
625  PRINT USING "RESISTANCE:  #.######";RESIST(F,I)
630    NEXT F
640 GOSUB 4250                'read thermocouple voltage
650 GOSUB 5000                'volt-temperature
660 TEMP3(I)=TEMP1
670 TEMP4(I)=TEMP2 : PRINT "temperature after : ";TEMP1,TEMP2
680 IF ABS(TEMP3(I)-TEMP4(I))>GRADMAX THEN GOTO 550 'check that the variation
690 IF ABS(TEMP3(I)-TEMP1(I))>GRADMAX THEN GOTO 550 'of temperature is lower
700 IF ABS(TEMP3(I)-TEMP2(I))>GRADMAX THEN GOTO 550 'than a given max gradient
710 IF ABS(TEMP4(I)-TEMP1(I))>GRADMAX THEN GOTO 550
720 IF ABS(TEMP4(I)-TEMP2(I))>GRADMAX THEN GOTO 550
730 TIM$(I)=TIME$: DAT$(I)=DATE$
740 TIME1$=TIM$(I-1): DATE1$=DAT$(I-1)
750 TIME2$=TIM$(I): DATE2$=DAT$(I)
760 GOSUB 2870                'derive the difference in minutes between t1 and t2
Ok
770 IF ABS(TEMP(I)-TEMP(I-1))<TEMPMIN THEN GOTO 550 ELSE GOTO 790
780 IF TIMEDIF<TIMMIN THEN GOTO 550
785 TEMP(I)=(TEMP1(I)+TEMP2(I)+TEMP3(I)+TEMP4(I))/4  'average temperature
```

```
790 GOSUB 2240              'introduce the data in the table
800 GOSUB 4250             'read thermocouple voltages
820    FOR F=1 TO NSPECI
825 GOSUB 5000             'conversion of voltage into temperature
830       GOSUB 2565         'creation of the disket file
840    NEXT F
842 PRINT: PRINT
845 I=I+1: PRINT"data: ";I  'increment the number of the data
850 GOTO 550                'begins a new serie of measurements
900 END
1950 '
1960 '*****************************************************************
1970 '
1980 '   BEGINING OF THE SUBROUTINES
1990 '
1995 '*****************************************************************
2000 '
2010 '
2020 '-------------------------------------------------------
2030 '           Subroutine Creation of the Table
2040 '-------------------------------------------------------
2050 '
2060 '
2070 'CLS
2080 LPRINT
2090 LPRINT
2100 LPRINT CHR$(27);"E"
2110 LPRINT "                          ";TITLE$
2120 LPRINT CHR$(27);"F"
2130 LPRINT
2140 LPRINT COMENT$(1);"        ";COMENT$(2);"              ";COMENT$(3)
2150 LPRINT
2155 LPRINT
2157 LPRINT "Date: ";DATE$
2159 LPRINT
2160 LPRINT "-------------------------------------------------------------
-----------"
2170 LPRINT " Time                  Temperature                          Resistance
     "
2180 LPRINT "                              ";UNITEMP$;"
     ";UNIRES$
2190 LPRINT
2200 LPRINT "          Tb1     Tb2     Ta1     Ta2       Tav       R1           R2
    R3     "
2210 LPRINT "-------------------------------------------------------------
-----------"
2211 RETURN
2212 '
2214 '
2215 '-----------------------------------------------------
2220 '     Subroutine  introduction of the lines of data
2230 '-----------------------------------------------------
2232 '
2234   I=I+1
2240   LPRINT USING "\    \";TIME$;: LPRINT " ";
2242   LPRINT USING "####.#";TEMP1(I);: LPRINT " ";
2243   LPRINT USING "####.#";TEMP2(I);: LPRINT " ";
2244   LPRINT USING "####.#";TEMP3(I);: LPRINT " ";
2245   LPRINT USING "####.#";TEMP4(I);: LPRINT " ";
2246   LPRINT USING "####.##";TEMP(I);: LPRINT "    ";
2247   LPRINT USING "#.######";RESIST(1,I);: LPRINT "  ";
2248   LPRINT USING "#.######";RESIST(2,I);: LPRINT "  ";
2249   LPRINT USING "#.######";RESIST(3,I)
2250   LPRINT USING "####.##";TEMPCOMP
2260   RETURN
2500   '
```

```
2510 '
2520 '------------------------------------------------------------
2530 '          Subroutine  creation of the files
2540 '------------------------------------------------------------
2550 '
2560 '
2567  IF I>1 THEN GOTO 2580           'no need to reopen the same file
2570  OPEN NAM$(F) FOR OUTPUT AS #F
2580  WRITE #F,TEMP(I),RESIST(F,I)
2600  RETURN
2800 '
2810 '
2820 '------------------------------------------------------------
2830 '             Subroutine Derive the difference in minutes
                          between two Times Values
2840 '------------------------------------------------------------
2850 '
2860 '
2865   'conversions of date and time in numeric values
2870 HOUR1=VAL(MID$(TIME1$,1,2)): MINUT1=VAL(MID$(TIME1$,4,2))
2880 HOUR2=VAL(MID$(TIME2$,1,2)): MINUT2=VAL(MID$(TIME2$,4,2))
2890 MONTH1=VAL(MID$(DATE1$,1,2)): DAY1=VAL(MID$(DATE1$,4,2))
2900 MONTH2=VAL(MID$(DATE2$,1,2)): DAY2=VAL(MID$(DATE2$,4,2))
2905 '
2910   'adjustments for the ends of days and months
2920 IF MONTH1>MONTH2 THEN DAY1=DAY2+1
2930 IF MONTH2>MONTH1 THEN DAY2=DAY1+1
2940 IF DAY1>DAY2 THEN HOUR1=HOUR1+24
2950 IF DAY2>DAY1 THEN HOUR2=HOUR2+24
2953 '
2955 '     difference of time (in minutes) between time1 and time2
2960 HOURDIF=HOUR2-HOUR1
2970 IF HOURDIF>0 THEN TIMEDIF=HOURDIF*60+MINUT2-MINUT1
2980 IF HOURDIF<0 THEN TIMEDIF=HOURDIF*60+MINUT1-MINUT2
2990 IF HOURDIF=0 THEN TIMEDIF=ABS(MINUT1-MINUT2)
2991 '
2992    PRINT " the time difference is : ";TIMEDIF,TIME$,DATE$
3000 RETURN
3100 '
3110 '
3120 '-----------------------------------------------------
3130 '   Subroutine INPUT of the informations for the Table
3140 '-----------------------------------------------------
3150 '
3160 '
3170 CLS
3180 PRINT "*************************************************************"
3190 PRINT "*                                                           *"
3200 PRINT "*       INPUT:  1  NO. OF SPECIMEN                          *"
3210 PRINT "*               2  TITLE OF THE TABLE                       *"
3220 PRINT "*               3  COMMENTS                                 *"
3225 PRINT "*               4  CHECK THE TITLE AND COMMENT              *"
3227 PRINT "*               5  NAMES OF THE FILES                       *"
3230 PRINT "*               6  VALUE OF STANDARD RESISTOR              *"
3240 PRINT "*               7  RETURN TO THE MAIN PROGRAM               *"
3245 PRINT "*                                                          *"
3250 PRINT "*************************************************************"
3260 ANSWER=0
3270 INPUT "INPUT YOUR CHOICE ";ANSWER
3280 IF ANSWER<1 OR ANSWER>7 THEN GOTO 3320
3290 ON ANSWER GOSUB  5210,3600,3400,3800,3900,5600,3310
3310 RETURN
3320 GOTO 3270
3400 '
3410 '
```

```
3420 '-------------------------------------------------------------
3430 '            Subroutine for the introduction of the comments
3440 '-------------------------------------------------------------
3450 '
3460 '
3463 CLS
3465 PRINT " YOU HAVE TO INPUT 3 COMMENTS "
3466 PRINT
3470    FOR I=1 TO 3
3480        INPUT"INPUT THE COMMENT ";COMENT$(I)
3490    NEXT I
3495 GOTO 3170
3500 RETURN
3600 '
3610 '
3620 '-------------------------------------------------------------
3630 '         Subroutine to introduce the TITLE of the table
3640 '            (name of the specimen or else)
3650 '-------------------------------------------------------------
3660 '
3670 '
3680 CLS
3690 INPUT "INPUT THE TITLE OF THE TABLE ";TITLE$
3695 GOTO 3170
3700 RETURN
3800 '
3810 '
3820 '-------------------------------------------------------------
3830 '         Subroutine to check the title and the comments
3840 '-------------------------------------------------------------
3850 '
3860 '
3870 PRINT "TITLE: ";TITLE$;"       COMMENT #1: ";COMENT$(1);"      COMMENT #2:
";COMENT$(2);"     COMMENT #3: ";COMENT$(3)
3875 INPUT R$      'used to give time to read
3880 GOTO 3170      'return to last menu (title,comments,program,check)
3890 RETURN         'used to mark the end of the subroutine but not used
3900 '
3901 '
3902 '-------------------------------------------------------------
3903 '        Subroutine to input the names of the files
3904 '-------------------------------------------------------------
3905 '
3906 '
3907 CLS
3908 PRINT "INPUT THE NAME OF THE FILE FOR THE SPECIMEN: "
3909 PRINT "(INPUT  N  FOR THE LAST ONE)"
3910 PRINT
3920  FOR F=1 TO 5
3930    PRINT "SPECIMEN # ";F;"     ";
3940    INPUT SPECI$(F)
3950    IF (SPECI$(F)="N" OR SPECI$(F)="n") THEN GOTO 3970
3951 NAM$(F)="B:"+SPECI$(F)+".DAT"
3960  NEXT F
3970 NSPECI=F-1
3975 GOTO 3170                  'return to the last menu
3980 RETURN
4000 '
4010 '
4020 '-------------------------------------------------------------
4030 '       Subroutine  set-up of the scanner
4040 '-------------------------------------------------------------
4050 '
4060 '
4065 PARAM$="SDR/17/": GOSUB 10000
4070 DATA.STRING$="A2P0T2D0H10X"   '2 poles,step scan,trigger on X,channel
                                   display mode,settling time 5 sec.
```

```
                                    display mode,settling time 5 sec.
4080 PARAM$="WR.STR/17//EOI/": GOSUB 10000
4090 RETURN
4100 '
4110 '
4120 '-------------------------------------------------------------------
4130 '        Subroutine set-up of the Multimeter 192 volt for temperature
4140 '-------------------------------------------------------------------
4150 '
4160 '
4165 PARAM$="SDR/8/": GOSUB 10000
4170 DATA.STRING$="F0R0T4S8X"   'DC volt,Auto range, Zero on, Trigger 1
                                 shot on X, rate integration 100 ms (6.5
                                 digits)
4180 PARAM$="WR.STR/8//EOI/": GOSUB 10000
4190 RETURN
4200 '
4210 '
4220 '-------------------------------------------------------------------
4230 '          Subroutine to read voltage with 192 multimeter
4240 '-------------------------------------------------------------------
4244 '
4250 '
4251 DATA.STRING$="N07N08C01X"           'channel used for thermocouple calibrat
ion
4252 PARAM$="WR.STR/17//EOI/": GOSUB 10000
4253 FOR T=1 TO 900: R=COS(0): NEXT T
4254 PARAM$="RD.STR/8//EOI/": GOSUB 10000       'read the volt
4265 VOLT=VAL(MID$(DATA.STRING$,7,6))/1000000!     'PRINT VOLT
4266 DATA.STRING$="N01X": PARAM$="WR.STR/17//EOI/": GOSUB 10000 'close chan 1
4267 TEMPCOMP=30+VOLT*10^3                      'temperature compensation
4268 VOLTCOMP=5.4295008#*TEMPCOMP+.011446885#*TEMPCOMP^2-.000011295306#*TEMPCOMP
^3+.000000005002049 6#*TEMPCOMP^4                       'volt compensation in uV
4269
     PRINT TEMPCOMP
4270 DATA.STRING$="N01C08N07X"                   'close channel 8 and open channe
1 7 and 1
4280 PARAM$="WR.STR/17//EOI/": GOSUB 10000
4285  FOR T=1 TO 300 : R=COS(0): NEXT T     'allow stabilization of volt
4290 PARAM$="RD.STR/8//EOI/": GOSUB 10000   'read voltage
4300 VOLT1=VAL(MID$(DATA.STRING$,7,6))/1000000!       'convert alpha in numeric v
olt
4305 VOLT1=VOLT1+VOLTCOMP/1000000!
4310 DATA.STRING$="C07N08X"                      'close 7 open 8
4320 PARAM$="WR.STR/17//EOI/": GOSUB 10000
4325  FOR T=1 TO 300 : R=COS(0): NEXT T      'allow stabilization of volt
4330 PARAM$="RD.STR/8//EOI/": GOSUB 10000   'read voltage
4340 VOLT2=VAL(MID$(DATA.STRING$,7,6))/1000000!
4345 VOLT2=VOLT2+VOLTCOMP/1000000!
4350 DATA.STRING$="N07X"
4360 PARAM$="WR.STR/17//EOI/": GOSUB 10000
4370 RETURN
4400 '
4420 '
4430 '-------------------------------------------------------------------
4440 '          Subroutine to measure the resistance  with AC bridge
4450 '-------------------------------------------------------------------
4460 '
4470 '
4480 DATA.STRING$="C"+CHANEL$+"X"              'close channel CHAN$(F)
4490 PARAM$="WR.STR/17//EOI/": GOSUB 10000
4500 DATA.STRING$="S"+CHR$(13)+CHR$(10)  'start and get resistance data
4510 PARAM$="WR.STR/9//EOI/": GOSUB 10000
4515  FOR T=1 TO 500: R=COS(0): NEXT T    'allow stabilization of resistance
4517 DATA.STRING$="LDE0"+CHR$(13)+CHR$(10)
4519 PARAM$="WR.STR/9//EOI/" : GOSUB 10000
```

```
4520 PARAM$="RD.STR/9//EOI/": GOSUB 10000 'read the resistance from AC bridge
4530 RESIST(F,I)=VAL(DATA.STRING$)          'conversion data string into value
4531 RESIST(F,I)=RESIST(F,I)*R       'conversion value of ratio into resistance
4532 DATA.STRING$="W"+CHR$(13)+CHR$(10)         'hold untill restart
4533 PARAM$="WR.STR/9//EOI/": GOSUB 10000
4535 DATA.STRING$="N"+CHANEL$+"X"               'open the chanel
4537 PARAM$="WR.STR/17//EOI/": GOSUB 10000
4540 RETURN
4600 '
4610 '
4620 '-------------------------------------------------------------------
4630 '       Subroutine to create the names of the files
4640 '-------------------------------------------------------------------
4650 '
4660 '
4680 'the name is chosen according to the evolution of the temperature
4690 ' C for a cooling cycle and H for the heating cycle
4700 'a difference of DELTATP is needed to change of cycle
4710 '(increase  DELTATP of temperature change from a cooling to a heating cycle

4720 SIGN(F,I)=SGN(TEMP(I)-TEMP(I-1))    'sign=-1 for cooling and 1 for heating
4725 SIGN(F,0)=1
4730 IF SIGN(F,I)=SIGN(F,I-1) THEN GOTO 4745   'still the same cycle
4732     ' PRINT"ABS: ";ABS(TEMP(I)-TEMP(I-1)),"DELTATP: ";DELTATP
4735 IF ABS(TEMP(I)-TEMP(I-1))<DELTATP THEN SIGN(F,I)=SIGN(F,I-1)
                                            'change in temperature is
                                                not significant
4736 IF ABS(TEMP(I)-TEMP(I-1))<DELTATP THEN GOTO 4745
4740 IF SIGN(F,I)=1 THEN CYCLNUM=CYCLNUM+1   'change of cycle
4745 IF SIGN(F,I)=1 THEN C$="H"
4747 IF SIGN(F,I)=-1 THEN C$="C"
4750 NAM$(F,I)="b:"+SPECI$(F)+C$+MID$(STR$(CYCLNUM),2,1)+".DAT"
4755 PRINT NAM$(F,I),F
4760 RETURN
4980 '
4990 '
5000 '-------------------------------------------------------------------
5010 '        Subroutine to convert volt into temperature
5020 '-------------------------------------------------------------------
5030 '
5040 '
5050 ' For Pt-Pt 13% Rh we use the following relationship
5060 '
5065 VOLT1=VOLT1*1000000!: VOLT2=VOLT2*1000000!
5070 TEMP1=.15239494#*VOLT1-.000013755675#*VOLT1^2+.0000000012610922#*VOLT1^3-4.
4281251D-14*VOLT1^4
5075 '
5080 TEMP2=.15239494#*VOLT2-.000013755675#*VOLT2^2+.0000000012610922#*VOLT2^3-4.
4281251D-14*VOLT2^4
5090 '
5095 RETURN
5200 '
5210 '
5220 '-------------------------------------------------------------------
5230 '     Subroutine to input the no. and channel of specimen
5240 '-------------------------------------------------------------------
5250 '
5260  PRINT "HOW MANY SPECIMEN YOU HAVE?", N
5270  NSPECI=N
5280  FOR I=1 TO N
5290  M=11+I
5300  CHAN$(I)="M"          'set the scannel channel for different specimen
5320  NEXT I
5350  RETURN
5400 '
5410 '
```

```
5420 '-------------------------------------------------------------------
5430 '      Subroutine to set up AC Bridge for resistance measurement
5440 '-------------------------------------------------------------------
5450 '
5460 '
5465 PARAM$="SDR/9/": GOSUB 10000
5470 DATA.STRING$="LDE0W"+CHR$(13)+CHR$(10)  'AUTO,OUTPUT STATUS,INTER Rs
5490 PARAM$="WR.STR/9//EOI/": GOSUB 10000
5500 RETURN
5600 '
5610 '
5620 '-------------------------------------------------------------------
5630 '        Introduce the value of standard resistor
5640 '-------------------------------------------------------------------
5650 '
5660 PRINT "WHAT IS THE VALUE OF THE STANDARD RESISTOR?", R
5670 RETURN
9600 '
9610 '
9620 '-------------------------------------------------------------------
9630 '         Subroutine to initialize IEEE interface
9640 '-------------------------------------------------------------------
9650 '
9660 '
9680 REM            IEEE-488 INTEFACE FOR THE IBM PC V4.2
9700 REM                  WRITTEN IN ADVANCED BASIC
9720 REM AND INCORPORATING ASSEMBLY LANGUAGE ROUTINES TO IMPLEMENT
9740 REM                DMA - DRIVEN GPIB TRANSACTIONS
9780 REM THE ASSEMBLY LANGUAGE ROUTINES MUST BE LOADED PRIOR TO ENTERING
9800 REM BASICA BY TYPING "SUBLIB".  THEN TYPE "BASICA", LOAD IEEE488.BAS,
9820 REM AND CALL SUBROUTINES AS DESCRIBED IN THE MANUAL.
9940 REM
9950 REM (C) Copyright Tecmar, Inc. 1982,1983,1984
9955 REM
9960 REM ********************* START OF SUBROUTINE ****************************
9999 END
10000 GOSUB 21560              'FETCH COMMAND
```

APPENDIX D

THE LATTICE PARAMETER - COMPOSITION RELATION FOR SOME TRANSITION METAL COMPOUNDS

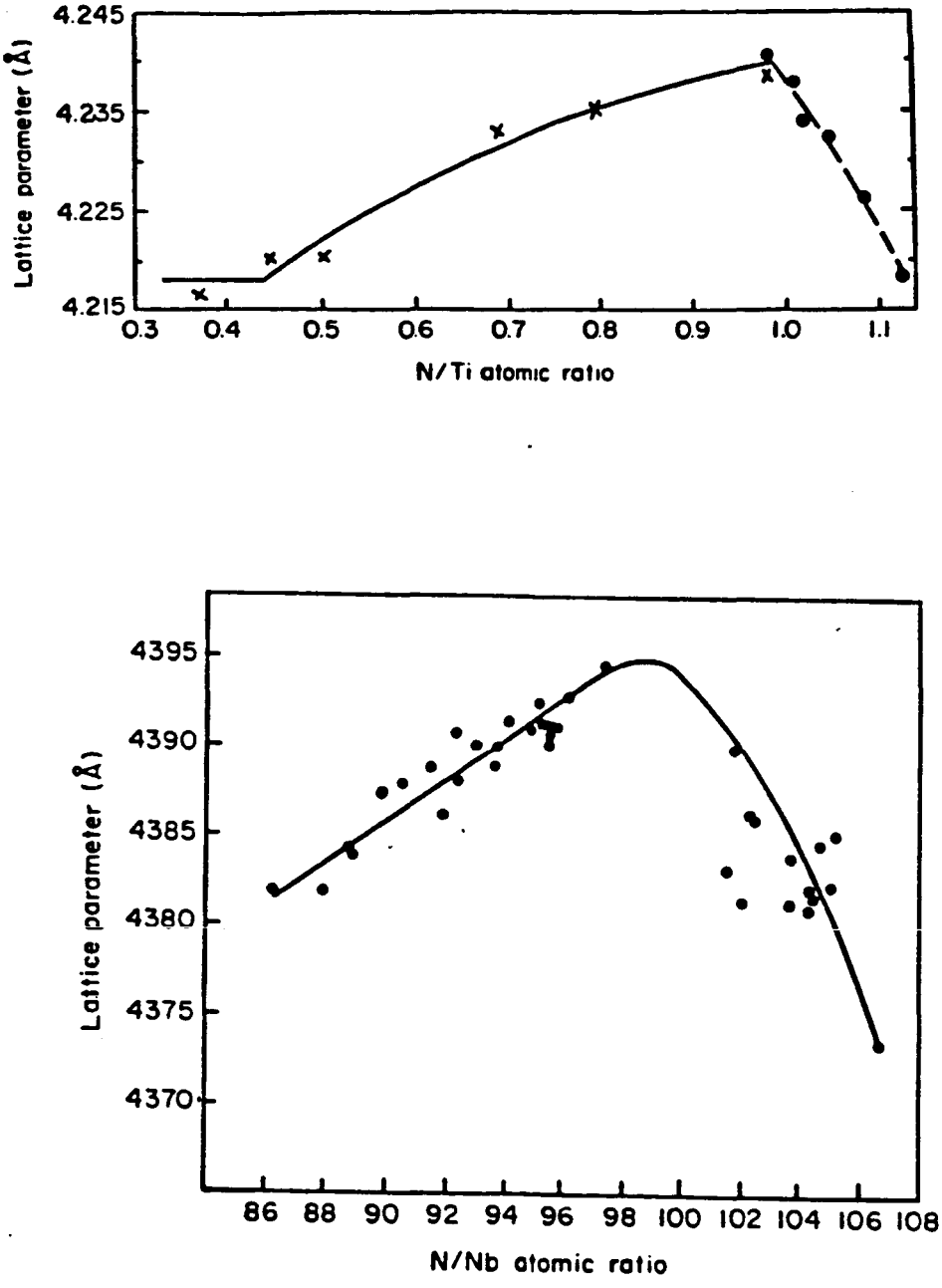

Fig. D-1. Dependence of the lattice parameter with N/M ratio for TiN (a) and NbN (b) (after Toth [65].

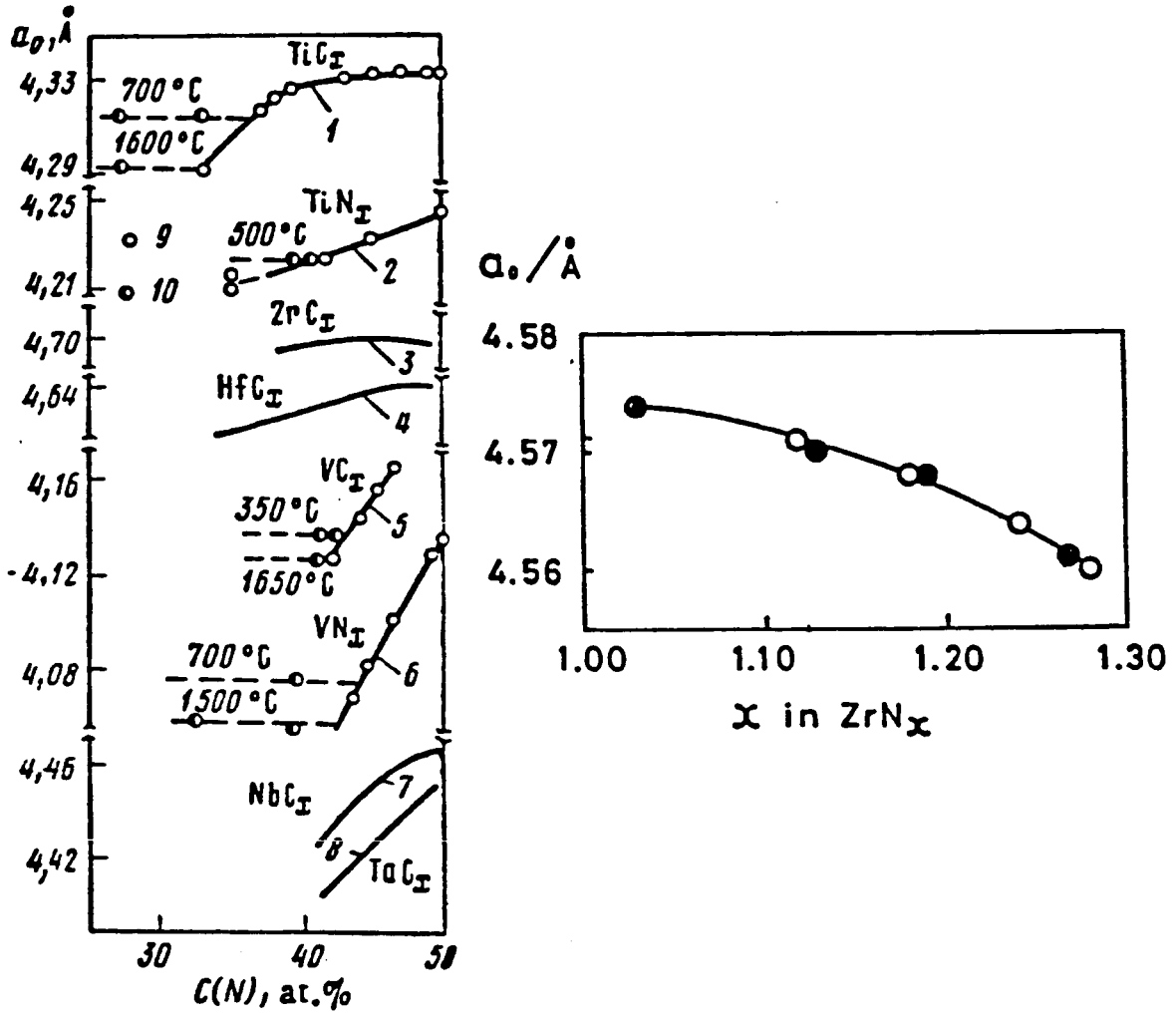

Fig. D-2. Dependence of the lattice parameter with nonmetal concentration for transition metal compounds (a)(after Khaenko [69]), and for hyperstoichiometry ZrNx (b) (after Yajima et al [70]).

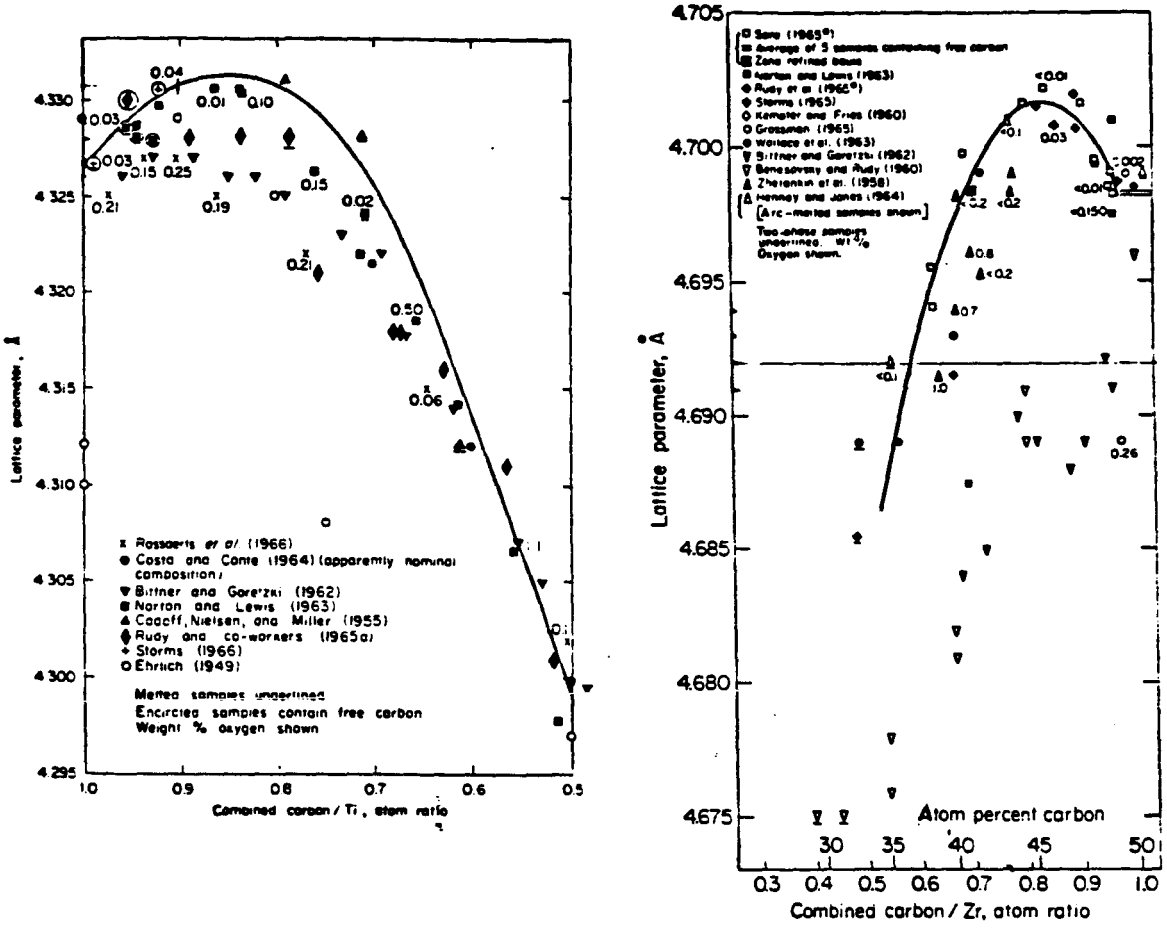

Fig. D-3. Lattice parameter as a function of composition for TiC (a) and ZrN (b). (after Storms [53]).

APPENDIX E

ORDER-DISORDER TRANSITION IN SOME OF THE TRANSITION METAL COMPOUNDS

TABLE E-1

Characteristics of Ordered Modifications of Cubic Carbides and Nitrides of Transition Metals of Groups IV and V. [69]

Basis phase	Ordered modification	Composition, at.% C or N	Temperature range of existence, °C	Crystallographic characteristics	
				lattice type	unit-cell period ($a_0 = a_{NaCl}$)
TiC_x	δ′	37–43	≈1100	Trigonal	$a=6{,}115$ Å$=\sqrt{2}a_0$ $c=14{,}90$ Å$=2\sqrt{3}a_0$
	δ′	~45,5	≈1000	»	$a=5{,}885$ Å$=\sqrt{2}a_0$ $c=14{,}43$ Å$=2\sqrt{3}a_0$
VC_x					$a=10{,}19$ Å$=\sqrt{6}a_0$ $c=28{,}85$ Å$=4\sqrt{3}a_0$
	δ″	~45,5	~1250–1000	»	$a=163{,}0$ Å$=16\sqrt{6}a_0$ $c=28{,}85$ Å$=4\sqrt{3}a_0$
	δ_x'	~46,6 (V_8C_7)	<1250	Cubic	$a=8{,}330$ Å$=2a_0$
ZrC_x	δ′	39–43	≈1100	Trigonal	$a=6{,}63$ Å$=\sqrt{2}a_0$ $c=16{,}26$ Å$=2\sqrt{3}a_0$
NbC_x	δ′	43–48	≈1000	»	$a=10{,}87$ Å$=\sqrt{6}a_0$ $c=30{,}76$ Å$=4\sqrt{3}a_0$
TiN_x	δ′	~37	≈800	Tetragonal	$a=4{,}144$ Å$=a_0$ $c=8{,}781$ Å$=2a_0$
VN_x	δ′	44–47	<520	»	$a=c=8{,}15$ Å$=2a_0$
NbN_x	δ′	~43 (Nb_4N_3)	≈1400	»	$a=4{,}382$ Å$=a_0$ $c=8{,}632$ Å$=2a_0$

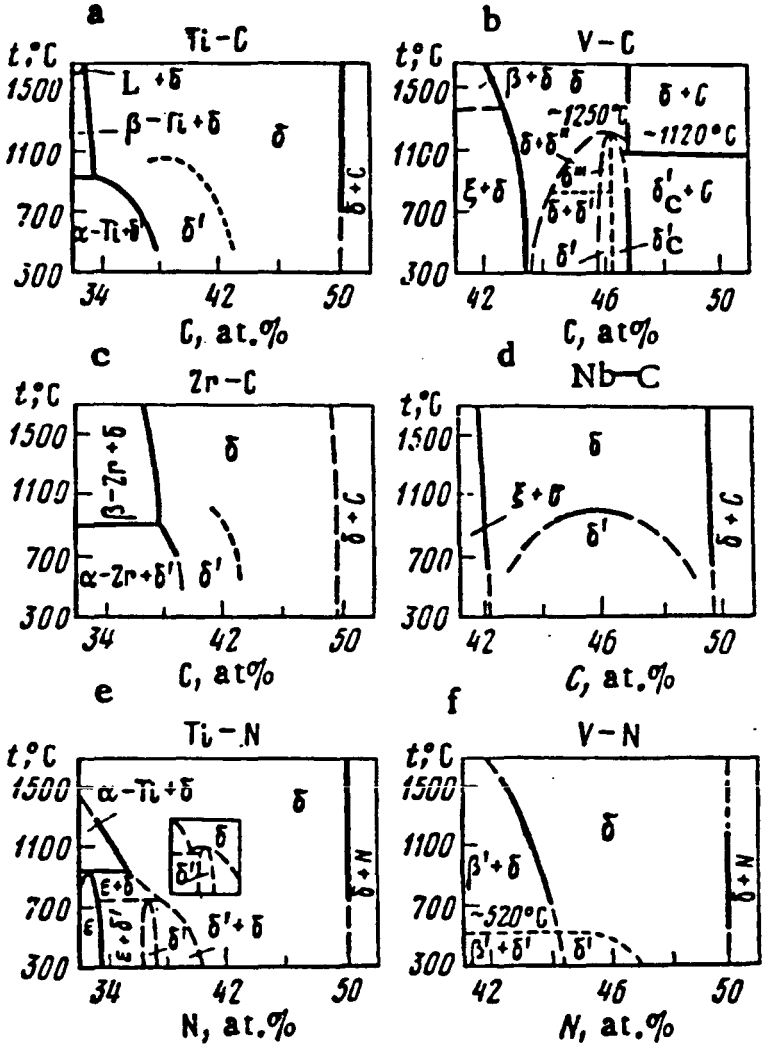

Fig. E-1. Fragments of phase diagrams for monocarbides and mononitrides of transition metals of Group IV and V. (after Khaenko [69]).

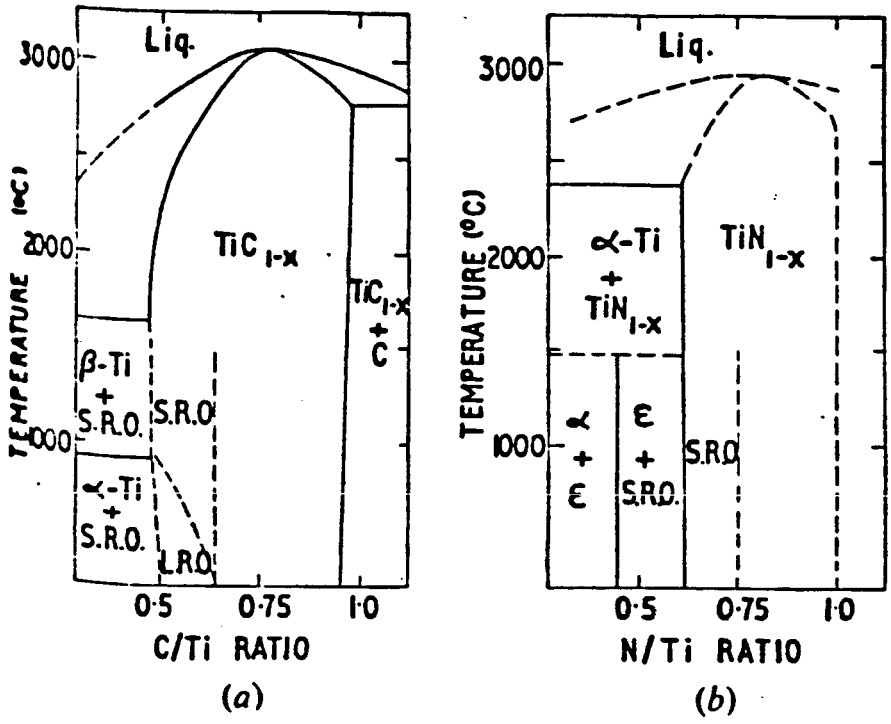

Fig. E-2. Part of a phase diagram for TiC (a) and TiN (b). (after Billingham [119]).

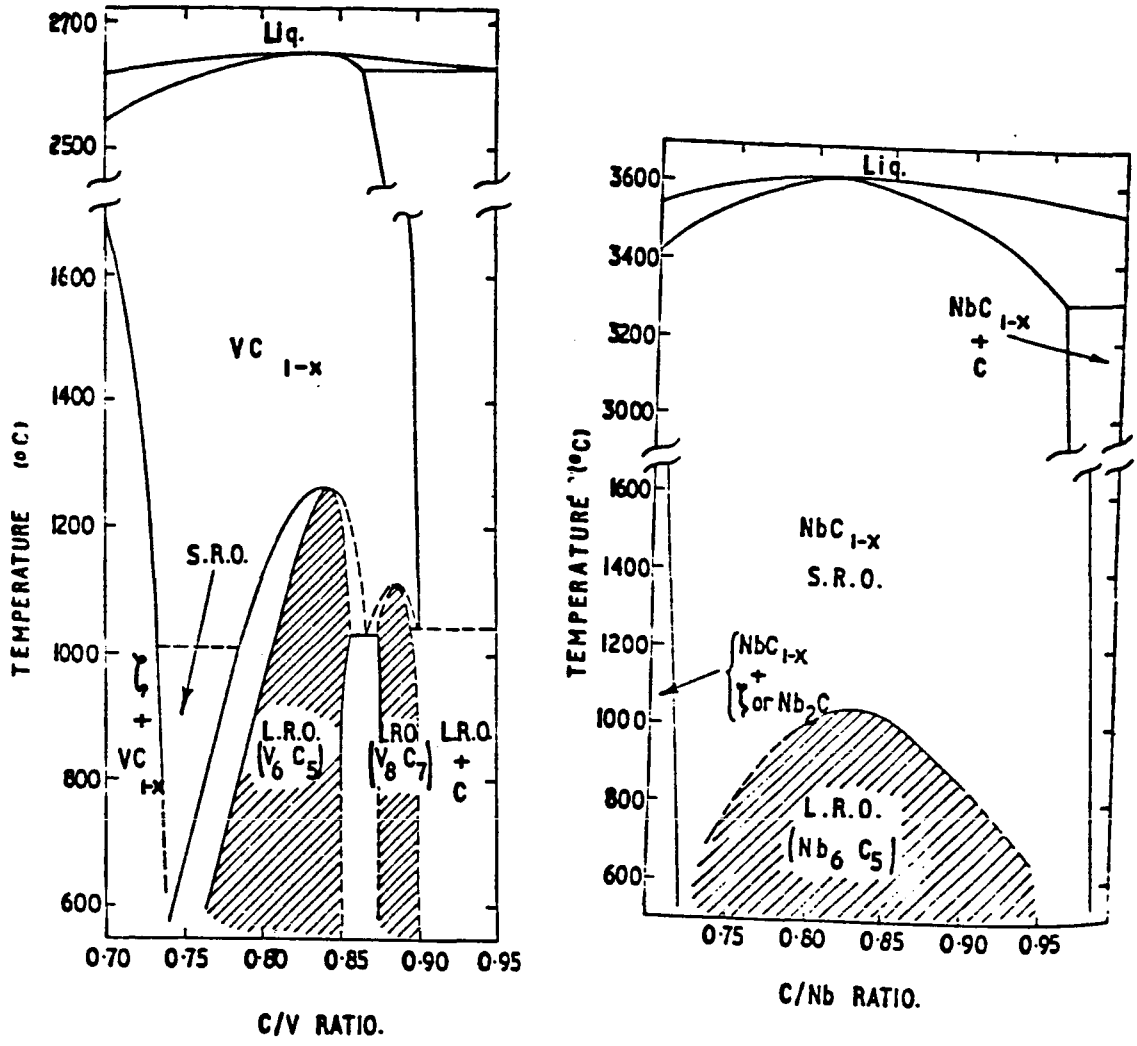

Fig. E-3. Part of the phase diagrams for VC (a) and NbC (b). (after Billingham [119]).

VITA

NAME : JIH-FEN LEI

BORN : [redacted]

EDUCATION:

Department of Materials Science and Engineering
Northwestern University
Evanston, Illinois U.S.A.
Janu. 1982 - Sept. 1984, July 1985 - present.

Department of Physics
Northwestern University
Sept. 1981 - Janu. 1982

B.S. in Department of Physics
Tsing - Hwa University
Shichu, TAIWAN, REPUBLIC OF CHINA
1981

PUBLICATION:

"Elevated Temperature Strain Gages", with J. O. Brittain and D. Geslin, Proceedings of a conference on Turbine Engine Hot Section Technology 1986, NASA Conference Publication 2444.

"Materials for Elevated Temperature Strain Gages Applications", with J. O. Brittain and D. Geslin, Proceedings of a conference on Turbine Engine Hot Section Technology 1985, NASA Conference Publication.

PRESENTATION:

"Selection Criteria for Materials for High Temperature Resistance Strain Gage Application", Materials Science and Engineering Spring Review, Northwestern University, May 22, 1986

"Elevated Temperature Strain Gages", Conference sponsored by NASA Lewis Research Center, Cleveland, Ohio, Octo. 21-22, 1986.